12-15-2014

Bio-Active Degradable Micellar Hydrogels for Osteogenic Differentiation of Mesenchymal Stem Cells

Seyedsina Moeinzadeh
University of South Carolina - Columbia

BIO-ACTIVE DEGRADABLE MICELLAR HYDROGELS FOR OSTEOGENIC DIFFERENTIATION OF MESENCHYMAL STEM CELLS

by

Seyedsina Moeinzadeh

Bachelor of Science
University of Tehran, 2007

Submitted in Partial Fulfillment of the Requirements

For the Degree of Doctor of Philosophy in

Chemical Engineering

College of Engineering and Computing

University of South Carolina

2014

Accepted by:

Esmaiel Jabbari, Major Professor

Melissa A. Moss, Committee Member

Francis Gadala-Maria, Committee Member

John J. Lavigne, Committee Member

John Weidner, Committee Member

Lacy Ford, Vice Provost and Dean of Graduate Studies

DEDICATION

To my family who have offered nothing but love and support over the years

ACKNOWLEDGEMENTS

First of all I must thank my research advisor, Dr. Esmaiel Jabbari who supported my scientific interests and guided me expertly toward completion of this dissertation. I would like to thank him for his undying encouragement, advice and support. I would also like to acknowledge my committee members, Dr. Melissa A. Moss, Dr. Francis Gadala-Maria, Dr. John J. Lavigne and Dr. John Weidner for their support and contribution. I would like to offer my sincere thanks to my research collaborators, Dr. Xuezhong He, Dr. Angel E Mercado, Dr. Ozan Karaman, Dr. Junyu Ma, Danial Barati, Samaneh K. Sarvestani, Dr. Tahereh Karimi, Dr. Seyedramin Pajoumshariati and Leily Daneshian. Further, I would like to thank my family members as well as my dear friends for their unending support.

ABSTRACT

A feasible approach to the restoration of injured bone tissue is the use of tissue engineering strategies to deliver mesenchymal stem cells (MSCs) to the site of regenration in degradable, in-situ gelling, bio-active hydrogels. Although inert Polyethylene glycol (PEG) hydrogels provide flexibility in controlling the cell microenvironment, their use for in vivo applications in tissue regeneration is limited by their persistence (nondegradability) in the site of regeneration. In an attempt to produce inert hydrolytically degradable matrices for encapsulation of MSCs, hydrogels based on star PEG macromonomers chain-extended with short hydroxy acid (HA) segments (SPEXA) were synthesized and characterized with respect to gelation kinetics, water content, degradation rate and mechanical properties. HA monomers included glycolide, lactide, p-dioxanone and ε-caprolactone. The degradation rate of SPEXA hydrogels was strongly dependent on HA type and number of HA repeat units. SPEXA gels chain-extended with the least hydrophobic glycolide completely degraded within days, lactide within weeks, and p-dioxanone and ε-caprolactone degraded within months. Further, there was a biphasic relationship between HA segment length and gel degradation. There was a significant decrease in gelation time of SPEXA macromonomers with HA chain-extension for all HA types due to micelle formation. Meso-scale simulations revealed formation of micellar structures within the SPEXA precursor solutions for all HA types.

The micellar SPEXA hydrogels supported osteogenic differentiation, collagen production, and mineralization of MSCs. We further investigated the effect of

concentration and hydrophobicity a BMP-2 protein derived peptide on osteogenic differentiation of mesenchymal stem cells (MSCs) encapsulated in a PEG based hydrogel. The dose-osteogenic response curve of the BMP-2 peptide was in the 0.0005-0.005 mM range, and osteoinductive potential of the BMP-2 peptide was significantly less than that of BMP-2 protein even at 1000-fold higher concentrations. There was a higher osteogenic differentiation of encapsulated hMSCs when the BMP-2 peptide was dissolved in the hydrogel matrix as compared to the peptide conjugated to the hydrogel network. The BMP-2 peptide with a positive index of hydrophobicity had a critical micelle concentration (CMC) and formed aggregates in aqueous solution. Results revealed that osteoinductive potential of the BMP-2 peptide is correlated with its CMC and the free peptide concentration in aqueous medium and not the total concentration.

TABLE OF CONTENTS

LIST OF TABLES

LIST OF FIGURES

CHAPTER 1

INTRODUCTION

The clinical needs for bone tissue regeneration are diverse and include applications arising from skeletal defects caused by fracture, trauma, infection, neurosurgical procedures, resection of tumors and spinal deformities. [1-3] There are more than 280000 and 700000 hip and vertebral fractures in the USA annually.[4] Approximately 500000 and 2.2 million bone grafting procedures are performed inside the US and worldwide respectively each year.[5] The total number of spinal fusion procedures in the U.S. was 673,000 in the year 2012. [6]

The gold standard for bone implantation is use of grafts harvested from the patient's body (Autologous grafts). However, autologous bone grafting needs an additional surgery for harvesting the bone from the donor site. Furthermore, the donor site may undergo morbidity, infection and pain after operation. [7] The use of cadaveric bone (allograft) suffers from a risk of disease transmission [8]. Further, the use of devitalized allografts was associated with 60% graft failure over 10 years due to the absence of bone osteoprogenitor cells within the graft.[9] It is well established that the presence of stem cells or osteoprogenitor cells has a significant role in bone regeneration.[10, 11] A 63% reduction in bone formation was reported when the stem cell containing periosteum and bone marrow were removed from a live bone graft in a murine segmental femoral bone graft model. [9] In addition, a significant increase in the

bone formation and neuvascularization were observed with immobalizing MSCs on the surface of allografts or directing MSCs to the surface of allografts in-vivo.[12, 13] However, MSCs had a limted viability and an extensive migration from the site of regeneration when they were incorporated into the grafts without a three dimensional carrier similar to the stem cell carrier matrix in the natural bone. [13]

Bone is a composite matrix consisting of a mineral and a gel phase.[14, 15] The mineral phase provides the mechanical strength as well as osteoconductivity while the gel phase, with a significantly lower stiffness than the mineral phase, plays a critical role in maturation and differentiation of stem cells and progenitor cells.[14, 15] Multiple bioactive ligands within the gel phase interact with stem cells to initiate the cascade of differentiation and mineralization.[16] For instance, the interaction between RGD, a ligand in collagen I and fibronectin proteins, and cell surface receptors, facilitates cell spreading and focal adhesion to the ECM which is critical for cell differentiation.[17] Also, a peptide corresponding to residues 73-92 of the knuckle epitope of the BMP-2 protein is shown to have an osteo-inductive potential. [18] Differentiation of stem cells to bone cells in the natural bone is regulated by an optimal matrix stiffness (mechanical cues) and optimal spatio-temporal distribution of bio-active ligands (biological cues) within the soft gels. [19]

An exciting approach to bone tissue engineering is to deliver progenitor cells to the regeneration site in natural or synthetic hydrogels modified with the bioactive lignds (see Figure 1.1). This allows the encapsulated cells to secrete the desired extracellular matrix (ECM).[20] In that approach, the gel degrades gradually, providing space for the new bone formation and eventually displacing the gel with the patient's own bone tissue.

Cell-laden bioactive hydrogels can be used alone for minimally invasive non-load bearing applications or combined with supportive structures for load bearing applications. Hydrogels are hydrophilic polymeric networks that retain a significant fraction of water in their structure in physiological solution. Nutrient molecules and proteins diffuse through hydrogels and cells immobilized in hydrogels display higher biological activity.[21-25] Due to these unique properties, hydrogels are very attractive as a matrix for cell encapsulation and delivery to the regeneration site in regenerative medicine.[26-30]

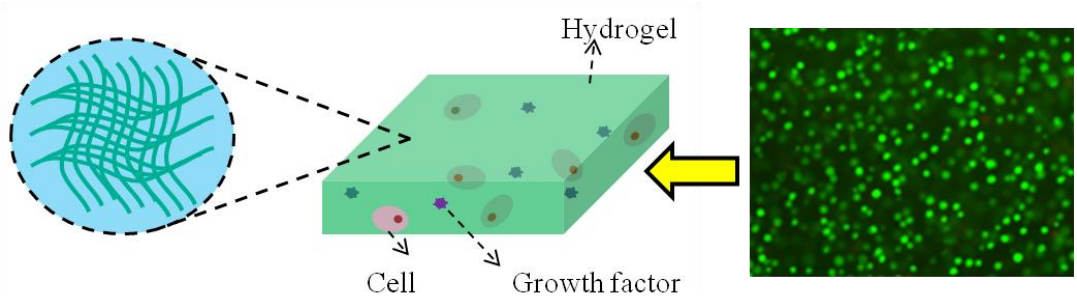

Figure 1.1. Schematic representation of cell-laden hydrogels for tissue regeneration. A fluorescent image of live MSCs (green dots) encapsulated in a PEG based hydrogel is shown at right.

Minor variation in the sequence distribution of natural gels can significantly affect the fate of encapsulated cells. With many cell-binding ligands and regulatory factors, it is difficult to adapt the properties of natural matrices to a particular application in regenerative medicine.[31] For instance, differentiation of mesenchymal stem cells (MSCs) shifted from osteogenic to chondrogenic lineage by changing the matrix from collagen type I to type II.[32, 33] Moreover, due to their low stiffness, natural gels are limited in practical applications by soft tissue compression.[34-36] Therefore, there is a need to synthesize novel hydrogels with tunable physical, mechanical, and biological

properties for a wide range of applications in regenerative medicine such as MSC implantation for treatment of skeletal defects and spinal fusion, chondrocyte implantation in cartilage regeneration or as cardiac patches to treat heart infarction.

Synthetic polyethylene glycol (PEG) based hydrogels are used extensively for cell encapsulation to elucidate the effect of physiochemical, mechanical, and biological factors in the microenvironment on cell fate *in vitro*.[36-39] PEG hydrogels, due to their inert, hydrophilic and immunogenic nature, provide enormous flexibility in designing and controlling the cell microenvironment.[40, 41] Unlike small-molecule monomers that cross the cell membrane, the flexible PEG macromonomers crosslink to produce hydrogels with high compressive modulus without adversely affecting the viability of the encapsulated cells.[42-46]

Although inert PEG hydrogels provide flexibility in controlling the cell microenvironment, their use for *in vivo* applications in tissue regeneration is limited by their persistence (non-degradability) in the site of regeneration.[30] In that regard, design and synthesis of PEG hydrogels with hydrolytically degradable hydroxyl acid (HA) links would substantially increase their use as cell delivery matrices in tissue regeneration.[47-49] We hypothesized that degradation and stiffness of PEG-HA gels are dependent on the length and characteristics of the HA segment as well as functionality, molecular weight and concentration of the PEG-HA macromonomer. To test the hypothesis, hydrogels based on star PEG macromonomers chain-extended with short HA segments (SPEXA) were synthesized and characterized with respect to gelation kinetics, degradation rate, sol fraction, mechanical properties and water content.[35, 50-52] Star PEG macromonomers have lower radius of gyration and shear viscosity, and higher density of functional groups

than the linear PEGs,[25, 53] leading to the formation of gels with higher crosslink density and modulus.[54-57] HA monomers included least hydrophobic glycolide, lactide, p-dioxanone, and most hydrophobic ε-caprolactone. Further, MSCs were encapsulated into the developed gels and their viability and differentiation to the osteogenic lineage were measured.[35, 51] In addition, Dissipative Particle Dynamics simulation method [58, 59] was used to simulate aggregation, micelle formation and the distribution of reactive groups in SPEXA hydrogel precursor solutions.[35, 51, 60] Experimental and simulation results demonstrated that SPEXA hydrogels with a wide range of degradation rate, gelation kinetics and mechanical properties can be synthesized with adjusting the hydrophobicity and length of the HA segment, functionality and molecular weight of the PEG and concentrations of the macromonomer and initiator. Further, results revealed the formation of micellar structures within the hydrogels' precursor solution at the nano-scale that affects the gelation kinetics, degradation rate and macroscopic properties of the hydrogels.[59]

It is well established that bone morphogenic protein (BMP-2) plays a dominant role in osteogenic differentiation of MSCs and formation of the new bone tissue.[16, 61] BMP-2 has been used extensively in certain clinical applications such as sinus augmentation, spinal fusion, and alveolar ridge augmentation to accelerate bone regeneration and reduce the chance of graft failure.[62, 63] Due to its short-half-life and diffusion of the protein away from the site of regeneration, doses much higher than the endogenous amount are used in clinical applications.[62, 64] High doses of BMP-2 protein *in vivo* cause undesired side effects such as bone overgrowth, immune response, and tumor formation.[65] For example, the probability of an adverse side effect with the

use of BMP-2 in spine fusion may be as high as 40%.[65] An attractive approach to reduce the protein's side effects in bone tissue engineering is to use peptides derived from the bioactive segements of BMP-2.[66] In order to design a BMP-2 peptide incorporated hydrogel for osteogenic differentiation of MSCs there is a need to know how peptide concentration, peptide aggregation and peptide grafting affect the bio-activity of the peptide within the hydrogel. The effect of concentration and hydrophobicity of a BMP-2 peptide on peptide aggregation and differentiation of MSCs encapsulated in an inert polyethylene glycol (PEG) hydrogel was investigated through experiments and simulations.[67] Results demonstrated that the osteo-inductive potential of the BMP-2 peptide within the PEG hydrogel is correlated with the peptide hydrophobicity and concentration of the non-aggregated peptide and not the total peptide concentration. [67]

CHAPTER 2

BACKGROUND AND LITERATURE REVIEW

2.1. OSTEOGENIC DIFFERENTIATION OF STEM CELLS IN BONE

Mesenchymal stem cells (MSCs) are multipotent stem cells that have self-renewal ability and also can differentiate to osteoblasts, chondrocytes or adipocytes. It is well established that MSCs and osteoprogenitor cells play a vital role in bone regeneration during development and bone healing. A 50% loss of bone graft strength and a 60% graft failure were observed after 10 years of the decellularized allograft implantation. [9] Further, a 63% reduction in bone formation was reported when the stem cell containing periosteum and bone marrow were removed from a live bone graft in a murine segmental femoral bone graft model. [9] In addition, a significant increase in the bone formation and neuvascularization were observed with immobalizin MSCs on the surface of the allografts or directing MSCs to the surface of allografts in-vivo.[12, 13] Stem cells and progenitor cells do not reside within the calcified part of the bone. Bone MSCs in adults mainly reside within the perivascular region of the bone marrow whereas osteoprogenitor cells exist in bone marrow, endostum and periostium. [68, 69] MSCs differentiate to osteoprogenitors in bone marrow. Osteoprogenitor cells undergo differentiation into preosteoblasts and osteoblasts in the osteoblastic region of the bone marrow as well as the soft osteogenic layer of the periosteum (see Figure 2.1). [19] The osteoblasts develop to osteocytes which participate in bone remodeling and bone regeneration. Osteoprogenitor

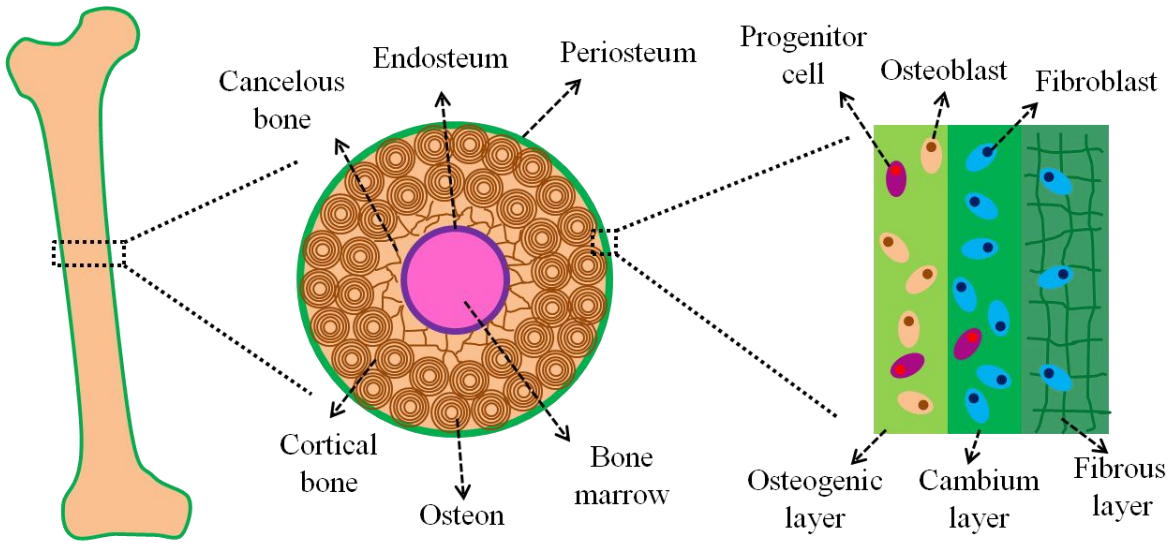

Figure 2.1. Schematic representation of the bone and periosteum micro-structures. Osteogenic differentiation of osteoprogenitor cells to bone cells occurs within the soft osteogenic layer of the periosteum.

cells in periosteum and bone marrow concurrently give rise to osteoblasts during bone repair. [15] Differentiation of stem cells to the bone cells in periosteum and endosteum is regulated by an optimal matrix stiffness (mechanical cues) and optimal concentration of growth factors (biological cues) at the site of differentiation. [19] While bone is composed of a stiff inorganic-organic composite matrix with elastic modulus of 17 GPa, the thin periosteum with an elastic modulus of 1.9 MPa is four orders of magnitude less stiff. [70, 71] Furthermore, the inner osteogenic layer of the periosteum, that hosts the differentiating of osteoprogenitor cells, is softer than the outer fibrous layer (see Figure 2.1). The process of bone remodeling in adults is compareable with intramembranous ossification in infants, in that they both initiate from the differentiation of stem cells to osteoblasts in soft un-calcified matrices.[72] It is well established that the stiffness of extracellular matrix (ECM) affects the fate of stem cells. [73, 74] For instance, MSCs encapsulated in a semi-synthetic alginate based hydrogel undewent osteogenic

differentiation when the matrix elastic modulus was in the 11-30 kPa range while the adipogenic differentiation occurred in softer matrices with elastic modulus of 2.5-5 kPa. [75] The osteogenic differentiation of MSCs increased when the elastic modulus of cell-laden PEG gels increased from 0.2 to 59 kPa. [76] In addition, MSCs underwent neuronal, myogenic and osteogenic differentiation when they were cultured on gels with low (0.1-1 kPa), intermediate (8-15 kPa) and high (25-40 kPa) elastic modulus respectively. [73]

In addition to the matrix stiffness, an optimal spatio-temporal distribution of growth factors plays a key role in differentiation of stem cells/osteoprogenitor cells to bone cells during bone remodeling or bone development. Although several growth factors including fibroblast growth factor (FGF), transforming growth factor-β (TGF-β), insulin-like growth factor (IGF) and vascular endothelial growth factor (VEGF) contribute in development and remodeling of a vascularized bone tissue, bone morphogenic proteins (BMPs) play a dominant role in osteogenic differentiation of MSCs. [16, 61] In intramembranous ossification, clustered MSCs in a soft matrix differentiate into osteoblasts by localized secretion of BMPs.[72, 77] In a developed bone tissue, migration of MSCs from bone marrow toward endosteum and secretion of BMPs promote bone formation. [78] Several clinical studies have shown that the rate of healing increases and the failure rate decreases with incorporation of BMP-2 and BMP-7 proteins in fracture repair or spinal fusion procedures. [62, 63, 79] All in all, the cascade of bone formation initiates with osteogenic differentiation of MSCs promoted by mechanical cues and growth factors specifically BMPs within a soft matrix.

2.2. CROSSLINKING OF POLYMER CHAINS AND GELATION

As mentioned before, hydrogels are crosslinked networks of hydrophilic polymeric chains. If monomers (or macromonomers) of a polymerization reaction show a functionality higher than 2, crosslinking between macromonomers will form branched structures (see Figure 2.2). If the expected number of chains in each succeeding generation of branched structures is greater than the number of chains in the preceding generation, crosslinking may result to formation of an infinite network (see Figure 2.2). Starting from a randomly chosen primary molecule "A", the probability that "A" belongs to an infinite network is dependent on the total number of crosslinks on a molecule "B" which is crosslinked to molecule "A". If ε is the average number of crosslinks on "B" excluding the one that primarily connects A to B, the crosslinking is finite when $\varepsilon < 1$ because each generation tends to be smaller than the preceding one. Infinite networks can be formed only if $\varepsilon \geq 1$.

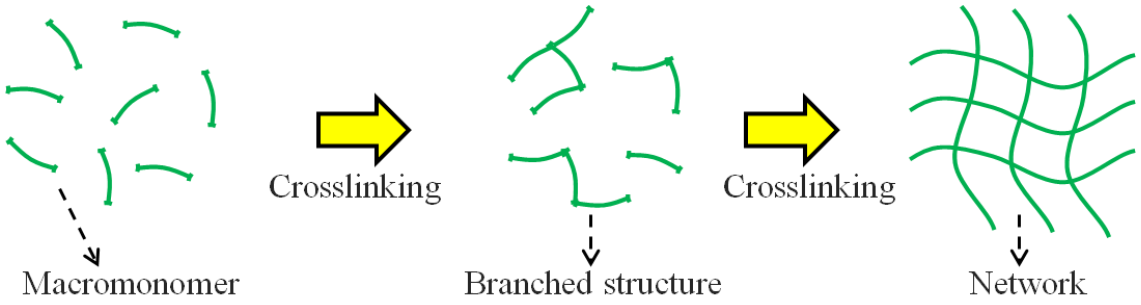

Figure 2.2. Schematic representation of crosslinking the multi-functional macromonomers (left) to form branched structures (middle) and an infinite network (right).

Therefore, the critical condition for gelation is $\varepsilon = 1$.[80] At the critical point of gelation ($\varepsilon = 1$), the number average molecular weight of the chains ($\overline{x_n}$) has a finite value but

the weight average molecular weight of chains ($\overline{x_w}$) is infinite. So the molecular weight distribution has an infinite breadth at the gelation point.[80]

2.3. APPLICATIONS OF HYDROGELS

Hydrogels have been used commercially to fabricate oscular contact lenses. [81] Furthermore, hydrogels based on poly(2-hydroxyethyl methacrylate) (pHEMA) copolymerized with methacrylic acid (MAA) and N-vinyl pyrrolidone (NVP) were used as ophthalmic drug carriers for treatment of glaucoma. [82, 83] In cancer treatment, biodegradable hydrogels based on PEG and PLGA were used for delivery of Paclitaxel to tumors and they were shown to be effective in localizing drug concentration and decreasing the systemic drug concentration. [84] In addition, pH, temperature or magnetic sensitive PEG based hydrogels have been used in cancer treatment. [85, 86]

Hydrogels, due to their high water content and high diffusivity of nutrients and biomolecules, can be potentially applied as carrier matrices for delivery of cells to the site of regeneration in cell based therapies and tissue regeneration.[21, 24, 28, 87, 88] Since injectable cell-laden hydrogels can be formed in-situ, they can be used for filling irregularly-shaped defects through minimally invasive procedures.[89] After injection and in situ hardening, the hydrogel matrix guides the development of seeded cell into the desired tissue.[24]. The mechanical properties of tissue engineering hydrogels can be tuned to prevent deformation or rupture and at the same time keep the cells viable. [44] In addition, resorption of biodegradable hydrogels provides volume for tissue formation and gradually displaces the hydrogel with cell secreted matrices.[48] Hydrogels have been used for encapsulation of different cell lines and regeneration of different tissues. For instance, PHEMA and PVA hydrogels were used for engineering of corneas. [90] MSCs

were encapsulated in a number of hydrogels including collagen, chitosan, alginate PEG and polypeptides for osteogenic differentiation.[30, 75, 91-93] Neural Stem Cells (NSCs) were encapsulated in alginate hydrogels and underwent neuronal differentiation when the the gel elatic mosulus was 180 Pa within the range of brain tissue modulus (100-1000 Pa).[94] Different hydrogels including PEG/agarose [95], collagen [96], PEG [97] chitosan [98] and hyaluronic acid/chitosan [99] were used for encapsulation of chondrocyte cells for cartilage tissue engineering. Co-cultures of Endothelial Colony Forming Cells (ECFCs) and Mesenchymal Stem Cells (MSCs) encapsulated in Gelatin Methacrylate hydrogels with a compressive modulus of 2 kPa underwent vasculogenic differentiation and generated extensive capillary like networks in-vitro. [100]

2.4 NATURAL VS SYNTHETIC HYDROGELS

Only those hydrogels that are biocompatible, support cell-matrix interactions and provide free volume for the newly formed tissue through degradation can be utilized as supporting matrices in regenerative medicine.[101, 102] Consequently, natural hydrogels, derived from the components of extracellular matrix (ECM) that degrade enzymatically, are frequently used as delivery matrices in clinical applications. Collagen gel, one of the main parts of mammalian tissues, is the most widely used natural hydrogel.[103] Collagen gel is formed from physically crosslinked collagen fibers self-asembled from triplehelic collagen molecules.[104] Gelatin is a thermosensitive gel formed from physically crosslinked gelatin protein molecules which are deformed collagen molecules with distorted secondary and tertiary structures.[105] Modified collagen and gelatin were also chemically crosslinked to make more robust hydrogels. [100, 106, 107] Fibrin gels were formed by the enzymatic polymerization of fibrinogen, a natural component of the

body, in the presence of thrombin.[103] Alginate is a biomaterial derived from brown algae and can be gelled in the presence of divalent cations such as: Mg^{2+}, Ca^{2+} and Ba^{2+}. [108] In addition to alginate, other polysaccharide based natural hydrogels including chitosan, hyaluronic acid and agarose have been extensively used in tissue engineering applications. [20, 109] With many cell-interactive ligands and regulatory factors, it is difficult to tailor the properties of natural hydrogels to a particular application in regenerative medicine.[31] Moreover, due to their low stiffness, natural gels are limited in practical applications by soft tissue compression.[34-36] Therefore, there is a need to synthesize hydrogels with adjustable physical, mechanical, and biological properties for a wide range of applications in tissue engineering.

Hydrogels based on several synthetic hydrophilic macromers including poly(hydroxyethyl methacrylate) (pHEMA), poly(ethylene glycol) (PEG), poly(vinyl alcohol) (PVA), polyurethane , polyacrylate and polypeptides have been synthesized and characterized.[20, 103, 110] pHEMA hydrogels have excellent biostability and are being used in fabrication of contact lenses.[103] Degradable pHEMA hydrogels were also synthesized with incorporation of oligomeric polycaprolactone (PCL) crosslinkers.[111] Polyethylene glycol (PEG) hydrogels are inert, non-immunogenic, and compatible with stem cells and can be conjugated with multiple bioactive peptides to modify the cell microenvironment and regulate cell fate.[112-114] Furthermore, the stiffness of PEG hydrogels can be changed in a wide range with altering the concentration of highly soluble PEG macromonomers in the aqueous precursor solution or using multifunctional PEG macromonomers. [35, 115] However, PEG hydrogels are non-degradable which limits their use as a supporting matrix in regenerative medicine. Degradable PEG based

hydrogels were synthesized via copolymerization of PEG macromonomer with hydrolytically degradable monomers or incorporation of hydrolytically or enzymatically crosslinkers within the hydrogel. [52, 116] PVA hydrogels have been synthesized using glutaraldehyde, acetaldehyde or formaldehyde as crosslinking reagents.[117] Chemical crosslinking of PVA macromonomers were also performed using electron beam or γ irradiation.[117] Physically crosslinked PVA hydrogels were developed by freeze-thawing the PVA aqueous solutions or by annealing the dried film. [118, 119] Furthermore, cytocompatable PVA based hydrogels for cell encapsulation were fabricated by photo-crosslinking of modified PVA chains. [120, 121] Self complementary β-sheet forming peptides and amphiphilic peptides have been used to synthesize physically bonded fibrous gels. [122, 123] The properties of peptide based gels were influenced by the hydrophobicity and flexability of the aminoacids within the peptide structure. [124, 125].

2.5. PHYSICALLY CROSSLINKED HYDROGELS

Physically crosslinked hydrogels are composed of macromonomers crosslinked through non-covalent bonds including hydrophobic, ionic or hydrogen bonds. Physically bonded macromonomers are capable of phase transition in response to external stimuli such as temperature, pH and ionic strength. Collagen and gelatin are thermo-sensitive natural gels and undergo gelation at physiological temperature. [105, 106] Aqueous solutions of Poly(N-isopropylacrylamide) (PNIPAAm) form thermo-sensitive physical gels with increasing the temperature above 32°C that is the Lower Critical Solution Temperature (LCST) for the aforementioned polymer solutions. [126, 127] The number of water molecules bound to isopropyl side chains of PNIPAAm decreases and inter-

molecular hydrophobic interactions increases with increasing the temperature above LCST that causes micro-phase separation and gelation.[128] Solutions of micelle forming block copolymers such as PEO-PPO-PEO or PEO-PLGA-PEO were shown to have reversible thermogelling properties.[129] Triblock copolymers containing a hydrophilic middle block and two hydrophobic blocks at the chains ends such as PPO-PEO-PPO or PCL-PEO-PCL underwent micelle formation with bridge and loop conformations in the aqueous solutions and formed gels with increasing the temperature due to the hydrophobic effect.[126]

Hydrogels based on Polyacrylic acid or macromonomers with amine group on the backbone are examples of pH responsive gels. The weak acidic or basic side groups on pH sensitive macromonomers undergo a transition from neutral to charged, leading to a structural transition from collapsed to extended chains with increasing or decreasing the pH respectively. [128, 130] β-sheet forming and surfactant like peptides were desi gned to form physical gels through hydrogen bonding and hydrophobic interactions. For example, peptides with alternating Arginine-Alanine-Aspartate (RAD) residues with 16 amino acids $(RADA)_4$ and $(RARADADA)_2$ with 1-10 mg/mL peptide concentration formed fibrous gels with 10-20 nm fiber diameter in physiological medium or in salt solution [123]. The self-assembly of aforementioned peptides to nanostructured gels was governed by inter-molecular hydrogen bonding between peptides' backbone in β-sheets, ionic interactions between the charged side chains on one side of β-sheets and hydrophobic interactions between hydrophobic side chains at the other side of β-sheet [123, 131, 132]. Solutions of a peptide with an alkyl tail of 16 carbon atoms and a head composed of 4 consecutive cysteines, 3 glycines, a serine and a segment of arginine-

glycine-aspartic acid (RGD) underwent self-assembly to form nanofibrous gels upon decreasing pH below 4 [122].

2.6. COVALENTLY CROSSLINKED HYDROGELS

Crosslinks can be generated by chemical reactions and formation of covalent bonds between macromonomers. Covalently crosslinked gels are significantly stiffer than those that are physically crosslinked [88, 133]. In addition, degradability of covalently-crosslinked gels can be controlled independently of gelation by the molecular weight and ratio of hydrophobic/hydrophilic domains [134-136]. Covalently crosslinked hydrogels have been synthesized using different types of reactions including conventional free radical reaction, Michael-type conjugation and click reaction.[110] The free radical reaction for synthesis of hydrogels can be initiated using redox or photo-initiators. [56, 137, 138] Synthetic or natural polymers modified with acrylate or methacrylate groups at the chain ends or fumarate groups on the backbone have been crosslinked via redox initiated free radical polymerization. For instance, acrylated PEG-PLA, oligo polyethylene glycol fumarate, PEG-PLA famarate and methacrylated chitosan were crosslinked using ammonium persulfate (APS, redox initiator) and tetramethylethylene diamine (TEMED, radical catalyst). [139-142] Advantages of photo-initiated reactions over redox-initiated ones include spatial and temporal control on the crosslinking reaction and faster gelation time. [143] Different photo-initiators including 2,2-Dimethoxy-1,2-diphenylethan-1-one (IRGACURE 651) [137], 1-[4-(2-Hydroxyethoxy)-phenyl]-2-hydroxy-2-methyl-1-propane-1-one (IRGACURE 2959) [35, 144, 145] and eosin/triethanolamine [146] were used for photo-crosslinking of macromonomer to synthesize hydrogels. Free radical photo-initiation was performed under visible light

[147] , UV [35, 52] or argon laser [146]. Acrylated or methacrylated PEG [148, 149], poly(ethylene oxide-co lactide-co glycolide) [52], poly(ethylene oxide-co lactide) fumarate [150], methacrylated gelatin[151], methacrylated hyaluronic acid[152] and methacrylated alginate[152] were used for synthesis of photo-crosslinked hydrogels. Acrylate or methacrylate functionalized macromers were crosslinked to thiol or amine functionalized macromers through Michael addition.[110, 153, 154] Furthermore, click chemistry was applied to synthesize hydrogels from PEG based macromers functionalized with acetylene and azide functional groups. [155]

2.7. MICELLAR HYDROGELS

A-B-A triblock copolymers can form micellar gels in selective solvents [156, 157]. These micelles are responsive to pH and temperature depending on the nature of "A" and "B" blocks. The formed micelles pack into an ordered phase at high concentrations (higher than 20 wt%) and form a gel when the "A" block is solvophilic [156, 158]. However, when the "B" block is solvophilic, gelation takes place by bridge formation between the micelles [159, 160]. Micelle formation in A-B-A triblock copolymers is illustrated schematically in Figure 2.3. At low concentrations, the block copolymers are freely dissolved in the solvent. As the concentration exceeds the critical micelle concentration (CMC), the solvophobic "B" blocks aggregate and form the core of the micelles and the solvophilic "A" blocks form the shell or corona.[161] Each macromer chain adopts one of four possible conformations: bridge, loop in which two chain ends are in the same micelle, tethered in which one chain end is free and free chains (see Figure 2.3.b and 2.3.c). The probability of bridge formation as well as total number of bridges increase with increasing the macromer concentration[162]. The increase in

macromer concentration beyond a finite percolation threshold leads to the formation of a transient micellar network cross-linked by inter-micellar bridges (see Figure 2.3.c). Each

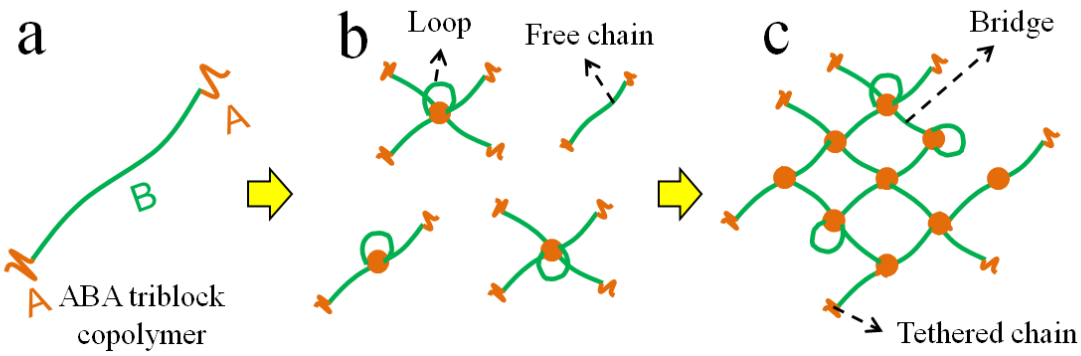

Figure 2.3. (a) Schematic diagram of an A-B-A triblock copolymer with solvophilic block B (green) and solvophobic block A (brown); (b) conformation of chains in A-B-A triblock copolymer chains in solution and formation of micellar structure by aggregation of solvophobic A blocks; (c) formation of a physical network in a solution of A-B-A triblock copolymers by aggregation and micelle formation of solvophobic A blocks. Solvophilic (B block) and solvophobic (A block) segments of the copolymer are shown in green and brown, respectively.(reprinted from [161])

bridge in a transient network has a finite residence time in the micelle. The stability of physical cross-links increases with increasing the solvophobicity and length of the solvophobic segment. A transient network of micelles is mechanically reinforced and permanently stabilized by the formation of covalent bonds within the core of the micelles. The confinement of the crosslinking reaction inside the micelle cores imparts unique features to the hydrogel. In the case of degradable hydrophobic segments, degradation of the hydrogel network is confined to the micellar domains. Furthermore, the cytotoxic low molecular weight molecules are not exposed to the live cells with positioning within the hydrophobic micelles' cores. [51]

2.8. HYDROGEL SWELLING AND MESH SIZE

Hydrophilic macromonomers are individually soluble in water or other selective solvents. However, the solubility of hydrophilic macromers decreases with formation of crosslinks and increasing the average molecular weight of the chains. When the degree of crosslinking exceeds the critical point of gelation, the resulting polymeric network can not be dissolved in water or selective solvents but it swells (see Figure 2.4). The degree of swelling (or water content) of a hydrogel is controlled by two opposing forces, namely thermodynamic force of mixing between polymer-water and elastic force of the extended polymer chains. The force of mixing tends to increase the water content of the gel by attractive interactions between water molecules and the network chains [80].

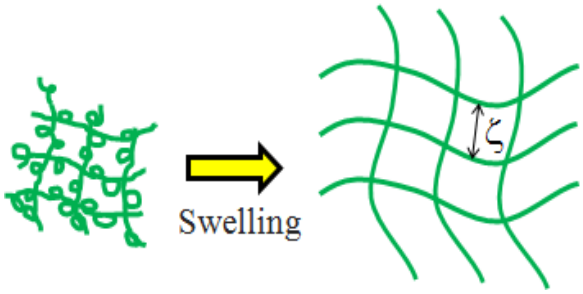

Figuure 2.4. Schematic representation of the swelling of a crosslinked network and the mesh size.

The elastic force of the polymeric chains on the other hand tends to decrease the water content of the gel due to the extension of favorable random coil chain conformation. The difference in the chemical potential of the gel penetrating solvent is given by: [80, 163]

$$\mu_1 - \mu_{1,0} = \Delta\mu_{mixing} + \Delta\mu_{elastic} \qquad \text{equation 2.1}$$

where μ_1 is the chemical potential of solvent within the polymeric gel, $\mu_{1,0}$ is the chemical potential of the pure solvent, $\Delta\mu_{mixing}$ is the change of chemical potential caused

by mixing and $\Delta\mu_{elastic}$ is the change of chemical potential due to the presence of elastic retractive forces of the polymer chains. At equilibrium, the difference between the chemical potential of the solvent inside and outside of the gel (left hand side of the equation 1) is zero. In other words, force of mixing and elastic force of extended chains become equal at equilibrium. Several factors including molecular weight, hydrophobicity, functionality and flexability of the macromonomers, degree of crosslining, nanostructure of the gel and temperature affect the swelling of hydrogels.[55, 164] Specifically, the swelling of hydrogels decreases with increasing the hydrophobicity of the chains and degree of crosslining (crosslinking density) through influencing the force of mixing and the elastic force of the chains respectively. [163]

The molecular weight between crosslinks ($\overline{M_c}$) can be found from equation 2.2 which is derived via incorporation of thermodynamic of mixing and theory of rubber elasticity into equation 2.1. [163]

$$\frac{1}{\overline{M_c}} = \frac{2}{\overline{M_n}} - \frac{\left(\frac{\bar{\nu}}{V_1}\right)\left[\ln(1-\nu_{2,s}) + \nu_{2,s} + \chi_1 \nu_{2,s}^2\right]}{\nu_{2,s}^{1/3} - \frac{\nu_{2,s}}{2}} \qquad \text{equation 2.2}$$

where $\overline{M_n}$ is the number average molecular weight of the chains, $\bar{\nu}$ is the specific volume of the polymer, V_1 is the molar volume of solvent, $\nu_{2,s}$ is the polymer volume fraction in the swollen state and χ_1 is the Flory-Huggins interaction parameter between the polymer and solvent. The mesh size of a gel, the average distance between two adjacent crosslinks (see Figure 2.4), can be obtained following determination of $\overline{M_c}$ from equation 2.2 by using:[163]

$$\zeta = \nu_{2,s}^{-1/3}\left(\frac{2C_n\overline{M_c}}{M_r}\right)^{1/2} l \qquad \text{equation 2.3}$$

where C_n, M_r and l are the Flory characteristic ratio, molecular weight of the repeating unit and length of the bond along the polymer backbone respectively. The degree of swelling and mesh size of the hydrogels are particularly important variables for controlling the diffusion rate of nutrients, oxygen, growth factors and waste products into or out of the cell-laden hydrogels in tissue engineering applications. [165, 166]

2.9. MECHANICAL PROPERTIES OF HYDROGELS

Mechanical properties of tissue engineering hydrogels need to be optimal to prevent deformation or rupture of the construct and at the same time keep the cells viable while tailoring them to a specific lineage.[167] It is well established that the stiffness of 3D matrix affects fate of the encapsulated cells. For instance, MSCs encapsulated in alginate hydrogels underwent adipogenic differentiation when the elastic modulus of the matrix was 2.5-5 kPa whereas they went through osteogenic differentiation in the gels with elastic modulus of 11-30 kPa.[75]

When a constant stress is applied on a hydrogel, an instantaneous strain is followed by an increasing strain over time.[168] Since hydrogels exhibit both viscous and elastic behaviors they are classified as viscoelastic materials. The time dependant (or frequency dependant in dynamic tests) response of hydrogels to an external force is related to the time needed for macromolecular motions. At short time scales, polymeric chains cannot be relaxed under an external force whereas at longer times polymeric chains have time to become relaxed.[168] The elastic behavior of hydrogels can be elucidated using the rubber elasticity theory which was developed by Treloar and

Flory[80] and modified by Peppas and Merrill[163]. The elastic behavior of a water swollen crosslinked gel is given by:

$$\tau = \frac{\rho RT}{\overline{M_c}}\left(1-\frac{2\overline{M_c}}{\overline{M_n}}\right)\left(\alpha-\frac{1}{\alpha^2}\right)\left(\frac{\nu_{2,s}}{\nu_{2,r}}\right)^{\frac{1}{3}} \qquad \text{equation 2.4}$$

Where τ is the stress, ρ, R, T, α and $\nu_{2,r}$ are the polymer density, gas universal constant, absolute temperature, elongation ratio and the polymer volume fraction before swelling respectively. Based on the constitutive relationships, the shear modulus (G) is:[168]

$$\mathrm{G} = \frac{\rho \mathrm{RT}}{\overline{\mathrm{M_c}}}\left(1-\frac{2\overline{\mathrm{M_c}}}{\overline{\mathrm{M_n}}}\right)\left(\frac{\nu_{2,s}}{\nu_{2,r}}\right)^{\frac{1}{3}} \qquad \text{equation 2.5}$$

According to equation 2.5 the modulus of hydrogels is inversely correlated with molecular weight between crosslinks ($\overline{M_c}$). Therefore, the shear modulus of the hydrogels increases with increasing the density of crosslinks (decreasing $\overline{M_c}$). The crosslink density can be enhanced with increasing the macromonomer concentration, macromonomer functionality or incorporation of multi-functional crosslinkers in the solution.[52] It is worth mentioning that intra-molecular reactions lead to the formation of loops that do not contribute to the network elasticity [150, 162]. Therefore, an increase in the probability of intra-molecular crosslinking through a decrease in macromonomer molecular weight or macromonomer concentration negatively affects the mechanical properties of hydrogel networks.[35]

2.10. DEGRADATION OF HYDROGELS

Although hydrogels provide flexibility in controlling the cell microenvironment, their use for *in vivo* applications in tissue engineering is limited by their persistence in the site of regeneration.[30] Therefore, hydrogels for tissue engineering applications need to be degradable with a degradation rate matched with tissue formation (ECM production) and remodeling. ECM production is limited by free volume when rate of matrix degradation is slower than that of ECM production. Conversely, ECM production is limited by cell adhesion when rate of matrix degradation is faster than that of ECM production. [102, 169] The essential role of matrix degradation in determining the cell fate has been shown for different cell lines. For example , the C2C12 mouse myoblast cells encapsulated in a degradable alginate gel had a higher extent of differentiation into myotubes and lower proliferation than those encapsulated in a non-degradable gel [170]. Similarly, MSCs encapsulated in a non-degradable hyaluronic acid (HA) gel did not spread and underwent adipogenic differentiation whereas those MSCs encapsulated in a degradable HA gel spread and differentiated to the osteogenic lineage [171].

Natural hydrogels are mostly enzymatically degradable. For instance, myofibroblast cell-laden fibrin gels were degraded after 2 days in the absence of inhibitor for enzymatical degradation. [172] Hyaluronic acid based hydrogels are degradable by hyaluronidase enzyme.[173] Gelatin based hydrogels were completely degraded over 6 hours in collagenase solution. [100] Alginate gels were degraded by alginase enzyme released from PLGA microspheres and the gel degradation rate increased with increasing the alginase loading concentration.[174]

Synthetic hydrogels can be made degradable with incorporation of enzymatic, hydrolytic or photolytic degradable segments into the macromonomer chains or crosslinkers. [175] For instance, Matrix Metalloproteinase (MMP) sensitive peptide was incorporated into the non-degradable PEG hydrogel using Michael addition reaction to make the gel enzymatically degradable. [176, 177] Fibroblast cells were shown to migrate within the MMP-sensitive PEG gels whereas the migration was limited within the non-degradable PEG gels or when the enzymatic degradation was inhibited. [176] Degradable PEG based gels were synthesizd with incorporation of poly(α-esters). For example, Copolymerization of PEG with poly(lactide) (PLA) has been used to impart degradability to PEG macromers. The degradation and water content of the copolymers could be adjusted by the fraction of hydrophobic lactide segments,[88, 178] but solubility of the copolymers in aqueous solution decreased with increasing lactide content.[56] Hydrogels synthesized from PEG and ε-caprolactone co-polymers were shown to be hydrolytically degradable, but the degradation rate was limited by the hydrophobicity of ε-caprolactone and formation of micellar aggregates in the solution.[179] Hydrogels based on PEG macromers co-polymerized with 5-15% (wt) glycolide underwent complete degradation over 2 to 8 days.[51] Due to a relatively fast degradation rate and hydrophilicity of the glycolide monomer, that has been extensively used with lactide or caprolactone for adjusting the degradation rate and water content of hydrogels.[52, 180, 181] In addition to poly(α-esters) , other hydrolytically degradable polymers including poly(ester amide)[182], polyphosphoester [183, 184], poly(amino-ester urethane) [185] were used to synthesize degradable hydrogels. Furthermore, photodegradable hydrogels

were synthesized with incorporation of a nitrobenzyl-ether-derived moiety into the PEG based hydrogels.[186]

Tissue engineered constructs often times require multiphase hydrogels with different but complementary microenvironments. For example, osteogenic differentiation of MSCs requires a supporting matrix with high compressive modulus and slow degradation [187] whereas vasculogenic differentiation of progenitor endothelial cells necessitates a low modulus, relatively fast-degrading matrix [100, 188]. This presents a need to develop synthetic hydrogels with tunable degradation and stiffness for wide-ranging applications in regenerative medicine.

2.11. BIOACTIVE MODIFICATION OF HYDROGELS

It is well established that cell-matrix interactions within a cell-laden hydrogel play a significant role in regulating cell function.[189, 190] In natural ECM, cell adhesive proteins such as laminin and fibronectin bind to the integrin cell surface receptors.[189, 191] It has been shown that cell-matrix attachment is crucial for cell proliferation and differentiation.[192] Furthermore, soluble or tethered growth factor proteins, present in the natural ECM, modulate cell functions including proliferation, migration and differentiation.[193]

Natural gels such as collagen, gelatin and fibrin possess cell-adhesive ligands. Despite this, it is difficult to adjust the properties of natural gels for a specific application in tissue engineering. [31] Further, the use of natural gels in regenerative medicine is limited due to their poor mechanical properties. [194] The properties of synthetic hydrogels including the matrix stiffness can be tuned for a specific application in regenerative medicine. However, synthetic hydrogels need to be modified with bioactive

ligands for optimal cell-matrix interactions. [195] A number of cell-adhesive peptides derived from laminin, fibronectin, elastin and collagen proteins have been incorporated into the synthetic inert hydrogels.[195] For example, when Arg-Gly-Asp (RGD), a laminin and fibronectin derived adhesive peptide, was added to PEG hydrogels the adhesion and mieralization of encapsulated osteoblest cells significantly increased. [17] The viability of human mesenchymal stem cells (hMSCs) was significantly higher in RGD modified PEG gels compared with non-modified PEG gels. [196] The viability and insulin secretion of β-cells significantly increased when acrylate terminated IKLLI and IKVAV cell-adhesive peptides were conjugated to the cell-laden PEG hydrogel. [197]

In addition to the cell-adhesive ligands, growth factors or growth factor derived peptides have been incorporated into the synthetic hydrogels to direct the stem cells into a specific liniage. A conjugation of SVVYGLR osteopontin derived peptide to the PEG based hydrogel, stimulated the formation of new blood vessels by encapsulated human umbilical vein endothelial cells (HUVECs). [198] Similarly, the vasculogenic differentiation of MSCs seeded on a PEG hydrogel increased when the osteopontin derived peptide was grafted to the hydrogel. [199] The collagen and glycosaminoglycan production by hMSCs increased significantly when KLER, a chondro-inductive decorin derived peptide, was incorporated into the PEG cell-laden hydrogels.[200] MSCs seeded on PEG hydrogels modified with RGD and an osteo-inductive BMP-2 protein derived peptide, KIPKASSVPTELSAISTLYL, showed 5 and 12 fold increase in ALP activity and calcium content after 14 and 21 days respectively. [113] The aformentioned BMP-2 derived peptide tethered to alginate gels induced new bone formation after 4 weeks in a rat tibial bone defect. [201, 202]

CHAPTER 3

SYNTHESIS AND GELATION CHARACTERISTICS OF PHOTO-CROSSLINKABLE STAR POLY(ETHYLENE OXIDE-CO-LACTIDE-GLYCOLIDE ACRYLATE) MACROMONOMERS

Seyedsina Moeinzadeh, Saied Nouri Khorasani, Junyu Ma, Xuezhong He, Esmaiel Jabbari, *Synthesis and gelation characteristics of photo-crosslinkable star Poly (ethylene oxide-co-lactide-glycolide acrylate) macromonomers*. Polymer, 2011. **52**(18): 3887-3896.

Reprinted here with permission of publisher.

3.1. INTRODUCTION

A novel approach to tissue regeneration is the use of injectable *in situ* crosslinkable hydrogels as a carrier for the delivery of therapeutic agents and cells [28, 203]. Less invasive injectable gels coupled with minimally invasive arthroscopic techniques are an attractive alternative to implantation of pre-formed polymers for treating irregularly shaped or inaccessible defects [27, 87, 204, 205]. Furthermore, diffusivity of nutrients [206, 207] and proteins [166, 208] in hydrogels is 4-5 orders of magnitude higher than solid polymers, thus providing a supportive matrix for differentiation, proliferation, and maturation of seeded cells into the desired tissue [209]. In addition, hydrogels can be reinforced with calcium phosphate nanoparticles to produce injectable cements for hard tissue applications [28, 210, 211].

Biodegradable polymers are widely used as a supportive carrier in tissue engineering and drug delivery [49, 212-215]. Among them, poly(lactide-co-glycolide) (PLGA) is the most widely used biodegradable polymer because its degradation products (lactic and glycolic acid) are resorbed through metabolic pathways [216, 217]. PLGA and poly(ε-caprolactone) (PCL) polymers have been copolymerized with poly(ethylene oxide) (PEO) to produce amphiphilic macromers that form thermally-induced physical gels [136, 218, 219]. Studies concerning the effect of macromer structure on water content and modulus [218, 220] demonstrate that physically crosslinked gels are significantly weaker than those that are chemically crosslinked [88, 133], limiting them for use in non load-bearing biomedical applications. In addition, degradability of chemically-crosslinked gels can be controlled independent of gelation by the molecular weight and ratio of hydrophobic/hydrophilic domains [134-136]. To control the hydrogel

water content (and therefore mechanical strength), degradation rate and the rate of crosslinking, our laboratory has previously developed a poly(lactide-co-ethylene oxide fumarate) (PLEOF) macromonomer consisting of low molecular weight poly(L-lactide) (LMW-PLA) and PEG blocks linked by unsaturated fumarate units [88, 205]. The water content of the PLEOF hydrogel could be adjusted by the ratio of hydrophilic PEG to hydrophobic PLA blocks and by PEG molecular weight [88]. Degradation rate of the network could be controlled by the ratio of PLA to PEG blocks or by the molecular weight of PLA segments [88]. However, due to steric hindrance of the fumarate groups along the chain and their lower reactivity (compared to acrylates and methacrylates) [88, 221, 222], the gelation kinetics depended strongly on UV initiator and small molecule monomer concentrations [88]. It is well established that the viability of cells encapsulated in synthetic gels is largely determined by the fraction of small-molecule initiators and monomers that cross the cell membrane [42, 223].

Terminal reactive groups at chain ends are less sterically hindered compared to those along the macromonomer chain. The reactivity of acrylates is an order of magnitude higher than fumarates [88, 141, 205]. In addition, star macromonomers have lower shear viscosity than linear ones at the same molecular weight [224], resulting in the onset of gelation at higher conversions and a higher extent of crosslinking. We hypothesized that a multi-arm star amphiphilic poly(ethylene oxide-co-lactide-glycolide) based macromonomer each arm terminated with an acrylate group would significantly increase the rate of crosslinking, thus reducing the minimum required concentration of initiator/monomer to produce robust networks. The objective of this work was to synthesize a novel star poly(ethylene oxide-co-lactide-glycolide acrylate) (SPELGA)

macromonomer and investigate the effect composition had on gelation kinetics and degradation of the hydrogels. In this work, SPELGA macromonomer was synthesized by ring-opening polymerization of lactide and glycolide monomers using hydrophilic pentaerythritol ethoxylate or poly(ethylene glycol) initiators, followed by acrylation of the chain ends with acryloyl chloride. The structure of the synthesized macromonomers was characterized by ^{1}H-NMR and GPC. The kinetics of photopolymerization of the SPELGA macromonomers in aqueous solution was investigated by rheometry. The SPELGA hydrogels were characterized with respect to sol fraction, swelling and degradation.

3.2. EXPERIMENTAL

3.2.1. MATERIALS

Lactide (LA; >99.5% purity by GPC) and glycolide (GL; >90% purity) monomers were purchased from Ortec (Easley, SC) and Boehringer Chemicals (Ingelheim, Germany), respectively. The ring opening polymerization initiators 4-arm pentaerythritol ethoxylate (PEE800; 15/4 EO/OH; M_n=797 Da; purity >98%) and 4-arm poly(ethylene glycol) (4PEG5K; nominal molecular weight of 5 kDa; purity >98%) were purchased from Sigma-Aldrich (St. Louis, MO), respectively. The initiators were dried by azeotropic distillation from toluene prior to the reaction. Triethylamine (TEA), tin (II) 2-ethylhexanoate (TOC), N-vinyl-2-pyrrolidone (NVP), and acryloyl chloride were purchased from Sigma-Aldrich. Methylene chloride (MC; VWR) was dried by distillation over calcium hydride (Sigma-Aldrich). All other solvents were reagent grade and used as received.

3.2.2. SYNTHESIS OF SPELGA MACROMONOMER

Star poly(ethylene oxide-co-lactide-glycolide) (SPELG) macromer was synthesized by ring-opening polymerization of LA and GA monomers with star 4PEE800 or 4PEG5K initiators, following a procedure similar to the synthesis of low molecular weight poly(L-lactide) [205, 225, 226]. The schematic diagram for the synthesis of SPELG with 4PEE800 is shown in Figure 3.1. TOC was used as the polymerization catalyst and LA/GL ratio was 100/0 for SPELGA-5K and 100/0, 75/25, 50/50 for SPELGA-800. In a typical procedure for the synthesis of 100/0 SPELGA, 30g LA (0.2084 mol) and 0.0116 mol initiator (7 ml 4PEE800 or 58 g 4PEG5K) were added to a three-neck reaction flask equipped with an overhead stirrer. The reaction flask was submerged in an oil bath and gradually heated to 110-120ºC to melt the monomers while under steady flow of nitrogen. After melting, 3 ml TOC as the polymerization catalyst was added to the reaction mixture with stirring. The reaction was allowed to proceed for 6 h at 135ºC. Upon completion, the product was dissolved in DCM and precipitated in ice cold methanol, ether, and hexane to fractionate the PLA product and remove the unreacted monomer and initiator [225]. The solvent was decanted and the star SPELG product was vacuum dried (<5 mmHg) to remove any residual solvent and stored at -20ºC. With TEA as the reaction catalyst, the chain ends of the star SPELG were acrylated by the reaction of acryloyl chloride with the hydroxyl end-groups of the SPELG (see Figure 3.1). Prior to this reaction the SPELG macromer was dried by azeotropic distillation from toluene to remove residual moisture. The polymer was cooled under steady flow of nitrogen and dissolved in dried DCM. The reaction flask was immersed in an ice bath to limit a temperature rise from the exothermic reaction. In a typical reaction

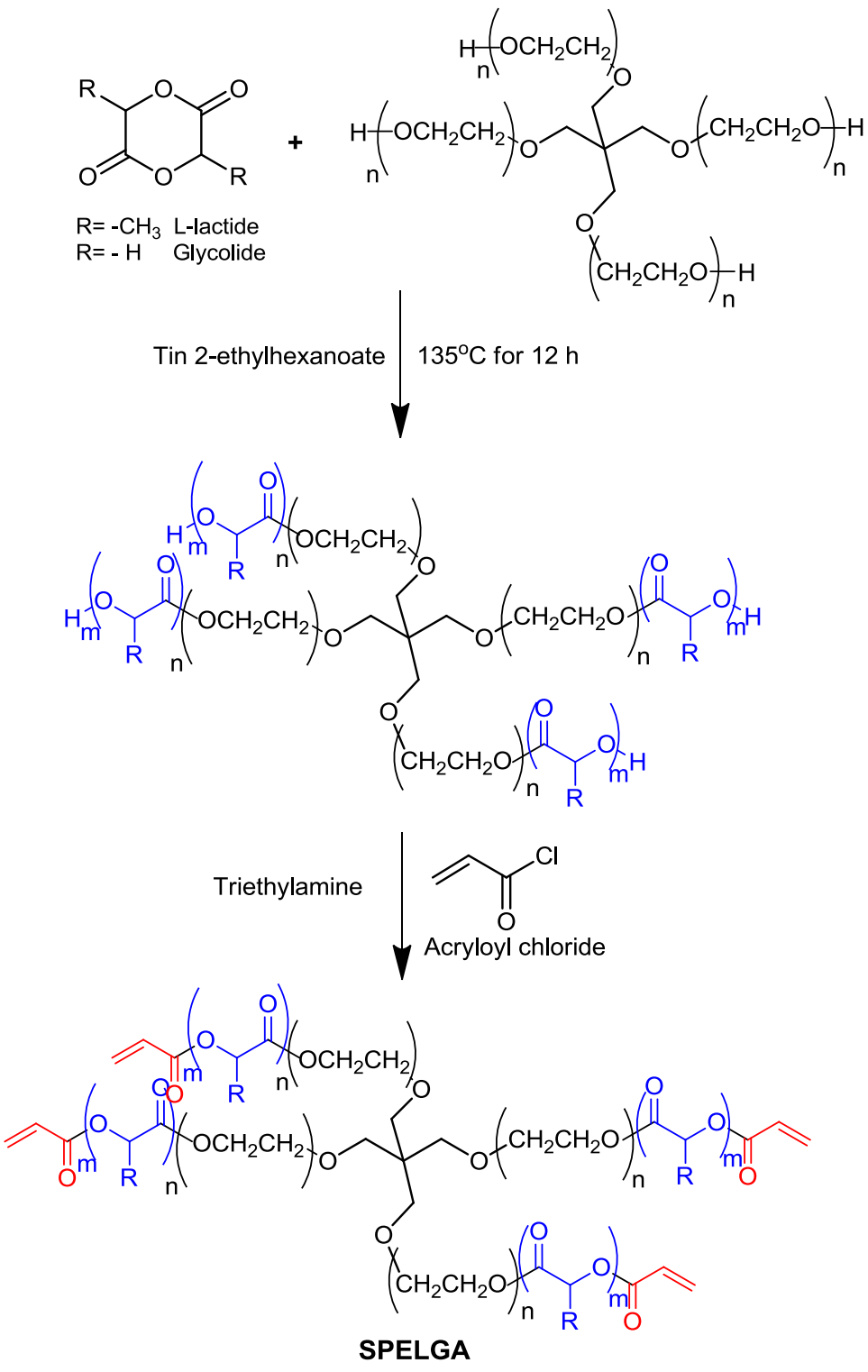

Figure 3.1. Reaction scheme for the synthesis of SPELGA macromonomer. The 4-arm PEG, lactide-co-glycolide segments, and terminal acrylate groups are shown by black, red, and blue colors, respectively.

5.6 ml acryloyl chloride and 9.7 ml TEA, each dissolved in DCM, were added drop-wise to the reaction with stirring. The reaction was allowed to proceed for 12 h under nitrogen flow. After completion of the reaction the solvent was removed by rotary evaporation and the residue was dissolved in anhydrous ethyl acetate to precipitate the by-product triethylamine hydrochloride salt. Next, ethyl acetate was removed by vacuum distillation; the macromonomer was re-dissolved in DCM and precipitated twice in ice cold ethyl ether. The macromonomer was dissolved in dimethylsulfoxide (DMSO) and further purified by dialysis to remove any unreacted acrylic acid. The SPELGA product was dried in vacuum (<5 mmHg) to remove residual solvent and stored at –20°C.

3.2.3. MACROMONOMER CHARACTERIZATION

The chemical structure of the SPELGA macromonomer was characterized by a Varian Mercury-300 ^{1}H-NMR (Varian, Palo Alto, CA) at ambient conditions with a resolution of 0.17 Hz as described [205]. The sample was dissolved in deuterated chloroform (Sigma-Aldrich, 99.8% deuterated) at a concentration of 50 mg/ml, and 1% v/v trimethylsilane (TMS; Sigma-Aldrich) was used as the internal standard. The molecular weight distribution of the macromonomer was measured by GPC [205]. Measurements were carried out with a Waters 717 Plus Autosampler GPC system (Waters, Milford, MA) connected to a model 616 HPLC pump, model 600S controller, and a model 410 refractive index detector. The columns consisted of a styragel HT guard column (7.8 x 300 mm, Waters) in series with a styragel HR 4E column (7.8 x 300 mm, Waters) heated to 37°C in a column heater. The Empower software was used for determination of number ($\overline{M_n}$) and weight ($\overline{M_w}$) average molecular weights and polydispersity index (PI). The sample (20 μl) with a concentration of 10 mg/ml in

tetrahydrofuran (THF) was eluted with degassed THF at a flow rate of 1 ml/min. Monodisperse polystyrene standards (Waters) with peak molecular weights (M_p) of 0.58-19.9, 66.35, and 143.4 kDa and polydispersities of <1.1 were used to construct the calibration curve.

3.2.4. SPELGA GELATION

The SPELGA macromonomer was crosslinked in aqueous solution by free-radical UV polymerization with 4-(2-hydroxyethoxy) phenyl-(2-hydroxy-2-propyl) ketone (Irgacure 2959; CIBA, Tarrytown, NY) photo-initiator [88, 141, 211]. The photo-initiator was dissolved in distilled deionized (DI) water at 50ºC. The SPELGA macromonomer was dissolved in DI water by vortexing and heating to 50ºC to aid dissolution. The initiator solution was added to the SPELGA solution, this mixture was then vortexed and loaded on the Peltier plate of the rheometer. To make 10, 15, and 20% SPELGA precursor solution, 30, 45, and 60 mg of the macromonomer solution was added to 270, 255 and 240 ml of the initiator solution, respectively. In samples with NVP added as a crosslinking agent, the initiator was first dissolved in the desired amount of NVP before addition to the macromonomer solution. The sample was irradiated with a BLAK-RAY 100-W mercury long wavelength (365 nm) UV lamp (Model B100-AP; UVP, Upland, CA) [88]. The notation "SPELGAa-Lb-Mc-Nd-Ie" is used to identify the composition of the samples, where a, b, c, d and e represent initiator molecular weight, lactide fraction and macromonomer molecular weight, NVP and initiator concentrations (wt%), respectively. The results are for SPELGA, NVP and initiator concentrations of 25 wt%, 0 mol%, and 0.16 mol%, respectively, unless otherwise specified.

3.2.5. RHEOLOGICAL MEASUREMENTS

Rheological measurements were carried out at 37°C on an AR-2000 rheometer (TA Instruments, New Castle, DE) equipped with a parallel plate geometry (acrylic plate transparent to UV light; 20 mm diameter; TA Instruments) [88]. A sinusoidal shear strain profile was exerted on the sample via the upper geometry at a constant frequency of 1 Hz. The deformation amplitude was kept at 1% to remain within the linear viscoelastic region. The polymerizing mixture was injected on the Peltier plate and the upper geometry was lowered to a gap of 500 μm. The sample was irradiated with a long wavelength UV lamp (Model B100-AP; UVP, Upland, CA) as described above. The elapsed time between mixing/injection and the start of data collection was ≤1 min for all experiments. The storage modulus (G') during the gelation process was monitored by the rheometer. The intensity of the transmitted UV light was measured by a BLAK-RAY long wave ultraviolet radiation meter (Model J-221; UVP). The transparency of the acrylic geometry to long wave (365nm) UV light was confirmed by comparing the intensity of the transmitted light through the geometry to the incident light (transmitted intensity was >95%). The measured UV intensities at distances of 10, 30, 35, and 40 cm from the lamp were 46,000, 5,300, 4,000, and 3,000 $\mu W/cm^2$, respectively. We have previously shown that a UV intensity of 46,000 $\mu W/cm^2$ applied 10 cm from the sample and exposure time of 1800 s results in the highest extent of crosslinking [88]. Therefore, all gelation results are with UV intensity, distance, and exposure time of 46,000 $\mu W/cm^2$, 10 cm, and 1800 s, respectively. In the text,"modulus" is defined as the storage shear modulus of the sample after 1800 s of UV radiation.

3.2.6. MEASUREMENT OF SWELLING RATIO AND SOL FRACTION

After crosslinking, samples with dimensions 20 mm diameter × 300 μm thickness were removed from the Peltier plate to measure their swelling ratio and sol fraction. Samples were dried at ambient conditions for 12 h followed by drying in vacuum for 1 h at 40°C and the total dry weights (W_i) were recorded. Next, dry samples were swollen in DI water for 24 h at 37°C and swelling medium changed every 6 h. After swelling the surface water was removed and the swollen weight (W_s) was recorded. Then, the swollen samples were dried as described above and the dry weight (W_d) were recorded. The weight swelling ratio (Q) and sol fraction (S) were calculated by the following equations:

$$Q = \frac{W_s - W_d}{W_d} \times 100 \qquad \text{equation 3.1}$$

$$S = \frac{W_i - W_d}{W_i} \times 100 \qquad \text{equation 3.2}$$

3.2.7. MEASUREMENT OF DEGRADATION

The SPELGA precursor solution was degassed, transferred into a PTFE mold (3cm × 5cm × 750μm), covered with a transparent glass plate fastened with clips, and UV crosslinked as described above. After crosslinking the sample was removed from the mold and disks were cut from the gel using an 8 mm cork borer. Degradation was measured as a function of time in primary culture media (5 ml per sample) without fetal bovine serum (FBS) at 37°C under mild agitation. To prepare the primary media 13.4 g of Dulbecco's Modified Eagle Medium (DMEM; 4.5 g/l glucose with L-glutamine and without sodium pyruvate; Mediatech, Herndon, VA) was dissolved in 900 ml of DI water containing 3.7 g sodium bicarbonate and 10 ml antibiotic and antimycotic agent (1% v/v).

At each time point samples were removed from the media, rinsed with DI water to remove excess electrolytes, and dried under vacuum. The dry sample weight was recorded and compared with the initial dry weight to determine fractional mass remaining with respect to time.

3.3. RESULTS

The ^{1}H-NMR spectrum of SPELGA800-L50 is shown in Figure 3.2. The chemical shifts with peak positions at 1.6 and 5.2 ppm were attributed to the methyl (-CH_3) and methine ($\equiv CH$) hydrogens of the lactide units in SPELGA, respectively [227]. The shift centered at 4.8 ppm was attributed to the methylene hydrogens (=CH_2) of the glycolide units in SPELGA. The shifts centered at 3.6 and 4.3 ppm were attributed to the methylene hydrogens (=CH_2) of the 4-arm initiator (4PEE800 or 4PEG5K) attached to the ether (-CH_2-O-CH_2-) and ester (-CH_2-OOC-) groups of lactide/glycolide units, respectively [227]. The chemical shifts with peak positions from 5.85-6.55 ppm were attributed to the vinyl hydrogens of the acrylate groups (-CH=CH2) at chain ends; the latter shifts were absent in the spectra of unacrylated SPELG (see the inset of Figure 3.2). The relative intensities of the NMR shifts of SPELGA macromonomers are presented in Table 3.1. The ratio of the shifts centered at 1.6 and 5.2 ppm (lactide hydrogens) to that at 4.8 ppm (glycolide hydrogens) was related to the molar ratio of LA/GL. The ratio of the shifts centered at 1.6, 5.2, and 4.8 (lactide+glycolide hydrogens) to those at 3.6 and 4.3 ppm (4-arm initiator hydrogens) was related to $\overline{M_n}$ of SPELGA. The ratio of the shifts centered at 5.85-6.55 ppm (acrylate hydrogens) to those at 3.6 and 4.2 ppm (initiator hydrogens) was related to the average number of acrylate groups per macromonomer. The LA/GL molar ratio, $\overline{M_n}$, and the number of acrylate groups per SPELGA800

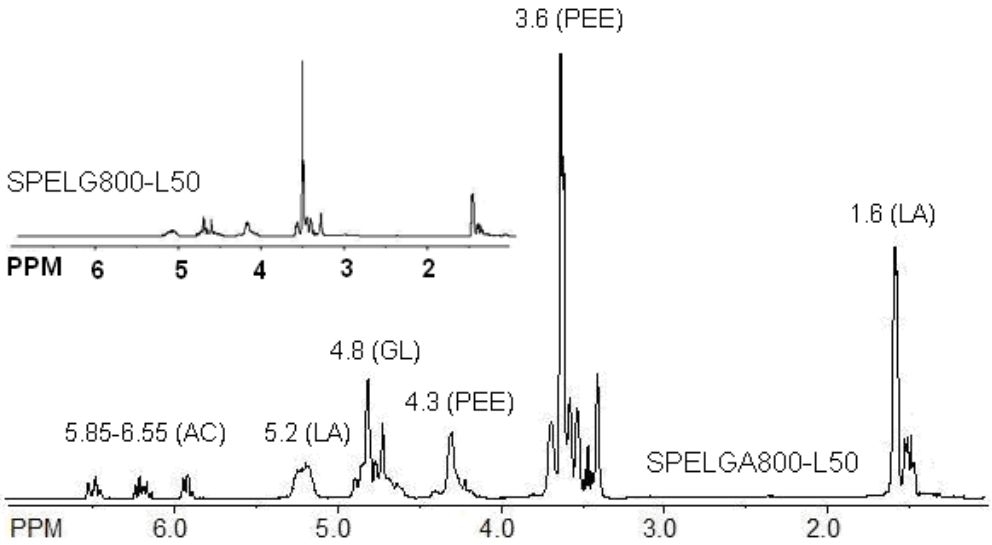

Figure 3.2. NMR spectra for SPELGA800-L50. The inset is the spectra of SPELG800-L50 before acrylation.

calculated from the NMR data are given in Table 3.1. For SPELGA800-L50 and SPELGA800-L75 with feed LA/GL ratios of 1.0 and 3.0, respectively, the actual ratios from the NMR data were 1.2 and 3.4. The actual LA/GL ratio was slightly higher than the feed indicating that the reactivity of lactide monomer with the growing chain was slightly higher than that of glycolide. The number of acrylate groups per macromonomer for SPELGA800-L50 and SPELGA800-L75 were 3.2 and 3.6, respectively.

$\overline{M_n}$, $\overline{M_w}$, and PI of the synthesized SPELGA macromonomers which were measured by GPC are presented in Table 3.2. $\overline{M_n}$, $\overline{M_w}$, and PI of SPELGA800 were independent of LA/GL ratio. SPELGA5K, due to higher PEG chain length, had the highest molecular weight and lowest PI. The $\overline{M_n}$ values measured by GPC were within 10% of the values calculated from the intensity of NMR shifts. All SPELGA macromonomers were dissolved in water, heated to 50ºC and crosslinked into a hydrogel.

Table 3.1. Relative intensity of the chemical shifts in the NMR spectra of SPELGA macromers.

NMR shift (ppm) / Macro-monomer (LA/GL feed)	5.85-6.55	5.16	4.77	4.28	3.64	1.56	LA/GL (NMR)	$\overline{M_n}$ (NMR)	# of acrylates/ Macro-monomer (NMR)
PLGA800-L50	---	1.0	2.42	1.52	6.03	1.82	1.2	1910	---
PLGAA800-L50	2.93	3.52	9.73	3.51	18.05	8.03	1.2	2260	3.2
PLGAA800-L75	2.96	5.64	5.41	3.41	15.81	12.61	3.4	2600	3.6

Table 3.2. $\overline{M_n}$, $\overline{M_w}$, and PI of the synthesized SPELGA macromers.

Macromonomer	$\overline{M_n}$	$\overline{M_w}$	PI
SPELGA800-L50	2490	4460	1.80
SPELGA800-L75	2650	4900	1.85
SPELGA800-L100	2640	4400	1.70
SPELGA5K-L100	6570	9460	1.40

The SPELGA800-L100 with low PEG molecular weight and 100% hydrophobic lactide fraction was not used in the subsequent gelation experiments due to its low solubility in aqueous solution. SPELGA5K-L100 had the highest solubility in water as measured by a turbidity test (data not shown).

To determine the effect of UV initiator on crosslinking, the gelation kinetics of SPELGA5K-L100-M25-N0 macromonomer were monitored by rheometry and the results are shown in Figure 3.3. As the initiator concentration was increased from zero to 0.11, 0.16, and 0.22 mol%, modulus increased from 1.3±0.3 to 10.0±2.1, 27.1±4.1, and 23.6±4.7, respectively. G' initially increased for up to 0.16 mol% initiator concentration and then decreased for >0.16 mol% concentration. Figures 3.4.a and 3.4.b show the effect of macromonomer concentration (based on the weight of polymerizing mixture) on the modulus and sol fraction of SPELGA5K-L100-N0-I0.16 gels, respectively. SPELGA5K, due to its higher solubility in water, was selected to study the effect of macromonomer concentration. There was a continuous increase in G' with increasing macromonomer concentration. G' increased from 0.16±0.03 to 0.47±0.12, 3.4±0.4, 5.9±1.0, 6.9±0.9, 13.4±2.4, and 27.1±4.1 kPa as the macromonomer concentrations increased from 10 to 12.5, 15, 17.5, 20, 22.5, and 25 wt%, respectively, with 170-fold overall increase in modulus. Sol fraction decreased from 17.8±1.1 to 15.6±1.5, 12.2±1.6, 13.8±3.0, 12.0±1.2, 9.4±0.9, and 7.6±0.9% as the macromonomer concentration increased from 10 to 12.5, 15, 17.5, 20, 22.5, and 25 wt%, respectively. The sol fraction of the PLEOF hydrogel with and without NVP monomer is also shown in Figure 3.4.b. SPELGA macromonomers with higher reactivity and lower steric hindrance of the acrylate groups had significantly lower sol fraction (S=8-18% in the absence of NVP) compared to PLEOF without (S=71%) or with (S=39%) NVP. It is well-established that the diffusivity/mobility of the growing chain affects gelation and the extent of crosslinking [88, 228]. Therefore, NVP was used to investigate the effect of a small molecule monomer on the plateau shear modulus of SPELGA hydrogels. Figures 3.5.a and 3.5.b

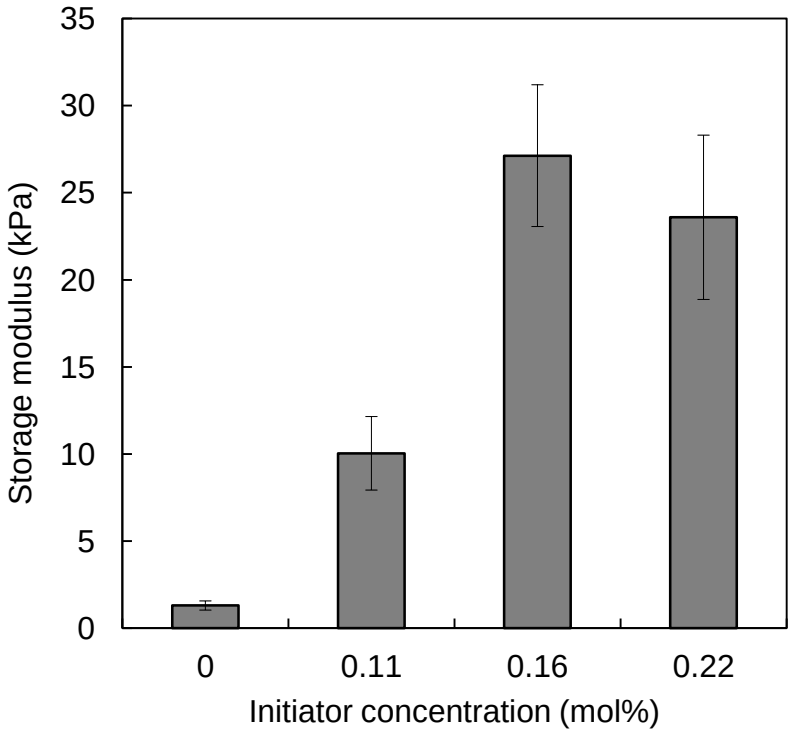

Figure 3.3 The effect of UV initiator concentration on shear storage modulus of SPELGA5K-L100-M25-N0 hydrogels. The intensity, distance from the sample, and exposure time of the UV radiation were 46,000 μW/cm^2, 10 cm, and 1800 s, respectively. Values are the mean of three samples with error bars representing one standard deviation from the mean.

show the effect of NVP concentration on the evolution and plateau modulus of SPELGA5K-L100-M25-I0.16 hydrogels, respectively. Addition of only 0.4 mol% NVP (0.004 moles NVP per mole of solution) to the polymerization mixture increased the modulus 2.2-fold from 27±4 (no NVP) to 60±10 kPa but the modulus did not change appreciably for concentrations >0.4 mol%. The gelation time of the samples was <60 s for all NVP fractions (50, 35, and 41 s for zero, 0.4, and 0.61% NVP, respectively). Based on Figure 3.5.a, addition of 0.4 mol% NVP affected modulus after the gelation point, but the curves were almost identical for higher NVP fractions. The effect of initiator molecular weight and LA/GL ratio of SPELGA-M15 on modulus is shown in Figure 3.6. SPELGA5K had a significantly lower modulus (3.3±0.4 kPa) compared to

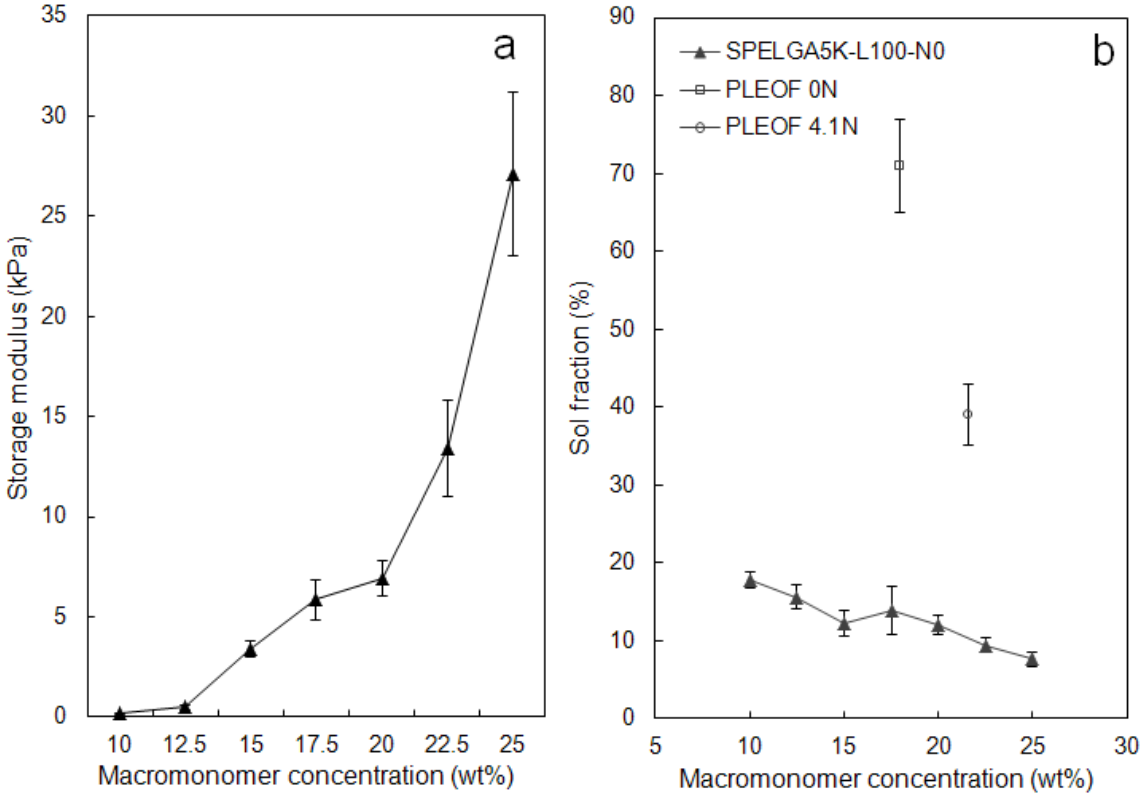

Figure 3.4. The effect of macromonomer concentration on the modulus (a) and sol fraction (b) of SPELGA5K-L100-N0-I0.16 hydrogel. The open square and open circle in (b) are the sol fractions of PLEOF hydrogels crosslinked without (17.5% macromonomer) and with (21% macromonomer) 4.1 mol% NVP crosslinker, respectively. The intensity, distance from the sample, and exposure time of the UV radiation were 46,000 μW/cm^2, 10 cm, and 1800 s, respectively. Values are the mean of three samples with error bars representing one standard deviation from the mean.

SPELGA800 (11.6±3.0 and 15.4±3.2 for SPELGA800-L75 and SPELGA800-L50, respectively). This can be attributed to the higher molecular weight of SPELGA5K compared to SPELGA800, resulting in lower density of reactive acrylate groups in the sample.

The effect of initiator molecular weight and LA/GL ratio on sample mass loss and swelling ratio is shown in Figures 3.7.a and 3.7.b, respectively. SPELGA800-L50 with the highest content of the less hydrophobic glycolide monomer had the highest mass loss over a period of 7 weeks, followed by SPELGA5K-L100 and SPELGA800-L75. For

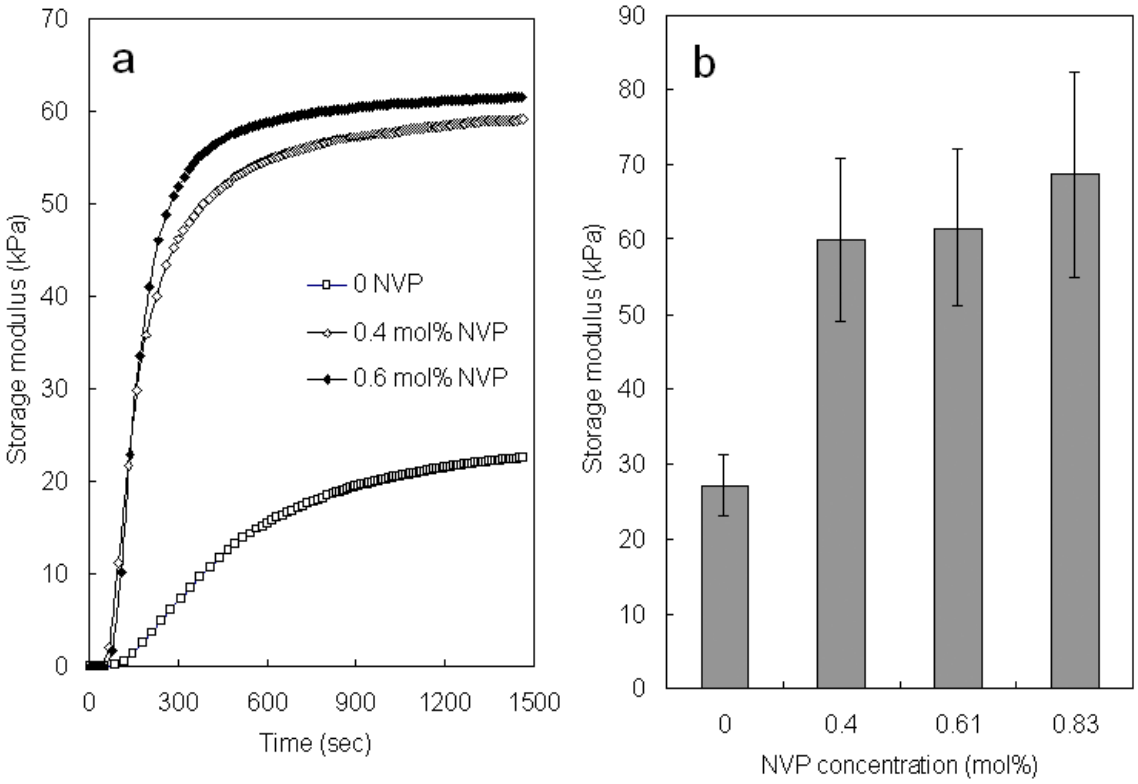

Figure 3.5. The effect of NVP monomer concentration on (a) evolution and (b) plateau shear storage modulus of SPELGA5K-L100-M25-I0.16 hydrogels. The intensity, distance from the sample, and exposure time of the UV radiation were 46,000 μW/cm^2, 10 cm, and 1800 s, respectively. Values are the mean of three samples with error bars representing one standard deviation from the mean.

example, after 4 weeks, SPELGA800-L50, SPELGA5K-L100, and SPELGA800-L75 lost 50.0±7.7, 33.0±1.9, and 23±0.4% mass, respectively. The swelling ratios support the mass loss results with SPELGA5K and SPELGA800-L75 showing the highest and lowest water contents, respectively. For example, after 4 weeks SPELGA5K-L100, SPELGA800-L50, and SPELGA800-L75 had swelling ratios of 645, 43, and 7%, respectively, corresponding to water fractions of 87, 30, and 6 wt%. Interestingly, SPELGA800 hydrogel showed delayed swelling characteristics, which could potentially be useful for the design of delayed drug release systems. For example, SPELGA800-L50

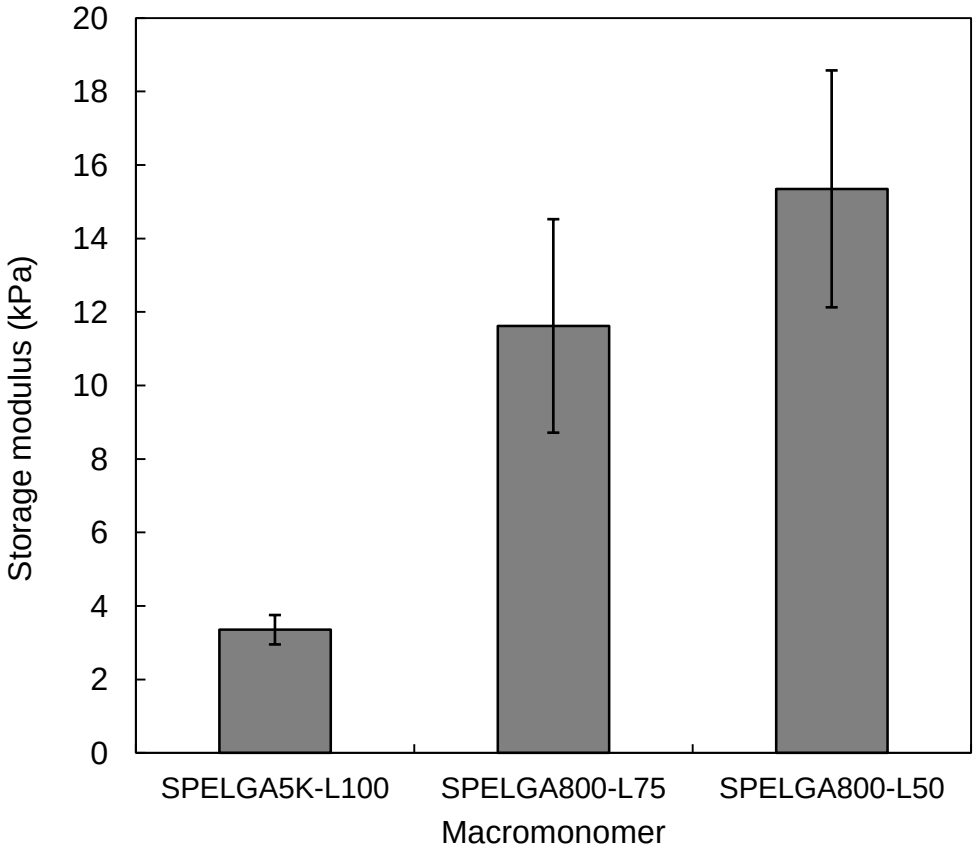

Figure 3.6. The effect of initiator molecular weight and LA/GL ratio of SPELGA macromonomer on shear storage modulus of SPELGA-M15-N0-I0.16 hydrogels. The intensity, distance from the sample, and exposure time of the UV radiation were 46,000 $\mu W/cm^2$, 10 cm, and 1800 s, respectively. Values are the mean of three samples with error bars representing one standard deviation from the mean.

and SPELGA800-L75 had only 5.7 and 3.8 wt% water content after 4 weeks of incubation; however, their water content increased to 83 and 11 wt% after 7 weeks.

3.4. DISCUSSION

SPELGA macromonomers crosslinked in the absence of NVP (see Figure 3.5) produced a relatively high modulus hydrogel (27±4 kPa). The results in Figures 3.3 and 3.5 demonstrate that initiator and NVP concentrations as low as 0.16 and 0.4 mol%, respectively, produced hydrogels with >10 kPa shear modulus. It should be noted that the

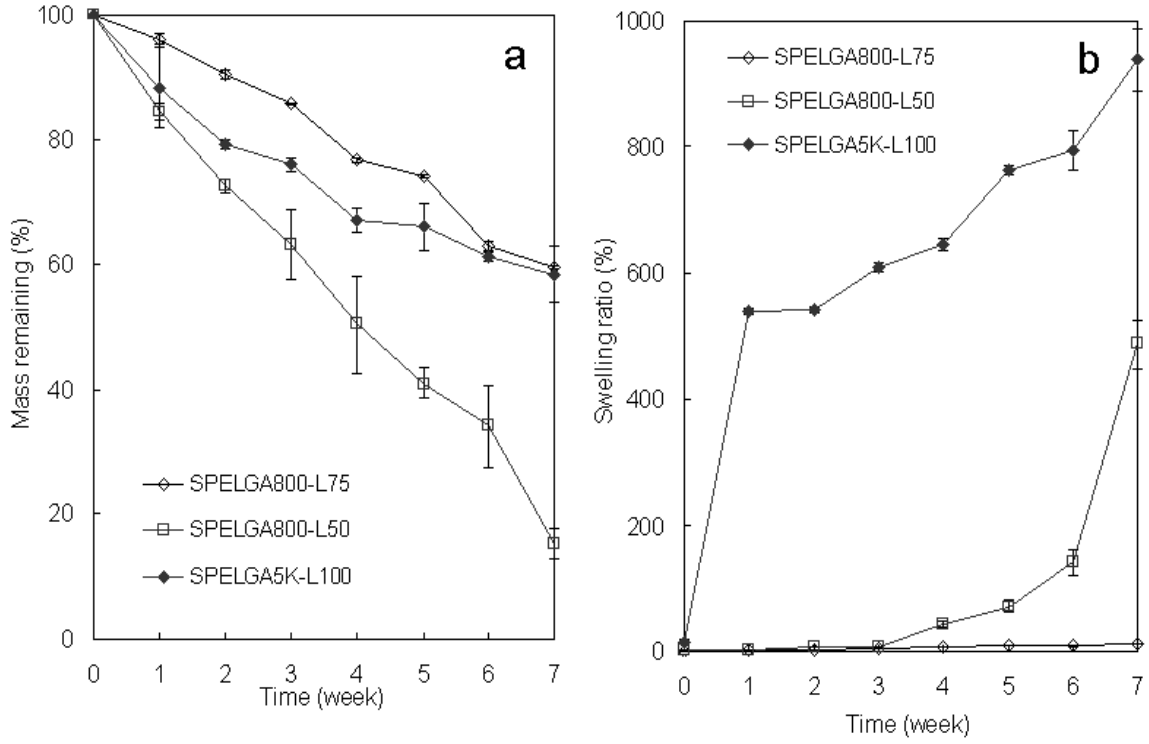

Figure 3.7. The effect of initiator molecular weight and LA/GL ratio of SPELGA macromonomer on (a) mass loss and (b) swelling ratio of SPELGA-N0-I0.16 hydrogels. The intensity, distance from the sample, and exposure time of the UV radiation were 46,000 μW/cm^2, 10 cm, and 1800 s, respectively. Values are the mean of three samples with error bars representing one standard deviation from the mean.

initiator and NVP concentrations used in this study were an order of magnitude lower than those used for gelation of the linear PLEOF macromonomer [88]. The higher reactivity of the acrylates in SPELGA compared to fumarates in linear PLEOF reduced the minimum required concentration of the initiator and NVP to produce robust networks. It is well established that the viability of cells encapsulated in hydrogels depends strongly on the concentration of small molecule initiator and monomer that can cross the cell membrane. Therefore, the lower initiator and NVP concentrations required for gelation has potential to improve biocompatibility of SPELGA hydrogels for cell encapsulation.

The modulus initially increased with initiator concentration for up to 0.16 mol% and then decreased at higher fractions. The dependence of propagation rate, R_P, on initiator concentration in the absence of NVP is given by [229]:

$$R_P = k_{P,AC}[AC]\left[\frac{R_{i,AC}}{k_t}\right]^{1/2} = k_{P,AC}[AC]\left[\frac{\phi \varepsilon I_0 \delta[I]}{k_t}\right]^{1/2} \qquad \text{equation 3.3}$$

where $k_{P,AC}$ and k_t are the rate constant for chain propagation and termination, $R_{i,AC}$ is the radical initiation rate, $[AC]$ is the concentration of unreacted SPELGA acrylates, ϕ is photo-initiation efficiency, ε is molar extinction coefficient, I_0 is incident radiation intensity, δ is gel thickness, and $[I]$ is the initiator concentration. Higher initiator concentrations below 0.16 mol% increased the rate of propagation, leading to a hydrogel with higher network density and higher modulus, as shown in Figure 3.3. At concentrations above 0.16 mol%, although the propagation rate continued to increase, there was a higher probability of localized formation of multiple radicals on growing chains, leading to cluster formation and increased cyclization within those clusters. This premise is supported by the decrease in gelation time from 460 s to 100, 50 and <30 s, as the initiator concentration was increased from zero to 0.11, 0.16, and 0.22 mole%, respectively. The increased cyclization and cluster formation reduced the modulus at initiator concentrations >0.16 mol%. Wang and collaborators observed a similar effect when UV intensity was increased above a threshold level in UV photocrosslinked polyacrylamide gels [230]. Similarly, a reduction in tensile modulus above a certain initiator concentration was reported for multi-functional methacrylamide, poly(ethylene glycol), and N-vinyl pyrrolidone hydrogels [231]. Results in Figure 3.3 indicate that the optimum initiator concentration in the absence of NVP was 0.16 mol%.

The addition of NVP monomer increased the hydrogel modulus, as shown in Figure 3.5. At any time there are monomers, linear and branched chains and a gel network in the polymerization reaction. The four propagation reactions involving the acrylate groups of NVP monomer and SPELGA macromonomer are given by:

$$\sim X^{*} \quad + \quad NVP \quad \overset{k_{P,Vs}}{\rightarrow} \quad \sim NVP^{*} \qquad \text{equation 3.4}$$

$$\sim X^{*} \quad + \quad AC \quad \overset{k_{P,As}}{\rightarrow} \quad \sim AC^{*} \qquad \text{equation 3.5}$$

$$> X^{*} \quad + \quad NVP \quad \overset{k_{P,Vg}}{\rightarrow} \quad > NVP^{*} \qquad \text{equation 3.6}$$

$$> X^{*} \quad + \quad AC \quad \overset{k_{P,Ag}}{\rightarrow} \quad > AC^{*} \qquad \text{equation 3.7}$$

where [NVP] and [AC] are concentrations of unsaturated vinyl groups of NVP and SPELGA, respectively, and symbols "~" and ">" denote a linear or branch chain in the sol (not part of the network) and the gel, respectively. For example, $\sim X^{*}$ is a growing chain in the sol with a radical attached to X terminal group, with X being NVP ($\sim NVP^{*}$) or SPELGA acrylate ($\sim AC^{*}$). Symbol $>X^{*}$ denotes a growing chain in the gel with a radical attached to X terminal group. There are also four propagation reactions involving unreacted acrylates of those SPELGA macromonomers that are part of a chain in the sol or the gel (~AC or >AC), which are given by:

$$\sim X^{*} \quad + \quad \sim AC \quad \overset{k_{P,br}}{\rightarrow} \quad \sim AC^{*} + br \qquad \text{equation 3.8}$$

$$\sim X^{*} \quad + \quad > AC \quad \overset{k_{P,dc1}}{\rightarrow} \quad > AC^{*} + d.c. \qquad \text{equation 3.9}$$

$$> X^{*} \quad + \quad \sim AC \quad \overset{k_{P,dc2}}{\rightarrow} \quad > AC^{*} + d.c. \qquad \text{equation 3.10}$$

$$> X^{*} \quad + \quad > AC \quad \overset{k_{P,nc}}{\rightarrow} \quad > AC^{*} + n.c. \qquad \text{equation 3.11}$$

Notation “br” stands for a branch in a chain (not part of the gel). Notations “d.c.” and “n.c.” denote a dangling (non-load bearing) and a network (load bearing) chain, respectively. In propagation reactions (3.4) and (3.5), a growing radical in the sol (~X^{*}) reacts with an NVP and SPELGA monomer, respectively, with rate constants $k_{P,Vs}$ and $k_{P,As}$. Reactions (3.4) and (3.5) produce linear or branched polymer chains that dilute the hydrogel network. In propagation reactions (3.6) and (3.7), a growing radical in the network (>X^{*}) reacts with an NVP monomer and SPELGA macromonomer, respectively, with rate constants $k_{P,Vg}$ and $k_{P,Ag}$, forming dangling radical chains in the network. In reaction (3.8), a growing radical in the sol reacts with a SPELGA acrylate that is part of a chain in the sol (~AC) with rate constant $K_{P,br}$, thus adding a branch to the chain. Reactions (3.9) and (3.10) form dangling chains attached to the gel by the reaction of a growing radical in the sol with a SPELGA acrylate in the gel (>AC^{*}; rate constant $k_{P,dc1}$) or by the reaction of a growing radical in the gel with a SPELGA acrylate on a chain in the sol (~AC, rate constant $k_{P,dc2}$). In reaction (3.11), a growing radical in the network (>X^{*}) reacts with a SPELGA acrylate in the network (>AC) with rate constant $k_{P,nc}$ forming a network chain, as shown in Figure 3.8. Since the ratio of NVP/SPELGA vinyl groups for 0.4, 0.61, and 0.83 mol% NVP is 1.3, 2.1, and 2.7, respectively, reactions (3.4) through (3.11) all contribute to the polymerization and gelation.

Reactions (3.4), (3.5), and (3.8) produce polymer chains in the sol which act as diluents and delay the onset of diffusion-controlled polymerization. The delay potentially

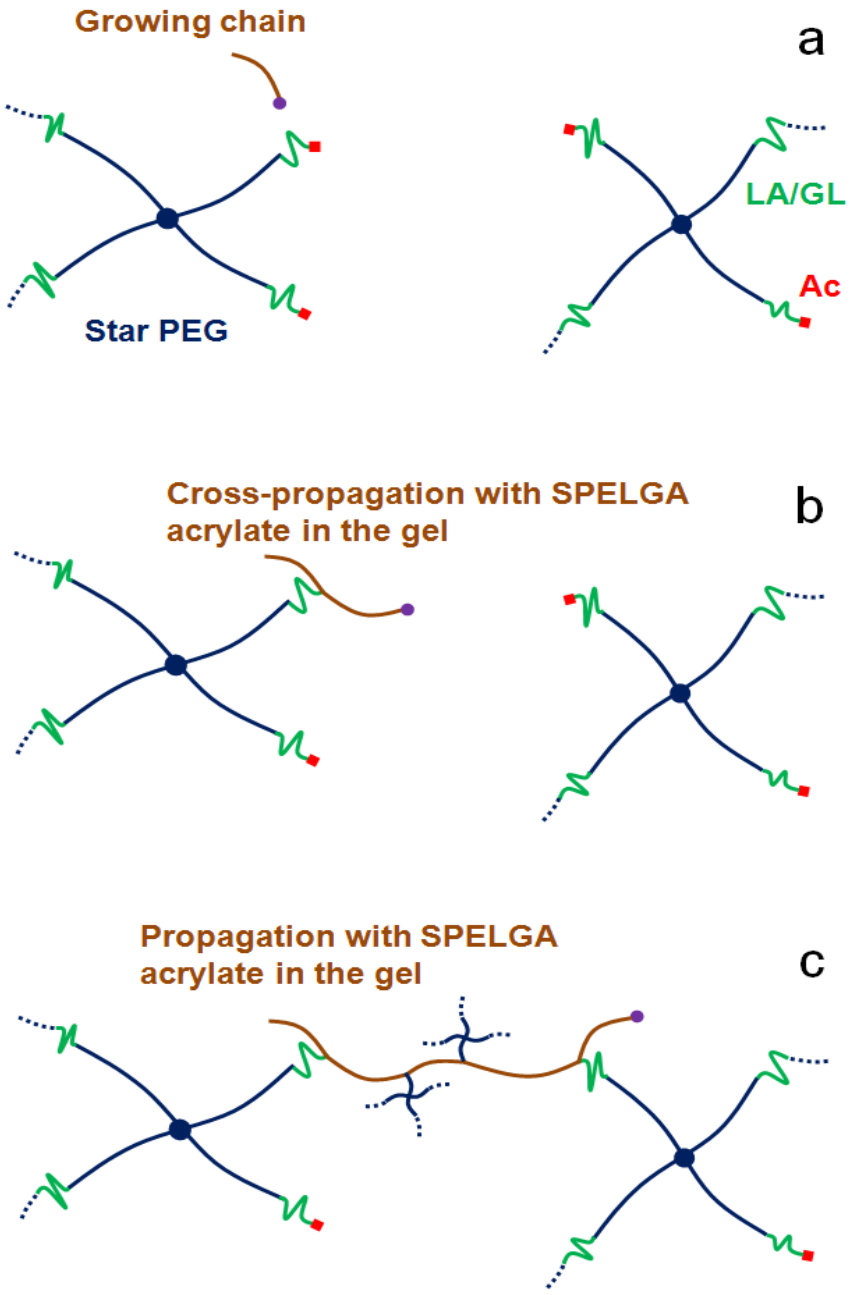

Figure 3.8. Schematic diagram to illustrate the cross-propagation reaction of the polymer chains in the sol with network-bound SPELGA acrylates to facilitate crosslinking: scheme a) SPELGA macromonomer with PEG (blue), LA/GL (green), and acrylate (red) groups; the growing polymer chain is shown with a purple dot at the chain end; scheme b) a growing chain in the sol (~X^*) cross-propagates by reaction with a network-bound SPELGA acrylate (>AC; reaction 3.9) followed by propagation with SPELGA and NVP monomers (reactions 3.6 and 3.7) to form a propagating chain bound to the gel; scheme c) the growing chain in the gel cross-propagates with a network-bound SPELGA acrylate to form a load-bearing network chain (reaction 3.11). Some SPELGA macromonomers (4-arm blue stars) are shown with a smaller size for clarity.

reduces the trapping of reactive acrylate groups in localized SPELGA clusters. This increases the overall conversion, resulting in a higher storage modulus as shown in Figure 3.5. Nowers and collaborators observed a similar effect when acrylated poly(ethylene glycol) (PEG) was added to epoxy polymerization [232]. Reactions (3.6) and (3.7) are propagation reactions between a growing radical on the network with NVP monomer and SPELGA macromonomer, respectively. In reactions (3.9) and (3.10), a growing radical on the network cross-propagates with a SPELGA acrylate on a chain in the sol, or a growing radical in the sol cross-propagates with a SPELGA acrylate on the network to form a dangling chain attached to the network. In reaction (3.11), a growing radical on the network ($>X^*$) reacts with a network-bound SPELGA acrylate to form a load-bearing crosslink point (see Figure 3.8), leading to a hydrogel with a higher modulus (Figure 3.5). As the NVP fraction is increased beyond a certain value, the delay in the onset of diffusion-controlled polymerization counteracts the dilution effect of polymer chains in the sol. Ultimately, this leads to no further increase in modulus (see Figure 3.5 for 0.4, 0.61, and 0.83 mol% NVP). Since the diffusivities of NVP monomer and NVP-rich growing chains (reactions 3.4 and 3.6) are relatively higher those that of SPELGA macromonomer and SPELGA-rich growing chains (reactions 3.5 and 3.7), the propagation reactions (3.6) and (3.7) and the cross-propagation reactions (3.9) and (3.10) serve as a bridge between the network-bound SPELGA acrylates to increase the number of network density. Therefore, the higher modulus of the hydrogels in the presence of NVP can be explained by the dilution effect of polymer chain in the sol to delay the onset of diffusion-controlled reaction, and by propagation of NVP monomer and growing chains with network-bound SPELGA acrylates to facilitate crosslinking.

The average molecular weight between crosslinks, $\overline{M_c}$, can be determined by the equation for rubber elasticity [233]:

$$\overline{M_c} = RT\frac{\rho}{G'}(1-S) \qquad \text{(equation 3.12)}$$

where ρ is the macromonomer mass density (1100 kg/m^3), G' is modulus (Pa), R is gas constant (8.31 J/mol K), T is absolute temperature (310 K), and S is sol fraction (see Eq. 3.2 and data in Figure 3.4.b). Using Eq. (3.12), $\overline{M_c}$ decreased from 97 ± 12 to 43 ± 5 kDa as the NVP concentration was increased from 0 to 3.6 wt% for SPELGA5K-L100-P25-I0.16 hydrogel.

Degradation of SPELGA gels depends on the gel water content and density of hydrolytically degradable ester linkages. The relatively fast degradation of SPELGA800-L50 can be contributed to the high density of degradable LA/GL units (70% LA/GL and 30% 4PEE800), higher content of less hydrophobic glycolide monomer (50% by weight), and the autocatalytic effect of acidic degradation products [234]. SPELGA5K-L100 with 76% by weight PEG content had high water content (540 wt% swelling ratio after 1 week as shown in Figure 3.7.b) but low density of degradable lactide units (24%), resulting in a degradation rate lower than that of SPELGA800-L50. SPELGA800-L75 with a high density of more hydrophobic lactide groups and low water content (see Figure 3.7.b) exhibited the lowest mass loss with time.

3.5. CONCLUSION

A novel star poly(ethylene oxide-co-lactide-glycolide acrylate) (SPELGA) macromonomer was synthesized and characterized with respect to gelation, sol fraction, degradation, and swelling in aqueous solution. We hypothesized that a multi-arm star

amphiphilic poly(ethylene oxide-co-lactide-glycolide) based macromonomer with each arm terminated with an acrylate group would significantly increase the rate of crosslinking, thus reducing the minimum required concentration of initiator/monomer to produce robust networks. Addition of only 0.4 mol% NVP to the polymerization mixture increased modulus by 2.2-fold but modulus did not change appreciably for higher NVP concentrations. The higher modulus can be explained by the dilution effect of polymer chains in the sol, to delay the onset of diffusion-controlled reaction, and by propagation of growing polymer chains with network-bound SPELGA acrylates to facilitate network formation. It is interesting to note that the minimum NVP concentration of 0.4% was at least an order of magnitude less than that used in previous studies for gelation of PLEOF macromonomers. Depending on macromonomer concentration, sol fraction ranged between 8-18%. The higher reactivity and lower steric hindrance of the acrylates in SPELGA compared to fumarates in PLEOF significantly reduced sol fraction and minimum NVP concentration to produce robust networks. SPELGA gels with highest LA/GL content (SPELGA800-L50) had the highest mass loss but lowest water uptake with incubation time which was attributed to the high fraction of degradable units and the autocatalytic effect of acidic degradation products. SPELGA gels with highest LA/GL content (SPELGA800-L75 and SPELGA800-L50) showed delayed swelling characteristics.

CHAPTER 4

GELATION CHARACTERISTICS AND OSTEOGENIC DIFFERENTIATION OF STROMAL CELLS IN INERT HYDROLYTICALLY DEGRADABLE MICELLAR POLYETHYLENE GLYCOL HYDROGELS

Seyedsina Moeinzadeh, Danial Barati, Xuezhong He, Esmaiel Jabbari, *Gelation Characteristics and Osteogenic Differentiation of Stromal Cells in Inert Hydrolytically Degradable Micellar Polyethylene Glycol Hydrogels.* Biomacromolecules, 2012. **13**(7): p. 2073-2086. Reprinted here with permission of publisher.

4.1. INTRODUCTION

The overall goal of this work was to synthesize inert and non-fouling degradable hydrogels as a matrix for cell encapsulation. Hydrogels are hydrophilic polymeric networks that retain a significant fraction of water in their structure in physiological solution without dissolving. Nutrient molecules and proteins diffusive readily through hydrogels and cells immobilized in hydrogels display higher biological activity.[21-25] Due to these unique properties, hydrogels are very attractive as a matrix for cell encapsulation and delivery to the regeneration site in regenerative medicine.[26-30]

Polyethylene glycol (PEG) hydrogels are used extensively as a matrix for cell encapsulation to elucidate the effect of physiochemical, mechanical, and biological factors in the microenvironment on cell fate *in vitro*.[36-39] PEG hydrogels, due to their inert, hydrophilic and immunogenic nature, provide enormous flexibility in designing and controlling the cell microenvironment.[40, 41] Unlike small-molecule monomers that cross the cell membrane, the flexible PEG macromonomers crosslink to produce hydrogels with high compressive modulus without adversely affecting the viability of the encapsulated cells.[42-46]

An exciting approach to *in vivo* tissue engineering is to deliver progenitor cells to the regeneration site in an inert matrix, such as the PEG hydrogel, and allow the encapsulated cells to secrete the desired extracellular matrix (ECM). In this approach, the encapsulated progenitor cells, guided by cell-cell interactions and soluble factors, create and reorganize their ECM as they go through lineage commitment, differentiation, and maturation. Although inert PEG hydrogels provide flexibility in controlling the cell microenvironment, their use for *in vivo* applications in tissue regeneration is limited by

their persistence (non-degradability) in the site of regeneration to provide free volume for tissue formation and remodeling. In that regard, design and synthesis of PEG hydrogels with hydrolytically degradable links would substantially increase their use as a cell delivery matrix in tissue regeneration.[47-49]

Copolymerization of PEG with poly(lactide) (PLA) has been used to impart degradability to PEG macromers. However, due to the hydrophobicity of lactide, these copolymers form thermo-responsive physical gels in aqueous solution with orders of magnitude lower modulus than the covalently crosslinked PEG hydrogels.[150, 235] The degradation and water content of the copolymers could be adjusted by the fraction of hydrophobic lactide segments,[88, 178] but solubility of the copolymers in aqueous solution decreased with increasing lactide content.[56] Furthermore, the covalently crosslinked copolymer gels had significantly lower modulus compared to PEG hydrogels due to entrapment of reactive groups in micellar domains.[56, 59, 236, 237]

We hypothesized that degradation and crosslink density of PEG-PLA gels and viability of encapsulated cells is strongly dependent on the number of lactides per macromonomer. We further hypothesized that PEG macromers with short lactide segments could produce mechanically robust hydrogels with tunable degradation rate. Previous molecular dynamic simulations demonstrated that the micelle size and reactivity of PEG-acrylates with short lactide segments depended strongly on the lactide segment length.[59]

The objective of this work was to synthesize star 4-arm poly(ethylene oxide-co-lactide) acrylate (SPELA) macromonomers and investigate the effect of number of lactides per macromonomer on gelation time, modulus, sol fraction, water content, and

degradation and to compare the results with the linear poly(ethylene oxide-co-lactide) acrylate (LPELA). Star PEG macromonomers have lower radius of gyration and shear viscosity, and higher density of functional groups than the linear PEGs,[25, 53] leading to the formation of gels with higher crosslink density and modulus.[54-57] Dissipative Particle Dynamics method[58, 59] was used to simulate aggregation and nanostructure formation and the distribution of reactive groups in SPELA and LPELA hydrogel precursor solutions. Bone marrow derived stromal cells (MSCs) were used to measure viability and differentiation of encapsulated cells to the osteogenic lineage.

4.2. MATERIALS AND METHODS

4.2.1.MATERIALS

Lactide monomer (LA; >99.5% purity) was purchased from Ortec (Easley, SC) and dried under vacuum at 40°C for at least 12 h prior to use. Calcium hydride, tetrahydrofuran (THF), deuterated chloroform (99.8% deuterated), trimethylsilane (TMS), triethylamine (TEA), tin (II) 2-ethylhexanoate (TOC), acryloyl chloride, dimethylsulfoxide (DMSO), Linear polyethylene glycol (LPEG, nominal M_w=4700), 4-arm PEG (SPEG, M_w=5000) Ethylenediaminetetraacetic acid disodium salt (EDTA), penicillin, streptomycin, and paraformaldehyde were purchased from Sigma-Aldrich (St. Louis, MO). The protected amino acids and Rink Amide NovaGel resin for the synthesis of acrylamide-terminated GRGD peptide were purchased from EMD Biosciences (San Diego, CA). Dichloromethane (DCM, Acros Organics, Pittsburgh, PA) was dried by distillation over calcium hydride. Diethyl ether and hexane were obtained from VWR (Bristol, CT). DCM Spectro/Por dialysis tube (molecular weight cutoff 3.5 kDa) was purchased from Spectrum Laboratories (Rancho Dominquez, CA). Dulbecco's phosphate-

buffered saline (PBS) and Dulbecco's Modified Eagle's Medium (DMEM; 4.5 g/L glucose with L-glutamine and without sodium pyruvate) were obtained from GIBCO BRL (Grand Island, NY). Fetal bovine serum (FBS, screened for compatibility with rat BMS cells) was obtained from Atlas Biologicals (Fort Collins, CO). Trypsin and Quant-it PicoGreen dsDNA reagent kit were obtained from Invitrogen (Carlsbad, CA). QuantiChrom calcium and alkaline phosphatase (ALPase) assay kits were purchased from Bioassay Systems (Hayward, CA). BMP2 solution (100 μL, 1.5 mg/mL in BMP2 buffer) was generously donated by Medtronic (Minneapolis, MN). The Live/Dead calcein AM (cAM) and Ethidium homodimer-1 (EthD) cell viability/cytotoxicity kit was purchased from Molecular Probes (Life Technologies, Grand Island, NY).

4.2.2. SYNTHESIS OF LPELA AND SPELA MACROMONOMERS

A two-step procedure was used to synthesize linear (LPELA) and star (SPELA) poly(ethylene glycol-co-lactide) acrylate macromonomers. In the first step, linear (LPEL) and star (SPEL) poly(ethylene glycol-co-lactide) macromers were synthesized by melt ring-opening polymerization with LPEG and SPEG, respectively, as polymerization initiators and TOC as the reaction catalyst, using a procedure similar to our previous work.[56] The PEG polymers were dried by azeotropic distillation from toluene.The LA and PEG were added to a three-neck reaction flask equipped with an overhead stirrer. The LA:PEG molar ratio was varied from 0 to 20 to synthesize macromonomers with different lactide segment lengths. The reaction flask was heated to 120ºC with an oil bath under steady flow of dry nitrogen to melt the reactants. Next, 1 ml of TOC was added and the reaction was allowed to continue for 8 h at 135ºC. After the reaction, the product was dissolved in DCM and precipitated in ice cold methanol followed by ether and hexane to

fractionate and remove the unreacted monomer and initiator. The synthesized LPEL and SPEL macromers were vacuum dried to remove any residual solvent and stored at -20ºC.

In the next step, the terminal hydroxyl groups of LPEL and SPEL macromers were reacted with acryloyl chloride to produce LPELA and SPELA macromonomers, respectively. Prior to the reaction, macromers were dissolved in DCM and dried by azeotropic distillation from toluene to remove residual moisture. After cooling under steady flow of nitrogen, the macromer was dissolved in DCM and the reaction flask was immersed in an ice bath. Equimolar amounts of acryloyl chloride and TEA were added drop-wise to the solution to limit the temperature rise of the exothermic reaction. The reaction was allowed to proceed for 12 h. After the reaction, solvent was removed by rotary evaporation, the residue was dissolved in ethyl acetate to precipitate the by-product triethylamine hydrochloride salt. Next, ethyl acetate was removed by vacuum distillation, the macromer was re-dissolved in DCM and precipitated twice in ice cold ethyl ether. The synthesized macromonomer was dissolved in DMSO and purified by dialysis to remove any unreacted acrylic acid. The LPELA and SPELA products were dried in vacuum to remove residual solvent and stored at –40°C.

4.2.3. MACROMONOMER CHARACTERIZATION

The chemical structure of the macromonomers was characterized by a Varian Mercury-300 H-NMR (Varian, Palo Alto, CA) at ambient conditions with a resolution of 0.17 Hz.[41] The sample was dissolved in deuterated chloroform at a concentration of 50 mg/ml and 1% v/v TMS as the internal standard.

4.2.4. MACROMONOMER GELATION AND RHEOLOGICAL MEASUREMENTS

The macromonomers were crosslinked in aqueous solution by UV free-radical polymerization with 4-(2-hydroxyethoxy)phenyl-(2-hydroxy-2-propyl) ketone (Irgacure 2959; CIBA, Tarrytown, NY) photoinitiator as described.[56, 150] The initiator was dissolved in distilled deionized (DI) water at 50ºC. The macromonomer was dissolved in DI water by vortexing and heating to 50ºC. The macromonomer solution was added to the initiator solution, vortexed for 5 minutes, and loaded on the Peltier plate of the rheometer (TA Instruments, New Castle, DE) to monitor the crosslinking reaction. A 20 mm plate acrylic geometry was used at a gap distance of 500 μm. A sinusoidal shear strain with frequency of 1 Hz and 1% strain was applied to the sample while sample was irradiated with a BLAK-RAY 100-W mercury long wavelength (365 nm) UV lamp (Model B100-AP; UVP, Upland, CA).[24, 45, 150] The UV exposure time for all samples was 1000s. The storage and loss moduli (G', G'') of the samples were recorded with irradiation time. The reported shear modulus is the measured G' after 1000 s of UV exposure. The notations LPELA-nLa-Mb and SPELA-nLa-Mb are used to identify the architecture (linear versus star) as well as composition of the samples, where a and b represent number of lactide monomers (nL) per macromonomer and macromonomer concentration (wt %), respectively.

4.2.5. MEASUREMENT OF SWELLING RATIO AND SOL FRACTION

After crosslinking, samples with dimensions 20 mm diameter × 300 μm thickness were removed from the Peltier plate to measure their swelling ratio and sol fraction. Samples were dried at ambient conditions for 12 h followed by drying in vacuum for 1 h at 40°C and the dry weight (w_i) was recorded. Next, dry samples were swollen in DI

water for 24 h at 37°C and swelling medium changed every 6 h. After swelling, the surface water was removed and the swollen weight (w_s) was recorded. Then, the swollen samples were dried as described above and the dry weight (w_d) was recorded. The weight swelling ratio (Q) and sol fraction (S) were calculated by the following equations:[56, 150]

$$Q = \frac{w_s - w_d}{w_d} \times 100 \qquad \text{(equation 4.1)}$$

$$S = \frac{w_i - w_d}{w_i} \times 100 \qquad \text{(equation 4.2)}$$

4.2.6. MEASUREMENT OF MASS LOSS

The macromonomer precursor solutions were degassed, transferred to a PTFE mold (5 cm × 3 cm × 750 μm), covered with a transparent glass plate, fastened with clips, and UV crosslinked as described.[41] Disc shape samples were cut from the gel using an 8 mm cork borer. The mass loss was measured in primary culture media (5 ml per sample) without fetal bovine serum at 37ºC and under mild agitation. The primary media was prepared by dissolving 13.4 g of Dulbecco's Modified Eagle Medium (DMEM) in 900 ml of DI water containing 3.7 g sodium bicarbonate and 10 ml antibiotic and antimycotic agents (1% v/v). At each time point, samples were removed from the media, washed with DI water several times to eliminate the excess salts and dried under vacuum. The dried sample weight was measured and compared with the initial dry weight to determine the fractional mass loss.

4.2.7. BONE MARROW STROMAL CELL ISOLATION

MSCs were isolated from the bone marrow of young adult male Wistar rats according to established protocols.[113, 238] Cell isolation was performed under a

protocol approved by the Institutional Animal Care and Use Committee of the University of South Carolina. The bone marrow cell suspensions were centrifuged at 200×g for 5 min, cell pellets were re-suspended in 12 mL basal medium (DMEM supplemented with 10% FBS, 100 units/mL penicillin (PEN), 100 µg/mL streptomycin (SP), 50 µg/mL gentamicin sulfate (GS) and 250 ng/mL fungizone (FZ)) and aliquoted into T-75 flasks. The flasks were subsequently maintained in a humidified 5% CO_2 incubator at 37°C. Cultures were replaced with fresh medium at 3 and 7 days to remove haematopoietic and other unattached cells. After 10 days, cells were detached from the flasks with 0.05% trypsin-0.53 mM EDTA and used for *in vitro* experiments.

4.2.8. ENCAPSULATION OF MSCS IN SPELA HYDROGEL

SPELA-nL14.8 macromonomer was dissolved in PBS at 15 %wt and sterilized by filtration with a 0.2 µm filter. Acrylamide-terminated GRGD peptide (Ac-GRGD) was synthesized on Rink Amide NovaGel resin in the solid phase, purified by HPLC, and characterized by electrospray ionization (ESI) mass spectrometry as described previously.[113] To the macromonomer solution, 1 wt% Ac-GRGD (based on SPELA) was added to improve cell viability and cell-matrix interaction after MSC encapsulation.[113] For experiments with BMP2, 200 ng/mL of the protein was added to the precursor hydrogel solution.[239] Next, $1x10^6$ MSCs, suspended in 100 µL of PBS, was added to the SPELA macromonomer precursor solution and mixed gently with a pre-sterilized glass rod. The density of MSCs in the gel was $2x10^6$ cells/mL. The mixture was injected between two sterile microscope glass slides and crosslinked by UV irradiation. After removing the gel from the glass slide under sterile condition, disks were cut with a sterile cork-borer and incubated in 2 ml PBS for 1 h with two PBS changes. Next, the

medium was replaced with osteogenic medium for two groups; with and without the addition of 200 ng/mL BMP2, and the encapsulated MSCs were incubated for 21 days. At each time point, some of the disks were stained with cAM/EthD live/dead assay (1 μg/ml) to image live and dead cells, respectively. Stained samples were imaged with an inverted fluorescent microscope (Nikon Eclipse Ti-ε, Nikon, Melville, NY).

At each time point, DNA content (cell number), ALPase activity, calcium content, and mRNA expression of osteogenic markers Dlx-5, Runx2, OP, and OC were measured.

4.2.9. MEASUREMENT OF DNA CONTENT, ALPASE ACTIVITY, AND CALCIUM CONCENTRATION

At each time point, some of the disks were homogenized and sonicated to rupture the membrane of the encapsulated cells and expose the DNA. Double stranded DNA (dsDNA) content of the homogenized samples were analyzed using a PicoGreen assay as described.[113] Analysis of dsDNA was performed using a Synergy HT plate reader (Bio-Tek, Winooski, VT) with emission and excitation wavelength of 485 and 528 nm, respectively. Alkaline phosphatase (ALPase) activity of the samples were measured with p-nitrophenyl phosphatase (Sigma-Aldrich) on a Synergy HT plate reader at 405 nm as described.[113] The measured p-nitrophenol concentration was correlated to ALPase activity in IU/L and normalized to cell numbers. Calcium content of the samples, as a measure of the total mineralized deposit in the sample, was measured using QuantiChrom Calcium Assay kit as described.[113] The absorbance was measured on a Synergy HT plate reader at 575 nm. Measured intensities were correlated to the amount of equivalent Ca^{2+} using a calibration curve made with calcium chloride solutions of known concentrations.

4.2.10. mRNA ANALYSIS

At each time point, total cellular RNA was isolated using TRIzol (Invitrogen, Carlsbad, CA) or RNeasy Mini-Kit (Qiagen, Valencia, CA) and analyzed with NanoDrop 2000 (Thermo Scientific, Waltham, MA) as described.[113] 1µg of the extracted total RNA was subjected to cDNA conversion using the Reverse Transcription System (Promega, Madison, WI). The obtained cDNA was subjected to real time polymerase chain reaction (PCR) amplification with appropriate gene specific primers. The expression level of ribosomal protein S16 was used as the endogenous control. Primers for real-time PCR analysis were designed and selected using the Primer3 web-based software as described.[188] The PCR products were analyzed by agarose gel electrophoresis. The annealing temperatures and other parameters for amplification were optimized by classical PCR and agarose gel electrophoresis as described.[188] Real-time PCR (RT-qPCR) was performed to analyze the differential expression of Dlx5 and Runx2, markers for osteogenic differentiation, osteopontin (OP, early marker), and osteocalcin (OC, late marker) with SYBR green RealMasterMix (Eppendorf, Hamburg, Germany) using Bio-Rad CXF96 PCR system (Bio-Rad, Hercules, CA). The following forward and reverse primers were synthesized by Integrated DNA technologies (Coralville, IA): OP: forward 5′-GAC GGC CGA GGT GAT AGC TT-3′ and reverse 5′-CAT GGC TGG TCT TCC CGT TGC-3′; OC: forward 5’-AAA GCC CAG CGA CTC T-3′ and reverse 5’-CTA AAC GGT GGT GCC ATA GAT-3′; Dlx5: forward 5′- CCT CAT GGC TAC TGC TCT CC-3′ and reverse 5′-CTC GGC CAC TTC TTT CTC TG-3′; Runx2: forward 5′-GCC GGG AAT GAT GAG AAC TA-3′ and reverse 5′-GGA CCG TCC ACT GTC ACT TT-3′; S16: forward 5′-AGT CTT CGG ACG CAA GAA AA-3′

and reverse 5′-AGC CAC CAG AGC TTT TGA GA-3′.[240] Quantification of gene expression was based on the crossing-point threshold value (CT) for each sample, which was evaluated by the Relative Expression Software Tool (RESTTM) as the average of three replicate measurements.[241] The model of Pfaffl was used to determine the expression ratio of the gene.[241] The expression of S16 housekeeping gene was used as the reference and the fold difference in gene expression was normalized to the first time point.

4.2.10. STATISTICAL ANALYSIS

Data are expressed as means±standard deviation. All experiments were done in triplicate. Significant differences between groups were evaluated using a two-tailed Student's t-test. A value of $p<0.05$ was considered statistically significant.

4.3. SIMULATION METHOD

The aqueous solutions of SPELA and LPELA macromonomers were simulated via Dissipative Particle Dynamics (DPD) approach, as described previously.[59] Figure 4.1 shows the molecular structure and different bead types on SPELA and LPELA macromonomers. The bead types with equal mass and volume in the simulation volume were L (one lactide monomer), EO (four ethylene oxide repeat units), Ac (the acrylate group), SPEGc (the star PEG center) and W (eight water molecules). In DPD, each bead represents a soft particle interacting with the other beads via a soft pair-wise force function given by:[242, 243]

$$f_{ij} = \sum_{i \neq j} F_{ij}^{C} + F_{ij}^{D} + F_{ij}^{R} + F_{ij}^{S} \qquad \text{(equation 4.3)}$$

where f_{ij} is the total force and F_{ij}^{C}, F_{ij}^{D}, F_{ij}^{R} and F_{ij}^{S} are the conservative, dissipative,

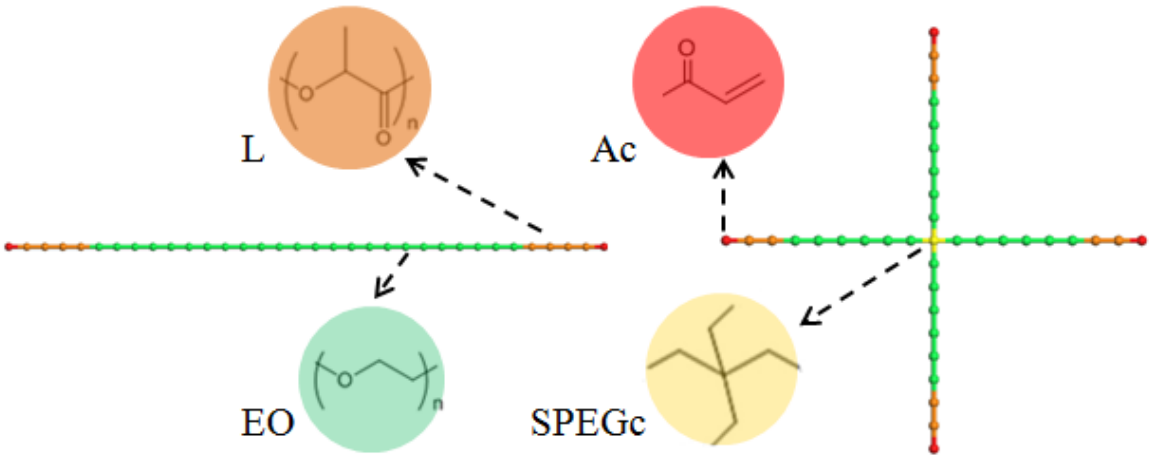

Figure 4.1. Coarse-grained representations of LPELA and SPELA macromonomers, respectively. Colors yellow, green, brown, and red represent SPEGc center, EO and L repeat units, and Ac terminal group. In a given arm, the length of lactide segment was significantly less than that of EO, leading to micellization and structure formation on the nanoscale.

random and spring components of the force, respectively. Different components of the force in a cutoff distance (r_c) are calculated by:

$$F_{ij}^{C} = \begin{cases} \alpha_{ij}(1-r_{ij})\,e_{ij} & |r_{ij}| < 1 \\ 0 & |r_{ij}| \geq 1 \end{cases} \qquad \text{(equation 4.4)}$$

$$F_{ij}^{D} = -\gamma\,[w^{D}(|r_{ij}|)]\,(e_{ij}.v_{ij})\,e_{ij} \qquad \text{(equation 4.5)}$$

$$F_{ij}^{R} = \sigma\,[w^{R}(|r_{ij}|)]\,\theta_{ij}\,e_{ij} \qquad \text{(equation 4.6)}$$

$$F_{ij}^{S} = \sum_{j} Cr_{ij} \qquad \text{(equation 4.7)}$$

where r_{ij} is the vector joining bead i to j, e_{ij} and $|r_{ij}|$ are the unit vector in the direction of r_{ij} and the magnitude of r_{ij} respectively. v_{ij} is the velocity vector given by $v_{ij} = v_i - v_j$. w^D and w^R are weight functions for dissipative and random forces, respectively, and γ, σ are the magnitude of the dissipative and random forces. The F_{ij}^{D} and F_{ij}^{R} act together

through the relation of their weight functions and constants ($w^D(r_{ij}) = [w^R(r_{ij})]^2$ and $\sigma^2 = 2k_B T\gamma$)[242] to preserve the dissipation as well as conservation of total momentum of the system. The spring force term acts to impose geometrical constraints on the covalently bonded beads[244]. The values of γ and C constants were 4.5 and 4 respectively[59, 244]. The repulsion between beads i and j is mainly dictated by the constant α_{ij} in the conservative force function. By choosing the system density $\rho = 3$ r_c^{-3}, the DPD length scale, r_c, was 8.18 Å and the pair-wise interaction parameter between beads i and j, α_{ij}, were determined using[58]:

$$\alpha_{ij} = 25 + 3.27\chi_{ij} \qquad \text{(equation 4.8)}$$

where χ_{ij} is the Flory-Huggins parameter between beads i and j. The values of χ_{ij} in turn are given by:

$$\chi_{ij} = \frac{(\delta_i - \delta_j)^2 V}{RT} \qquad \text{(equation 4.9)}$$

where δ_i and δ_j are the solubility parameters of beads i and j, respectively, V is the bead molar volume, T is absolute temperature, and R is the gas constant. The solubility parameters were calculated via atomistic molecular dynamics simulation (Forcite and Amorphous Cell modules, Materials Studio v5.5, Accelrys)[152] using the COMPASS force field, which is an *ab initio* force field optimized for condensed-phase systems[245].

The position and velocity of the beads at each time point were determined by solving the equation of motion (equation 4.10)[242] using the force function (equation 3):

$$\frac{dr_i}{dt} = v_i \quad , \quad m_i \frac{dv_i}{dt} = f_i \qquad \text{(equation 4.10)}$$

All DPD simulations were performed in a $30 \times 30 \times 30$ r_c simulation box with 3D periodic boundary conditions with over 200000 time steps and dimensionless time step of 0.05. The Mesocite module of the Materials Studio (v5.5) was used to perform the DPD calculations.[152]

4.4. RESULTS AND DISCUSSION

4.4.1. MACROMONOMERS CHARACTERIZATION

^1H-NMR spectrum of SPELA-nL14.8 macromonomer is shown in Figure 4.2. NMR spectra of other SPELA macromonomers and LPELA are provided in Figures 4.3. The chemical shifts with peak positions at 3.6 and 4.3 ppm were attributed to the methylene hydrogens ($=CH_2$) of PEG attached to ether ($-CH_2-O-CH_2-$) and ester ($-CH_2-OOC-$) groups of lactide respectively.[246] The shifts with peak positions at 1.6 and 5.2 ppm were attributed to the methyl ($-CH_3$) and methine ($\equiv CH$) groups of lactide respectively.[246] The shifts with peak positions from 5.85 to 6.55 ppm (see the insets in Figure 4.2 and Figure 4.3) were attributed to the vinyl hydrogens ($-CH=CH_2$) of the acrylate group at the end of each macromonomer arm as follows: Peak positions in the 5.82-5.87 ppm range were associated with the trans proton of unsubstituted carbon of the Ac; those in the 6.10-6.20 ppm range corresponded to the protons bonded to monosubstituted carbon of the Ac; and those in the 6.40-6.46 ppm range were associated with the proton of unsubstituted carbon of the acrylate group. The $\overline{M_n}$ of SPELA was determined from the ratio of shifts centered at 1.6 and 5.2 ppm (lactide hydrogens) to those at 3.6 and 4.3 ppm (PEG hydrogens). The number of acrylate groups per macromonomer was determined from the ratio of shifts between 5.85 and 6.55 ppm

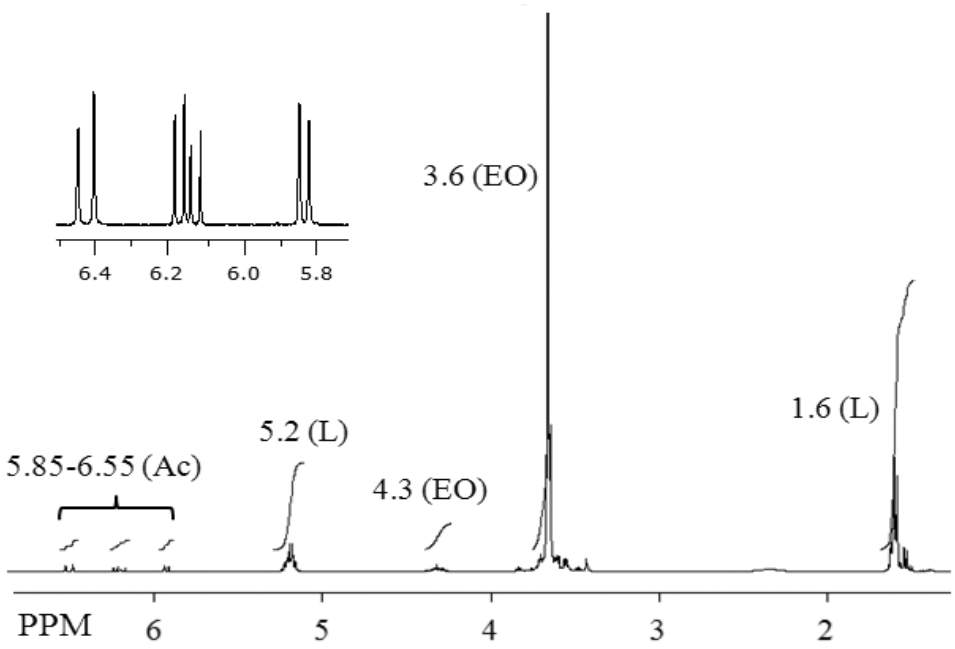

Figure 4.2. ^{1}H-NMR spectrum of SPELA-nL14.8 macromonomer. The inset shows the chemical shifts with peak positions between 5.8 and 6.5 at higher intensity.

(acrylate hydrogens) to those at 3.6 and 4.2 ppm (PEG hydrogens). The number of lactide monomers (nL) and functional acrylate groups per macromonomer, and $\overline{M_n}$ for LPELA and SPELA macromonomers as a function of lactide to PEG (LEGF) molar feed ratio are summarized in Table 4.1. LEGF ratio was varied from zero to 20 with intervals of 5. The nL values, shown in the first column, changed from 0 to 3.4, 6.4, 11.6 and 14.8 for SPELA and from 0 to 3.6, 7.4, 9.6 and 14.8 for LPELA as LEGF values were increased from zero to 5, 10, 15, and 20, respectively. As LEGF ratio was increased from zero to 20, $\overline{M_n}$ of SPELA (column 2) increased from 5.2 to 7.4 kDa and $\overline{M_n}$ of LPELA increased from 4.7 to 6.8 kDa. As LEGF ratio was increased from zero to 20, number of lactides per arm of the macromonomer (column 4) increased from zero to 3.7 for SPELA and from zero to 7.4 for LPELA. The range for acrylate fraction per arm of SPELA and LPELA macromonomers was 0.75-0.86 and 0.71-0.89, respectively. It should be noted

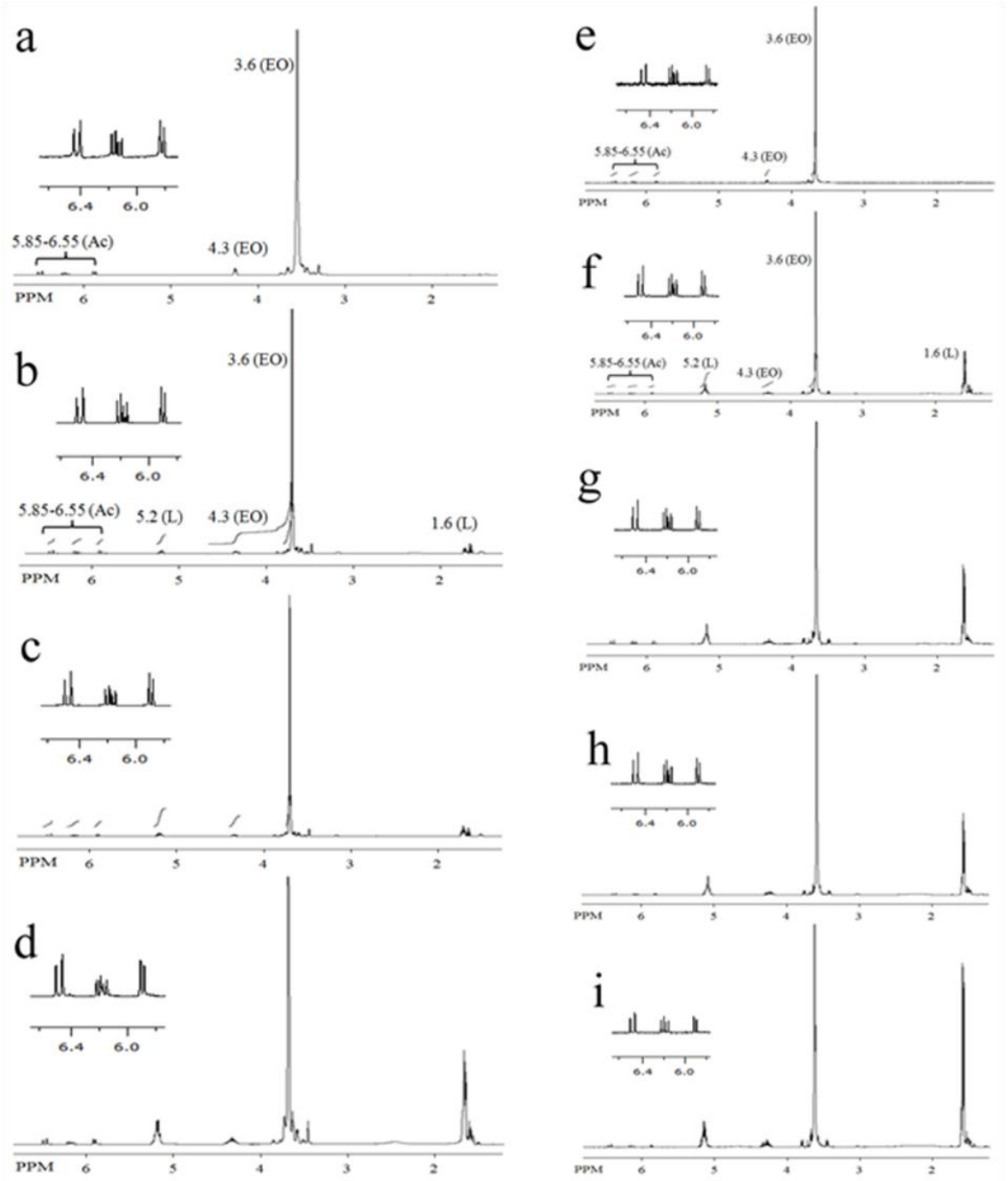

Figure 4.3. ^{1}H-NMR spectrum of (a) SPELA-nL0 , (b) SPELA-nL3.4 , (c) SPELA-nL6.4 and (d) SPELA-nL11.6, (e) LPELA-nL0 , (f) LPELA-nL3.6 , (g) LPELA-nL7.4 , (h) LPELA-nL9.6 and (i) LPELA-nL14.8 macromonomers. The inset shows the chemical shifts with peak positions between 5.8 and 6.5 at higher intensity. EO, L, and Ac represent ethylene oxide and lactide repeat units, and acrylate terminal group, respectively.

Table 4.1. Number of lactide monomers (nL), number-average molecular weight ($\overline{M}_n$), average number of lactide units per end group, and average number of acrylate groups per end group for SPELA and LPELA macromonomers as a function of lactide to PEG molar feed ratio in the polymerization reaction.

Macromonomer	$\overline{M}_n$	Lactide units per end group in the feed	Lactide units per end group	Acrylate groups per end group
SPELA-nL0	5300	0	0	0.85
SPELA-nL3.4	5800	1.25	0.8	0.86
SPELA-nL6.4	6200	2.5	1.6	0.82
SPELA-nL11.6	6900	3.75	2.9	0.74
SPELA-nL14.8	7400	5	3.7	0.75
LPELA-nL0	4700	0	0	0.89
LPELA-nL3.6	5200	2.5	1.8	0.85
LPELA-nL7.4	5800	5	3.7	0.87
LPELA-nL9.6	6100	7.5	4.8	0.77
LPELA-nL14.8	6800	10	7.4	0.71

that the standard deviation from the mean (s.d.) for, $\overline{M_n}$, average number of lactide units per end group, and average number of acrylates per end group were 100 Da, 0.1, and 0.05, respectively. Therefore, the differences in acrylate groups per end group for SPELA-nL0, SPELA-nL3.4, and SPELA-nL6.4 (0.85, 0.86, and 0.82, respectively) and those between LPELA-nL0, LPELA-3.6 nL, and LPELA-7.4 nL (0.89, 0.85, and 0.87, respectively) were not statistically significant. In general, there was a decrease in the average number of acrylates per arm with increasing nL. This decrease was related to higher steric hindrance of hydroxyl endgroups in LPELA and SPELA macromonomers with longer length of lactide segments, leading to a lower effective reactivity with acryloyl chloride. In general, polydispersity of SPELA and LPELA macromonomers was <1.5.

4.4.2. GENERAL OBSERVATIONS IN RHEOLOGICAL EXPERIMENTS

Time evolution of the shear storage modulus (G') for gelation of SPELA macromonomer as a function of number of lactide monomers (nL) is shown in Figure 4.4. The intersection of storage and loss moduli (G'', not shown in the figure), where $G' = G''$, was used to determine the gelation time. All time sweep tests exhibited a lag or induction time, a developing portion, and a plateau region.[24] However the length of each region as well as the final value of G' were affected by the macromonomer structure, i.e., linear versus star and the number of lactides. In general, the time for induction/lag time decreased with increasing nL, because the average distance between the reactive acrylate groups of the macromonomers decreased with increasing nL (see Figure 4.3). The slope and duration of the developing portion of the gelation curve decreased with increasing nL, mainly due to micelle/cluster formation by the hydrophobic lactide segments (See Figure 4.3). There was also a decrease in plateau shear modulus with increasing nL due to micelle/cluster formation (see Figure 4.3).

4.4.3. EFFECT OF INITIATOR ON GELATION KINETICS

The effect of initiator concentration on the storage modulus and gelation time of LPELA-nL7.4 and SPELA-nL14.8 macromonomers (both having 3.7 lactide monomers per end group) is shown in Figure 4.5.a and 4.5.b, respectively. SPELA-nL14.8 had the longest hydrophobic lactide segment length, compared with other SPELA macromonomers, potentially leading to highest steric hindrance of the acrylate groups in each arm in aqueous solution and lowest effective reactivity during cross-linking. Therefore, the effect of initiator concentration on gelation was investigated with SPELA-nL14.8 as the least favorable case, and LPELA-nL7.4 with a similar lactide segment

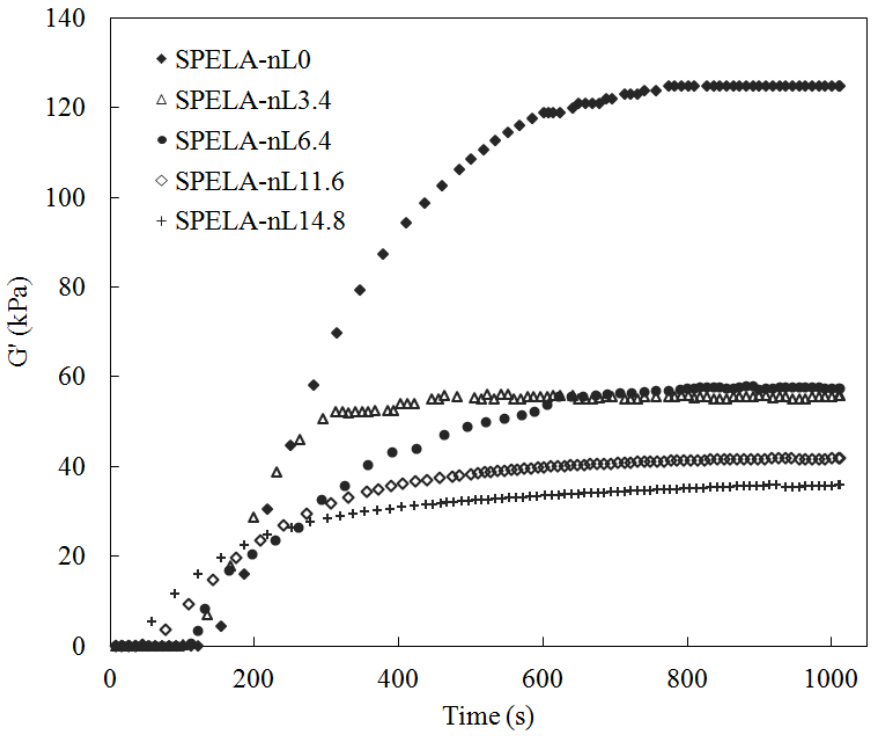

Figure 4.4. Effect of number of lactide monomers per macromonomer on time evolution of the storage modulus of SPELA-M20 hydrogels.

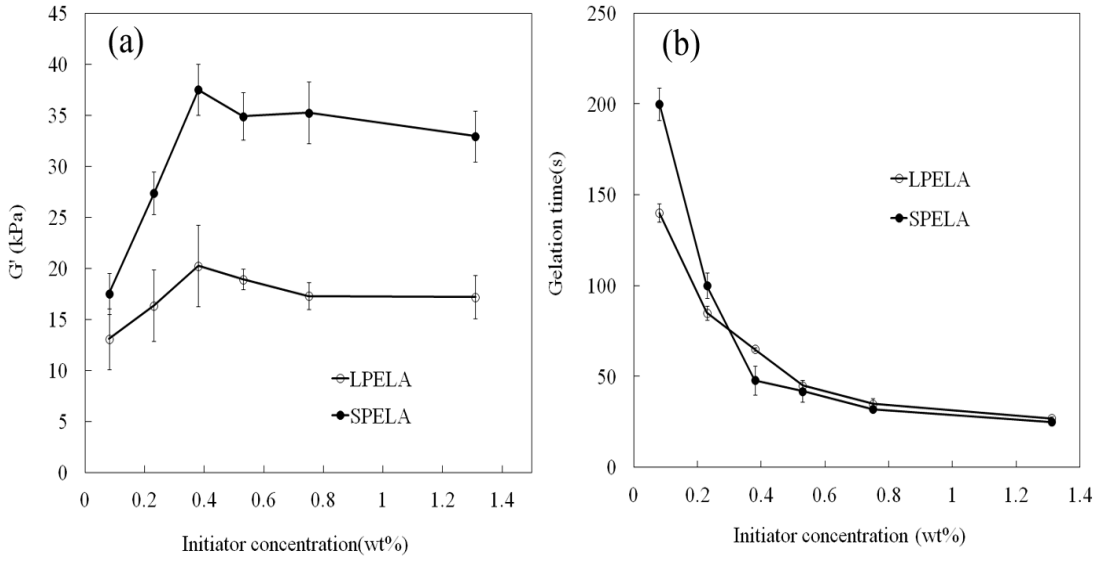

Figure 4.5. Effect of UV initiator concentration on (a) storage modulus and (b) gelation time of LPELA-nL7.4-M20 and SPELA-nL14.8-M20 hydrogels. Error bars correspond to means ± 1 SD for n = 3.

length was used for comparison. It is well established that the viability of cells encapsulated in synthetic gels is adversely affected by low molecular weight species such as initiator, crosslinker, and small-molecule monomers that cross the cell membrane.[42] On the basis of previous studies, photoinitiator concentrations >2 wt% (based on the weight of macromonomer) significantly decreased viability of the seeded cells.[43] Therefore, the effect of initiator on gelation of SPELA and LPELA was tested with concentrations <1.4 wt%. In the absence of photoinitiator (0.00 wt%) the modulus of LPELA-nL7.4 and SPELA-nL14.8 systems was 0.13 and 0.08 Pa respectively and (G''/G') was 5.3 and 1.8. Therefore, the precursor solutions without initiator did not form a hydrogel network with UV irradiation (no gelation time in Figure 4.5.b). For each initiator concentration, the modulus of SPELA gel was significantly higher than that of LPELA. The modulus of the hydrogels showed a maximum at 0.38 wt % initiator concentration for both LPELA-nL7.4 and SPELA-nL14.8 macromonomers. As the initiator concentration was increased from 0.08 to 0.38 wt%, the modulus of LPELA and SPELA gels initially increased from 13.1 ± 3.0 to 20.2 ± 4.1 kPa and from 17.5 ± 2.0 to 37.5 ± 2.5 kPa, respectively. After that, the modulus decreased to 17.2 ± 2.1 and $32.9 \pm$ 2.5 kPa for LPELA and SPELA hydrogels, respectively, when the initiator concentration was increased to 1.31 wt%. The modulus of the gels did not change for initiator concentrations >0.8 wt%. The initial increase in the gel modulus with initiator concentration can be attributed to an increase in propagation rate (R_p) given by:[229]

$$R_P = K_P [AC] \left[\frac{R_i}{K_t} \right]^{1/2} \qquad \text{(equation 4.11)}$$

$$R_i = \phi \varepsilon I_0 \delta [I] \qquad \text{(equation 4.12)}$$

where K_P and K_t are the rate constants for chain propagation and termination respectively, R_i is the radical initiation rate, [AC] is the concentration of unreacted acrylates, ϕ is initiation efficiency, ε is molar extinction coefficient, I_0 is the intensity of incident radiation, δ is sample thickness, and $[I]$ is photoinitiator concentration. According to equation 4.12, the rate of radical production increased with increasing initiator concentration to 0.38 wt% leading to a higher propagation rate of acrylates and higher extent of crosslinking. For initiator concentrations exceeding 0.38 wt%, the probability of formation of more than one radical on the same macromonomer increased, which led to the formation intra-molecular crosslinks, as opposed to inter-molecular crosslinks, and cluster formation and a decrease in storage modulus.[56] For initiator concentrations >0.8 wt%, the increase in propagation rate was offset by the increase in the rate of intra-molecular crosslinking, resulting in no change in modulus with increase in initiator concentration.

As the initiator concentration was increased from 0.08 to 0.78 wt%, gelation time of LPELA and SPELA macromonomers decreased from 140 ± 5 to 45 ± 1 s and from 200 ± 9 to 42 ± 2 s, respectively. At low initiator concentrations (0.08 to 0.23 wt%), SPELA had higher gelation times than LPELA but the two macromonomers reached similar gelation times for concentrations >0.5 wt%. The total volume of the hydrophobic domains in SPELA-nL14.8 was higher than LPELA-nL7.4. As a result, at low initiator concentrations, it was more likely for the SPELA polymerization reaction to become diffusion controlled than LPELA, leading to a higher gelation time for SPELA. As the initiator concentration was increased above 0.23 wt%, the reaction became less controlled by diffusion, leading to comparable gelation times for LPELA and SPELA at higher

concentrations. In addition, the higher concentration of reactive acrylates in SPELA was offset by the higher probability of intra-molecular crosslinking, leading to comparable gelation times for SPELA and LPELA at initiator concentrations >0.23 wt%. In the experiments that follow, the initiator concentration of 0.75 wt% was used, unless otherwise specified, to have low gelation times as well as high shear storage moduli.

4.4.4. EFFECT OF MACROMONOMER CONCENTRATION ON GELATION KINETICS

The effect of macromonomer concentration in the hydrogel precursor solution on gelation time and modulus of LPELA-nL7.4 and SPELA-nL14.8 hydrogels is shown in Figures 4.6.a and 4.6.b, respectively. The gelation time of SPELA gels decreased from 45 ± 8 to 30 ± 1 s whereas LPELA gels decreased from 65 ± 8 to 32 ± 6 s as the macromonomer concentration increased from 10 to 25 wt%. The storage modulus of LPELA and SPELA gels increased from 1.2 ± 0.5 to 28.3 ± 3.5 kPa and from 1.5 ± 0.6 to 61.0 ± 6.2 kPa, respectively, with increasing macromonomer concentration from 10 to 25 wt%. In the absence of a crosslinker, the dependence of propagation rate of the crosslinking reaction on the concentration of reactive acrylate groups is given by Eq. 4.11. According to that equation, higher acrylate concentrations increase propagation rate and density of crosslinks for both LPELA and SPELA macromonomers. Therefore, the decreasing trend of gelation time with increasing SPELA and LPELA macromonomer concentrations as well as the lower gelation time of SPELA at constant concentration (see Figure 4.6.a) can be attributed to the higher concentration of acrylates.[56]

The shear modulus of an ideal network is proportional to the density of elastically active links according to the theory of rubber elasticity:[247]

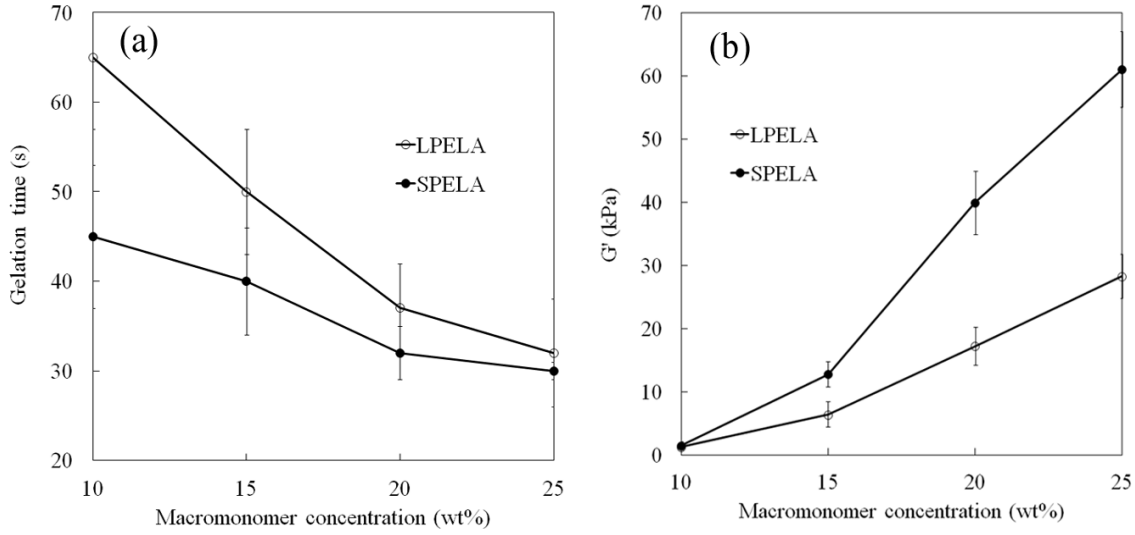

Figure 4.6. Effect of macromonomer concentration on (a) storage modulus and (b) gelation time of LPELA-nL7.4 and SPELA-nL14.8 hydrogels. Error bars correspond to means ± 1 SD for n = 3.

$$G = \nu_E RT \qquad \text{(euation 4.13)}$$

where ν_E is the concentration of elastically active chains, R is the gas constant and T is absolute temperature. The higher acrylate densities for SPELA compared to LPELA and higher macromonomer concentrations led to higher propagation rates, higher density of elastically active chains, and higher modulus. Furthermore, due to a larger average distance between the macromonomers at low concentrations, the probability of intra-molecular crosslinks that lead to loop formation and cyclization was higher.[24] Since intra-molecular crosslinks are not elastically active and do not contribute to the network modulus, the higher density of acrylates in SPELA was offset by higher intra-molecular crosslinks, leading to a smaller difference between the moduli of SPELA and LPELA gels at low concentrations (see Figure 4.5.b). As macromonomer concentration was increased, the probability of intra-molecular links decreased,[162] leading to higher

fraction of elastically active crosslinks in SPELA and larger difference between the moduli of SPELA and LPELA.

As shown in Figure 4.6.b, the shear modulus of SPELA gels was significantly higher than those of LPELA for all macromonomer concentrations. For example, the ratio of G'_{SPELA} / G'_{LPELA} increased from 1.2 at 10 wt% macromonomer concentration to 2.2 at 25 wt%. As mentioned in the last paragraph, the lower values of G'_{SPELA} / G'_{LPELA} at low concentrations can be attributed to the macromonomer architecture and its effect on nano-scale structure formation. DPD simulations of the macromonomers in aqueous solution showed a uniform distribution of Ac beads over the simulation box in the absence of L beads [60]. With the addition of lactide segments to the macromonomer, the hydrophobic L and Ac beads aggregated and formed core of the micelles, as shown in Figure 4.7.a for SPELA-nL14.8-M20 . (W, EO and SPEGc beads are not shown for clarity.) The cross-section of one of the micelles corresponding to the DPD simulations in Figure 4.7.a is shown in the Figure 4.6.b. According to simulation results, hydrophilic ethylene oxide segments (EO beads) of the macromonomers surrounded the core and formed the micelle's corona. Localization of Ac beads in the micelles' cores led to the formation of elastically active inter-molecular and elastically inactive intra-molecular crosslinks. To quantify the proximity of Ac beads to other beads on the same macromonomer, the average number of intra-molecular acrylate beads [$(IN_{intra-Ac}(R)]$ in a sphere of radius R around an Ac bead or the running integration number (IN) is calculated by:[248]

$$IN_{intra-Ac}(R) = 4\pi\rho_{Ac0}\int_0^R g_{intra-Ac}(r)\, r^2 dr \qquad \text{(equation 4.14)}$$

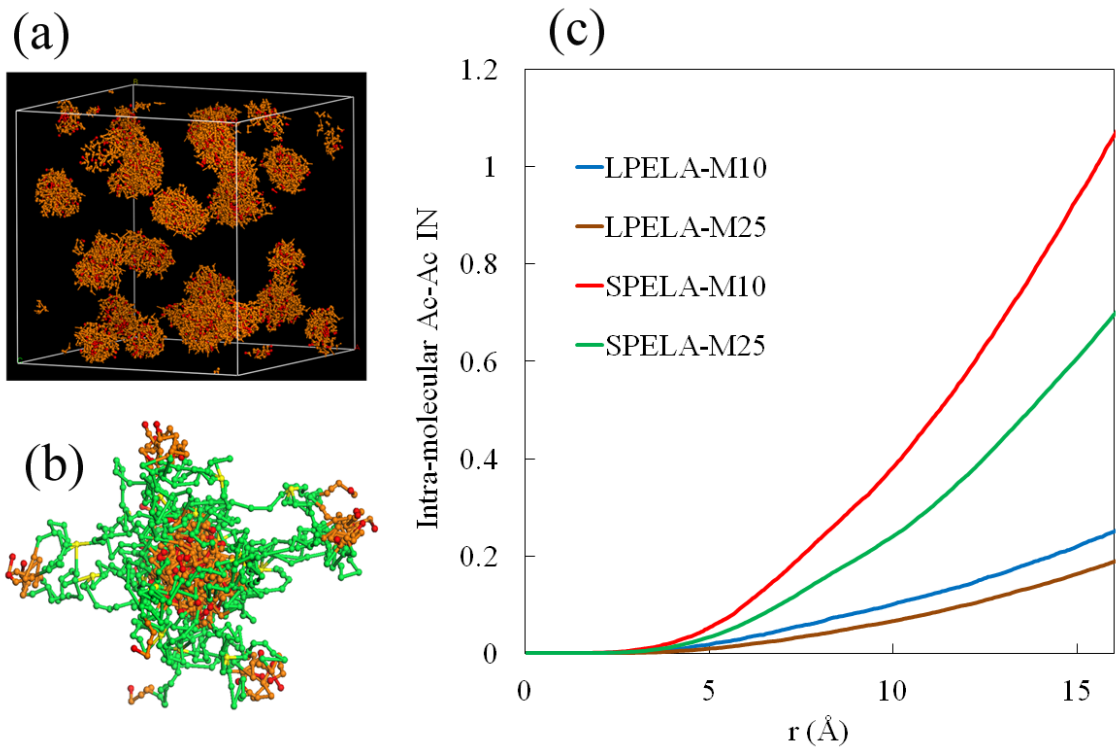

Figure 4.7. (a) DPD simulation of micellar cores for SPELA-nL14.8- M20; L and Ac beads are shown in brown and red, respectively, whereas other beads are not shown for clarity. (b) simulated crosssection of one of the micelles in panel a; L, Ac, EO, and SPEGc beads are shown in brown, red, green, and yellow, respectively, whereas water beads are not shown for clarity. (c) Intramolecular running integration number (IN) for Ac−Ac beads as a function of radius around an Ac bead for LPELA-nL7.4 and SPELA-nL14.8 macromonomers in aqueous solution. SPELA macromonomers have significantly higher Ac−Ac integration number than LPELA, leading to shorter gelation times and higher modulus.

where ρ_{Ac0} is the overall number density of Ac beads and $g_{intra-Ac}(r)$ is the radial distribution function of intra-molecular acrylates in a shell of infinitesimal thickness at distance r from each Ac bead, located at the origin. The $IN_{intra-Ac}$ profile for LPELA and SPELA hydrogels at 10% and 25% macromonomer concentrations is shown in Figure 4.7.c. The $IN_{intra-Ac}$ for LPELA and SPELA at R=15 Å decreased from 0.22 to 0.16 and from 0.93 to 0.60, respectively, with increasing macromonomer concentration from 10% to 25%. Therefore, the probability of intra-molecular reaction for SPELA was more

sensitive to macromonomer concentration than that of LPELA. This effect is reflected in the higher G'_{SPELA}/G'_{LPELA} ratios at higher macromonomer concentrations. Hiemstra et al. synthesized star eight-arm methacrylate-functionalized PEG-PLLA (L-lactide) and PEG-PDLA (D-lactide) with molecular weight of 28 kDa and 12 lactides per macromonomer. The modulus of those gels was generally <10 kPa, which is significantly lower than the four-arm SPELA gel synthesized in this work [57]. The effect of macromonomer concentration on swelling ratio and sol fraction of LPELA-nL7.4 and SPELA-nL14.8 hydrogels is shown in Figures 4.8.a and 4.8.b, respectively. The LPELA-nL7.4-M10 samples disintegrated upon removal from peltier plate of the rheometer, so the swelling and sol fraction of that sample was not measured. The swelling ratio of SPELA and LPELA gels decreased from 430 to 300% and from 810 to 580%, respectively, as the macromonomer concentration increased from 10/15% to 25%. The higher swelling ratio of LPELA gels compared to SPELA was related to the lower fraction of hydrophobic segments per macromonomer in LPELA along with lower crosslink density of LPELA gels. Sol fraction of LPELA gels decreased from $32.1 \pm 2.0\%$ to $26.8 \pm 1.5\%$ as concentration increased from 15 to 25%. The sol fraction of SPELA decreased from 13.2 ± 1.1 to 11.6 ± 1.1, 6.4 ± 1.0 and 4.9 ± 0.9 as macromonomer concentration increased from 10 to 15, 20 and 25%, respectively. Sol fraction of the hydrogels decreased by 2.7, 4.8 and 5.4 folds by changing macromonomer architecture from linear to star at 15, 20 and 25% concentration, respectively. The significantly lower sol fraction of SPELA hydrogel compared to LPELA was due to the higher concentration of reactive acrylate groups in SPELA at the same macromonomer concentration. The decreasing trend in sol fraction with macromonomer concentration was related to the

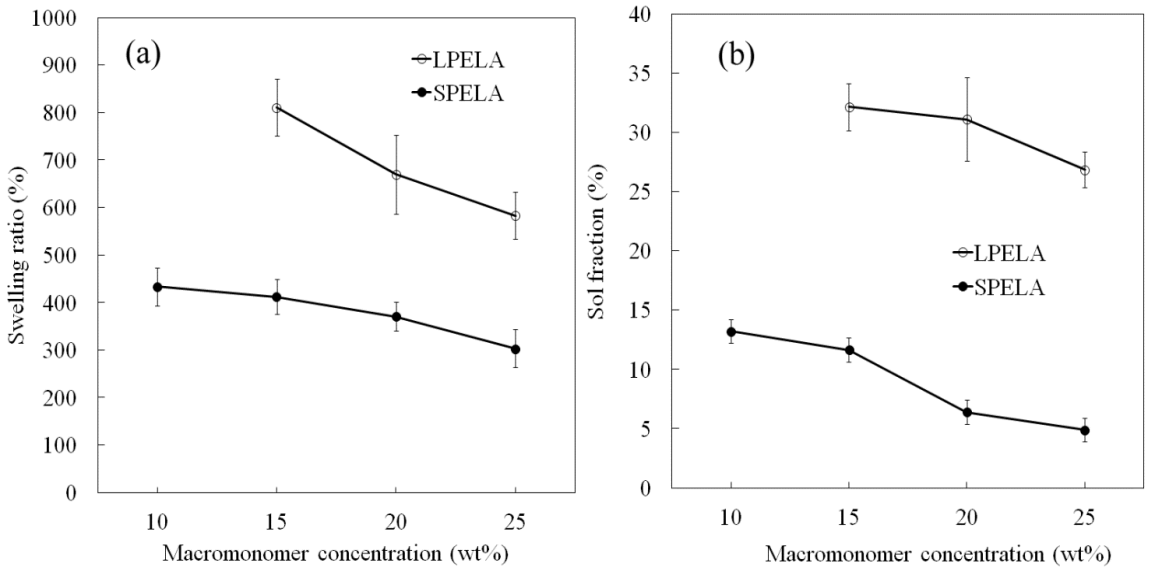

Figure 4.8. Effect of macromonomer concentration on (a) swelling ratio and (b) sol fraction of LPELA-nL7.4 and SPELA-nL14.8 hydrogels. Error bars correspond to means ± 1 SD for n = 3.

decrease in inter-molecular distance between the acrylate groups with concentration, which enhanced the probability of formation of elastically active crosslinks.

4.4.5. EFFECT OF NUMBER OF LACTIDES PER MACROMONOMER ON GELATION KINETICS

Figure 4.9 (a,b) shows the effect of number of lactide monomers per macromonomer on shear modulus and gelation time, respectively, for LPELA-M20 and SPELA-M20 hydrogels. G′ of the hydrogels initially decreased from 116 ± 10 kPa to 58 ± 2 kPa and from 69 ± 8 kPa to 26 ± 4 kPa with the addition of 3.6 and 3.4 lactide monomers per macromonomer (nL) for SPELA and LPELA hydrogels, respectively, corresponding to 1.8 and 0.85 monomers per arm of LPELA and SPELA hydrogels. Afterward, G′ decreased at a slower rate to 6.5 ± 2.5 kPa and 37.0 ± 2.0 kPa for LPELA and SPELA gels, respectively, when nL increased to 14.8. The gelation time of SPELA hydrogel decreased from 115 ± 10 s to 32 ± 1 s whereas that of LPELA decreased from 85

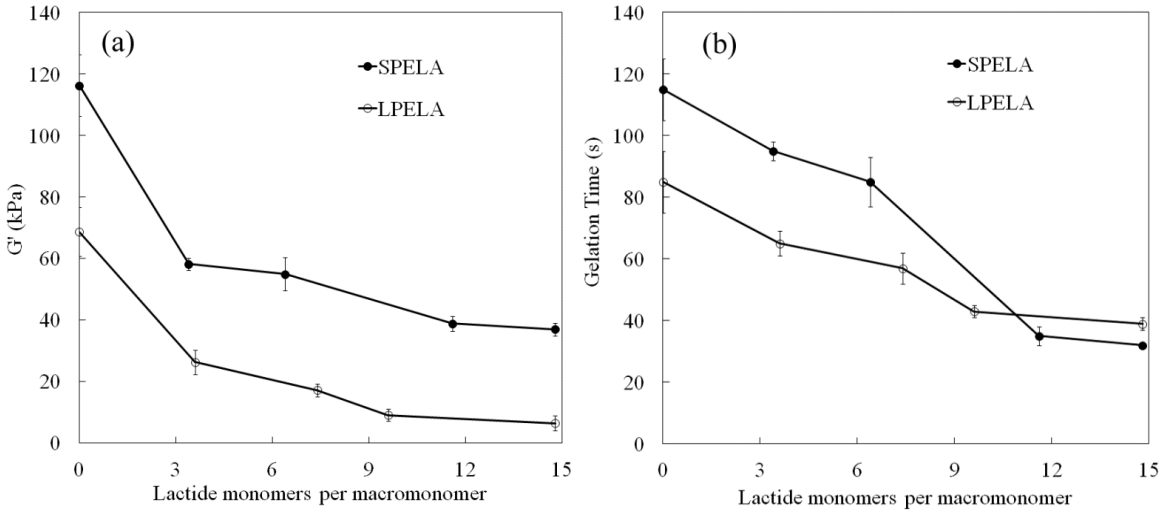

Figure 4.9. Effect of number of lactide monomers per macromonomer (nL) on (a) storage modulus and (b) gelation time of LPELA-M20 and SPELA-M20 hydrogels. Error bars correspond to means ± 1 SD for n = 3.

$\pm$ 10 s to 39 $\pm$ 2 s with increasing nL from 0 to 14.8. The decrease in G' and gelation time of the hydrogels with increasing lactide segment length is related to aggregation and micelle formation of the macromonomers in aqueous solution. The size of the micelles' core increased with increasing lactide segment length[60]. At any given time, macromonomer arms can have one of three conformations, namely bridge, which connects two different micelle cores, loop with at least two arms of a macromonomer in the same micelle, and free arm which is in solution (not part of the micelles).[59] The dynamic nature of these conformations leads to the formation of a transient physical network in the precursor solution. In SPELA-nL0 system, the gelation time was high due to a relatively large average distance between the uniformly distributed acrylate groups. The localization of reactive acrylate groups in the micelles core with increasing lactide content decreased the average distance between the acrylate groups.[59] As a result, the reaction rate between acrylates increased with increasing lactide segment length. In addition, the lifetime of the bridging arms in the core increased with increasing lactide

segment length.[59, 249] Those factors worked together to decrease gelation time with increasing lactide content of the macromonomer. At the same time, due to very low water content of the micelles, mobility of the acrylate groups and diffusion of initiator in the micelles significantly decreased with increasing micelles' core size. As a result, a fraction of the acrylates, trapped in the micelles' core, did not react to form elastically active crosslinks, which led to a decrease in the hydrogel modulus with increasing macromonomer lactide content.

The effect of number of lactides per macromonomer on sol fraction and swelling ratio of LPELA and SPELA hydrogels is shown in Figure 4.10.a and 4.10.b, respectively. The swelling ratio of LPELA gels decreased dramatically from 700% to 110% when nL increased from 0 to 14.8 while that of SPELA decreased slightly from 430% to 350%. The decrease in network density with increasing nL had a positive effect on swelling ratio whereas the increase in hydrophobicity with increasing nL had a negative effect on swelling ratio. . The molecular weight between crosslinks, $\overline{M_c}$, for an ideal network in the affine model is given by:[55, 247]

$$\frac{1}{\overline{M_c}} = \left(\frac{F}{F-2}\right)\frac{1}{\overline{M_n}} + \frac{G\bar{\nu}}{RT}\left(\frac{\nu_{2,r}}{\nu_{2,s}}\right)^{1/3} \qquad \text{(equation 4.15)}$$

where F is functionality of crosslinks (three for crosslinks at chain ends), $\overline{M_n}$ is macromonomer molecular weight, G is the network modulus, $\bar{\nu}$ is specific volume of the macromonomer, and $\nu_{2,r}$ and $\nu_{2,s}$ are the macromonomer volume fraction in the crosslinked gel before and after swelling equilibrium, respectively. According to the above equation, in the absence of inhomogeneity in the gel (e.g. PEG networks with no

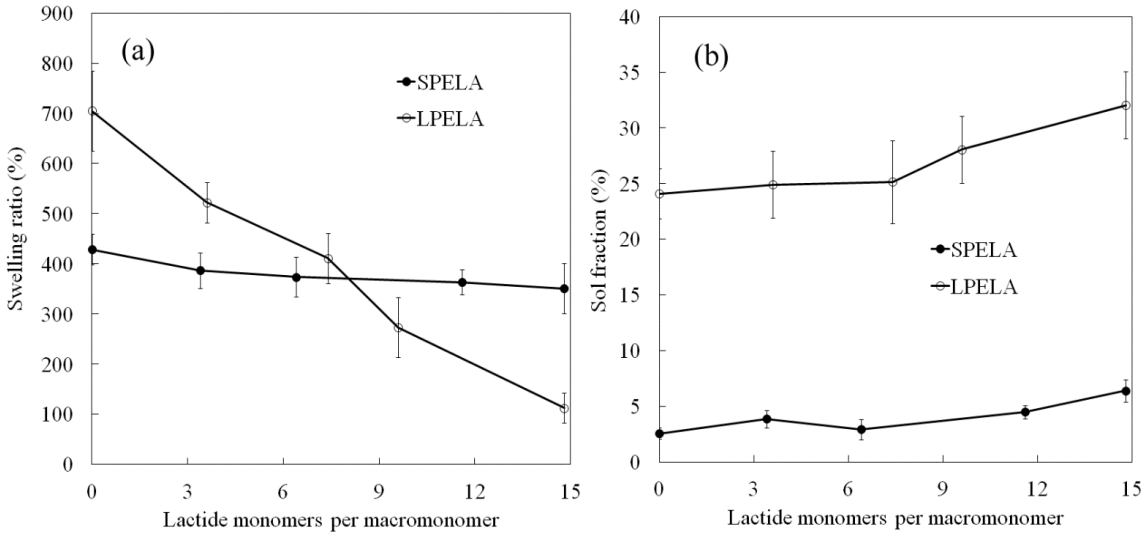

Figure 4.10. Effect of number of lactide monomers per macromonomer (nL) on (a) swelling ratio and (b) sol fraction of LPELA-M20 and SPELA-M20 hydrogels. Error bars correspond to means ± 1 SD for n = 3.

lactide segments), $\overline{M_c}$ increases and G decreases with $\overline{M_n}$. Therefore, the higher swelling of LPELA-nL0 compared with SPELA-nL0 is attributed to the lower crosslink density of the linear LPELA compared with star SPELA. In the presence of lactide, aggregation of hydrophobic segments produced micellar inhomogeneity in the network and increased hydrophobicity. On the basis of simulation results, water content of the hydrophobic domains was <1%. So the SPELA and LPELA gels may be better described as nanophase separated networks.[250] The interfacial free energy of the micelles with the aqueous phase increased with increasing nL for both SPELA and LPELA macromonomers. However, the micelles in SPELA had a lower interfacial energy than LPELA. The ethylene oxide chains in star SPELA macromonomer provided greater surface coverage for micelles' core, as predicted by DPD simulation (data not shown), thus lowering the interfacial energy of SPELA compared with LPELA. In addition, the lower radius of gyration of star SPELA led to higher steric repulsion between the EO

units in the macromonomer, which reduced the equilibrium core size and the average distance between the micelles in SPELA compared with LPELA. Therefore, as nL increased, SPELA macromonomers formed smaller micelles closer to each other while LPELA formed larger micelles farther away from each other. The higher inter-micellar distance in LPELA and extension of the bridging arms of the cores sharply reduced swelling ratio of LPELA as nL was increased (see Figure 4.10.a) while the swelling ratio of SPELA was unaffected by nL. SPELA hydrogel had a significantly lower sol fraction than LPELA, as shown in Figure 4.11.b. For example, sol fraction of LPELA and SPELA hydrogels increased from $24 \pm 2\%$ to $32 \pm 3\%$ and from $2.5 \pm 0.5\%$ to $6.4 \pm 1.0\%$ as nL increased from 0 to 14.8. This was attributed to the higher density of reactive acrylate groups in SPELA compared to LPELA, which increased the probability of incorporating macromonomers in the gel network.

The effect of lactide content per macromonomer on mass loss of the SPELA and LPELA hydrogels is shown in Figure 4.11(a,b) respectively. There was no significant difference between the mass loss curves of SPELA-nL6.4 and SPELA-nL14.8 ($p = 0.34$), but there was a significant difference between the mass loss of all other SPELA pairs ($p < 0.05$). There was a significant difference between the mass loss of all LPELA pairs ($p < 0.05$). Mass loss of SPELA-nL0 and LPELA-nL0 was <10% after 42 days. For a given time, mass loss of SPELA increased with increasing nL up to nL = 11.6, followed by a decrease in mass loss for higher nL values, but it was higher than LPELA at any incubation time. Mass loss of LPELA increased with nL. For example, mass loss of SPELA hydrogels after 28 days changed from 7 to 37, 80, 100, and 87% as the number of lactide monomers in SPELA increased from zero to 3.4, 6.4, 11.6, and 14.8, respectively,

whereas those of LPELA increased from 7 to 15, 26, 38, and 46% as the number of lactide monomers in LPELA increased from zero to 3.6, 7.4, 9.6, and 14.8. Sawhney et al. reported degradation time of 50 days for LPELA with PEG molecular weight of 6 kDa and 5 lactide units per macromonomer, but the swelling ratio of those gels were significantly higher than our gels.[251] The addition of only 3.4 lactides per macromonomer (<9 wt % of dry macromonomer and <2 wt % of swollen hydrogel) increased mass loss to 50% after 42 days.

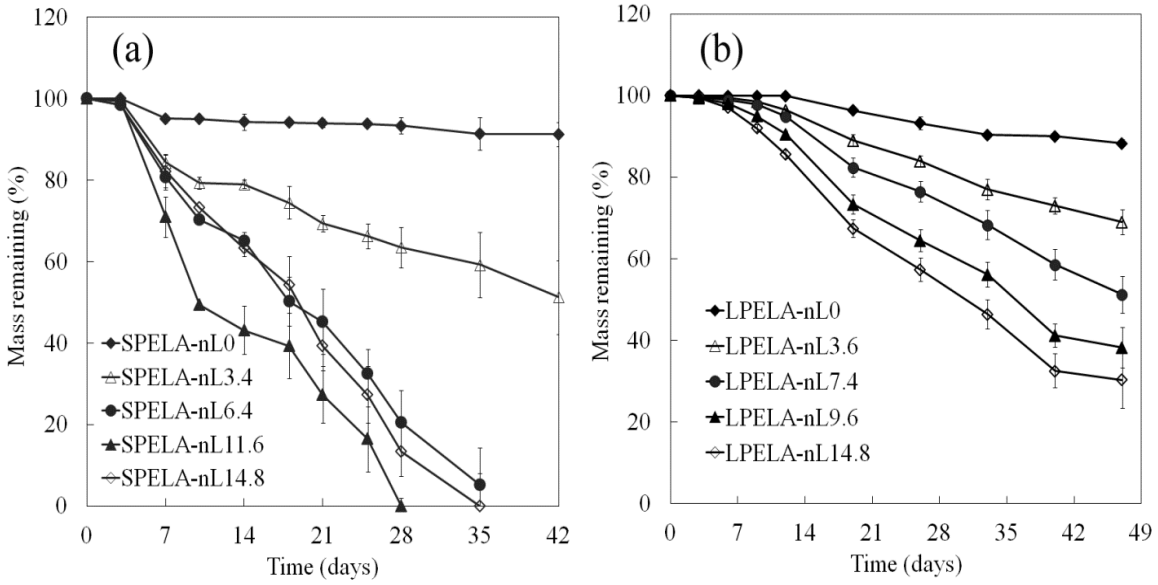

Figure 4.11. Effect of number of lactide monomers per macromonomer (nL) on mass loss of (a) SPELA-M20 and (b) LPELA-M20 hydrogels with incubation time. Error bars correspond to means ±1 SD for n = 3.

The SPELA hydrogel with 11.6 lactides per macromonomer completely degraded after 28 days. Assuming the formation of carboxylic acid groups by degradation of lactides does not significantly affect mass loss, degradation rate of SPELA is given by:

$$R_{\deg,SPELA} = k[-COO-][H_2O] \qquad \text{(equation 4.16)}$$

where k is the degradation rate constant, and [-COO-] and [H_2O] are the concentrations of ester groups and water in the hydrogel, respectively. Degradation of PLA matrices is

controlled by the low concentration of water in the matrix while degradation of SPELA hydrogel is controlled by relatively low concentration of degradable ester units. The decline in the concentration of ester groups in the hydrogel with degradation was offset by the increase in water content (increased swelling ratio), leading to nearly constant degradation rate, as shown in Figure 4.12. The increase in mass loss with nL (up to 11.6) was attributed to the higher concentration of ester groups in SPELA hydrogel. The decrease in mass loss for nL>11.6 was attributed to micelle formation with significantly reduced local concentration of water, leading to reduced rate of degradation.

Images a−d in Figure 4.12 show live (green) and dead (red) cells 1 h after encapsulation in SPELA-nL3.4, SPELA-nL6.4, SPELA-nL11.6, and SPELA-nL14.8 hydrogels, respectively. On the basis of the images, the number of lactides per macromonomer did not have a significant effect on cell viability. Cell viability was quantified by dividing the image into smaller squares and counting the number of live and dead cells. The fraction of viable cells for SPELA-nL0, SPELA-nL3.4, SPELA-nL6.4, SPELA-nL11.6, and SPELA-nL14.8 gels was 92 ± 3, 90 ± 4, 92 ± 4, 94 ± 4, and 91 ± 3, respectively.

DNA content, ALPase activity, and extent of mineralization of MSCs encapsulated in SPELA are shown in Figure 4.13(a−c), respectively. The cell free gels did not have DNA count, ALPase activity, and mRNA expression (Figure 4.13) but showed slight calcium content. For all time points, MSCs in BM had higher cell count than those cultured in OM, and the addition of BMP2 did not affect DNA count. At day 21, DNA count of MSCs in BM decreased slightly (statistically significant) compared with days 4−14. For days 14 and 21, DNA content of MSCs in OM and OM+BMP2

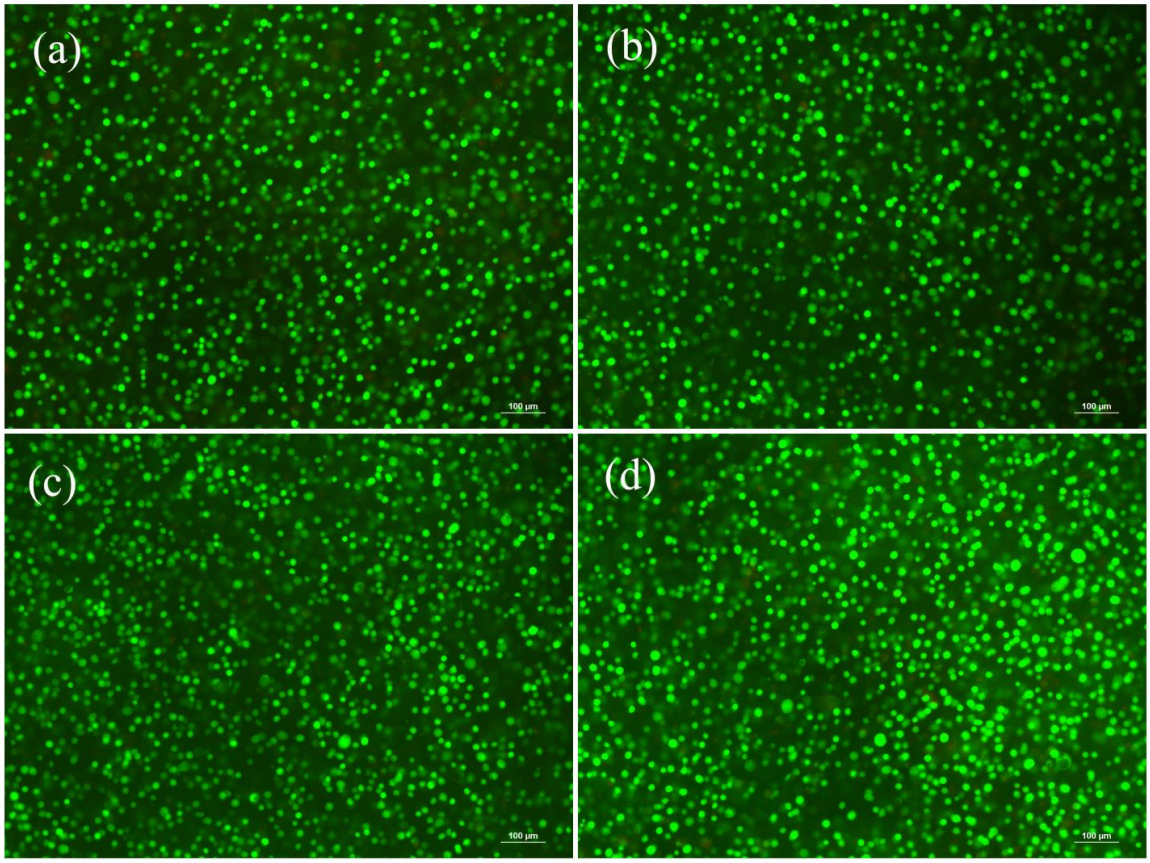

Figure 4.12. Live (green) and dead (red) image of MSCs 1 h after encapsulation in (a) SPELA-nL3.4, (b) SPELA-nL6.4, (c) SPELA-nL11.6, and (d) SPELA-nL14.8 hydrogels (without BMP2). The scale bar is 100 µm.

groups was statistically lower than days 4 and 7 (indicated by a star in Figure 4.13.a) and statistically lower than BM group. This trend is consistent with previous reports that cell number decreases with differentiation of MSCs in osteogenic medium. Wang et al. reported a decrease of 24 and 51% in DNA content after 3 and 6 weeks, respectively, with osteogenic differentiation of human umbilical cord MSCs seeded in PLGA scaffolds.[252] Oliveira et al. reported a decrease of 20% in DNA content after 7−14 days with osteogenic differentiation of rat MSCs.[253] Burdick et al. observed a decreasing trend in cell viability in 2 weeks for rat calvarial osteoblasts encapsulated in PEGDA hydrogels.[17] MSCs in BM group (green in Figures 4.13 and 4.14) had significantly

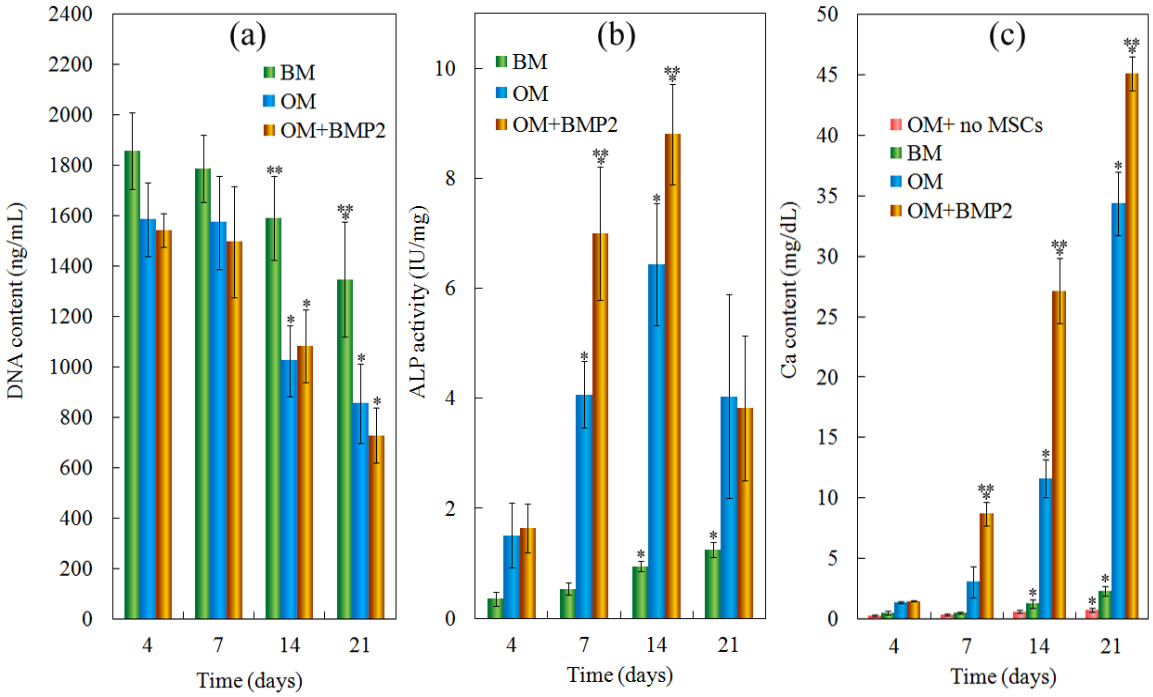

Figure 4.13. (a) DNA content, (b) ALPase activity, and (c) calcium content of MSCs encapsulated in SPELA-14.8 hydrogel. Experimental groupsinclude gels without MSCs incubated in osteogenic media (OM+no MSCs, red, control), gels with MSCs incubated in basal media (BM, green,control), gels with MSCs incubated in osteogenic media (OM, blue), and gels with MSCs and BMP2 incubated in osteogenic media (OM+BMP2,orange). One star indicates statistically significant difference (s.d.; $p < 0.05$) between the test time point and first time point (day 4) in the samegroup, and two stars indicate significant difference between the test group and all other groups at the same time point. Error bars correspond tomeans ±1 SD for n = 3.

lower ALPase activity, calcium content, and expression of osteogenic marker than OM and OM+BMP2. ALPase activity of both groups (with and without BMP2) significantly increased (indicated by one star) from day 4 to 7 and 14 and returned to the baseline level after 21 days. This was consistent with our previous results that the peak ALPase activity is the start of mineralization.[113] ALPase activity of BMP2 group at days 7 and 14 was significantly higher than that of OM (without BMP2, indicated by two stars). Calcium content of both groups increased significantly on days 7−21 compared with day 4 (indicated by one star). However, calcium content of the BMP2 group was significantly higher that the OM group for days 7−21 (indicated by two stars). For example, calcium

contents of the BMP2 group after 7, 14, and 21 days were 8.7 ± 1.0, 27.1 ± 2.7, and 45.1 ± 1.4 mg/dL, respectively, whereas those of OM were 3.1 ± 1.3, 11.6 ± 1.6, and 34.4 ± 2.6 mg/dL. Results in Figure 4.13.c demonstrate that the calcium content of MSCs in OM and OM+BMP2 groups was due to osteogenic differentiation and mineralization of MSCs and not due to the calcium in osteogenic media. mRNA expression levels of Dlx5, Runx2, OP, and OC of the MSCs for both groups (with and without BMP2) are shown in Figure 4.14(a−d) with incubation time. The fold differences in mRNA expression of the markers are normalized to those at time zero. BMP2 protein forms complexes with type I and type II BMP2 receptors (BRI and BRII) on the surface of MSCs, which activates the Smad-dependent and Smad-independent p38 pathways as well as internalization of the receptors.[254] The expression of Dlx5 and Runx2 is the early event in the BMP2 signaling cascade. Dlx5 regulates the activity of osteogenic master transcription factor Runx2 by Smad-dependent pathways, which in turn drives the expression of osteogenic genes. The expressions of Dlx5 and Runx2 were up-regulated for all time points (Figure 4.14.a,b) for both OM and BMP2 groups. However, for BMP2 group, there was a sharp increase in the expression of Dlx5 on days 7 and 14 and the expression of Runx2 on day 7. mRNA expression of OP and OC increased gradually for both OM and BMP2 groups with incubation time, but the fold difference was significantly higher for BMP2 group at each time point. For example, the fold differences in OC mRNA expression for OM group increased from 0.4 ± 0.2 to 1.1 ± 0.4, 3.5 ± 0.5, and 6.0 ± 0.4 after 4, 7, 14, and 21 days of incubation, respectively, whereas those for BMP2 group increased from 0.6 ± 0.2, 2.2 ± 0.2, 7.4 ± 1.1, and 11.5 ± 1.3. Results in Figures 4.13 and 4.14 taken together demonstrate that the encapsulated MSCs in OM and OM+BMP2 groups differentiated in

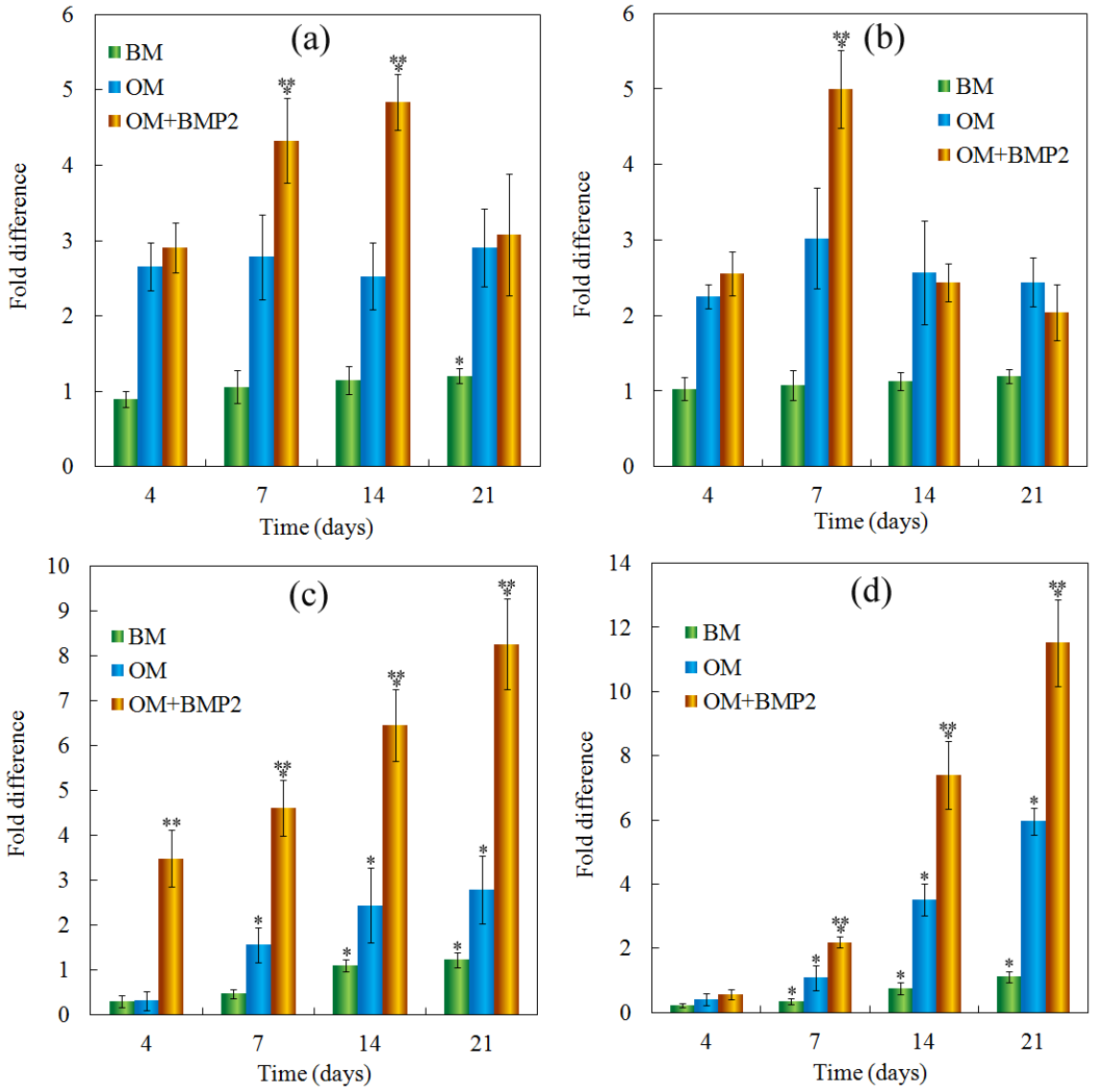

Figure 4.14. mRNA Expression levels, as fold difference, of (a) Dlx5, (b) Runx2, (c) OP, and (d) OC of MSCs encapsulated in SPELA-14.8 hydrogels. Experimental groups include gels with MSCs incubated in basal media (BM, green, control), gels with MSCs incubated in osteogenic media (OM, blue), and gels with MSCs and BMP2 incubated in osteogenic media (OM+BMP2, orange). One star indicates statistically significant difference (s.d.; $p < 0.05$) between the test time point and the first time point (day 4) in the same group, and two stars indicate significant difference between the test group and all other groups at the same time point. Error bars correspond to means ±1 SD for n = 3.

osteogenic media, whereas those incubated in BM did not undergo osteogenic differentiation. Yang et al. investigated osteogenic differentiation of MSCs encapsulated in RGD-conjugated PEG hydrogels.[114] The calcium content of MSCs with optimum

RGD density after 21 days was 0.00008 mg/mg DNA, compared with 0.057 mg/mg DNA in this work. The higher calcium content in this work may be related to the degradable nature of SPELA matrix, leading to increase in water content, free volume, and greater cell-matrix interaction with incubation time. The addition of inductive factors like BMP2 significantly enhanced differentiation and mineralization of MSCs. Kim et al. reported that the addition of BMP2 to MSCs encapsulated in hyaluronic acid gels increased OC expression by 80%.[255] Na et al. reported that the addition of BMP2 to MSCs encapsulated in poly(N-isopropylacrylamide-co-acrylic acid) gels increased the expression of OC after 8 weeks of incubation.[256]

4.5. CONCLUSION

A novel approach to tissues regeneration is to encapsulate progenitor cells in inert and biodegradable hydrogels loaded with soluble growth factors to guide their differentiation and maturation. To this end, linear (LPELA) and star (SPELA) poly(ethylene glycol-co-lactide) acrylate macromonomers with short lactide segments were synthesized. SPELA hydrogels had significantly higher modulus, lower gelation time, and lower sol fraction compared with LPELA. Mass loss of the SPELA hydrogel depended strongly on the number of lactides per SPELA macromonomer (nL) and showed a biphasic behavior. Molecular dynamic simulations demonstrated that the biphasic behavior mass loss was related to aggregation and micelle formation of the lactide monomers of SPELA in aqueous solution. MSCs encapsulated in SPELA-nL14.8 and incubated in osteogenic media had significantly higher ALPase activity, extent of mineralization, and expression of osteogenic markers compared with those incubated in basal media. The expression of osteogenic markers and extent of mineralization increased

with coencapsulation of BMP2 with MSCs in the SPELA hydrogel and incubation in osteogenic media when compared to without BMP2. Results demonstrate that the PEG-based SPELA hydrogels are potentially useful as a degradable matrix for MSCs in tissue regeneration.

CHAPTER 5

NANOSTRUCTURE FORMATION AND TRANSITION FROM SURFACE TO BULK DEGRADATION IN POLYETHYLENE GLYCOL GELS CHAIN-EXTENDED WITH SHORT HYDROXY ACID SEGMENTS

Seyedsina Moeinzadeh, Danial Barati, Samaneh K. Sarvestani, Ozan Karaman, Esmaiel Jabbari *Nanostructure Formation and Transition from Surface to Bulk Degradation in Polyethylene Glycol Gels Chain-Extended with Short Hydroxy Acid Segments*, Biomacromolecules, 2013. ***14****(8): p. 2917-2928*. Reprinted here with permission of publisher.

5.1. INTRODUCTION

Hydrogels are used extensively in medicine for soft tissue repair.[176, 257-259] Due to their high diffusivity of nutrients and biomolecules,[24-26] hydrogels are very useful as a matrix in tissue engineering for *in situ* delivery of cells to the site of regeneration and regulation of cell fate.[21, 29, 30, 41] Only those hydrogels that degrade and provide free volume for the newly formed tissue can be utilized as a matrix in regenerative medicine.[101, 102] However, viability and fate of the encapsulated cells are limited by toxic side effects of gelation and degradation reactions in the hydrogel matrix. Consequently, natural hydrogels derived from the components of extracellular matrix (ECM) of biological tissues that physically crosslink and degrade enzymatically are frequently used as the delivery matrix in clinical applications.

Minor variation in the sequence distribution of natural gels can dramatically affect the fate of encapsulated cells. With many cell-interactive ligands and regulatory factors, it is difficult to tailor the properties of natural matrices to a particular application in regenerative medicine.[31] For example, differentiation of mesenchymal stem cells (MSCs) shifted from osteogenic to chondrogenic lineage by changing the matrix from collagen type I to type II.[32, 33] Moreover, due to their low stiffness, natural gels are limited in practical applications by soft tissue compression.[34-36] Therefore, there is a need to synthesize novel hydrogels with tunable physical, mechanical, and biological properties for a wide range of applications in regenerative medicine such as chondrocyte implantation in cartilage regeneration or as cardiac patches to treat heart infarction.

Polyethylene glycol (PEG) hydrogels are inert, non-immunogenic, and compatible with stem cells and can be conjugated with multiple bioactive peptides to modify the cell

microenvironment and regulate cell fate.[112-114] However, PEG hydrogels are non-degradable which limits their use as a supporting matrix in regenerative medicine. PEG macromonomers copolymerized with hydroxy acid (HA) monomers produce block copolymers that have limited solubility in aqueous solution[35] and self-assemble to form nanoparticles for drug delivery.[260-266] We previously demonstrated that star PEG macromonomers chain-extended with very short hydrolysable lactide segments (SPELA) dissolved in aqueous solution and formed a micellar gel.[35] Remarkably, the results showed a biphasic relationship between the lactide segment length and gelation or degradation rate. We hypothesized that the observed biphasic dependence was related to the transition from surface to bulk hydrolysis in the micelle phase with increasing lactide segment length. To test the hypothesis, we investigate in this work gelation and degradation of star PEG macromonomers chain-extended with short hydroxy acid (HA) segments (SPEXA where "X" is HA monomer type) with a wide range of hydrophobicity. HA monomers included least hydrophobic glycolide (G), lactide (L), p-dioxanone (D), and most hydrophobic ε-caprolactone (C). All HA chain-extended PEG hydrogels showed the transition from surface to bulk degradation with increasing HA segment length. Chain extension of PEG macromonomers with short HA segments localized the reactive moieties within micelles and reduced their average distance, thereby increasing gelation and degradation rates with increasing segment length. As the micelle size was increased above a certain value, the average distance between the reactive moieties within the micelles began to increase and degradation rates decreased.

5.2. SIMULATION METHOD

Solution of SPEXA macromonomers in water was simulated via Dissipative Particle Dynamics (DPD) using an approach described previously.[35, 60] The molecular structure of the macromonomer was divided into different beads with equal mass, as shown in Figure 5.1. The beads included L (lactide repeat unit), G (glycolide), D (p-dioxanone), C (ε-caprolactone), EO (ethylene oxide repeat unit), Ac (acrylate functional group), SPEGc (star PEG core), and W (three water molecules). The meso-structure of the macromonomer is also shown in Figure 5.1. The notations SPEXA-nA or SPEXA-mB are used to identify length of the degradable segment, where A is the number of repeat units or ester groups per arm, B is the number of monomers per arm, and X is HA monomer type (G, L, D, and C). When X is C or D, A equals B but A=2B when X is G or L. In DPD, each bead represents a soft particle interacting with the other beads via a soft pairwise force function given by[242, 243]

$$f_{ij} = \sum_{i \neq j} F_{ij}^{C} + F_{ij}^{D} + F_{ij}^{R} + F_{ij}^{S} \qquad \text{(equation 5.1)}$$

where f_{ij} is the total force and F_{ij}^{C}, F_{ij}^{D}, F_{ij}^{R} and F_{ij}^{S} are the conservative, dissipative, random and spring components of the force, respectively. Different components of the force in a cutoff distance (r_c) are calculated by[58]

$$F_{ij}^{C} = \begin{cases} \alpha_{ij}\,(1 - r_{ij})\,e_{ij} & \left|r_{ij}\right| < 1 \\ 0 & \left|r_{ij}\right| \geq 1 \end{cases} \qquad \text{(equation 5.2)}$$

$$F_{ij}^{D} = -\gamma\ [\,w^{D}(\left|r_{ij}\right|)]\ (e_{ij}.v_{ij})\ e_{ij} \qquad \text{(equation 5.3)}$$

$$F_{ij}^{R} = \sigma\ [\,w^{R}(\left|r_{ij}\right|)]\ \theta_{ij}\ e_{ij} \qquad \text{(equation 5.4)}$$

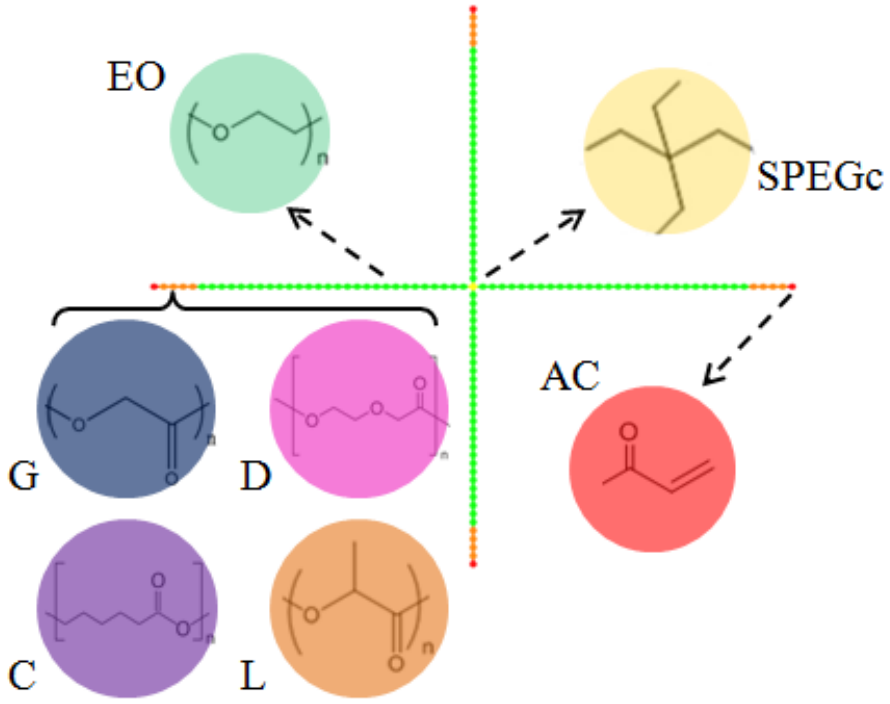

Figure 5.1. Bead reperesentation of SPEXA (X= L, G, C or D) macromonomer in DPD. Beads SPEGc (yellow), EO (green), G (blue), D(pink), L (orange), C (purple) and Ac (red) represent star PEG core, ethylene oxide repeat unit, glycolide, p-dioxanone, lactide, ε-caprolactone repeat unit, and acrylate functional group, respectively.

$$F_{ij}^{S} = \sum_{j} C r_{ij} \qquad \text{(equation 5.5)}$$

where r_{ij} is the vector joining bead i to j, e_{ij} and $|r_{ij}|$ are the unit vector in the direction of r_{ij} and the magnitude of r_{ij}, respectively. v_{ij} is the velocity vector given by $v_{ij} = v_i - v_j$. w^D and w^R are weight functions for dissipative and random forces, respectively, and γ, σ are the magnitude of dissipative and random forces. F_{ij}^{D} and F_{ij}^{R} act simultaneously to preserve dissipation and to conserve the total momentum in the system. The dissipative and random force constants and weight functions are interrelated by $w^D(r_{ij}) = [w^R(r_{ij})]^2$ and $\sigma^2 = 2 k_B T \gamma$ in order to satisfy the dissipation-fluctuation condition.[244] The

spring force term imposes geometrical constraints on the covalently bonded beads. Values of γ and C constants were 4.5 and 4, respectively.[60] The repulsion between beads i and j is mainly dictated by the constant α_{ij} in the conservative force function. By choosing the system density $\rho = 3\ r_c^{-3}$, the DPD length scale, r_c, was 6.74 Å and the values of α_{ij} were determined using[58]

$$\alpha_{ij} = 78 + 3.27\chi_{ij} \qquad \text{(equation 5.6)}$$

where χ_{ij} is the Flory-Huggins parameter between beads i and j. Values of χ_{ij} in turn are given by

$$\chi_{ij} = \frac{(\delta_i - \delta_j)^2 V}{RT} \qquad \text{(equation 5.7)}$$

where δ_i and δ_j are solubility parameters of beads i and j, respectively, V is bead molar volume, T is absolute temperature, and R is gas constant. Solubility parameters were calculated via atomistic molecular dynamics simulation performed via Forcite and Amorphous Cell modules, Materials Studio (v5.5, Accelrys)[267] using the COMPASS force field, which is an *ab initio* force field optimized for condensed-phase systems.[245] Position and velocity of the beads at each time point were obtained by solving the following equations of motion using the force function (equation 5.1).

$$\frac{dr_i}{dt} = v_i \quad , \qquad m_i \frac{dv_i}{dt} = f_i \qquad \text{(equation 5.8)}$$

All DPD simulations were performed in $30 \times 30 \times 30$ r_c boxes with 3D periodic boundary conditions over 2×10^5 time steps and dimensionless time step of 0.05. The

Mesocite module of Materials Studio (v5.5, Accelrys)[267] was used for DPD calculations.

5.3. EXPERIMENTAL METHODS

5.3.1. MATERIALS

Lactide (L), glycolide (G) and p-dioxanone (D) monomers with >99.5% purity were purchased from Ortec (Easley, SC). ε-Caprolactone (C) monomer with >99% purity was purchased from Alfa Aesa (Ward Hill, MA). All monomers were dried under vacuum at 40°C for at least 12 h prior to use. 4-(2-hydroxyethoxy)phenyl-(2-hydroxy-2-propyl) ketone (Irgacure-2959) photoinitiator was obtained from CIBA (Tarrytown, NY). Calcium hydride, tetrahydrofuran (THF), deuterated chloroform (99.8% deuterated), trimethylsilane (TMS), triethylamine (TEA), tin (II) 2-ethylhexanoate (TOC), acryloyl chloride (Ac) , dimethylsulfoxide (DMSO), 4-arm PEG (SPEG, 4 arm, nominal Mw=5 kDa), ethylenediaminetetraacetic acid disodium salt (EDTA), and paraformaldehyde were purchased from Sigma-Aldrich (St. Louis, MO). The protected amino acids and Rink Amide NovaGel resin for the synthesis of acrylamide-terminated GRGD peptide were purchased from EMD Biosciences (San Diego, CA). Dichloromethane (DCM, Acros Organics, Pittsburgh, PA) was dried by distillation over calcium hydride. Other solvents were obtained from VWR (Bristol, CT) and used as received. Dulbecco's phosphate-buffer saline (PBS) and Dulbecco's Modified Eagle's Medium (DMEM; 4.5 g/L glucose with L-glutamine and without sodium pyruvate) were obtained from GIBCO BRL (Grand Island, NY). Fetal bovine serum (FBS), screened for compatibility with rat MSCs, was purchased from Atlas Biologicals (Fort Collins, CO). TRIzol for isolation of cellular RNA and trypsin were purchased from Invitrogen (Carlsbad, CA). Penicillin (PN),

streptomycin (SP), fungizone (FG), gentamicin sulfate (GS), dexamethasone (DEX), ascorbic acid (AA), and ß-sodium glycerophosphate (GP) were purchased from Sigma-Aldrich. Quant-it PicoGreen dsDNA reagent kit was obtained from Invitrogen (Carlsbad, CA). QuantiChrom calcium and alkaline phosphatase (ALP) assay kits were purchased from Bioassay Systems (Hayward, CA). Sircol total collagen assay kit was obtained from Biocolor (Carrickfergus, UK).

5.3.2. CHARACTERIZATION

The chemical structure of SPEXA macromonomers was characterized by a Varian Mercury-300 ^{1}H-NMR (Varian, Palo Alto, CA) at ambient conditions with a resolution of 0.17 Hz as described previously.[35] The sample was dissolved in deuterated chloroform at a concentration of 50 mg/ml, and 1% v/v TMS was used as the internal standard. Number- (M_n) and weight-average molecular weight (M_w) and polydispersity index (PI) of the macromonomers were measured by Gel Permeation Chromatography (GPC, Waters 717 System, Milford, MA) in THF with 1 mL/min flow rate as previously described.[52]

5.3.3. MACROMONOMER SYNTHESIS

SPEG macromer chain-extended with short HA segments was synthesized by ring opening polymerization (ROP) as described.[35] SPEG and TOC were the polymerization initiator and catalyst, respectively. Briefly, dry HA monomer and SPEG were added to a three-neck reaction flask with an overhead stirrer and immersed in an oil bath (only SPEG was added to the flask for D monomer). Molar ratio of SPEG to monomer was selected based on the desired theoretical length of the HA segment. Next, the reaction flask was heated to 120°C under nitrogen to melt the mixture, maintained at

that temperature for 1 h to remove moisture, and TOC was added to the mixture. The reaction was run at 140°C for 12 h for C and L monomers and 160°C for 10 h for G monomer. Since equilibrium was shifted toward monomer in polycondensation of p-dioxanone for temperatures >100°C, SPEG and catalyst mixture was heated to 130°C for 10 min to remove moisture, the mixture was cooled to 85°C, D monomer was added, and reaction was run at that temperature for 48 h. After the reaction, the product was purified by precipitation in ice-cold hexane to remove any unreacted monomer, initiator and catalyst.

In the next step, chain ends of the macromer were acrylated to produce SPEXA macromonomer. SPEX macromer (product of the first reaction) was dried by azeotropic distillation from toluene. The macromer was dissolved in DCM, the flask was immersed in an ice bath, and the reaction was carried out by the addition of equimolar amounts of AC and TEA drop-wise to the macromer solution under dry nitrogen. After 12 h, solvent was removed by rotary evaporation and the residue was dissolved in ethyl acetate to precipitate the byproduct triethylamine hydrochloride salt. After vacuum distilling ethyl acetate, the product was re-dissolved in DCM and precipitated in ice-cold ethyl ether twice. The product was dissolved in DMSO and dialyzed against water in a 3.5 kDa MW cutoff Spectro/Por dialysis tube (Spectrum Laboratories, Rancho Dominquez, CA) to remove any remaining impurities. SPEXA macromonomer was dried in vacuum to remove residual solvent and stored at –20°C.

5.3.4. MACROMONOMER GELATION AND RHEOLOGICAL MEASUREMENTS

The aqueous SPEXA hydrogel precursor solution was crosslinked by UV free-radical polymerization with Irgacure-2959 photoinitiator as previously described.[150]

To monitor gelation kinetics, the hydrogel precursor solution of the photoinitiator and macromonomer on the peltier plate of an AR-2000 rheometer (TA Instruments, New Castle, DE) was irradiated with a long wavelength (365 nm) mercury UV lamp (Model B100-AP; UVP, Upland, CA) at a distance of 10 cm from the sample. The gap distance between the peltier plate and the upper 20 mm transparent acrylic geometry was 500 μm. A sinusoidal shear strain with frequency of 1 Hz and amplitude of 1% was exerted on the sample via the upper geometry and the storage (G') and loss moduli (G'') was recorded with time. The time at which $G' = G''$ was recorded as the gelation time. The notation X-mN is used for the hydrogels with X representing the HA monomer, m for monomer, and N for the number of HA monomers per macromonomer arm. For example, m0 denotes PEG hydrogel without chain extension with HA monomer and C-m1.8 denotes SPECA hydrogel with average of 1.8 ε-caprolactone monomers per macromonomer arm.

5.3.5. MEASUREMENT OF EQUILIBRIUM WATER CONTENT AND MASS LOSS

Hydrogels 20 mm diameter and 300 μm thickness were removed from the rheometer and dried in ambient conditions for 12 h followed by drying in vacuum for 1 h at 40°C. Dry samples were swollen in DI water for 24 h at 37°C with a change of swelling medium every 6 h. After swelling, surface water was removed and the swollen weights (w_s) were measured. The swollen samples were dried as described above and dry weights (w_d) were recorded. The equilibrium water content was calculated by dividing the weight of water (the difference between swollen and dry weights) by the swollen weight as described.[35] To measure mass loss, the hydrogel precursor solution was crosslinked in a polytetrafluoroethylene (PTFE) mold (5 cm × 3 cm × 750 μm) covered with a transparent glass plate. Disk-shape samples were cut from the gel and their mass

loss was measured in 5 mL PBS at 37ºC under mild agitation. At each time point, samples were washed with DI water several times and dried under vacuum. The dried sample weight was measured and compared with the initial dry weight to determine mass loss as described.[35]

5.3.6.MARROW STROMAL CELL ISOLATION AND ENCAPSULATION IN HYDROGELS

MSCs were isolated from the bone marrow of young adult male Wistar rats as described.[35, 268] Cell isolations were performed under a protocol approved by the Institutional Animal Care and Use Committee of the University of South Carolina. The suspension of bone marrow cells was centrifuged at 200g for 5 min and the cell pellets were resuspended in 12 mL basal medium consisting of DMEM supplemented with 10% FBS, 100 units/mL PEN, 100 μg/mL SP, 50 μg/μL GS and 250 ng/mL FZ, and cultured in a humidified 5% CO_2 incubator at 37°C. Cultures were replaced with fresh medium at 3 and 7 days to remove hematopoietic and other unattached cells. After 10 days, cells were detached from the flasks with 0.05% trypsin-0.53 mM EDTA and used for *in vitro* experiments. The experimental groups for encapsulation of MSCs in SPEXA hydrogels included m0, L-m1.7, D-m1.7 and C-m1.8. SPEGA hydrogel was not used for cell encapsulation because it completely degraded in a few days (see Figure 6d). Cell encapsulation and osteogenic differentiation experiments were carried out in SPEXA hydrogels while maintaining a constant compressive modulus of 50 kPa by varying the concentration of SPEXA macromonomer in the hydrogel precursor solution. Acrylamide-terminated GRGD peptide (Ac-GRGD) was synthesized on Rink Amide NovaGel resin in the solid phase, purified by high-performance liquid chromatography (HPLC), and

characterized by electrospray ionization (ESI) mass spectrometry as previously described.[113] Ac-GRGD peptide in the amount of 2 wt%, based on the macromonomer weight, was added to the hydrogel precursor solution to facilitate cell adhesion to SPEXA matrix, and the mixture was sterilized by filtration. Next, 1×10^6 MSCs suspended in 100 μL PBS was gently mixed with the hydrogel precursor solution to reach the final density of 5×10^6 cells/mL. The mixture was injected between two sterile glass slides and crosslinked as described above. UV exposure time for all cell-seeded precursor solutions was 200 s, which was the minimum required time for the gel to reach its plateau modulus. After gelation, samples were incubated in 2 mL PBS for 1 h with two PBS changes. Next, the medium was replaced with complete osteogenic medium (basal medium supplemented with 100 nM DEX, 50μg/mL AA, 10mM GP) and cultured for 28 days. To measure the effect of photoinitiator on cell viability, 10 mg/mL initiator was added to the suspension of MSCs in SPEXA precursor solution. After 10 min, the suspension was centrifuged and cells were re-suspended and cultured in basal medium (without initiator). After incubation for 2 days, MSCs were counted with a hemocytometer and cell numbers were normalized to those cells cultured in PBS (no exposure to initiator).

5.3.7. BIOCHEMICAL ANALYSIS AND MRNA ANALYSIS

At each time point (7, 14, 28 days), gel samples were washed with serum-free DMEM for 8 h to remove serum components, washed with PBS, lysed with lysis buffer (10 mM tris and 2% triton), and sonicated. After centrifugation, the supernatant was used for measurement of total collagen content, alkaline phosphatase (ALP) activity and calcium content. Total collagen content was measured with a Sircol collagen assay based on selective binding of G-X-Y amino acid sequence of collagen to Sircol dye, according

to manufacturer's instructions.[269] Briefly, 1 mL Sircol dye was added to the sonicated cell lysate, incubated for 30 min and centrifuged at 10,000 rpm for 5 min to separate the collagen–dye complex. After removing the supernatant, the collagen-dye complex was mixed with 1 mL Sircol alkali reagent and absorbance was measured on a plate reader at 555 nm. ALP activity and calcium content as a measure of the total mineralized deposit were measured using QuantiChrom ALP and calcium assays as previously described.[199] For mRNA analysis, at each time point, total cellular RNA of the sample was extracted and converted to cDNA as described.[199] The cDNA was amplified with gene specific primers designed using the Primer3 software as previously described.[188] Expression of collagen type I (Col-I), ALP and osteocalcin (OC) was measured by performing real-time quantitative polymerase chain reaction (RT-qPCR) using a CXF96 PCR system (Bio-Rad, Hercules, CA) with the following primers (synthesized by Integrated DNA technologies, Coralville, IA): Col-1: forward 5'-GCA TGT CTG GTT AGG AGA AAC C-3' and reverse 5'-ATG TAT GCA ATG CTG TTC TTG C-3'; ALP: forward 5`CCT TGA AAA ATG CCC TGA AA-3` and reverse 5`-CTT GGA GAG AGC CAC AAA GG-3; OC: forward 5`-AAA GCC CAG CGA CTC T-3` and reverse 5`-CTA AAC GGT GGT GCC ATA GAT-3`; S16: forward 5′-AGT CTT CGG ACG CAA GAA AA-3′ and reverse 5′-AGC CAC CAG AGC TTT TGA GA-3′.[269] The expression ratio of the gene of interest to that of S16 housekeeping gene was determined using Pfaffl model[241] and normalized to the first time point.

5.3.8. STATISTICAL ANALYSIS

Data are expressed as means ±standard deviation. All experiments were done in triplicate. Significant differences between groups were evaluated using a two-way

ANOVA with replication test followed by a two-tailed Student's t-test. A value of $p<0.05$ was considered statistically significant.

5.4. RESULTS AND DISCUSSION

5.4.1. CHARACTERIZATION OF MACROMONOMERS

^{1}H-NMR spectra of star-PEG (m0), SPEGA (G-m2.8), SPEDA (D-m2.9), SPELA (L-m2.9) and SPECA (C-m2.8) are provided in Figures 5.2.a to 5.2.e, respectively. The assignment of chemical shifts for PEG macromer in the NMR spectra of lactide chain-extended SPEXA was previously described by us.[35] The shifts with peak position at 3.6 and 4.3 ppm in Figure 5.2(a-e) corresponded to methylene protons of PEG attached to ether and ester groups of HA repeat units, respectively. The shifts with peak position at 4.8-4.9 ppm in Figure 5.2.b corresponded to methylene protons of glycolide; those at 3.7, 4.2 and 4.4 ppm in Figure 5.2.c corresponded to β, α, γ methylene protons of p-dioxanone, respectively; those at 1.6 and 5.2 ppm in Figure 5.2.d corresponded to methyl and methine protons of lactide; and those at 1.4, 1.7, 2.3 and 4.1 ppm in Figure 5.2.e corresponded to γ, β, α, ε ethylene protons of ε-caprolactone. The shifts with peak position from 5.85 to 6.55 ppm were attributed to vinyl hydrogens of the Ac as follows: peak positions in the 5.82-5.87 ppm range corresponded to the trans protons of unsubstituted carbon in Ac; those in the 6.10-6.20 ppm range corresponded to the protons bonded to monosubstituted carbon; and those in the 6.40-6.46 ppm range corresponded to the proton of unsubstituted carbon. The number of HA repeat units per macromonomer (m) was determined from the ratio of the shifts centered at 4.8-4.9 ppm (glycolide hydrogens), 3.7, 4.2 and 4.4 ppm (p-dioxanone), 1.6 and 5.2 ppm (lactide) and 1.4, 1.7, 2.3 and 4.1 ppm (ε-caprolactone) to those at 3.6 and 4.3 ppm (PEG). The number of

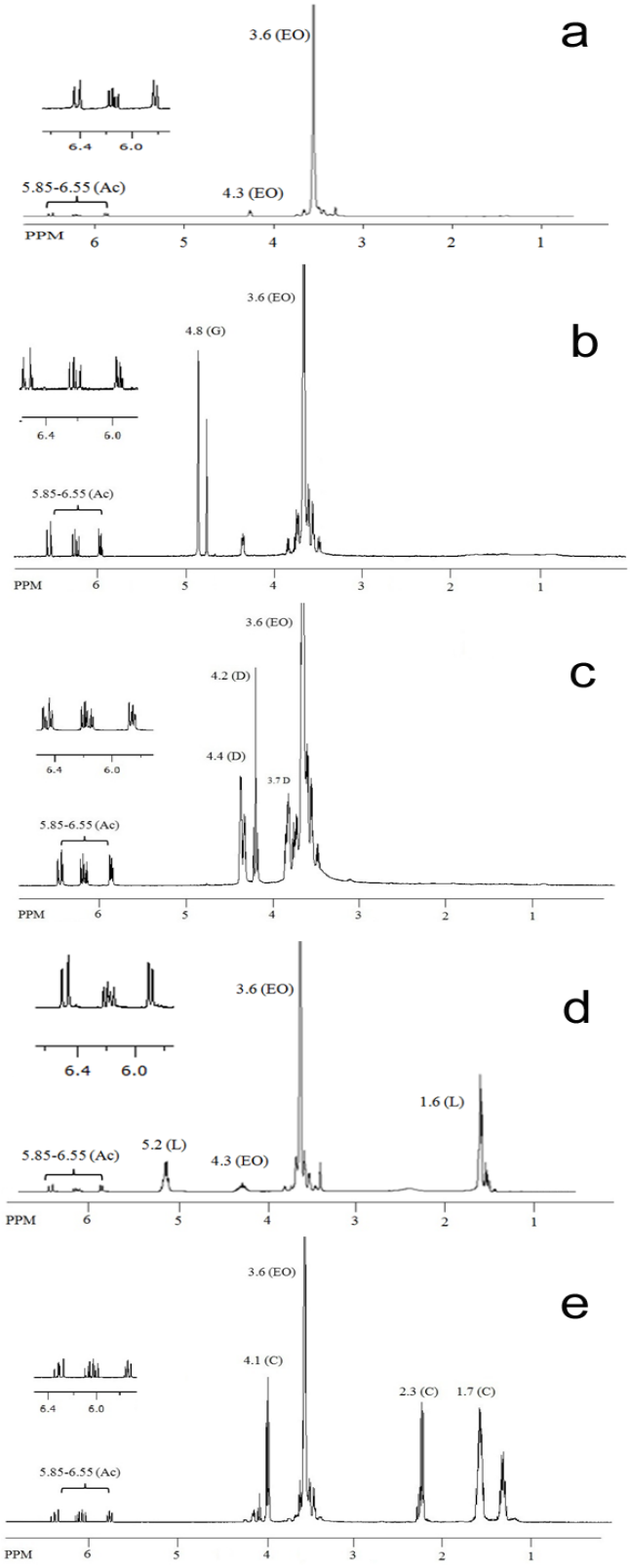

Figure 5.2. H-NMR spectra of (a) star PEG, (b) SPEGA (G-m2.8), (c) SPEDA (D-m2.9), (d) SPELA (L-m2.9) and (e) SPECA (C-m2.8).

acrylate groups per macromonomer was determined from the ratio of the shifts between 5.85 and 6.55 ppm (acrylate hydrogens) to those at 3.6 and 4.2 ppm (PEG). $\overline{M_n}$ of SPEGA, SPELA, SPEDA, and SPECA macromonomers depending on HA segment length was in the range of 5.6-6.5 kDa, 5.8-7.4 kDa, 5.4-6.3 kDa and 5.5-6.4 kDa, respectively, and the corresponding fraction of acrylated chain-ends was in the range of 0.78-0.87, 0.75-0.86, 0.73-0.82 and 0.75-0.85. Polydispersity of SPEGA, SPELA, SPEDA, and SPECA macromonomers was in the range of 1.24-1.44, 1.17-1.34, 1.20-1.35 and 1.22-1.38 respectively.

5.4.2. STRUCTURE FORMATION IN SPEXA PRECURSOR SOLUTIONS

Formation of nanoscale structure by SPEXA macromonomers in aqueous medium is shown in Figure 5.3. In the absence of HA monomer, the distribution of acrylate groups attached to SPEXA chain ends was uniform in aqueous medium[60] but the extension of SPEXA arms with hydrophobic X segments induced aggregation as shown in Figure 5.3. For SPEGA and SPEDA with n=2, hydrophobic segments were not sufficiently long to form stable micellar structures. However, SPELA and SPECA macromonomers (see first column of Figure 5.3), due to higher hydrophobicity of lactide and ε-caprolactone monomers, formed stable micelles with n=2. All four SPEXA macromonomers formed stable micelles for n=4 (second column of Figure 5.3). The aggregate size increased and number density decreased with increasing n from 4 to 8. According to the theory of micellization in block copolymers in solution, degree of aggregation increases with increasing block size, driven by the decrease in overall surface free energy of solvophobic blocks.[270] Cross-sectional view of one of the aggregates along with its EO beads is shown in Figure 5.4 for different number of HA repeat units.

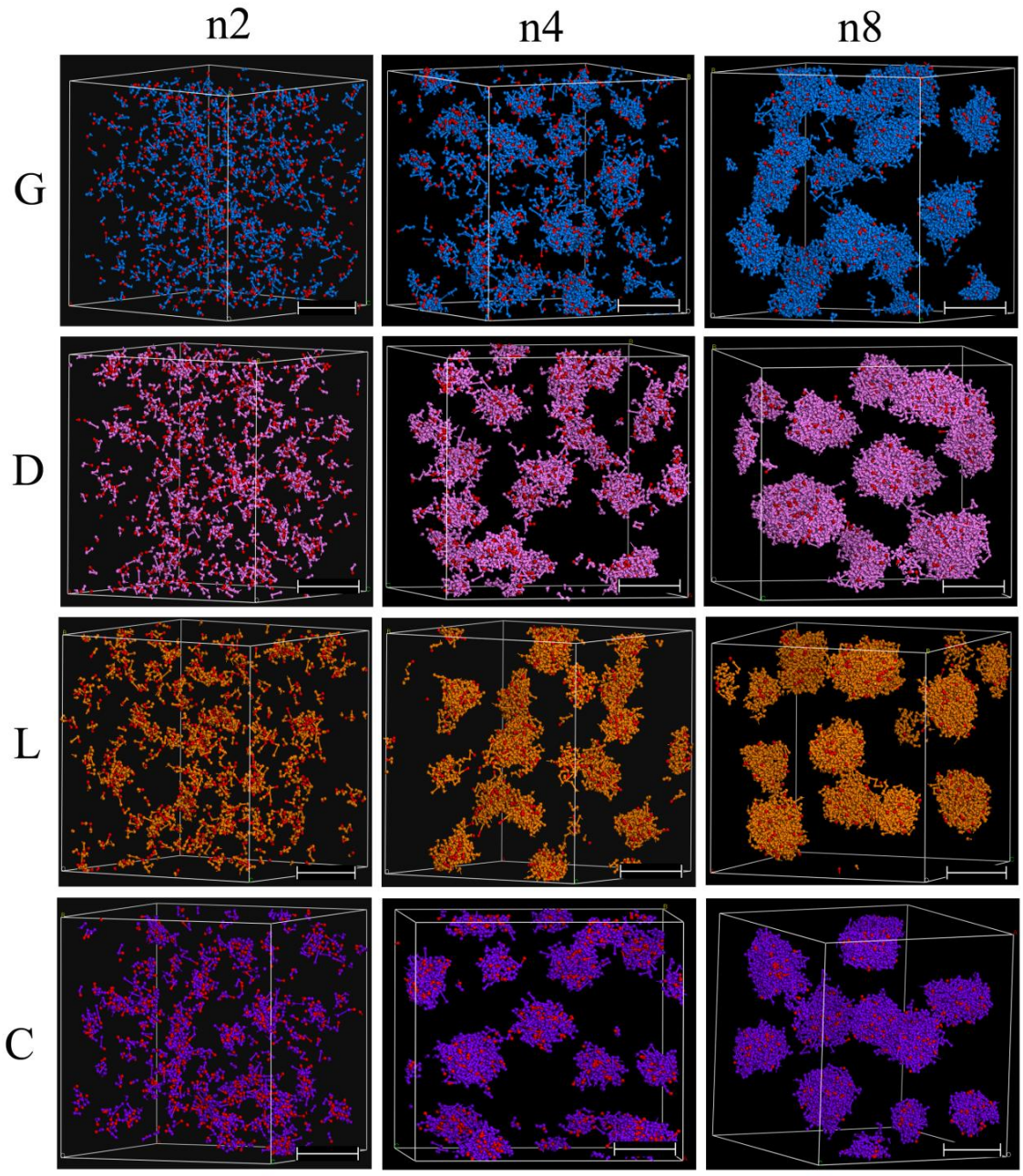

Figure 5.3. Evolution of core of the micelles in 20% aqueous solutions of SPEXA. Only X and Ac (red) beads are shown for clarity. “n” is the number of HA repeat units. G, D, L and C beads are shown by blue, pink, orange and purple, respectively. The scale bars are 5 nm.

In the images of Figure 5.3, hydrophobic HA segments and hydrophilic EO beads formed the core and corona of the micelles, respectively. In our previous work, we showed that a

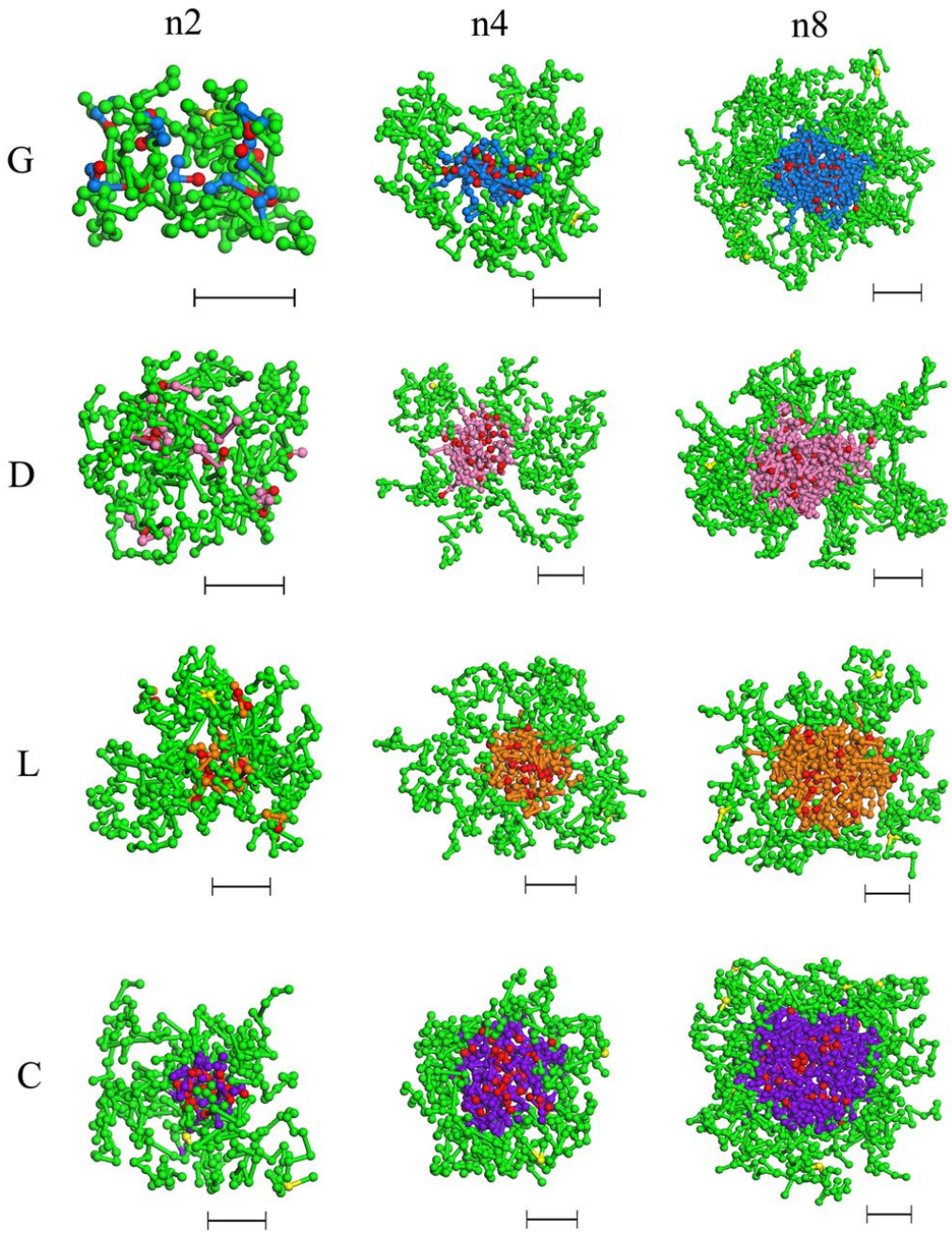

Figure 5.4. Cross section of the micelles formed in 20% aqueous solutions of SPEXA. "n" is the number of HA repeat units. SPEGc, EO and Ac beads are shown by yellow, green and red, respectively. G, D, L and C beads are shown by blue, pink, orange and purple, respectively. Water beads are not shown for clarity. The scale bars are 2 nm.

change in core size and aggregation number for SPELA micelles is dominated by interfacial free energy (the product of interfacial tension γ and interface area a).[60] Due to the presence of hydrophilic EO segments at the interface, the effective interfacial

tension in SPEXA micelles is different from the interfacial tension between the micelle core and water, γ_{C-W}.[249] γ can be calculated by minimizing the chemical potential of the aqueous solution at equilibrium[271]

$$\gamma = \gamma_{C-W} + \frac{kT}{s^2}\left[\ln\frac{1-C_i}{1-C_b} - \frac{N-1}{N}(C_i - C_b) + \chi_{W-EO}(\frac{1}{2}C_i^2 - \frac{3}{4}C_b^2)\right] \qquad \text{(equation 5.9)}$$

where γ_{C-W} is interfacial tension between the micelles' core and water, k, T, s and N are Boltzmann constant, absolute temperature, statistical EO segment length, and number of statistical EO segments on each SPEXA arm. C_i and C_b are concentrations of EO segments at the interface and in bulk, respectively. Equation 5.9 implies that an increase in C_i has a negative contribution to interfacial tension. In other words, dense EO coverage of the interface decreases effective interfacial tension between the hydrophobic domains and water. According to Figure 5.4, the micelle core size of SPECA macromonomers with n=8 was similar to that of other monomers even though ε-caprolactone was significantly more hydrophobic than the other monomers. This discrepancy can be explained by higher packing of EO segments in the corona, thus decreasing the effective interfacial tension of SPECA micelles.

Effect of number of hydrophobic X beads on core diameter of micelles, number of macromonomers per micelle (aggregation number), number density of micelles, and fraction of macromonomer free arms is shown in Figures 5.5.a to 5.5.d, respectively. Assuming there were only X and Ac beads in the core, total number of beads taking part in core formation per macromonomer equals $4(n+1)$ and aggregation number is[60]

$$n_{agg} = \frac{\rho V_c}{4(n+1)} \qquad \text{(equation 5.10)}$$

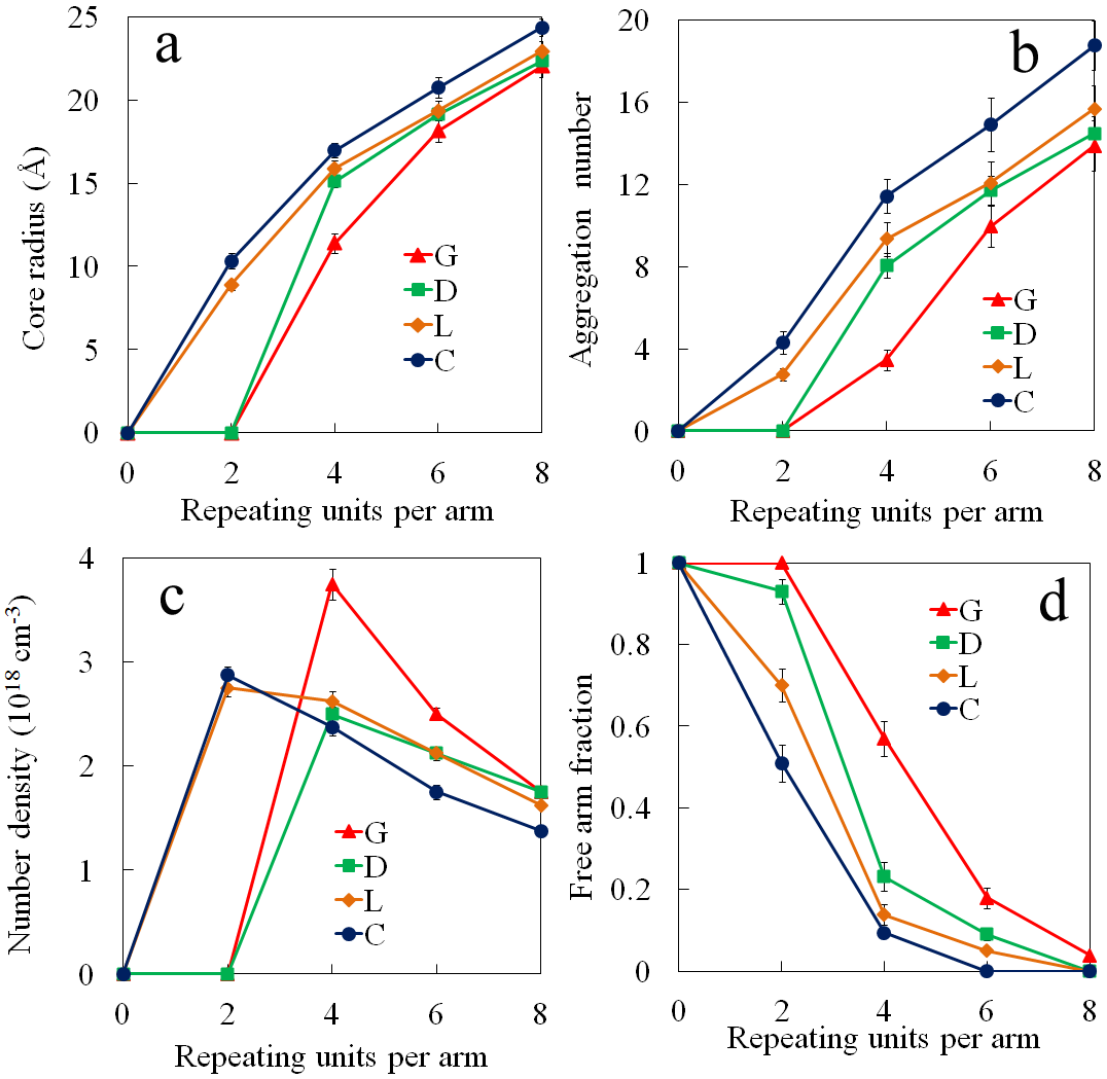

Figure 5.5. Effect of number of degradable HA repeat units on each arm on (a) core radius (a), aggregation number (b), number density of micelles (c) and free arm fraction of the micelles (d) in 20% aqueous solutions of SPEXA. Error bars correspond to means ± SD for 5 simulation runs.

where ρ and V_c are bead number density and micelle core volume, respectively. Core radius of SPEGA and SPEDA micelles increased from 0 to 22 Å when n increased from 2 to 8. Core radius of SPELA and SPECA micelles increased from 9 and 11 Å to 23 and 24 Å, respectively, with increasing n from 2 to 8. Aggregation number showed an increasing trend with n after micelle formation (n=2 for L and C and n=4 for G and D). Average

aggregation number of SPECA increased from 4 to 19 when n increased from 2 to 8 which was the highest aggregation number among the four macromonomers. SPEGA had the lowest aggregation number, which ranged from 0 to 14 when n increased from 2 to 8. The increase in SPEXA aggregation number with increasing n is attributed to the increase in the volume of hydrophobic segments and the decrease in corona thickness of micelles, leading to an increase in effective interfacial tension between the core and water with increasing n.[60]

Number density of micelles initially increased with n due to a transition from uniform distribution of macromonomers in the system to the formation of micelles. The number density then decreased with n due to the increase in size and aggregation number of micelles. Figure 5.5.d shows the effect of number of HA monomers on each arm (n) on the fraction of free arms. For n=0, acrylate groups were uniformly distributed in solution and fraction of free arms was unity. Fraction of free arms for SPELA decreased from 1 to 0.70, 0.14, 0.05 and zero as n increased from zero to 2, 4, 6 and 8, respectively, whereas for SPEDA it decreased from 1 to 0.93, 0.23, 0.09 and zero. Fraction of free arms decreased at a faster rate for SPECA and reached zero for n=6. SPEGA macromonomers with $n \leq 2$ did not form micelles and had a free arm fraction of unity, and fraction of SPEGA free arms decreased to 0.57, 0.18 and 0.04 as n increased from 2 to 4, 6 and 8, respectively. The slower rate of decrease in fraction of free arms in SPEGA was consistent with lower hydrophobicity of glycolide compared to the other monomers.

5.4.3. GELATION KINETICS OF SPEXA PRECURSOR SOLUTION

Rate of crosslinking of SPEXA macromonomers in aqueous solution depended on the proximity of acrylate groups to photo-activated acrylates while the rate of photo-

activation of acrylates depended on the proximity of initiator molecules to acrylate groups. Therefore, rate of crosslinking depended on average distance between the acrylates and initiator molecules. Distribution of photoinitiator beads (pink color) in SPELA-m3 solution and cross-section of one of the micelle cores are shown in Figures 5.6.a and 5.6.b, respectively. Simulation images indicate that 98% of the photoinitiator beads partitioned to the hydrophobic core of the micelles in the proximity of acrylates (see pink beads in Figures 5.6.a and 5.6.b). The simulated fraction of initiators in the aqueous phase (those not partitioned to the micelles' core) in SPELA solutions is shown in Figure 5.6.c. Fraction of initiators in the aqueous phase decreased from 100% to 7.4, 3.3 and 2% when m increased from 0 to 1, 2 and 3, respectively. Partition of a large fraction of initiators to the micelles' core confined the gelation reaction to the micelle phase, thus potentially reducing the exposure of encapsulated cells to toxic initiator molecules. MSCs in 20 wt% SPEXA solutions were exposed to 10 mg/mL photoinitiator for 10 min, the cells were re-suspended in basal medium (without initiator) and cultured for 2 days. Figure 5.6.d compares the normalized cell numbers for SPEXA solutions after exposure to photoinitiator to that in SPEXA-m0 (acrylated star PEG without HA chain-extension). Groups included SPEGA (G-m1.6), SPELA (L-m1.7), SPEDA (D-m1.7), SPECA (C-m1.8) and PEG (m0). The cell number was significantly higher for SPELA (0.87±0.04) and SPECA (0.84±0.05) solutions compared to SPEXA-m0 (0.77±0.05) which can be explained by partitioning of initiator molecules to the hydrophobic micelle phase (see Figure 5.6.c), whereby the exposure of encapsulated cells to initiator molecules was reduced.

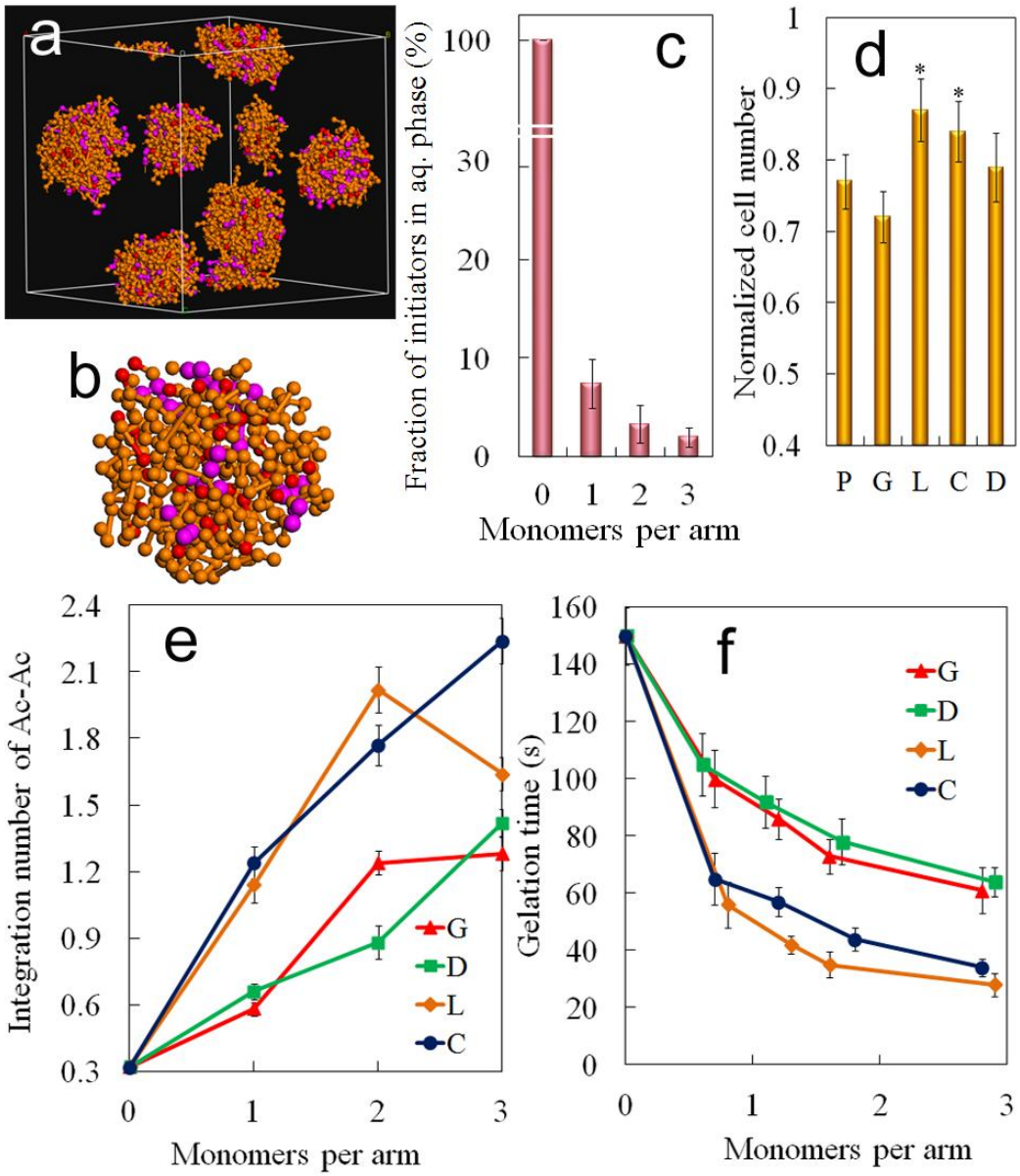

Figure 5.6. (a) Distribution of photoinitiator molecules in the simulation box in SPELA-m3 precursor solution and (b) in the corresponding cross-section of one of the micelles. L and Ac beads in (a-b) are shown in orange and red, respecctively, while the initiator bead is in purple. EO and water beads are not shown for clarity. (c) DPD simulation of the effect of number of degradable lactide monomers per SPELA arm on fraction of initiators in aqueous solution. (d) Effect of exposure of MSCs to photoinitiator (10 mg/mL) in 20 wt% SPEXA precursor solution on the fraction of viable cells as a function of HA type. P, G, L, C and D in (d) represent PEG (no HA, control group), SPEXA with glycolide, lactide, ε-caprolactone and p-dioxanone HA monomer, respectively. "star" indicates a statistically significant difference between the test group and P. (e) Effect of number of degradable HA monomers per arm on simulated Ac-Ac running integration number and (f) experimental gelation time of 20% SPEXA precursor solutions.

Micelle formation sharply reduced the average inter-acrylate and acrylate-initiator distance, leading to a significant increase in the rate of initiation and propagation of the acrylates. To quantify the average inter-acrylate distance (related to crosslinking rate) or proximity of water beads to ester groups on SPEXA macromonomers (related to hydrolytic degradation rate), the average number of Ac (or W) beads in a sphere of radius R around an Ac (or ester) bead or the running integration number of beads "a" around beads "b", $IN_{ab}(R)$ was calculated by[248]

$$IN_{ab}(R) = 4\pi\rho_{b0}\int_0^R g_{ab}(r)\, r^2 dr \qquad \text{(equation 5.11)}$$

where ρ_{b0} is overall number density of type "b" beads and $g_{ab}(r)$ is radial distribution function of bead "b" around bead "a", located at the origin. The running integration number of Ac-Ac beads in SPELA solutions (IN_{Ac-Ac}) at $R = r_c$ (the DPD length scale 6.74 Å, see Methods section) initially increased with increasing m from 0 to 2, as shown in Figure 5.6.e, and then decreased as m increased from 2 to 3. Conversely, a unimodal increase in IN_{Ac-Ac} was observed for SPEGA, SPECA and SPEDA solutions with increasing m from 0 to 3. The increase in IN_{Ac-Ac} with m was attributed to a decrease in average Ac-Ac distance in the micelles' core. As the core of the micelles continued to increase in size and their separation distance continued to increase for m>2, average distance between the Ac beads began to increase, leading to a decrease in IN_{Ac-Ac}, as predicted for SPELA in Figure 5.6.c. Furthermore, SPELA and SPECA macromonomers had higher IN_{Ac-Ac} than SPEGA and SPEDA for $m \le 3$. The predicted IN_{Ac-Ac} values are related to gelation time of the macromonomers in aqueous solution. Gelation time of

20 wt% SPEXA solutions was measured with a rheometer as a function of number of HA monomers per arm and the results are shown in Figure 5.6.f. Gelation times of SPELA and SPECA precursor solutions were shorter than those of SPEGA and SPEDA, as predicted by simulation (see Figure 5.6.e). Gelation time of 20 wt% SPEGA, SPEDA, SPELA and SPECA solutions decreased from 150 s to 61, 64, 28 and 34 s, respectively, with increasing m from 0 to 3 (see Figure 5.6.f). The initial sharp decrease in gelation time was attributed to aggregate formation and an increase in IN_{Ac-Ac}. Simulation results in Figure 5.6.e predict that the IN_{Ac-Ac} value for SPELA should decrease for m>2. However, a decrease in IN_{Ac-Ac} for SPELA at higher m values was offset by an increase in residence time of the arms in the micelle core, leading to no change in gelation time. Residence time of a hydrophobic segment in the micelle core is proportional to[249, 272]

$$\tau \sim \gamma . n^{2/3} \qquad \text{(equation 5.12)}$$

where γ is effective interfacial tension between the hydrophobic domains and water. As a result, residence time of the unreacted Ac groups in the micelles' core increased with n, which increased the rate of crosslinking, thereby gelation time was reduced. Furthermore, fraction of bridging arms between micelles increased with increasing residence time, which in turn increased the extent of physical gelation. Therefore, gelation time of the macromonomer solutions continued to decrease with increasing n.

5.4.4. DEGRADATION OF SPEXA HYDROGELS

Degradation of SPEXA hydrogels depended on the proximity of water beads to ester links on HA segments. Local distribution of water beads around hydrophobic cores of SPEXA-n4 micelles is shown in Figure 5.7.g. Water beads were in close proximity to G beads in SPEGA solution. The relatively small size of G cores along with lower

hydrophobicity of G beads compared to other HA monomers led to a short average distance between G and W beads. when SPEGA was replaced with SPELA, size of the micelles' core increased and local concentration of W beads around the core decreased (Figure 5.7.g, see image "L"), thereby increasing the average L-W bead distance. A dip in the concentration of W beads observed proximal to the micelle core in SPELA was attributed to the higher hydrophobicity of L beads, compared to G, leading to a higher packing of EO beads at the core-water interface. Concentration of W beads proximal to the micelles' core increased by exchanging SPELA with SPEDA but core size in SPEDA was significantly larger than SPEGA. The lowest concentration of W beads at the core margins was observed for SPECA micelles where the higher hydrophobicity of C cores compared to other HA monomers overcame the energy of chain extension and forced EO beads to undergo high-entropy packing at the core-water interface by repelling water beads from the interfacial layer.

The running integration number of water beads around ester links, $IN_{ester-W}$, for SPEXA macromononers (data not shown) initially increased with the addition of one monomer to SPEXA-m0. Then, $IN_{ester-W}$ decreased for all SPEXA solutions with m>1 due to increase in micelle size and decrease in total micelle surface area. SPEGA and SPECA solutions had the highest and lowest $IN_{ester-W}$ for all m values, respectively. However, degradation rate of SPEXA hydrogels depended on the density of ester groups as well as proximity of ester groups to water beads. Assuming that the formation of carboxylic acid groups by ester dissociation did not affect hydrolysis rate (this is a good assumption since degradation was performed in a buffered aqueous medium), the relative

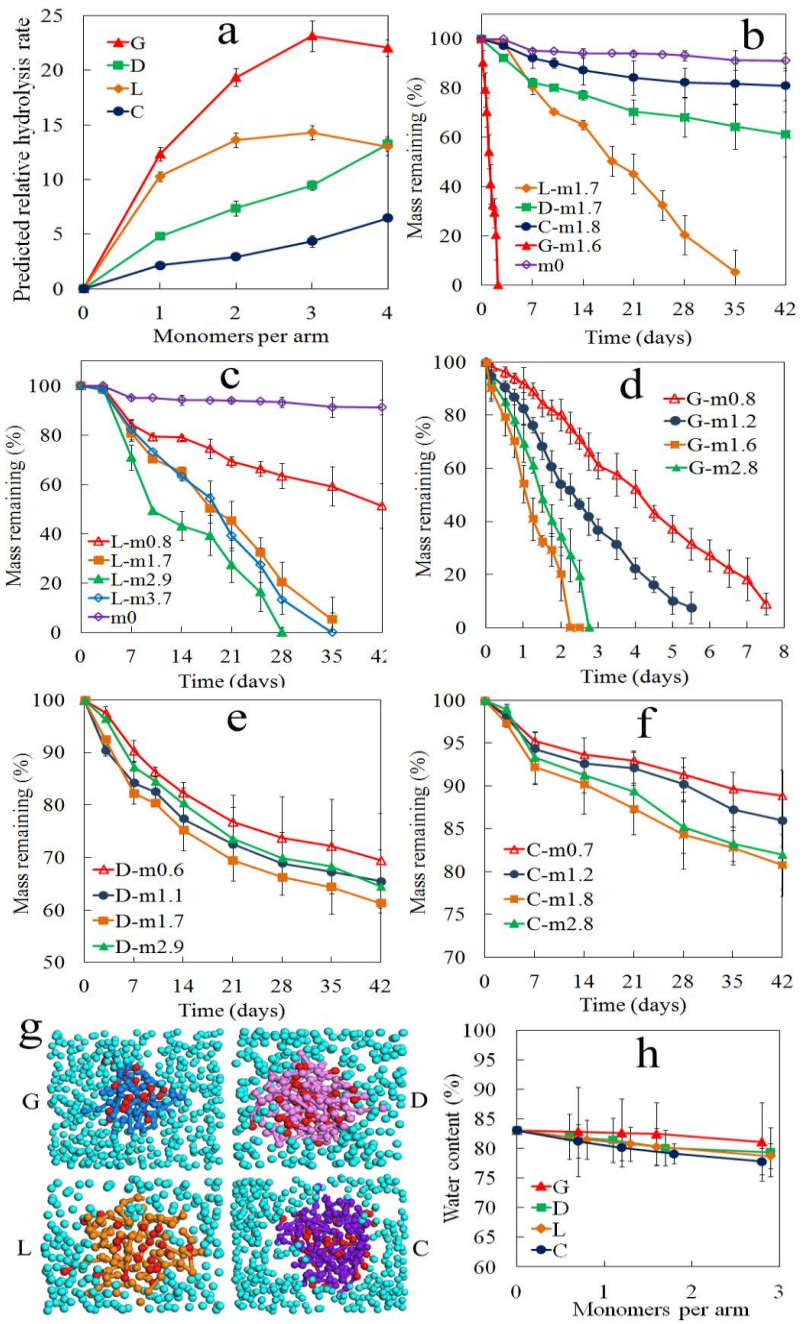

Figure 5.7. (a) Effect of number of HA monomers per arm (m) on predicted hydrolysis rate of 20 wt% SPEXA precursor solutions. (b) Effect of HA monomer type on experimental mass loss of SPEXA hydrogels with incubation time. (c-f) Effect of number of HA monomers per macromonomner on experimental mass loss of SPELA, SPEGA, SPEDA and SPECA hydrogels, respectively, with incubation time. (g) Effect of degradable HA monomer type on distribution of water beads around core of the micelles. (h) Effect of number of HA monomers per arm on experimentally-measured equilibrium water content of SPEXA hydrogels. In (g), G, D, L, C, Ac and water beads are shown by

blue, pink, orange, purple, red and light blue, respectively, and EO beads are not shown for clarity.

hydrolysis rate (P) at the mesoscale scale, which is proportional to the rate of degradation at the macroscale, is defined by

$$P = IN_{ester-W} \times IN_{ester-ester} \quad \text{(equation 5.13)}$$

In the above equation, $IN_{ester-W}$ and $IN_{ester-ester}$ are proportional to the concentration of water and ester groups in the micelles, respectively. The simulated relative hydrolysis rate in the reaction volume for 20 wt% SPEXA macromonomers in aqueous solution is shown in Figure 5.7.a as a function of m. For all m values, SPEGA had the highest relative hydrolysis rate followed by SPELA, SPEDA and SPECA. Relative hydrolysis rate for SPECA and SPEDA solutions increased from zero to 5.2 and 12.5, respectively, with increasing m from zero to 4. Likewise, relative hydrolysis rate of SPELA and SPEGA solutions increased from zero to 13.4 and 22.5, respectively, with increasing m from zero to 3 and then decreased to 12.3 and 21.0 with increasing m from 3 to 4. The relatively large difference in predicted relative hydrolysis rates between SPEXA macromonomers for a given m indicated that hydrolysis was related to equilibrium water content and concentration of ester groups in the micelles, not to the bulk water concentrations (the solutions had similar bulk water contents, see Figure 5.7.h). The predicted biphasic hydrolysis rate for SPELA and SPEGA in Figure 5.7.a was attributed to the low proximity of water to ester beads in larger micelle cores at higher m values. SPECA with the most hydrophobic micelles had the lowest predicted hydrolysis rate while SPEGA with the least hydrophobic micelles had the highest hydrolysis rate. Mass loss of 20 wt% SPELA, SPEGA, SPEDA and SPECA hydrogels with incubation

time for different m values are shown in Figures 5.7(c-f). SPELA-0L without lactide chain extension had <5% mass loss after 6 weeks of incubation.

Mass loss of SPELA gels was linear with incubation time for all m values. SPELA hydrogels lost 6%, 37%, 80% and 100% mass after 4 weeks as m increased from zero to 0.8, 1.6 and 2.9, respectively. However, SPELA mass loss decreased from 100% to 87% as m increased from 2.9 to 3.7, which was consistent with the predicted decrease in SPELA hydrolysis rate for $3 \leq m \leq 4$ in Figure 5.7.a (brown curve). SPEGA gels had the fastest degradation rate among HA monomers. The time for complete degradation of SPEGA gels initially decreased from 8 to 2 days with increasing m from 0.8 to 1.6. However, SPEGA degradation time increased from 2 to 3 days when m increased from 1.6 to 2.8 mainly due to a transition from surface (controlled by the number of ester groups) to bulk degradation (domination by water content of the micelles). The difference in experimental ($1.6 < m < 2.8$) and simulated ($3 < m < 4$) transition range for SPEGA was attributed to the polydispersity of G segments, leading to a wider distribution of micelle core sizes. Mass loss of SPEDA and SPECA gels after 42 days ranged between 30-39% and 80%-89% respectively. The non-linear degradation trend for SPEDA was attributed to a wider micelle size distribution, which was not taken into account in the simulations. The experimentally measured mass losses for SPEXA hydrogels at similar m values ($1.6 \leq m \leq 1.8$) are compared in Figure 5.6.b. SPEGA and SPELA hydrogels completely degraded in 3 days and 5 weeks, respectively, whereas SPEDA and SPECA hydrogels lost 40% and 20% their mass in 6 weeks. Equilibrium water content of SPEXA hydrogels as a function of m is shown in Figure 5.7.h. The difference in water content of SPEXA gels was not statistically significant (p values for the difference between water

contents were >0.17). Therefore, the wide range of degradation rates from a few days to many months observed for SPEXA gels, as shown in Figure 5.7.b, can only be explained by differences in equilibrium water content of the micelles with HA type and number of HA monomers per segment.

5.4.5. OSTEOGENIC DIFFERENTIATION OF MARROW STROMAL CELLS IN SPEXA HYDROGELS

MSCs were encapsulated in SPEXA gels and the effect of HA monomer type on osteogenic differentiation of MSCs was evaluated. SPEGA gel due to its relatively fast degradation (see Figure 5.7.d) was not used for MSC encapsulation. Groups included 20 wt% SPELA (L-m1.7), SPEDA (D-m1.7), SPECA (C-m.18) and PEG (m0). The effect of HA type on total collagen content with incubation in osteogenic medium is shown in Figure 5.8.a. Total collagen content of L-m1.7 gel increased from 54 μg/μg DNA at day 7 to 83 and 122 μg/μg DNA at days 14 and 21, respectively. Total collagen content of L-m1.7 gel was significantly higher than those of C-m1.8, D-m1.7 and m0 gels for all incubation times. The higher secretion of collagen by MSCs seeded in L-m1.7 gels is attributed to hydrolytic degradation of the matrix concurrent with ECM production. Rate of ECM production is related to the rate of matrix degradation.[102, 169] ECM production is limited by free volume when rate of matrix degradation is slower than that of ECM production. Conversely, ECM production is limited by cell adhesion when rate of matrix degradation is faster than that of ECM production. ALP activity and extent of mineralization of MSCs in SPEXA gels are shown in Figures 5.8.b and 5.8.c, respectively. Consistent with previous results, ALP activity of all groups increased from day 7 to 14 and then decreased after 28 days with mineralization.[35, 113] At day 14,

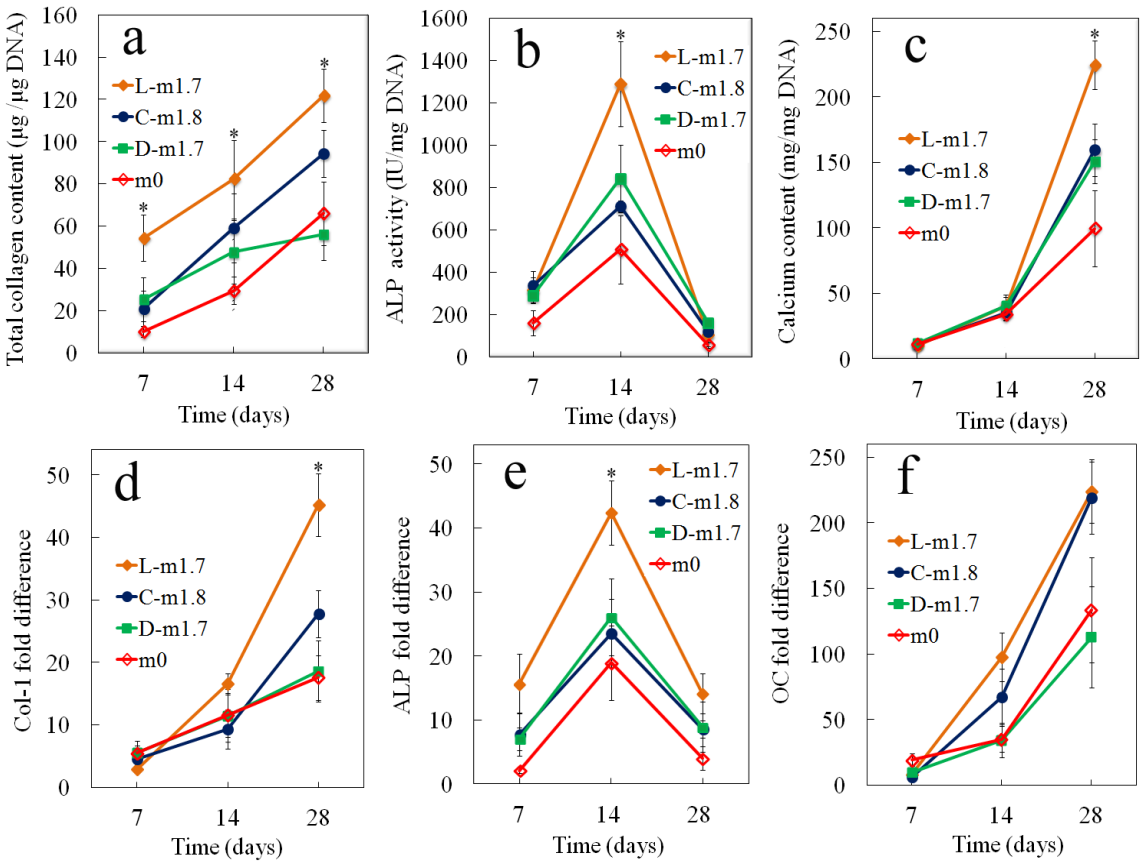

Figure 5.8. (a) Total collagen, (b) ALP activity and (c) alcium content of MSCs encapsulated in SPEXA hydrogels with incubation time in osteogenicc medium. mRNA expression of (d) Col-1, (e) ALP and (f) OC of MSCs encapsulated in SPEXA hydrogels with incubation time in osteogenicc medium. "star" indicates statistically significant difference ($p<0.05$) between the test group and all other groups at the same time point. Error bars correspond to mean ± SD for 3 experiments.

ALP activity of L-m1.7 was significantly higher than the other groups. Calcium content of all groups had an increasing trend with time. Calcium content of L-m1.7 increased from 10.3±1.2 to 40.8±8.5 and 224.7±18.5 mg/mg DNA with incubation time from day 7 to 14 and 28. After 28 days, calcium content of L-m1.7 was significantly higher than the other groups. Furthermore, at day 28, calcium content of D-m1.7 and C-m1.8 was significantly higher than that of m0 group. It can be inferred from the results that degradation of SPEXA gels contributed significantly to mineralization with L-m1.7 gel having 2.3-fold higher mineral deposition compared to non-degradable m0 (PEG gel).

Higher extent of mineralization of MSCs in degradable gels is consistent with previous reports. In one study, Human MSCs encapsulated in a hydrolytically degradable PEG matrix and incubated in osteogenic medium displayed higher cell-cell contact and cell spreading compared to non-degradable PEG.[30, 273] In another study, mineralization of osteoblasts increased by three folds with conjugation of lactide segments in PEG dimethacrylate hydrogels.[101]

mRNA expression levels of Col-1, ALP and OC are shown in Figures 5.8(d-f), respectively. Col-1 expression for all groups was significantly higher at day 28 compared to day 7. For example, Col-1 mRNA expression of L-m1.7 increased from 2.9±0.7 to 16.6±1.7 and 45.2±5.0 when incubation time increased from day 7 to 14 and 28. At day 28, Col-1 mRNA expression of L-m1.7 was 2.5 fold higher than PEG gel. ALP mRNA expression (Figure 5.8.e) showed a trend similar to its bioactivity in Figure 7b. At day 14, ALP mRNA expression of L-m1.7 was significantly higher than the other gels and 2.2 times higher than PEG gel. OC expression of all groups increased from day 7 to 28 with L-m1.7 and C-m1.8 gels showing significantly higher OC expression at day 28 compared to D-m1.7 and PEG gels. Taken together, the findings of this work demonstrate that chain extension of PEG hydrogels with short HA segments resulted in the formation of micellar hydrogels that support differentiation and mineralization of MSCs with a wide range of degradation rates from a few days to many months.

5.5. CONCLUSIONS

Structure formation and gelation kinetics of SPEXA macromonomers in aqueous solution and degradation of SPEXA gels were investigated by simulation and experimental measurement. In the absence of HA monomer, distribution of acrylate

groups was uniform in aqueous solution but the extension of the macromonomer arms with hydrophobic X segments induced aggregation and micelle formation. Core radius of SPEGA and SPEDA micelles increased from 0 to 22 Å when number of HA repeating units per arm (n) increased from 2 to 8 while that of SPELA and SPECA micelles increased from 9 and 11 Å to 23 and 24 Å, respectively. Aggregation resulted in partitioning of the polymerization photoinitiator to the micelle phase, which confined the gelation reaction to the micelle phase, thereby improving viability of encapsulated MSCs. Micelle formation sharply reduced the average inter-acrylate and acrylate-initiator separation distance, leading to a significant increase in gelation rates of SPEXA gels. For example, gelation time of 20 wt% SPEGA, SPEDA, SPELA and SPECA solutions decreased from 150 s to 61, 64, 28 and 34 s, respectively, with increasing number of HA monomers per arm (m) from 0 to 3. The simulated hydrolysis rates of SPEXA gels were strongly dependent on HA type and number of HA repeat units, consistent with experimentally measured degradation rates. For all HA types, hydrolysis rate of SPEXA gels was biphasic. For example, as m increased from 0.7 to 1.2, 1.8 and 2.8, mass loss of SPEGA gels after 2 days increased from 20% to 46% and 80% and then decreased to 66%, respectively. Similarly, as m increased from 0.8 to 1.7, 2.9 and 3.7, mass loss of SPELA gels after 3 weeks increased from 32% to 50% and 62% and then decreased to 46%. All SPEXA gels had similar initial water contents irrespective of HA type and n. A biphasic relationship between HA segment length and gel degradation rate indicated a transition from surface to bulk hydrolysis in the micelle phase. The micellar SPEXA hydrogels supported osteogenic differentiation, collagen production and mineralization of MSCs.

CHAPTER 6

MESOSCALE SIMULATION OF THE EFFECT OF A LACTIDE SEGMENT ON THE NANOSTRUCTURE OF STAR POLY(ETHYLENE GLYCOL-CO-LACTIDE)-ACRYLATE MACROMONOMERS IN AQUEOUS SOLUTION

Seyedsina Moeinzadeh and Esmaiel Jabbari, *Mesoscale Simulation of the Effect of a Lactide Segment on the Nanostructure of Star Poly(ethylene glycol-co-lactide)-Acrylate Macromonomers in Aqueous Solution*, Journal of Physical Chemistry B, 2012. **116**(5): p. 1536-1543 Reprinted here with permission of publisher.

6.1. INTRODUCTION

Hydrogels, due to their high water content and high diffusivity of nutrients and biomolecules, are very attractive as a carrier for delivery of stem cells to the site of defect in regenerative medicine.[21, 24, 28, 87, 88] After injection and in situ hardening, the hydrogel matrix guides the development of seeded cell into the desired tissue.[24] In most in situ applications, the hydrogel should have robust mechanical stability to prevent deformation and rupture by soft tissue compression or other mechanical loads.[44] In addition, the hydrogel should be degradable to provide volume for tissue regeneration.[48] Hydrogels based on small-molecule monomers, due to their potentially high network density, have excellent structural stability, but viability of the seeded cells is severely reduced by the diffusion of toxic monomers across the cell membrane.[42] Naturally based injectable gels have excellent biocompatibility and support cell-matrix interaction, but they have very low cross-link density and mechanical strength.[31, 274] Physically cross-linked hydrogels, due to the transient nature of the cross-links, also suffer from low mechanical strength.[36, 235] There is a need to develop synthetic biodegradable macromonomers for applications in regenerative medicine with robust mechanical properties. In that regard, hydrogels based on functionalized poly(ethylene glycol) (PEG) macromers are inert and nonimmunogenic and have a compressive modulus exceeding 1 MPa.[169, 275] PEG hydrogels have been used extensively to investigate the effect of matrix physiochemical, mechanical, and biological factors on cell function in vitro.[26, 44] To impart degradability to the hydrogels, short degradable lactide segments can be attached to the PEG macromer by ring opening polymerization prior to acrylate functionalization to produce a degradable PEG based hydrogel.[136,

218, 276] However, the hydrophobic lactide segments in the hydrophilic PEG, in addition to reducing the solubility of the macromonomer in aqueous solution and the water content of the resulting PEG hydrogel, cause micelle formation.[134, 135] Experimental results with four-arm star poly(ethylene glycol-co-lactide)-acrylate (SPELA) macromonomer demonstrate that the hydrogel modulus increases slightly with the addition of 1−2 lactides per arm followed by a sharp decrease in modulus for higher lactide segment lengths.[52] The formation of nanostructure by macromonomers in the hydrogel precursor solution alters the spatial distribution and accessibility of the reactive functional groups, which in turn affects the rate and extent of cross-linking.[277] Therefore, a molecular-scale understanding of the factors that affect nanostructure formation in these mixtures will aid us in designing hydrogels from macromonomers with improved physical and mechanical properties. Atomistic molecular simulations are limited to the atomic time and length scales.[278] Mesoscale methods in which the dynamics of the system is based on course-grained beads made up of a group of atoms have been developed to simulate the nanostructure of copolymers.[244, 279, 280] Hoogerbugge and Koelman[243] introduced the dissipative particle dynamics (DPD) approach, later revised by Espanol and Warren,[242] to simulate the dynamics of soft spherical beads interacting through pairwise additive force fields. The DPD approach has been used to simulate the mesoscale dynamics of polymer systems [281-285] after Groot and Warren related the conservative force terms to the Flory− Huggins interaction parameter.[58, 80] DPD has been used to simulate the microstructure and microphase separation for linear and multiarm block copolymer mixtures and solutions.[184, 244, 286-290] The objective of this work was to simulate the nanostructure and micelle

formation of SPELA macromonomer, a four-arm PEG with short lactide chains terminated with acrylates. In this work, the effect of the four-arm SPELA lactide segment length and macromonomer concentration in aqueous solution on micelle formation and distribution of the acrylate groups will be simulated with DPD. The distribution of the acrylates, namely free from the micelles, tethered, and trapped in the micelles, provide information on the crosslinking efficiency of the SPELA macromonomer and then ultimate modulus of the hydrogel.

6.2. METHODS

6.2.1. THEORY

In DPD simulation, the polymer solution is divided into different beads (set of atoms) with equal mass and volume. The SPELA macromonomer is synthesized by ringopening polymerization of lactide monomers initiated by a four-arm star PEG (MW of 5 kDa), followed by acrylation of the chain ends with acryloyl chloride. Figure 6.1 shows the molecular structure and different bead types on SPELA macromonomer. The bead types included lactide (L, dark brown), ethylene oxide (EO, green), acrylate (Ac, red), and star PEG center (SPEGc, light brown). Three water molecules were used for the solvent bead. The evolution of the position and velocity of all beads is governed by Newton's equation of motion:[242, 243]

$$\frac{d\mathbf{r_i}}{dt} = \mathbf{v_i} \ , \quad m_i \frac{dv_i}{dt} = f_i \qquad \text{(equation 6.1)}$$

where $\mathbf{r_i}$, m_i , $\mathbf{v_i}$ and $\mathbf{f_i}$ are the position vector, mass, velocity vector, and total force vector acting on bead i respectively. The total force in a cutoff radius (r_c) is[242]:

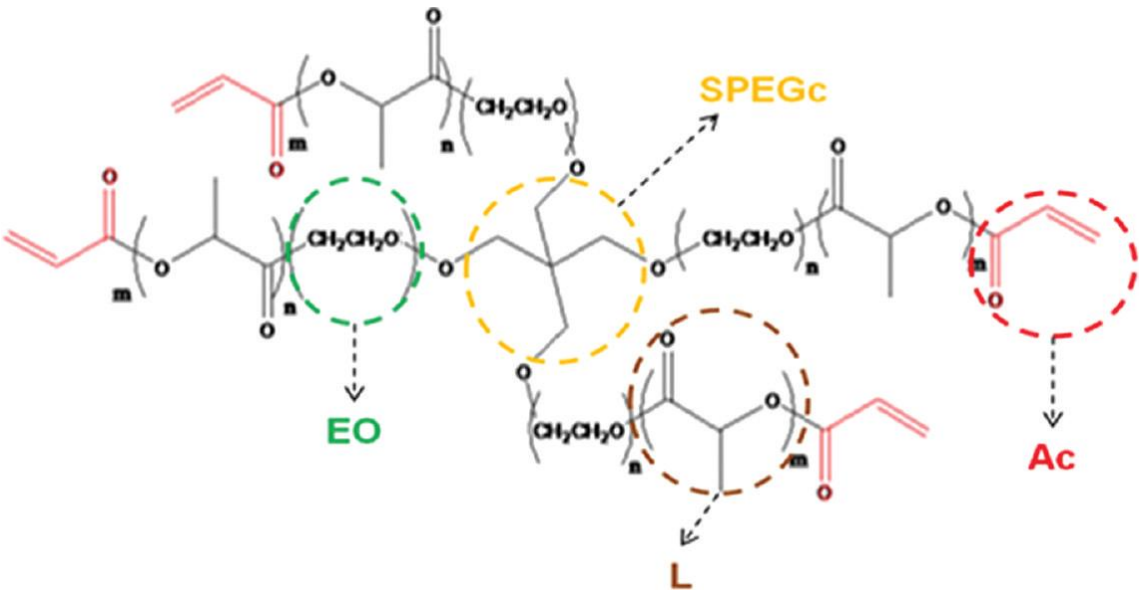

Figure 6.1. Bead representation of SPELA macromonomer in DPD.

$$\mathbf{f}_i = \sum_{i \neq j} \mathbf{F}_{ij}^{C} + \mathbf{F}_{ij}^{D} + \mathbf{F}_{ij}^{R} \qquad \text{(equation 6.2)}$$

where $\mathbf{f}_i$ is the total force and $\mathbf{F}_{ij}^{C}$, $\mathbf{F}_{ij}^{D}$, $\mathbf{F}_{ij}^{R}$ are the conservative, dissipative and random components of the force respectively. Different parts of the force are given by [242]:

$$\mathbf{F}_{ij}^{C} = \begin{cases} \alpha_{ij}(1-r_{ij})\,\mathbf{e_{ij}} & r_{ij} < 1 \\ 0 & r_{ij} \geq 1 \end{cases} \qquad \text{(equation 6.3)}$$

$$\mathbf{F}_{ij}^{D} = -\gamma w^{D}(r_{ij})(\mathbf{e_{ij}}.\mathbf{v_{ij}})\mathbf{e_{ij}} \qquad \text{(equation 6.4)}$$

$$F_{ij}^{R} = \sigma w^{R}(r_{ij})\theta_{ij}\,e_{ij} \qquad \text{(equation 6.5)}$$

where r_{ij} and $\mathbf{e_{ij}}$ are the magnitude and unit of the vector joining bead i to j ($\mathbf{r_{ij}} = \mathbf{r_i} - \mathbf{r_j}$), $\mathbf{v_{ij}}$ is given by $\mathbf{v_{ij}} = \mathbf{v_i} - \mathbf{v_j}$, and α_{ij} is a constant that describes the maximum repulsion between the interacting beads i and j. α_{ij}, which is dependent on the characteristics of the mixture plays a significant role in determining the nanostructure of the equilibrated

macromonomer solution. The system contains dissipation as well as total momentum conservation due to the simultaneous action of $\mathbf{F}_{ij}^{D}$ and $\mathbf{F}_{ij}^{R}$. w^{D} and w^{R} are r-dependant weight functions for dissipative and random forces respectively, and γ, σ are the magnitude of dissipative and random forces. θ_{ij} is a random variable with a Gaussian probability distribution. Espanol and Warren showed that the parameters of the dissipation and random forces have to satisfy fluctuation-dissipation conditions $w_D(r_{ij}) = [w_R(r_{ij})]^2$ and $\sigma^2 = 2k_B T\gamma$.[242]. The optimized weight function $w_D(r_{ij}) = (1 - r_{ij})^2$ within the cutoff distance for soft chains in aqueous solution was used in the simulation. [58]

According to the force balance (equation 6.2), the beads on the macromonomer that are not directly connected move like soft spheres in the solution. However, the motion of the adjacent beads that are directly connected is constrained by covalent bonds. Thus, an additional spring force has to be included to simulate the motion of adjacent beads on the macromonomer chains. The spring force acting on the bonded consecutive beads of a chain is given by[58]

$$\mathbf{F}_i^S = \sum_j C\,\mathbf{r}_{ij} \qquad \text{(equation 6.6)}$$

where beads j are those that are connected to bead i. A value of 4 was used in the simulation for spring constant C to properly account for the distance between connected beads.[244] Due to the domination of repulsive forces between soft spheres in the mean segment length,[244] the end point distribution of the macromonomer is not very sensitive to the value of constant C.

6.2.2. SIMULATION PARAMETERS

The parameters of the conservative force were set by choosing the mapping of three water molecules per DPD bead in order to simulate the diffusivity and compressibility of water.[291-293] This mapping made it possible to simulate the structure of SPELA macromer with small L:EO ratio and one acrylate per arm. All beads in the simulation system had the same volume of 90 $Å^3$ and the same mass 54 amu. By choosing the system density $\rho = 3r_c^{-3}$, the DPD fundamental length scale, r_c, was 6.46 Å and the bead−bead interaction parameters were determined by[58]

$$\alpha_{ij} = \alpha_{ii} + 3.27\chi_{ij} \qquad \text{(equation 6.7)}$$

where χ_{ij} is the Flory-Huggins parameter between beads i and j and α_{ii} is the repulsion parameter between beads of the same type. To satisfy the compressibility of water, the mapping of three water molecules per bead led to $\alpha_{ii} = 78$.[291]. Flory-Huggins parameters were calculated using:

$$\chi_{ij} = \frac{(\delta_i - \delta_j)^2 V}{RT} \qquad \text{(equation 6.8)}$$

where δ_i and δ_j are the solubility parameters of beads i and j respectively, V is the bead molar volume, T is the absolute temperature, and R is the gas constant. The solubility parameters were calculated via atomistic Molecular Dynamics simulation (Forcite module in Materials Studio V. 5.5 (Accelrys)) using the COMPASS forcefield which is an ab initio forcefield optimized for condensed-phase systems[245]. To arrive at the initial packing for each bead type, 64 beads were simulated in a cubic unit cell with 3D periodic boundary conditions using the rotational isomeric state (RIS) method,[294]

subject to equilibration at 298 K. After geometric optimization, the unit cell was equilibrated by the annealing dynamics simulation method, which included five cycles of NVT ensemble dynamics between 300 and 800 K to prevent the system from being trapped in a local minimum. After reaching the lowest energy configuration, 1500 ps of thermalizing NPT dynamics (1 fs time step) was performed to reach the actual system temperature and pressure. Next, the cohesive energy density (CED) was determined by sampling the system and collecting data for 500 ps. The CED was related to the solubility parameter of bead i, δ_i, by

$$\delta_i = \left(\frac{\Delta H_{v,i}}{V_{m,i}} \right)^{\frac{1}{2}} = (CED)^{\frac{1}{2}} \qquad \text{(equation 6.9)}$$

where $\Delta H_{v,i}$ and $V_{m,i}$ are the molar enthalpy of vaporization and molar volume of bead i respectively. The bead−bead repulsion parameters, α_{ij}, calculated from the solubility parameters using eqs 6.7 and 6.8, are given in Table 6.1.

The initial condition of each simulation was the random distribution of coarse-grained SPELA-nL macromonomers and water beads inside the simulation box with 3D periodic boundary conditions. The parameter "n" in SPELA-nL is equal to the number of L beads on each arm of the macromonomer. The total numbers of L and EO beads were held constant at 32 while n was varied, and the macromer concentration was 30% v/v unless otherwise specified. The macromonomer was simulated in cubic boxes with lengths of $30r_c$, $40r_c$, and $50r_c$. The relative distribution and structure of the macromonomer after equilibration was independent of size of the simulation box. The simulated root-mean-square radius of gyration (R_g) of the four-arm PEG (MW of 5.9 kDa with 33 beads on each arm) was 25.4 Å, which was in the theoretical range 21.2−27.8

Table 6.1. DPD Interaction Parameters (α_{ij}) Used in the Simulation.

	Ac	L	EO	SPEGc	W
Ac	78.0	83.2	91.9	118.7	98.9
L	83.2	78.0	86.8	86.3	92.3
EO	91.9	86.8	78.0	93.3	80.5
SPEGc	118.7	86.3	93.3	78.0	115.6
W	98.9	92.3	80.5	115.6	78.0

Å.[53, 295] Furthermore, the length of the simulation box (197 Å for $30r_c$) was an order of magnitude larger than R_g, indicating that the finite size effects may have no effect on our results.[289] Bead diffusivities reached steady-state values after 150000 time steps. All simulations ran 200000 times with a dimensionless time step of 0.05. For each sample, the DPD simulation was repeated five times (with randomly seeded macromonomers in the simulation box) and the results were reported as the mean ± standard deviation. All atomistic and mesoscale calculations were performed via the Amorphous Cell, Forcite, and Mesocite modules of Materials Studio v5.5 (Accelrys, San Diego, CA).[267]

6.3. RESULTS AND DISCUSSION

6.3.1. EFFECT OF LACTIDE FRACTION

Figure 6.2 shows the effect of the number of lactides on structure formation of SPELA-nL macromers in water (30% v/v). It should be noted that the W, EO, and SPEGc beads are not shown in Figure 6.2 for clarity. In the absence of lactide (n = 0), the acrylates were uniformly distributed over the volume of the simulation box. Addition of lactide segments ($n \geq 2$) to the macromonomer led to the formation of micellar structures. The hydrophobic lactide and acrylate beads of the arms belonging to different

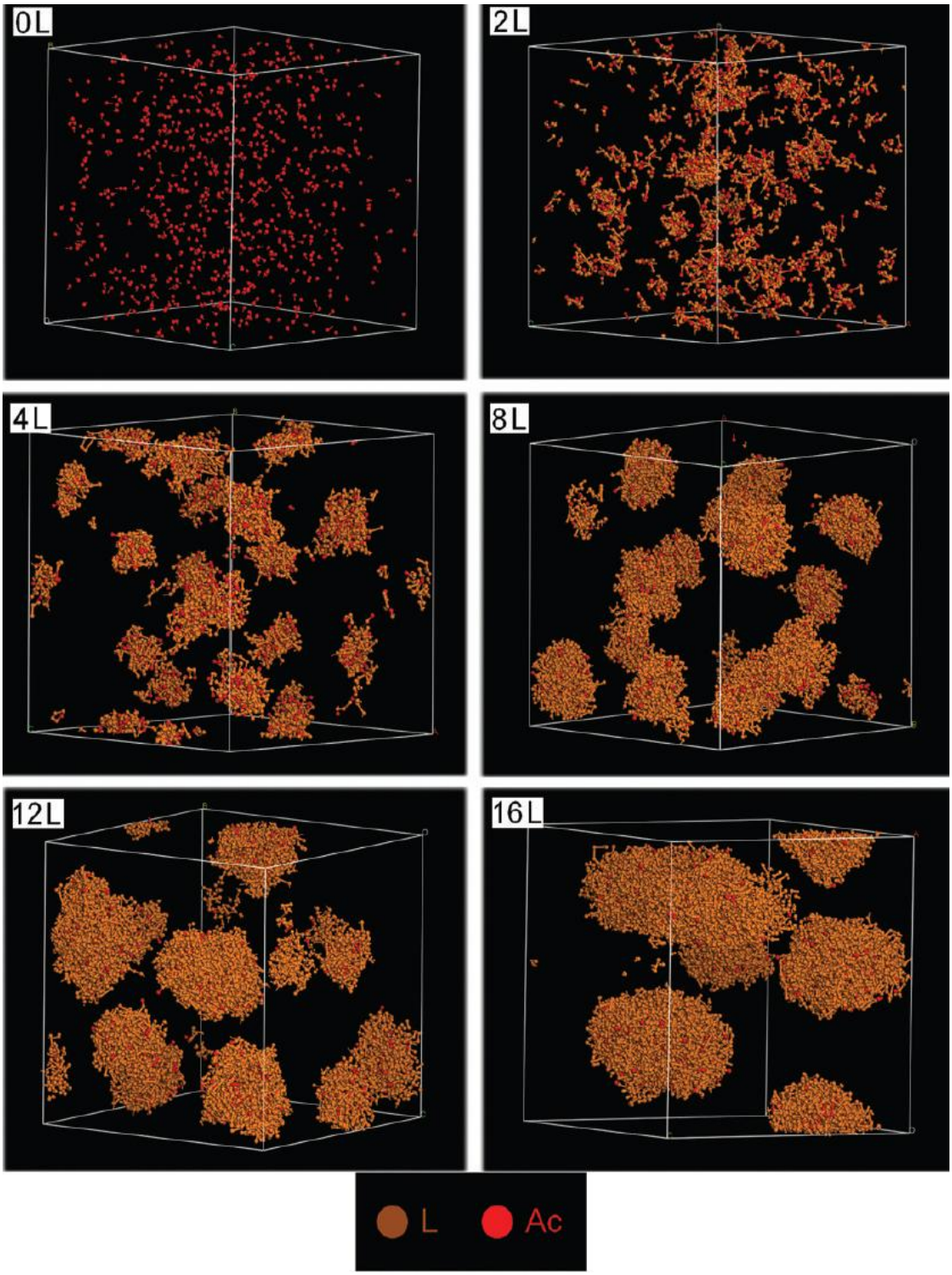

Figure 6.2. Evolution of micellar cores for SPELA-nL macromonomers in 30% aqueous solution. “L” and “Ac” represent lactide and acrylate beads respectively. The other beads in the image are not shown for clarity.

macromonomers aggregated and formed the core of the micelles while the hydrophilic EO segments, facing the aqueous phase, formed the micelle's corona. Those arms that are not part of the hydrophobic core of the micelles are referred to as "free arms". With increasing number of lactides per arm, the core size of the micelles increased while the number of free arms decreased. A cross section of the structures, corresponding to those in Figure 6.2, is shown in Figure 6.3. With increasing n, more arms of each macromonomer participated in the formation of the micellar core. Consequently, the core size increased with n while the corona thickness decreased, as shown in Figure 6.3. At low n with small hydrophobic domains, the EO segments had an extended conformation in the aqueous phase at the water−micelle interface. However, as n and the volume of the hydrophobic domain increased, the EO segments adopted a 2D stretched conformation on the surface of the micelles. This change in conformation is caused by repulsive interactions between water and lactide segments at the interface dominating over the reduction in entropy as the EO segments adopt a 2D conformation on the micelle surface.

The effect of number of lactides on each arm on the core radius and number density of micelles is shown in Figure 6.4.a. The core size increased with the volume fraction of lactide segments, while the number density decreased. Although the aggregation of lactide segments and formation of micelles reduces the total free energy of the solution, two positive contributions to the free energy controlled the core size and number density.[296] One factor is the free energy of the water−micelle interface, which is proportional to the core surface area per macromonomer. The other factor is the steric repulsive energy between the hydrophilic EO segments positioned at the corona−core interface of the micelles, which is inversely proportional to the core surface area per

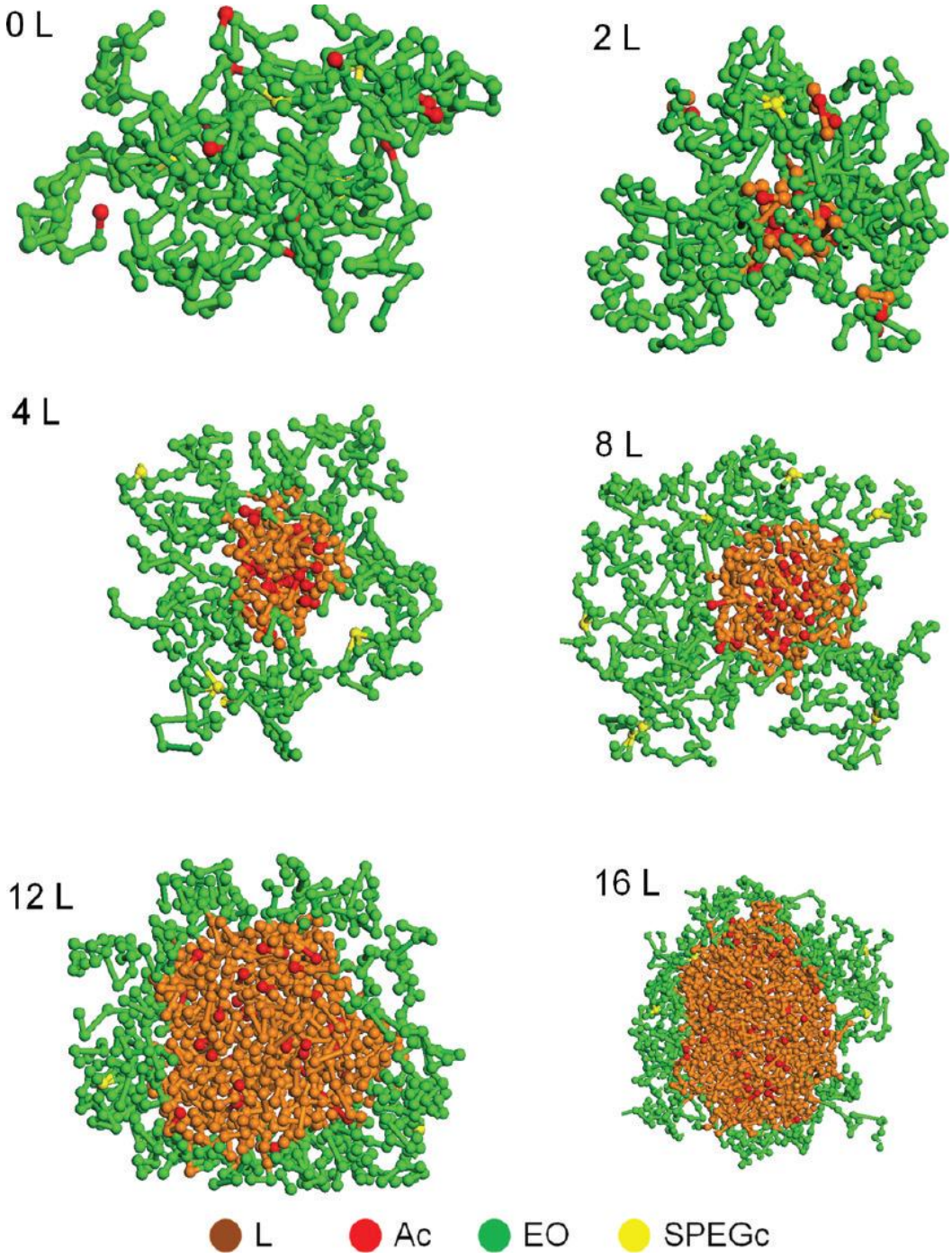

Figure 6.3. Cross section of the micelles for SPELA-nL macromonomers in 30% aqueous solution. “L”, “Ac”, “EO”, and “SPEGc” represent lactide, acrylate, ethylene oxide, and the star PEG core, respectively. The water beads are not shown for clarity.

macromer. The number of EO beads per unit core surface area deceases with increasing n, leading to a decrease in repulsive energy between the EO segments. At the same time,

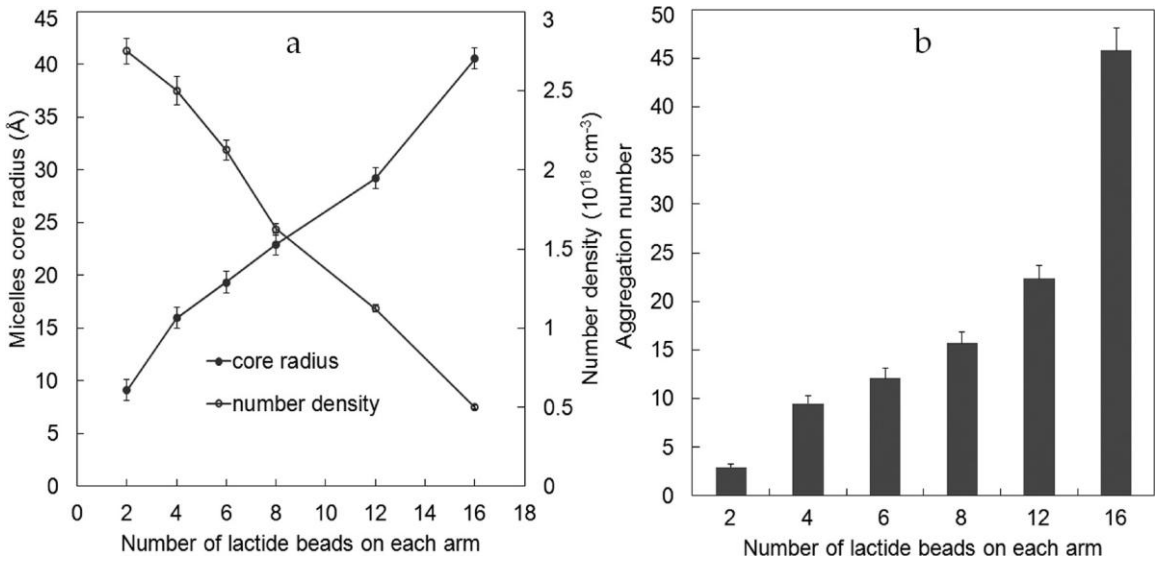

Figure 6.4. The effect of the number of lactide beads on each arm on (a) the micelle core size and number density and (b) the aggregation number of micelles in 30% aqueous solution of SPELA-nL macromonomers. n represents the number of lactide beads on each macromonomer arm, which has a total of 32 L and EO beads. Error bars correspond to means ± 1 SD for n = 5 simulations.

the EO layer thickness on the core surface decreases with increasing n, thus leading to an increase in interfacial free energy. Since the core size increased with n (see Figures 6.2 and 6.3), the net effect is the domination of interfacial over repulsive free energy, which led to the formation of micelles with smaller core surface areas per molecule, larger cores, and lower number density of micelles. The average number of SPELA macromonomers in a micelle or aggregation number, n_{agg}, can be calculated by the following equation, assuming there are only L and Ac beads in the micelle's core:

$$n_{agg} = \frac{\rho V_c}{4(n+1)} \qquad \text{(equation 6.10)}$$

where ρ and V_c are the bead number density and micelle core volume, respectively. Figure 4b shows that the aggregation number increased with n. According to Figure 6.4.b, there was a sharp increase in n_{agg} from 3 to 9 when n was raised from 2 to 4. That

increase can be related to the transition from macromonomer density fluctuation (size < R_g) to micelle formation (see Figure 6.2). n_{agg} also increased sharply when n was raised from 12 to 16, which can be related to the transition from micellar to microphase separated solution. For the case of SPELA-20L, the small interfacial surface area per macromonomer could not be achieved for minimization of free energy by spherical packing, which led to the formation of continuous phases in the simulation box (data not shown).

6.3.2. EFFECT OF MACROMONOMER CONCENTRATION

The effect of macromonomer concentration on core radius and number density of micelles for SPELA-4L is shown in Figure 6.5. The core radius slightly increased from 14.9 to 16 Å as the SPELA concentration was increased from 5 to 30%. The ratio of water to lactide beads was higher for lower SPELA concentrations, resulting in a stronger repulsive interaction at the micelle−water interface and smaller core size. Since there was a slight change in core size with concentration, the number density of micelles increased with increasing macromonomer concentration. In addition, the distribution of acrylates in the core of the micelles did not change significantly with increasing SPELA concentration.

6.3.3. INTER-MICELLAR BRIDGING

The cross sections in Figure 6.3 show that the center of the macromonomers (SPEGc) is positioned in the corona of the micelles. Therefore, the arms can possess three different conformations, namely, the intermicellar bridges, loops in which at least two arms of a macromonomer are in the same micelle, and free arms. The three conformations are shown schematically in Figure 6.6. For SPELA-0L with n = 0, the

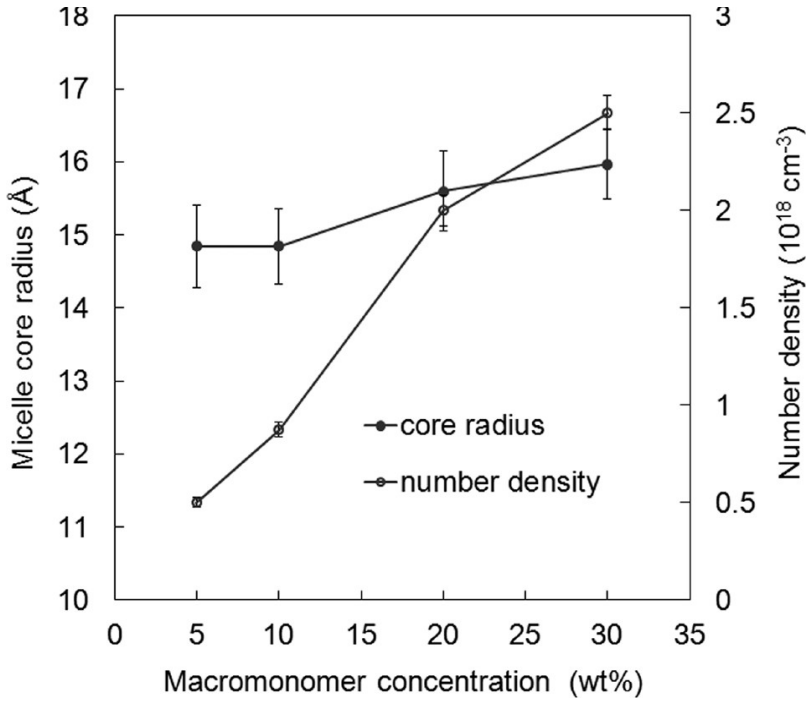

Figure 6.5. The effect of macromonomer concentration on the core size and number density of the micelles in aqueous solution of SPELA-4L macromonomers. Error bars correspond to means ± 1 SD for n = 5 simulations.

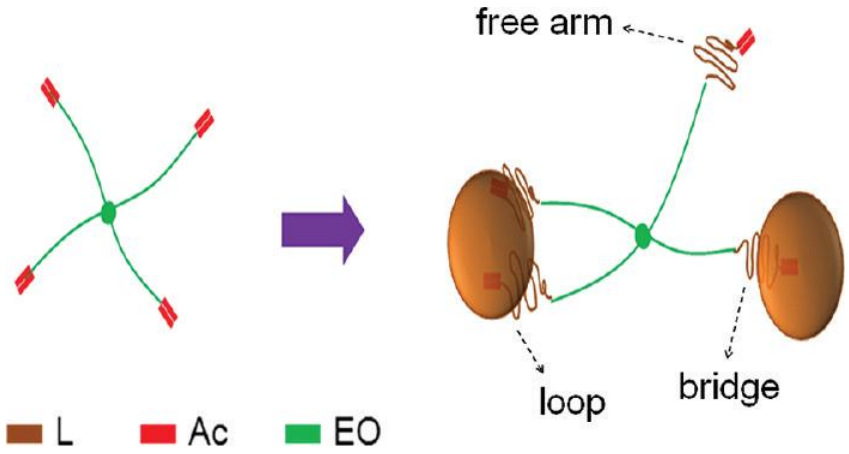

Figure 6.6. Schematic representation of bridge, loop ,and free arm conformations of SPELA macromonomers in aqueous solution. "L", "Ac", and "EO" represent lactide, acrylate, and ethylene oxide beads, respectively.

arms are in solution and considered free. For SPELA macromonomer with n > 0, aggregation of hydrophobic lactide groups and micelle formation results in the creation of loops and bridges. Assuming ideal solution and connectivity of the macromonomer arms

does not affect partitioning, the relation between the mole fraction of arms in the micelles (X_{ma}) and free arms (X_{fa}) at thermodynamic equilibrium is given by[297]

$$\frac{\ln(X_{ma})}{4n_{agg}} = -\frac{\mu^0_{mic} - \mu^0_f}{RT} + \ln(X_{fa}) + \frac{\ln(4n_{agg})}{4n_{agg}} \qquad \text{(equation 6.11)}$$

where ($\mu^0_{mic} - \mu^0_f$) is the standard chemical potential of micellization per arm, n_{agg} is the aggregation number of macromonomers in a micelle, and R and T are the gas constant and absolute temperature, respectively. According to Figure 6.5, macromonomer concentration has a slight effect on micelle core size and thus the aggregation number. Therefore, on the basis of eq 6.11, the fraction of free arms, X_{fa}, does not change significantly with an increase in the total macromonomer concentration $X_T = X_{ma} + X_{fa}$. However, it significantly increases the fraction of arms with bridge and loop conformation. Therefore, there is a smaller fraction of free arms and larger fraction of loops and bridges at higher macromonomer concentrations. As the ratio of L to EO increases at constant X_T, the fraction of free arms decreases. The number of bridges per micelle and the bridge fraction of the arms as a function of n are shown in Figure 6.7. The number of bridges per micelle continuously increased with n, while the bridge fraction showed a biphasic behavior. The bridge fraction initially increased when n increased from 2 to 4, which can be attributed to the decrease in the fraction of free arms from 70 to 14% of total arms. With increasing n to values >4, the intermicellar distance increased while the length of hydrophilic EO segments connecting the micelles decreased, thus reducing the probability of bridge formation and the bridge fraction.

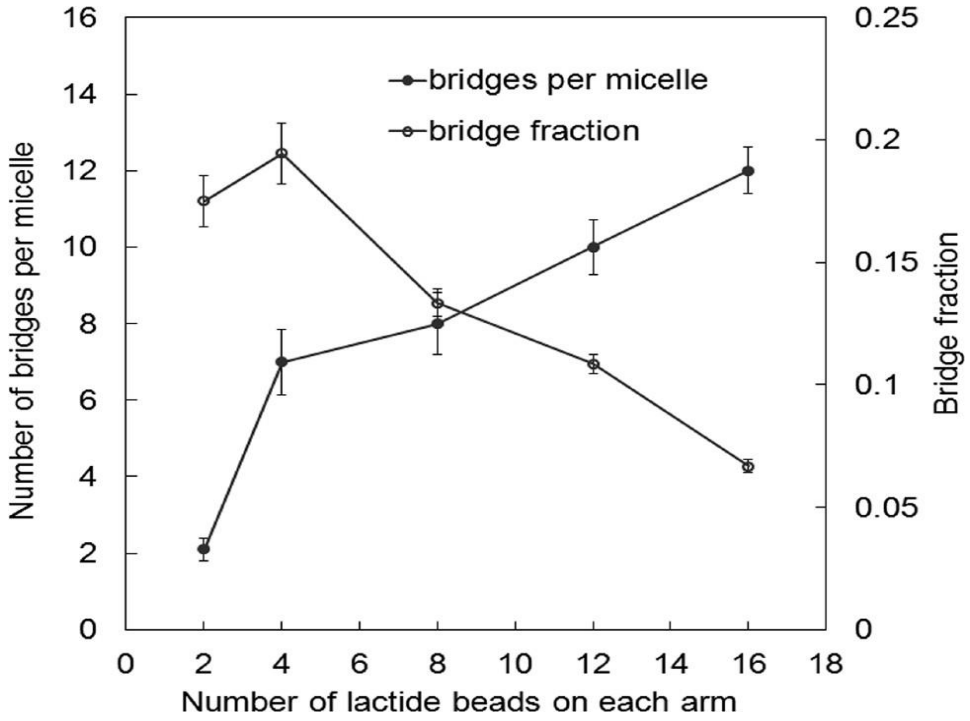

Figure 6.7. The effect of the number of lactide beads on each arm on the number of bridges per micelle and bridge fraction in 30% aqueous solution of SPELA-nL macromonomers. Error bars correspond to means ± 1 SD for n = 5 simulations.

The contribution of each bridge to the elastic modulus of the physically formed network is related to the residence time of the arm in the micelle's core, which is proportional to[249]

$$\tau \sim \gamma . n^{2/3} \qquad \text{(equation 6.12)}$$

where γ is the effective interfacial tension between the micelle's core and solution. With increasing n, the EO segments adopt a thinner interfacial layer on the core surface with lower entropy, thus increasing the interfacial tension of the micelle−water interface. Therefore, both n and γ increased the residence time of the bridges with increasing number of lactides per arm. As a result, the contribution of each bridge to the elastic modulus of the network increased with n [298] even though the fraction and number

density of bridges decreased for n > 4. That effect, in turn, reduced the mobility and accessibility of the reactive acrylate groups with increasing n.

6.3.4. DISTRIBUTION OF REACTIVE ACRYLATE BEADS

The reactivity of an acrylate group in the macromonomer depends on its mobility and its proximity to other acrylates in the solution. The acrylate mobility, in turn, depends on the concentration of water in the microenvironment. To quantify the proximity of an acrylate bead to water beads or other acrylate beads, the average number of water (n_{Ac-w}) or acrylate (n_{Ac-Ac}) beads in a sphere of radius R around an acrylate bead or the running integration number of beads "a" around beads "b", n_{ab}, was calculated by[248]

$$n_{ab}(R) = 4\pi\rho_{b0}\int_0^R g_{ab}(r)\, r^2 dr \qquad \text{(equation 6.13)}$$

where ρ_{b0} is the overall number density of beads of type 'b' and $g_{ab}(r)$ is the radial distribution function of bead "b" around bead "a" located at the origin. [299] The effect of the number of lactides in the SPELA macromonomer on n_{Ac-w} and n_{Ac-Ac} in a radius of 20 Å is shown in Figure 6.8.a and 6.8.b, respectively. n_{Ac-w} increased with radial distance, but the SPELA-0L macromonomer (n = 0) had the highest integration number with maximum coverage of acrylate groups by water beads. With increasing n and formation of larger lactide cores, the fraction of hydrophobic acrylates facing water decreased, leading to a decrease in n_{Ac-w}. The n_{Ac-w} value for SPELA-0L at radial distance r_c was an order of magnitude higher than that of SPELA-16L. This large difference emphasizes the higher accumulation of water beads around acrylates, and hence higher accessibility to the aqueous phase, for macromonomers with a low number

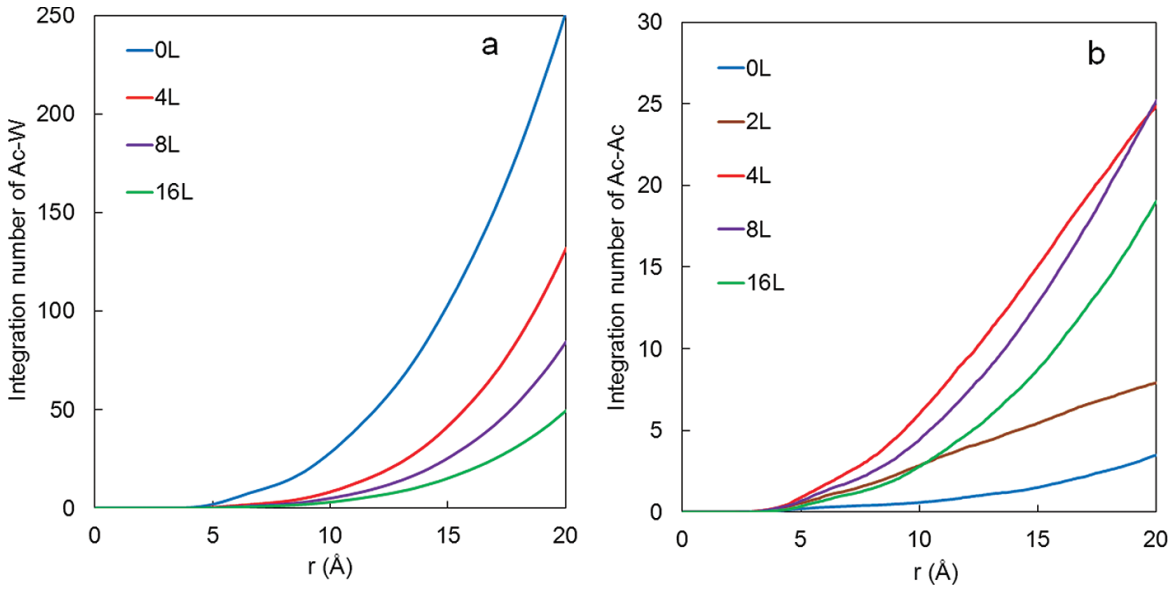

Figure 6.8. The running integration numbers for (a) Ac−W beads and (b) Ac−Ac beads of SPELA-nL macromonomers in 30% aqueous solution.

of lactides. According to Figure 6.8.b, SPELA- 0L with the most uniform distribution of acrylate beads had the lowest n_{Ac-Ac}. The hydrophilic EO segments in SPELA-0L served as an energy barrier against the formation of acrylate aggregates; thus, the acrylate local density was the same as the overall density. Increasing n and the phase separation of lactide and acrylate beads led to an increase in n_{Ac-Ac}, as shown in Figure 6.8.b. As n increased from 0 to 2 and 4, the fraction of macromonomer arms incorporated in the micelles increased from 0 to 30 and 86%, respectively, which led to a higher local density of acrylates and a decrease in the average Ac−Ac bead distance. With further increase in n, the local density of acrylates in the micelles' core decreased and the intermicellar distance increased which led to an overall decrease in n_{Ac-Ac} for n > 4. Therefore, n_{Ac-Ac} reached a maximum value for n = 4.

Figure 6.9 shows the effect of n on the radial distribution of acrylates in the core of micelles. Due to its hydrophobic nature, there was a high density of acrylate beads in

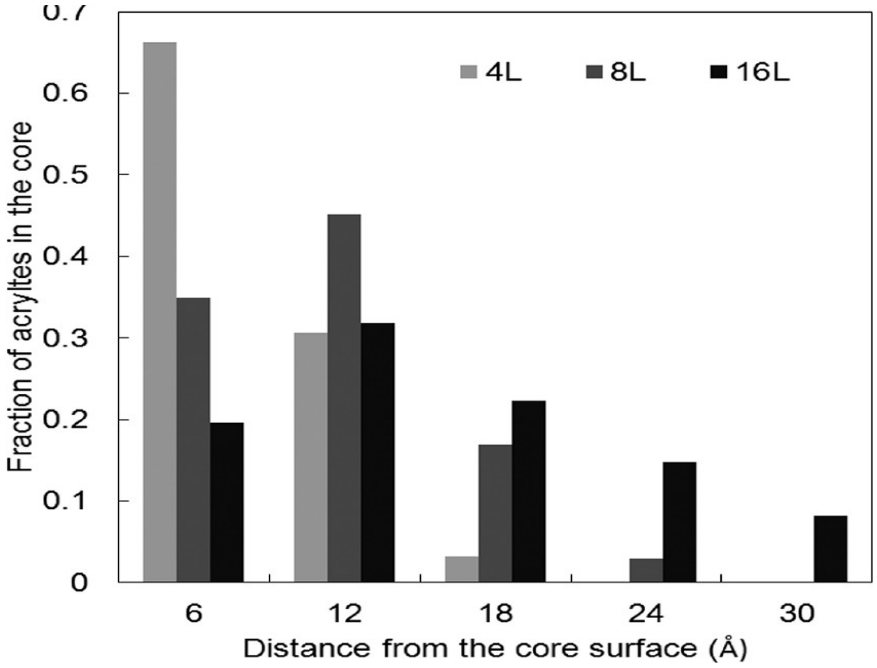

Figure 6.9. The distribution of Ac beads in the core of micelles for SPELA-nL macromonomers in 30% aqueous solution.

the central part of the micelles' core. However, a significant fraction of acrylate beads in micelles with smaller cores, due to volume constraints, were positioned near the surface layers. For example, in SPELA-4L with relatively smaller core size, 66% of the acrylates were positioned near the surface layer, away from the core's center. The average size of the micelles' core increased with n, which relaxed the volume constraint, thus increasing the fraction of acrylates in the core's inner layers. Therefore, the maximum fraction of Ac beads for macromonomers with n = 8 and n = 16 were located below the surface layer to minimize the interfacial free energy, as shown in Figure 6.9. Figure 6.10 shows the variation of free and tethered fractions of acrylates with the number of lactides in each arm. All acrylates were distributed uniformly in SPELA-0L. Increasing n led to the formation of larger micelles and a decrease in the fraction of free arms. The fraction of free arms decreased dramatically from 0.70 to 0.14 when n was increased from 2 to 4, which can be explained by a sharp increase in the volume to surface area ratio of the

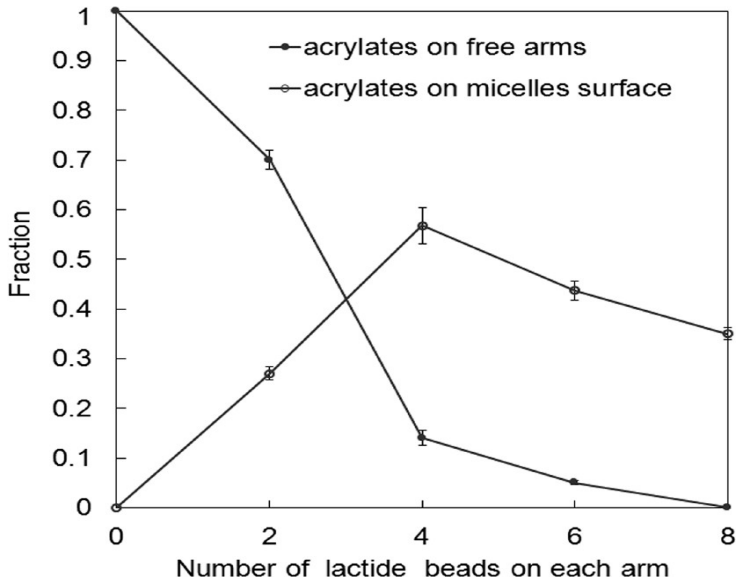

Figure 6.10. The effect of the number of lactide beads on each arm on the fraction of Ac beads on free arms and core surface of the micelles for SPELA-nL macromonomers in 30% aqueous solution. Error bars correspond to means ± 1 SD for n = 5 simulations.

micelles. A 66% increase in the size of the lactide segment of the arms (n changing from 2 to 4) led to a 420% increase in the core volume of the micelles, while the number density of micelles decreased by only 10%. When n was increased to 8, almost all acrylates (>99%, see Figure 6.10) became part of the core volume of the micelles. The reactive acrylate groups on SPELGA macromonomers cross-link by photopolymerization in aqueous solution and form mechanically robust hydrogel networks.[52] The covalent cross-links are stronger than the transient physical bridges between micelles. The reaction between the free acrylates, which are in contact with the aqueous phase, forms intermolecular cross-links and increases the cross-link density. The reaction between the acrylates in the micelle's core that belong to the same macromonomer (loops) increases the residence time of the bridges, while the reaction between those acrylates on different macromonomers (bridges) changes a transient bridge to a permanent cross-link. Since there is a high fraction of loops in the micelles' core (see the bridge fraction in Figure

6.7), a large fraction of the core acrylates undergo cyclization, which do not contribute to the elastic modulus of the network.

The effect of the number of lactide beads, n, on the reaction of acrylates and network formation can be divided into two regimes. SPELA-0L with 100% free acrylates produces networks with the highest and most uniform cross-link density. For low n values ($n \leq 4$), most of the acrylates are free (see Figure 6.7.a) and the average distance between the acrylates in the micelles' core is relatively small (see Figure 6.3). Therefore, both free acrylates in the aqueous phase and core acrylates in the micelle phase contribute to network formation. With increasing n, the Ac−Ac integration number grows, which increases the rate of propagation reaction between the acrylates, leading to a reduction in gelation time (formation of infinite network). For $n > 4$, the fraction of free acrylates is negligible, so cross-linking is dominated by the reaction between the core acrylates. Since the solvent concentration in the micelle's core is very low, the core acrylates have significantly low diffusivity compared to free acrylates. Also, the average distance between the acrylates in the micelles' core increases with n. Thus, the rate of cross-linking decreases with increasing n for $n > 4$, leading to decreasing density of permanent bridges and lower elastic modulus of the network.

6.4. CONCLUSION

The mesoscale structure of the four-arm star poly(ethylene glycol-co-lactide)-acrylate (SPELA) macromonomer in aqueous solution was simulated by dissipative particle dynamics (DPD). The short lactide segments on each arm led to the formation of micelles. The micelle size, aggregation number (average number of macromonomers per micelle), and the number of intermicellar bridges increased with increasing number of

lactides per arm. Among three possible conformations of the arms (free, loop, and bridge), the fraction of free arms decreased with increasing n while the fraction of loops decreased. The fraction of bridges showed a maximum at n = 4. There was a transition from the uniform distribution of acrylates for n = 0 to nearly complete incorporation in the micelles for n > 4. For the acrylates incorporated in the micelles, the fraction tethered to the core surface (those within a volume element facing the aqueous phase) decreased with increasing n. The average integration number of water beads around the acrylates was highest for the SPELA-0L (n = 0) and decreased with increasing n. The average integration number of acrylates around an acrylate had a biphasic behavior with a maximum at n = 4. The macromer concentration did not have a significant effect on the distribution of acrylates and the size of the micelles. The results predict that the conversion of SPELAnL acrylates in the cross-linking reaction decreases with increasing n, thus reducing the modulus of the hydrogel. The results also predict that there is a trade-off between the hydrogel modulus and degradation with higher n values favoring degradation. The predictions of the simulation can be used to design novel PEG-based hydrogels with robust mechanical properties and the desired degradation rate by changing the composition of the macromonomer.

CHAPTER 7

EXPERIMENTAL AND COMPUTATIONAL INVESTIGATION OF THE EFFECT OF HYDROPHOBICITY ON AGGREGATION AND OSTEOINDUCTIVE POTENTIAL OF BMP-2 DERIVED PEPTIDE IN A HYDROGEL MATRIX

Seyedsina Moeinzadeh, Danial Barati, Samaneh K. Sarvestani, Tahereh Karimi and Esmaiel Jabbari, *Experimental and Computational Investigation of the Effect of Hydrophobicity on Aggregation and Osteoinductive Potential of BMP-2 Derived Peptide in a Hydrogel Matrix,* Tissue Engineering Part A, 2014. Reprinted here with permission of publisher.

7.1. INTRODUCTION

A feasible approach to the restoration of injured bone tissue is the use of tissue engineering strategies to transplant undifferentiated human mesenchymal stem cells (hMSCs) in a supportive carrier loaded with bone morphogenetic proteins. In particular, *human recombinant* bone morphogenetic protein (BMP-2) is used extensively in certain clinical applications such as spine fusion, sinus augmentation and alveolar ridge augmentation to accelerate bone regeneration and healing.[62] Due to its short-half-life and diffusion of the protein away from the site of regeneration, doses much higher than the endogenous amount are loaded in the implant to induce bone formation.[62, 64] High doses of BMP-2 protein *in vivo* cause undesired side effects such as bone overgrowth, immune response, and tumorigenesis.[65] For example, the probability of an adverse side effect with the use of BMP-2 in spine fusion may be as high as 40%.[65] Encapsulation or grafting in nano- and microspheres is used to localize the protein to the site of regeneration and reduce diffusion,[239, 300, 301] however tumor formation and inflammatory response persists in some patients.[302]

The side effects of BMP-2 protein stems from its ability to promote cell migration and vascularization and its involvement in tumor angiogenesis.[303] Therefore, an attractive approach to reduce the protein's side effects in bone tissue engineering is to use peptides derived from the bioactive domains of BMP-2 and other morphogenetic proteins.[66] BMP-2 protein is a homodimer of two 114 amino acid residues with two distinct epitopes. The wrist epitope is assembled around the central α-helix while the knuckle epitope is located on the two aligned double-stranded β-sheets.[304, 305] It has been shown that the activity of BMP-2 protein is mainly due to the interaction of the

knuckle epitope with type II BMP receptor (BMP-II).[304] Multiple peptides derived from the knuckle epitope of BMP-2 protein have been shown to have osteoinductive potential.[18, 202] Among those, a peptide corresponding to residues 73-92 (hereinafter referred to as BMP-2 peptide) showed highest alkaline phosphatase (ALP) and osteogenic differentiation of MSCs, but the peptide activity was significantly lower than BMP-2 protein.[66] The higher activity of the protein compared to the BMP-2 peptide may be due to conformations differences between the native and free states of the peptide in aqueous medium. Peptides have recently been used to generate tubular, fibrillar, micellar, or vesicular nanostructures due their amphiphilic nature.[306-309] For example, peptides with a hydrophilic head and a hydrophobic tail spontaneously self-assemble to form vesicular structures in aqueous solution.[310] Peptide aggregation may alter the overall conformation and presentation of the amino acid sequence that interacts with cell surface receptors which adversely affects the osteoinductive potential of the peptide. Although the structure and activity of BMP-2 protein has been extensively investigated *in vitro* and *in vivo*, there is limited data on aggregation and nanostructure formation by osteogenic peptides in aqueous solution and its effect on osteogenesis.

The objective of this work was to investigate the effect of concentration and hydrophobicity of the BMP-2 peptide on peptide aggregation and differentiation of hMSCs encapsulated in an inert polyethylene glycol (PEG) hydrogel. To test the effect of BMP-2 peptide on differentiation, the encapsulated hMSCs were cultured in osteogenic medium without dexamethasone (DEX). Molecular dynamic simulation was used to predict the effect of concentration and hydrophobicity on peptide aggregation and critical micelle concentration (CMC) using a MARTINI coarse-grained force field.[60, 311, 312]

The peptide concentration was varied by 1000-fold from 0.005 mM to 5 mM with BMP-2 protein as the positive control. Hydrophobicity of the peptide was varied by capping PEG chain ends with 0-6 lactide monomers. PEG as an inert matrix with tunable properties[51, 52, 113] was used for encapsulation of hMSCs to isolate and investigate the effect of BMP-2 peptide hydrophobicity on its osteoinductive potential. Experimental and simulation results revealed that osteoinductive potential of the BMP-2 peptide is correlated with its CMC and the concentration of free peptide in aqueous medium and not the total peptide concentration.

7.2. MATERIALS AND METHODS

7.2.1. REAGENTS

Linear polyethylene glycol (PEG) with nominal molecular weight of 3.4 kDa was purchased from Acros (Pittsburg, PA). Lactide (L) monomer with >99.5% purity was purchased from Ortec (Easley, SC) and it was dried under vacuum at 40°C for at least 12 h prior to use. 4-(2-hydroxyethoxy)phenyl-(2-hydroxy-2-propyl) ketone (Irgacure-2959) photoinitiator was obtained from CIBA (Tarrytown, NY). The protected amino acids and Rink Amide NovaGel^{TM} resin were purchased from EMD Biosciences (San Diego, CA). Piperidine, calcium hydride, tetrahydrofuran (THF), trimethylsilane (TMS), triethylamine (TEA), tin (II) 2-ethylhexanoate (TOC), acryloyl chloride (Ac), acrylic acid, dimethylsulfoxide (DMSO), and ethylenediaminetetraacetic acid disodium salt (EDTA) were purchased from Sigma-Aldrich (St. Louis, MO). Dichloromethane (DCM, Acros) was dried by distillation over calcium hydride. Other solvents were obtained from VWR (Bristol, CT) and used as received. The protected amino acids and Rink Amide NovaGel resin for peptide synthesis were purchased from EMD Biosciences (San Diego, CA).

N,N-dimethylformamide (DMF), acetonitrile (MeCN), N,N-diisopropylethylamine (DIEA), N,N'-diisopropylcarbodiimide (DIC), triisopropylsilane (TIPS), N,N-dimethylaminopyridine (DMAP), hydroxybenzotriazole (HOBt) and trifluoroacetic acid (TFA) were received from Acros. Dulbecco's phosphate-buffer saline (PBS) and Dulbecco's Modified Eagle's Medium (DMEM; 4.5 g/L glucose with L-glutamine and without sodium pyruvate) were received from GIBCO BRL (Grand Island, NY). Fetal bovine serum (FBS) was purchased from Atlas Biologicals (Fort Collins, CO). TRIzol for isolation of cellular RNA and trypsin were purchased from Invitrogen (Carlsbad, CA). Penicillin (PN), streptomycin (SP), fungizone (FG), gentamicin sulfate (GS), dexamethasone (DEX), ascorbic acid (AA), and ß-sodium glycerophosphate (βGP) were purchased from Sigma-Aldrich. Quant-it PicoGreen dsDNA reagent kit was obtained from Invitrogen (Carlsbad, CA). QuantiChrom calcium and alkaline phosphatase (ALP) assay kits were purchased from Bioassay Systems (Hayward, CA). Human mesenchymal stem cells (hMSCs), harvested and cultured from normal human bone marrow, were purchased from Lonza (Allendale, NJ). The cells were tested for purity by high expression of CD105, CD166, CD29, and CD44 and low expression of CD14, CD34 and CD45 markers as described by the supplier (Lonza).

7.2.2. SYNTHESIS OF LACTIDE-CAPPED PEG MACROMER

The PEG macromer was capped with short lactide segments (<6 monomers) by condensation polymerization as we previously described.[35, 52] Briefly, the residual moisture was removed from the PEG macromer by azeotropic distillation from toluene. The PEG macromer and lactide monomers were heated to 120°C under dry nitrogen atmosphere in a reaction flask equipped with an overhead stirrer. After melting, 1 mL of

TOC catalyst was added and the reaction was allowed to proceed for 8 h at 135°C. After the reaction, the product was dissolved in DCM and precipitated in ice cold methanol, followed by precipitation in ether and hexane to remove the unreacted monomer and PEG. Then, the product was dried in vacuum and stored at -20°C. In the next step, the lactide-capped PEG was functionalized by reaction with AC using the following procedure. Equimolar amounts of AC and TEA were added dropwise to a cooled solution of the capped macromer in DCM and the reaction was allowed to continue for 12 h. After the reaction, solvent was removed by rotary evaporation and the residue was re-dissolved in ethyl acetate to precipitate the byproduct triethylamine hydrochloride salt. Next, ethyl acetate was removed by vacuum distillation and the functionalized macromer was dissolved in DCM and precipitated twice in ice cold ethyl ether. The product was dissolved in DMSO, purified by dialysis, freeze dried and stored at -20°C. A similar procedure was used for functionalization of PEG to produce PEG diacrylate (PEGDA) macromer. The synthesized macromers were characterized by ^{1}H-NMR (Varian, Palo Alto, CA) as we previously described.[35] The synthesized macromer is hereinafter referred to as Ln where "L" stands for lactide-capped PEG macromer and "n" is the number of lactide monomers per chain end.

7.2.3. BMP-2 peptide synthesis and conjugation to the macromer

The amino acid sequence KIPKA SSVPT ELSAI STLYL (BMP-2 peptide, Figure 7.1.a) was synthesized manually on Rink Amide NovaGel^{TM} resin in the solid phase as we previously described.[113] The pseudoproline dipeptides (oxazolidine) Fmoc-Ser(tBu)-Thr($\Psi^{Me,Me}$pro)-OH, Fmoc-Leu-Ser($\Psi^{Me,Me}$pro)-OH, and Fmoc-Ala-Ser($\Psi^{Me,Me}$pro)-OH were used in the peptide synthesis to improve the coupling efficiency

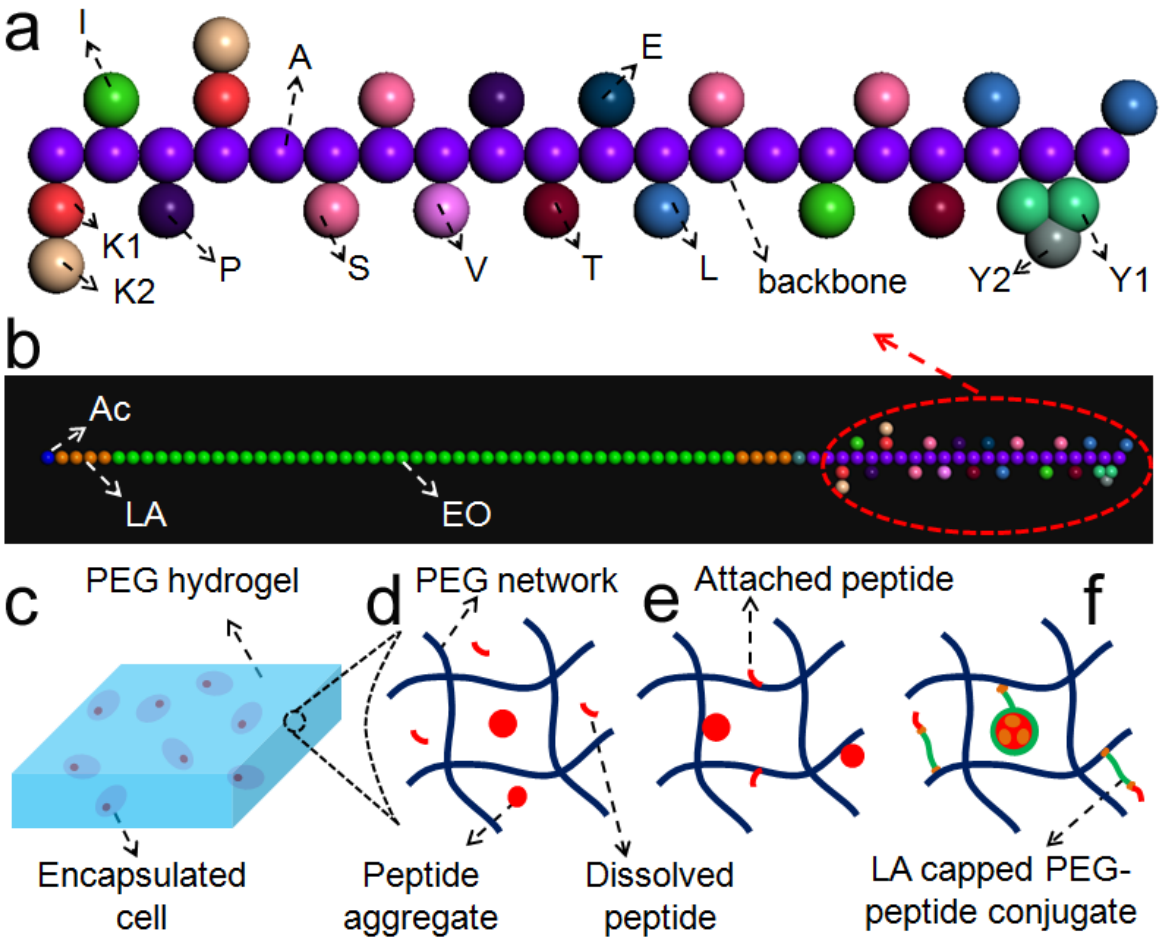

Figure 7.1. Bead representation of the BMP-2 peptide (a) and the peptide/lactide-capped PEG conjugate (b). Lactide, ethylene oxide and acrylate units in (b) are shown in brown, green and blue beads respectively. (c) Schematic representation of hMSCs encapsulated in the PEGDA (blue network) hydrogel matrix for all groups. Experimental groups included the peptide (shown in red) dissolved in the hydrogel network (d), peptide covalently attached to the hydrogel network (e), and peptide/lactide-capped PEG conjugate attached to the hydrogel network (f). The red lines and circles in (d-f) represent the peptide chain and peptide aggregate, respectively. The lactide-capped PEG macromer in (f) is shown by brown-green colors.

and product yield.[313] Briefly, the Fmoc-protected amino acid (1 equiv), HOBt (2 equiv) and DIC (1.1 equiv) were added to 100 mg resin swelled in DMF. Next, 0.2 mL of 0.05 M DMAP was added to the mixture and the coupling reaction was allowed to proceed for 4-6 h at 30°C with orbital shaking. After each coupling reaction, the resin was tested for the presence of unreacted amines using the Kaiser reagent.[314] The

coupling reaction was repeated if the test result was positive. Otherwise, the resin was treated with 20% piperidine in DMF and the next Fmoc-protected amino acid was coupled. For direct conjugation of BMP-2 peptide to the hydrogel matrix, acrylamide-terminated BMP-2 peptide was synthesized by the reaction between N-terminal amine of the peptide with acrylic acid directly on the resin under reaction conditions used for amino acid coupling. Acrylamide-terminated cell-adhesive GRGD peptide (Ac-GRGD) was synthesized using a similar procedure. For conjugation of the peptide to lactide-capped PEG macromer, the amino acid sequence cysteine-glycine-glycine (CGG) was coupled to the lysine end of the BMP-2 peptide directly on the resin. After coupling the last amino acid, the peptide was cleaved from the resin by treating with 95% TFA/2.5% TIPS/2.5% water for 2 h and precipitated in cold ether. The peptide was further purified by preparative HPLC and characterized by electrospray ionization (ESI) mass spectrometry as we previously described.[113]

The Michael addition reaction between the cysteine's sulfhydryl group on the peptide and the acrylate on the macromer was used for conjugation, similar to a procedure we previously described.[315] Figures 7.1.a and 7.1.b show the bead structure of the BMP-2 peptide and peptide-macromer conjugate, respectively. Blue, brown, and green beads in Figure 7.1.b represent acrylate, lactide, and ethylene oxide units of the macromer, respectively. Briefly, a solution of the peptide in sodium borate buffer was added to the solution of macromer in DMF in a 1:1 molar ratio to terminate on average one end of the macromer with peptide and leaving the unreacted acrylate-terminated end for attachment to the hydrogel matrix. The conjugation reaction was allowed to proceed for 24 h at 30°C. After the reaction, the solution was dialyzed against distilled deionized

(DI) water to remove the unreacted monomer and peptide, and freeze dried to obtain the dry peptide-macromer conjugate. The number of peptides per lactide-capped PEG chain was determined by ^{1}H-NMR as we described previously.[315] The conjugate is hereinafter referred to as PLn where "P", "L" and "n" stand for BMP-2 peptide, lactide-capped PEG macromer, and number of lactide monomers per chain end, respectively.

7.2.4. DYNAMIC LIGHT SCATTERING

Dynamic light scattering (DLS) was used to determine CMC of the peptide as described.[316] Solutions with different concentration of the peptide in PBS were prepared by sonication for 10 min. A 20 µL aliquot of the peptide solution was used for DLS measurements on a DynaPro MSX DLS instrument (Wyatt Technology, Santa Barbara, CA). The intensity of scattered light at 90° angle was collected and averaged over 50 data points using the DynaPro software (Wyatt Technology). Intersection of the two linear lines fitted to the data for scattered light intensity at low and high concentrations was used to define CMC for the peptide as previously described.[317]

7.2.5. CELL ENCAPSULATION AND CULTURE

Prior to cell encapsulation, hMSCs were cultivated at 5000 cells/cm^2 in a high glucose DMEM medium supplemented with 10% FBS, 100 units/mL penicillin and 100 µg/mL streptomycin. The medium was refreshed every 3 days. When the cultivated hMSC colonies reached approximately 70% confluency, the cells were detached with 0.1% trypsin- 0.03% EDTA and sub-cultivated at 1:3 ratio. According to supplier's instructions (Lonza, Allendale, NJ), all hMSCs used in cell culture experiments were passaged <5 times. The following procedure was used for encapsulation of hMSCs in BMP-2 peptide incorporated PEGDA hydrogels by UV polymerization, as shown in

Figure 7.1.c.[35, 51] First, BMP-2 peptide, with or without conjugation to the lactide-capped macromer, was dissolved in a solution of Irgacure-2959 photoinitiator (1 wt% of PEGDA) in PBS. Next, 1 wt% Ac-GRGD adhesive peptide was dissolved in a solution of PEGDA macromer (15 wt%) in PBS to improve cell viability and cell-matrix interaction after encapsulation. After sterilization by filtration, the initiator and macromer solutions were mixed by vortexing for 5 min to generate the hydrogel precursor solution. Then, $1x10^6$ hMSCs, suspended in 100 μL PBS, was added to the precursor solution and mixed gently with a pre-sterilized glass rod. The suspension of cells in the precursor solution was injected between two sterile microscope glass slides and crosslinked by UV irradiation with a BLAK-RAY 100-W mercury long wavelength (365 nm) UV lamp (Model B100-AP; UVP, Upland, CA) as we described previously.[88] The final density of hMSCs in the gel was $2x10^6$ cells/mL. Experimental groups included peptide dissolved in PEGDA gel (Figure 7.1.d, peptide in red), peptide covalently attached to PEGDA gel (Figure 7.1.e), and peptide/lactide-capped PEG conjugate attached to PEGDA gel (Figure 7.1.f). Abbreviations "P" and "cP" denote BMP-2 peptide dissolved in and conjugated to PEGDA hydrogel, respectively, "PLn" denotes BMP-2 attached to lactide-capped macromer and dissolved in PEGDA gel, and "cPLn" denotes BMP-2 peptide attached to lactide-capped macromer and conjugated to PEGDA gel. After removing from the glass slide and cutting the gel with a cork borer, the disk-shape samples were incubated in basal medium for 24 h with two medium changes. The medium was then replaced with osteogenic medium without DEX (50 μg/mL AA and 10 mM βGP) and incubated for 28 days. The cell-encapsulated gels (without BMP-2 peptide) incubated in basal medium and osteogenic medium without DEX were used as negative controls while those with 0.0004

mM BMP-2 protein dissolved in the gel (and medium) were used as the positive control.[318, 319] For the groups with peptide dissolved in the gel, the peptide was also added to the culture medium for concentration uniformity.

7.2.6. BIOCHEMICAL AND mRNA ANALYSIS

At each time point, the samples were divided in two groups. One group was homogenized and sonicated to rupture the membrane of the encapsulated cells and expose the DNA. Double stranded DNA (dsDNA) content of the homogenized samples was analyzed using the PicoGreen assay as described.[35] Analysis of dsDNA was performed using a Synergy HT plate reader (Bio-Tek, Winooski, VT) with emission and excitation wavelength of 485 and 528 nm, respectively. Alkaline phosphatase (ALP) activity of the samples was measured using the QuantiChrom ALP assay kit on a Synergy HT plate reader at the wavelength 405 nm as described.[35] The measured intensity was correlated to ALP activity in IU/L and normalized to cell numbers. Calcium content of the samples, as a measure of the total mineralized deposit, was measured using the QuantiChrom Calcium Assay kit as described.[35] The absorbance was measured on a Synergy HT plate reader at the wavelength of 575 nm. Measured intensities were correlated to the amount of equivalent Ca^{2+} using a calibration curve made with calcium chloride solutions of known concentrations. For mRNA analysis, total cellular RNA was isolated using TRIzol as described.[113] 250 ng of the extracted total RNA was subjected to cDNA conversion using Promega reverse transcription system (Madison, WI). The obtained cDNA was subjected to real-time quantitative polymerase chain reaction (rt-qPCR) amplification with SYBR green RealMasterMix (Eppendorf, Hamburg, Germany) using Bio-Rad CXF96 PCR system (Bio-Rad, Hercules, CA) and the appropriate gene specific

primers. PCR experiments were performed to analyze the differential expression of osteogenic markers ALP and RunX-2 with time for hMSCs encapsulated in the gels. Primers for rt-qPCR were designed and selected using the Primer3 web-based software as described.[188] The following forward and reverse primers were synthesized by Integrated DNA technologies (Coralville, IA): ALP: forward 5'-ATG GGA TGG GTG TCT CCA CA-3' and reverse 5'- CCA CGA AGG GGA ACT TGT C-3'; RunX-2: forward 5'-ATG ACA CTG CCA CCT CTG A-3' and reverse 5'-ATG AAA TGC TTG GGA ACT GC-3'; GAPDH: forward 5'-CAT GAC AAC TTT GGT ATC GTG G-3' and reverse 5'-CCT GCT TCA CCA CCT TCT TG-3'.[320] The model of Pfaffl was used to determine the expression ratio of the gene.[241] The expression of GAPDH housekeeping gene was used as the reference, and the fold difference in gene expression was normalized to the first time point.

7.2.7. Statistical analysis

Data are expressed as means ± standard deviation. All experiments were done in triplicate. Significant differences between groups were evaluated using a two-way ANOVA with replication test, followed by a two-tailed Students t-test. A value of $p < 0.05$ was considered statistically significant.

7.2.8. Simulation Method

The atomistic structure of the BMP-2 peptide and lactide-capped PEG macromer were coarse-grained into different beads (set of atoms) using the MARTINI coarse graining model.[311, 312] The MARTINI force field has been parameterized and applied previously to the simulation of proteins, peptides, polymers, and polymer-peptide conjugates.[321-326] This model is based on the four to one mapping with each bead in

the coarse-grained model representing four heavy atoms in the atomistic model. The coarse graining of the peptide and macromer is schematically illustrated in Figure 7.1.a. There were a total of 16 bead types for the peptide backbone, amino acid side chains, ethylene oxide repeat unit (EO), acrylate group (Ac) and lactide repeat unit (L). Each amino acid was coarse grained into a backbone bead and between zero to three side chain beads, based on the original MARTINI model developed for simulation of proteins.[311, 312] After coarse graining, the beads were assigned pairwise interactions that included polar (P), nonpolar (N), apolar (C), and charge (Q) interactions. To accurately represent its real nature, the interactions were grouped into subtypes based on the extent of hydrogen bonding or the degree of polarity of the beads. The polar beads were divided into five subtypes based on the degree of polarity from low (P1) to high (P5). Apolar beads were divided into five subtypes from high (C1) to low apolar (C5). The nonpolar as well as charged beads were divided into four subtypes, namely hydrogen donor, hydrogen acceptor, hydrogen donor and acceptor and incapable of hydrogen bonding. For example, 4 water molecules were represented by a polar bead with degree of polarity of 4 or P4. For non-bonded interactions, the following Lennard-Jones potential function $V_{LJ}(r)$ was used [312]

$$V_{LJ}(r) = 4\varepsilon_{ij}\left[\left(\frac{\sigma_{ij}}{r}\right)^{12} - \left(\frac{\sigma_{ij}}{r}\right)^{6}\right] \qquad \text{(equation 7.1)}$$

where ε_{ij} is the depth of the potential well which is related to the strength of interaction between beads i and j, and σ_{ij} is the minimum distance of approach between beads i and j. To account for electrostatic interaction between charged beads, the following columbic function was used [312]

$$V_{EL} = \frac{q_i q_j}{4\pi\varepsilon_0 \varepsilon_{rel} r_{ij}} \quad \text{(equation 7.2)}$$

where q_i and q_j are values of the point charges on beads i and j, ε_0 is the dielectric constant of free space and ε_{rel} is the relative dielectric constant of the medium. To account for interaction between bonded beads, the following potential functions were used: harmonic function (V_b) for bond length, cosine harmonic function (V_a) for bond angle, and dihedral function (V_d) for bond torsion [312]

$$V_b = \frac{1}{2} K_b (r_{ij} - d_b)^2 \quad \text{(equation 7.3)}$$

$$V_a = \frac{1}{2} K_a [(\cos(\theta_{ijk}) - \cos(\theta_a)]^2 \quad \text{(equation 7.4)}$$

$$V_d = K_d [1 + \cos(n\psi_{ijkl} - \psi_d)] \quad \text{(equation 7.5)}$$

where K_b, K_a and K_d are force constants for bond stretching, bond angle bending and bond torsional rotation, respectively. r_{ij}, θ_{ijk} and ψ_{ijkl} represent the distance between bonded beads i and j, the angle between bonded beads i, j, and k, and the dihedral angle between beads i, j, k , and l respectively. d_b, θ_a, ψ_d and n are the equilibrium bond length, bond angle, phase angle, and periodicity, respectively. Simulations were performed under NVT ensemble dynamics. A time step of 10 fs was employed and the total simulation time was 5 μs. The temperature was held at 37°C using the Nose thermostat.[327] The simulations were performed in a 200×200×200 Å box with 3D periodic boundary conditions. To cover a broader range of concentrations, a bigger 400×400×400 Å box was used to simulate the effect of peptide concentration. The

Mesocite module of Materials Studio (v5.5, Accelrys) was used for the mesoscale simulations.[267]

For simulations to investigate the interaction of BMP-2 peptide with the cell membrane, a template membrane with a width of 40 Å was generated using Dipalmitoylphosphatidylcholine (DPPC) lipid as one face of the simulation box with the box filled with water. The coarse graining of DPPC has been described elsewhere.[328] The cell membrane was simulated under NVT ensemble for 100 ns to form the bilayer structure. After forming the lipid bilayer, the other components of system (peptide or peptide-macromer conjugate) were added to the simulation box. Next, the interaction type of all lipid bilayer beads was constrained to P4 type in order to account for the interaction with water beads. Then, dynamic simulations were run for 5 μs to allow the formation of peptide or peptide-macromer aggregates in aqueous solution similar to the simulations without the lipid bilayer membrane. Next, the constraint was removed from the membrane beads and the pairwise bead interaction potential was changed accordingly. Finally, the system was simulated for 5 μs similar to that without the lipid bilayer membrane.

7.3. RESULTS

The average number of lactides per chain end of lactide-capped PEG, average number of acrylates per chain end, and average number of BMP-2 peptides per conjugate was determined from the NMR spectra of macromers as we previously described.[35, 315] The number of lactide repeat units per chain end of the lactide-capped PEG macromer was determined from the ratio of the peaks at 1.6 and 5.2 ppm (lactide hydrogens) to those at 3.6 and 4.3 ppm (PEG hydrogens).[35] The average number of

lactide repeat units per chain end for L2, L4 and L6 macromers was 1.9, 3.6 and 5.6 respectively. The number of reactive acrylate groups per chain end was determined from the ratio of the peaks between 5.85 to 6.55 ppm (acrylate hydrogens) to those at 3.6 and 4.2 ppm (PEG hydrogens).[35] The average number of acrylates per chain end before peptide conjugation for L0, L2, L4 and L6 macromers was 0.85, 0.85, 0.83 and 0.82, respectively. The number of peptides in a peptide/lactide-capped PEG conjugate was determined using the acrylate/PEG molar ratios before and after conjugation as previously described.[315] The average number of peptides per conjugate for L0, L2, L4 and L6 macromers was 0.57, 0.49, 0.52 and 0.45, respectively. Several studies have demonstrated that >95% of acrylated PEG/peptide conjugates are integrated in PEGDA hydrogel network during photo-crosslinking.[113, 329, 330]

Figure 7.2 (a-e) shows the effect of dissolved (not attached to the gel network) BMP-2 peptide concentration on osteogenic differentiation of hMSCs encapsulated in the PEGDA hydrogel incubated in osteogenic medium without DEX. Peptide concentration ranged from 0.00025 mM to 5 mM. Negative and positive control groups were gels without peptide and with 0.0004 mM BMP-2 protein, respectively. The clinically used concentration of BMP-2 protein is 1 mg/mL (~ 0.04 mM) [331] but the typical concentration used for *in vitro* 3D experiments is in the 1-10 µg/mL (~0.00004-0.0004 mM) range.[318, 319] In this work, the upper concentration of 0.0004 mM was used to elucidate the effect of peptide on differentiation of hMSCs. DNA content, ALP activity and calcium content of the groups are shown at a single time point (7, 14 and 21 days, respectively) in Figure 7.2(a-c). DNA content of the groups at day 7 did not change appreciably with peptide concentration (Figure 7.2.a). ALP activity of all groups reached

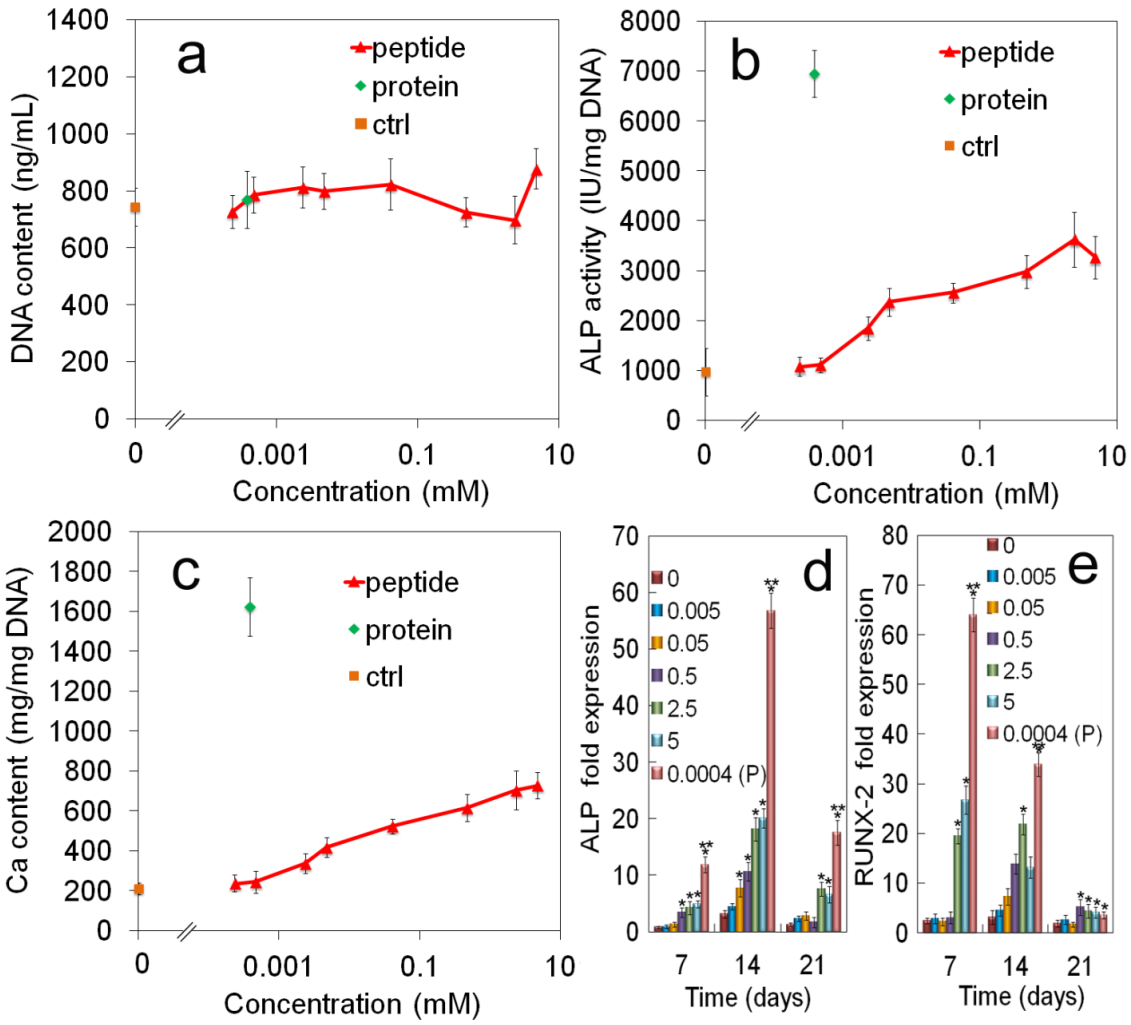

Figure 7.2. DNA content (a, day 7), ALP activity (b, day 14), and calcium content (c, day 21) of hMSCs encapsulated in PEGDA hydrogel (15 wt%) and incubated in osteogenic medium without DEX as a function of dissolved BMP-2 peptide concentration in the hydrogel matrix. Control groups included hMSCs encapsulated in PEGDA hydrogel (15 wt%) and cultured in osteogenic medium without DEX (OM) and without the BMP-2 peptide (0 mM, negative control) and those cultured in OM with 0.0004 mM BMP-2 protein (0.01 Pr, positive control). Effect of the BMP-2 peptide concentration on ALP (d) and RunX-2 (e) mRNA marker expression of hMSCs encapsulated in PEGDA hydrogel.

a maximum on day 14 consistent with the biphasic activity of ALP in osteogenic differentiation of MSCs.[332] ALP activity of the groups at day 14 did not significantly change when the peptide concentration increased from 0 to 0.00025 and 0.0005 mM (Figure 7.2.b). The ALP activity of the groups at peptide concentrations above 0.0005

mM was significantly higher than the ALP activity of the group without peptide (Figure 7.2.b). The ALP activity of groups increased by 1.7 and 2.2 fold when the peptide concentration increased from 0.0005 mM to 0.0025 and 0.005 mM respectively. The growth rate of ALP activity of groups decreased with increasing the peptide concentration above 0.005 mM. A 1000-fold increase in the concentration of peptide in the gel from 0.005 mM to 5 mM increased ALP activity only by 1.4-fold at day 14 (Figure 7.2.b). ALP activity of hMSCs encapsulated in PEGDA gel with 0.005 mM BMP-2 peptide was 2.4-fold higher than the gel without peptide (ctrl group in Figure 7.2.b) after 14 days while that with 0.0004 mM BMP-2 protein (same weight concentration as peptide, 10 μg/mL) was 7.2-fold higher. The effect of peptide concentration on the extent of mineralization of encapsulated hMSCs (Figure 7.2.c), as measured by calcium content, was consistent with ALP activity. Calcium content of the gels did not significantly change with the addition of 0.00025 and 0.0005 mM peptide to the gels. The calcium content increased from 245 ± 50 to 340 ± 40 and 420 ± 50 mg/mg DNA with increasing the peptide concentration by 5 and 10 folds from 0.0005 to 0.0025 and 0.005 mM respectively, but the calcium content increased at a slower rate from 420 ± 50 to 700 ± 100 mg/mg DNA with 500-fold increase in peptide concentration from 0.005 mM to 2.5 mM. Further increase in peptide concentration from 2.5 to 5 mM did not significantly change calcium content. The ALP and RunX-2 mRNA expression as a function of peptide concentration in Figures 7.2.d and 7.2.e, respectively, were consistent with ALP activities and calcium contents (Figures 7.2.b and 7.2.c). Notably, osteoinductive potential of BMP-2 peptide was significantly less than that of BMP-2 protein as the calcium content and ALP mRNA expression of hMSCs cultured with 10 μg

protein/mL (0.0004 mM) BMP-2 protein were 4-fold and 12-fold higher than those cultured with the same 10 μg peptide/mL mass concentration of the peptide (0.005 mM) , respectively. Furthermore, RunX-2 expression of hMSCs cultured with BMP-2 protein (0.0004 mM, pink bar in Figure 7.2.e) and those cultured with BMP-2 peptide at highest concentrations (2.5 and 5 mM, light green and light blue) peaked on day 7 while those cultured with 0.005-0.5 mM peptide peaked on day 14. To summarize, the results in Figure 7.2 indicated that the osteoinductive potential of BMP-2 peptide was significantly less than that of the protein and even 12000-fold higher peptide molar concentrations could not achieve the osteoinductive potential of BMP-2 protein.

The results in Figure 7.2 prompted us to investigate stability of the peptide in aqueous solution. The hydrophobicity index for each amino acid, from N-terminus (left side) to C-terminus (right side) of the BMP-2 peptide, based on the difference in free energy of the aqueous and condensed phases,[333] is shown in Figure 7.3.a. The positive and negative indices indicate hydrophobic and hydrophilic residues, respectively. The distribution of hydrophobicity was not uniform along the peptide chain as the average hydrophobicity indices on N- (left) and C-terminus (right) sides of the peptide were -0.28 and 0.84, respectively (see the dash lines in Figure 7.3.a). Overall the peptide was hydrophobic with an average hydrophobicity index of 0.28. The overall hydrophobicity suggested that the peptides form aggregates in aqueous solution to reduce the overall free energy. Indeed, molecular dynamic simulations in Figure 7.3.c show that the aggregation number (number of peptides per aggregate) increased with concentration of the peptide in aqueous solution. By extrapolating to aggregation number of one in Figure 7.3.c, the critical micelle concentration (CMC) of 0.040 mM was obtained for the peptide. Similar

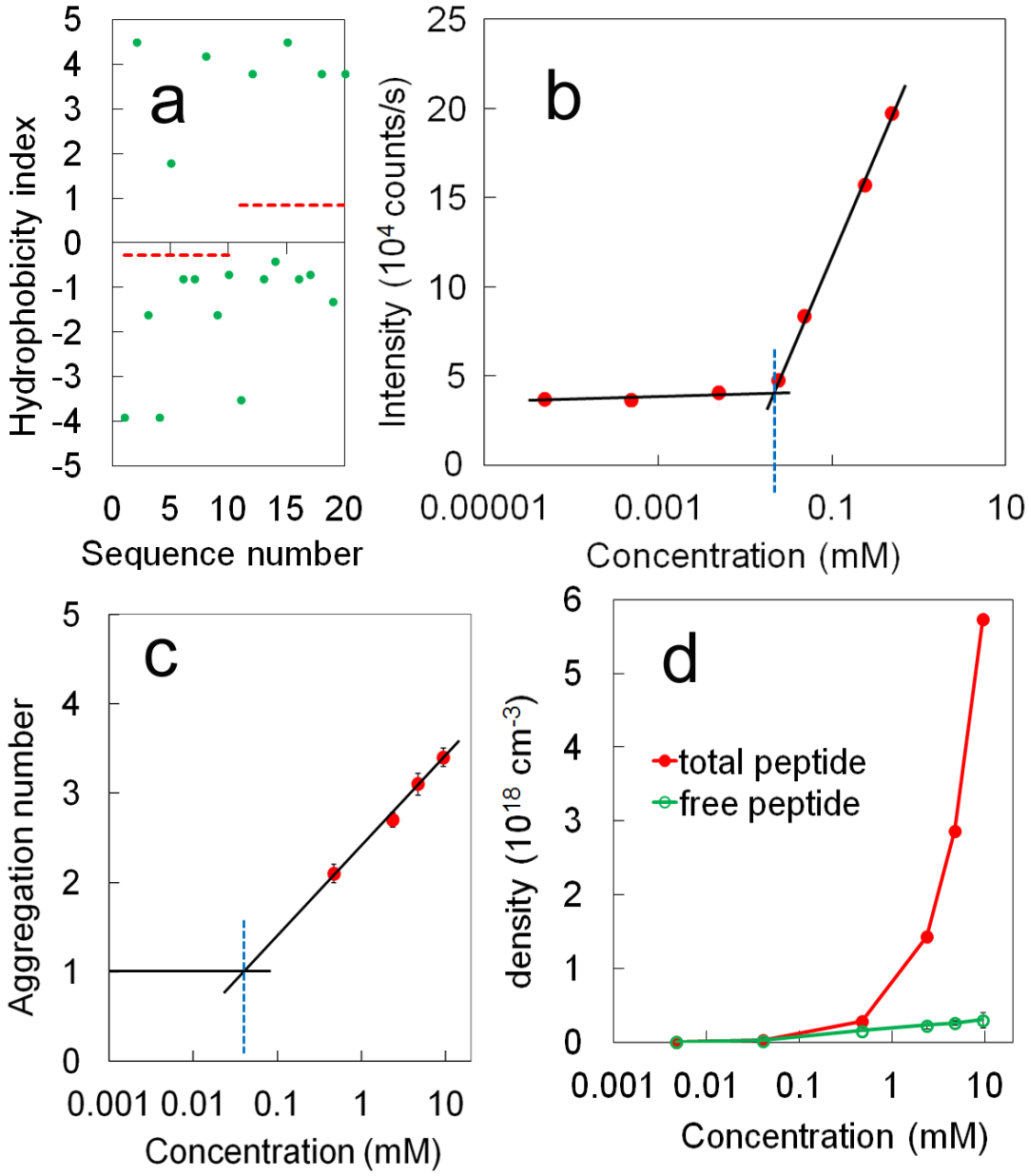

Figure 7.3. (a) Hydrophobicity index for each amino acid from N-terminus (left side) to C-terminus (right side) of the BMP-2 peptide. (b) intensity of scattered light as a function of peptide concentration in aqueous solution. (c) Simulated aggregation number of the BMP-2 peptide (number of peptides per aggregate) as a function of the peptide concentration in aqueous solution. (d) density of free BMP-2 peptide and total peptide density as a function of peptide concentration in aqueous solution.

to surfactants, the peptide is soluble in aqueous solution below CMC but it forms aggregates in equilibrium with the free peptide in solution above CMC with the propensity for aggregation increasing with peptide concentration.[334] CMC of the

peptide was measured by dynamic light scattering from the intersection of the two lines fitted to the scattered light intensity at high and low concentrations, as shown in Figure 7.3.b. The intensity of scattered light did not change significantly at low concentrations in the absence of aggregation but it increased exponentially above CMC with aggregation. The experimentally measured CMC was 0.019 mM which was lower than the predicted value of 0.04 mM from simulations (Figure 7.3.c). The predicted higher CMC was most likely due to the error in extrapolating the aggregation number from higher concentrations to the aggregation of unity at CMC. However, the experimental and simulated CMCs were within the range of 0.005-0.05 mM which was observed in the cell studies (Figure 7.2). A lower growth rate of ALP activity and mineralization of hMSCs in PEGDA gels with peptide concentration when the peptide concentration was in the 0.005-0.05 mM range compared to the 0.0005-0.005 range can be related to the initiation of aggregation within the former range (see Figure 7.2.b and 7.2.c). The predicted total and free peptide densities as a function of peptide concentration in solution are compared in Figure 7.3.d. According to simulation results, the fraction of free peptide above CMC concentration decreased sharply from 0.54 to 0.16, 0.09 and 0.06 as the peptide concentration was increased from 0.5 mM to 2.5, 5 and 10 mM, respectively. However, the decrease in fraction of free peptide was offset by an increase in peptide number density. Therefore, the density of free peptide in solution increased by 1.9-folds from $0.16x10^{18}$ to $0.3x10^{18}/cm^3$ while the total peptide density increased by 20-folds from 0.28 $x10^{18}$ to 5.73 $x10^{18}/cm^3$ (Figure 7.3.d). The effect of peptide concentration, added to the gel and culture medium, on ALP activity (day 14) and calcium content (day 21) of hMSCs encapsulated in 15% PEGDA gel is shown in Figure 7.2.b and 7.2.c, respectively.

Note that concentration scale in the figures is logarithmic. As the total peptide concentration was increased by 10-folds from 0.5 to 5 mM in a range well above CMC, ALP activity and calcium content increased by 1.1 and 1.2 folds, respectively, while the free peptide concentration increased by 1.6-fold from 0.26 to 0.42 mM (see Figure 7.4). Therefore, the data suggests a better correlation between osteogenic activity and the free peptide concentration. Further, the significantly lower osteogenic activity of the peptide compared to BMP-2 protein even at 12000-fold higher concentration, can be partially (see other effects due to peptide interaction with the cell membrane) explained by aggregation in aqueous solution.

The effect of peptide hydrophobicity and its conjugation to the PEGDA network on DNA content, ALP activity and calcium content of the encapsulated hMSCs is shown in Figures 7.5.a to 7.5.c, respectively. Groups included gels incubated in basal medium (BM), osteogenic medium without DEX (OM), OM with peptide conjugated to the gel (cP), OM with peptide dissolved in the gel (P), OM with peptide/lactide-capped PEG macromer with zero (cPL0), 2 (cPL2), 4 (cPL4), and 6 (cPL6) lactides conjugated to the gel. DNA content of hMSCs cultured in BM increased with incubation time while those incubated in OM decreased, with or without peptide (Figure 7.5.a). The increase in DNA content in BM indicated that hMSCs were able to grow in the encapsulating PEG matrix but DNA content decreased with incubation time as the encapsulated cells underwent differentiation in osteogenic medium consistent with previous reports.[252, 253] Addition of BMP-2 peptide, peptide hydrophobicity, or peptide conjugation to the PEG matrix did not have a significant effect on cell number with incubation time.

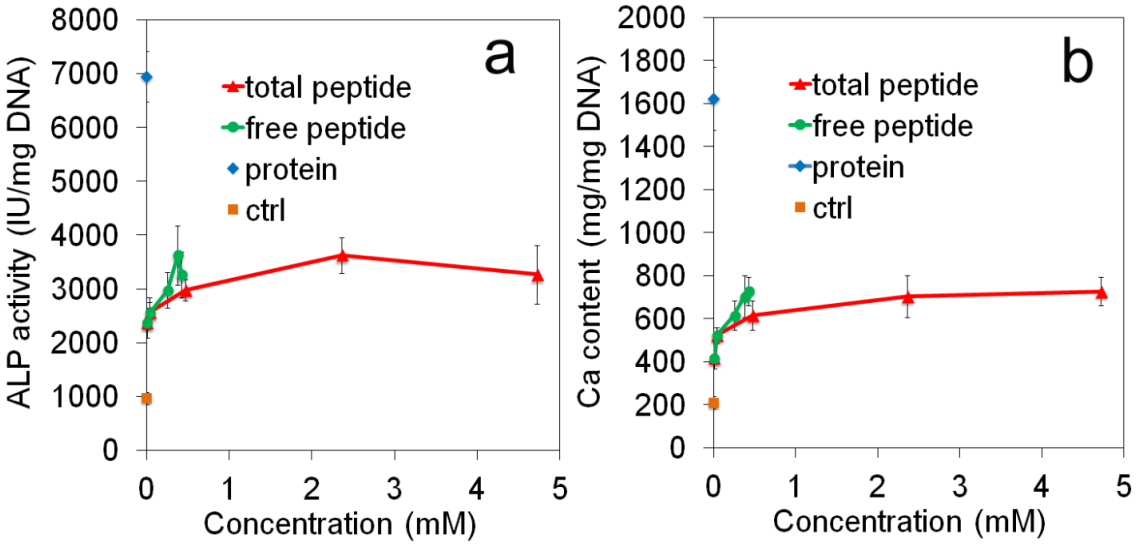

Figure 7.4. ALP activity (b, day 14), and calcium content (c, day 21) of hMSCs encapsulated in PEGDA hydrogel (15 wt%) and incubated in osteogenic medium without DEX as a function of dissolved BMP-2 peptide concentration in the hydrogel matrix. Control groups included hMSCs encapsulated in PEGDA hydrogel (15 wt%) and cultured in osteogenic medium without DEX (OM) and without the BMP-2 peptide (0 mM, negative control) and those cultured in OM with 0.0004 mM BMP-2 protein (0.01 Pr, positive control).

ALP activity of the encapsulated hMSCs cultured in BM did not change with incubation time while those cultured in OM, with or without peptide, peaked on day 14. The addition of BMP-2 peptide to the culture medium significantly increased the peak ALP activity on day 14, as shown by one star in Figure 7.5.b. Further, the group with BMP-2 peptide dissolved in the medium (P) had significantly higher ALP activity on day 14 compared to those groups in which the peptide was conjugated to the PEG gel (cP, cPL0, cPL2, cPL4, cPL6), as shown by two stars in Figure 7.5.b. This is consistent with the fact that BMP-2 protein is associated with the soluble, not the insoluble fraction of the bone matrix.[335] Further, ALP activity for cPL0 group (peptide-PEG conjugate attached to the gel) was 3000 ± 450 IU/mg DNA which was higher than that for cP group (peptide attached to the gel) with 2200 ± 260 IU/mg DNA. Notably, ALP activity of the encapsulated hMSCs decreased when the PEG chain conjugated to the peptide was

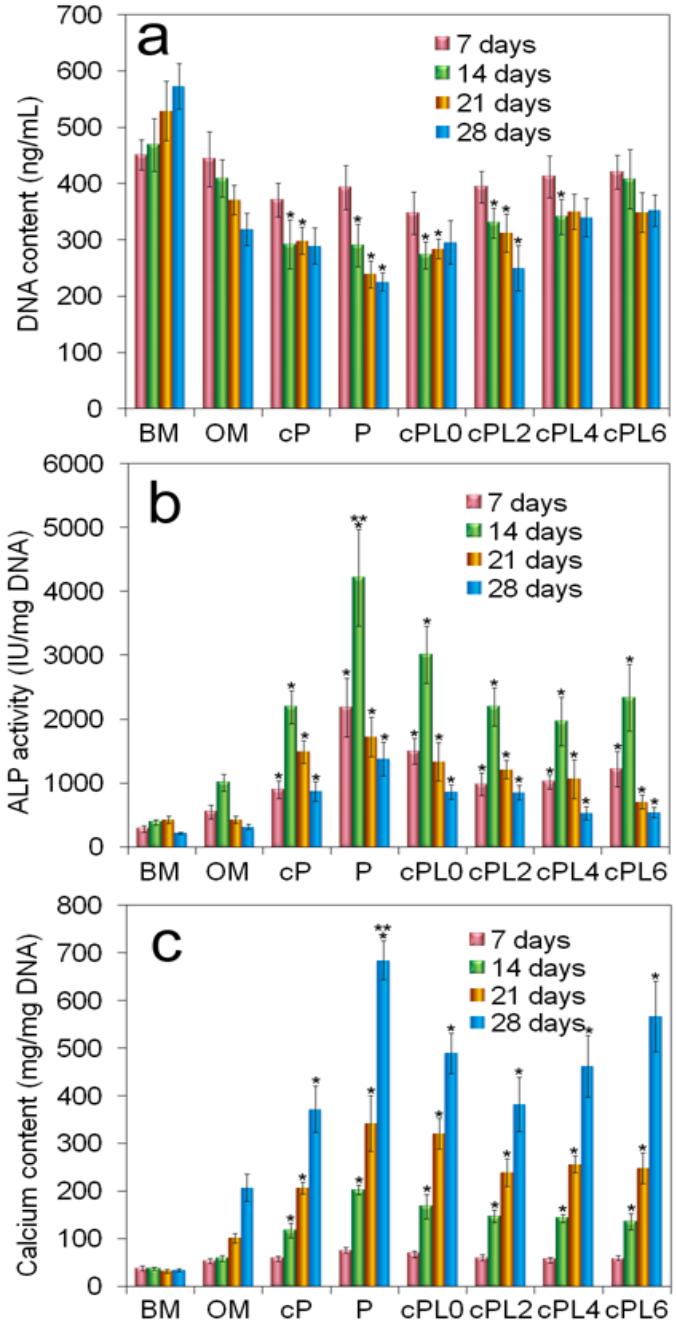

Figure 7.5. DNA content (a), ALP activity (b), and calcium content (c) of hMSCs encapsulated in PEGDA hydrogel and incubated in basal medium (BM, control group), osteogenic medium without DEX (OM, control group), OM with the BMP-2 peptide covalently attached to the hydrogel network (cP), OM with BMP-2 peptide dissolved in the hydrogel (P), OM with peptide/lactide-capped PEG conjugate with zero (cPL0), 2 (cPL2), 4(cPL4) and 6 (cPL6) lactide units, attached to the hydrogel network. One star indicates a statistically significant difference ($p<0.05$) between the test and OM groups at each time point. Two stars indicates a statically significant difference between the test and all other groups at each time point. Error bars correspond to means±1 SD for n=3.

capped with a hydrophobic lactide segment (cPL2, cPL4 and CPL6 groups). However, the lactide segment length did not significantly change the peak ALP activity of hMSCs.

The extent of mineralization of hMSCs, as measured by calcium content, did not change with incubation time in BM but it increased in all OM groups (with or without peptide), as shown in Figure 7.5.c. The addition of BMP-2 peptide to the gel (P group, Figure 7.5.c) significantly increased calcium content compared to that without peptide (OM medium, Figure 7.5.c). Consistent with ALP results, the calcium content of hMSCs cultured in the gel with dissolved peptide (P group) was 680 ± 40 mg/mg DNA which was significantly higher than that conjugated to the gel (cP group, 370 ± 50 mg/mg DNA), as shown by two stars in Figure 7.5.c. Extension of the peptide with a PEG chain increased the calcium content of hMSCs from 370 ± 50 to 500 ± 40 mg/mg DNA at day 28. However, extension of the peptide with a lactide-capped PEG chain (lactide segment length of two, cPL2) significantly reduced calcium content at day 28 compared to PEG-extended peptide. The length of the lactide segment in lactide-capped PEG conjugated peptide did not affect calcium content of hMSCs.

We hypothesized that the lower osteoinductive potential of the peptide groups conjugated to PEG or lactide-capped PEG was due to increased aggregation. The images in Figure 7.6 show the simulated equilibrium structure of BMP-2 peptide or peptide/lactide-capped PEG conjugates in aqueous solution (15 wt%). The blue and brown beads are for acrylate and lactide units, respectively, and ethylene oxide beads are not shown for clarity. Images 7.6.a to 7.6.g correspond to acrylate-terminated (blue beads) PEG, lactide-capped PEG (2 lactides, L2), PL0, PL2, PL4 and PL6, respectively. The acrylate-terminated PEG chains without lactide were uniformly distributed in the

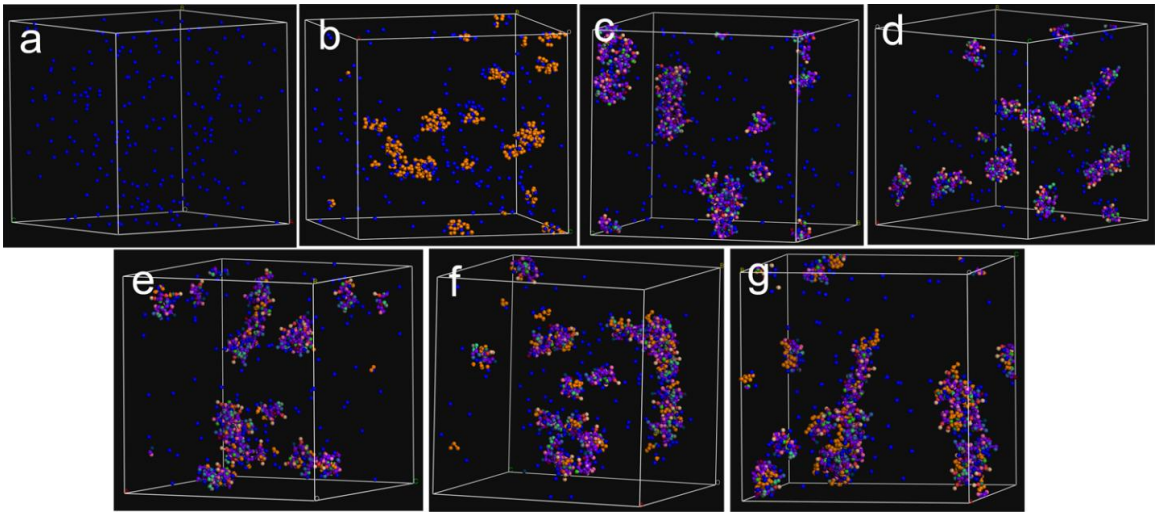

Figure 7.6. Evolution of the BMP-2 peptide aggregates in PEGDA hydrogel (15 wt%) without the peptide or lactide-capped PEG macromer (a, control), with lactide-capped PEG macromer (b, control, L0 group), the peptide (c, P group), the peptide-PEG conjugate (d, PL0 group), the peptide/lactide-capped PEG conjugate with 2 (e, PL2 group), 4 (f, PL4 group), and 6 (g, PL6 group) lactides. The blue and brown beads correspond to acrylate and lactide beads, respectively. Ethylene oxide and water beads are not shown for clarity.

simulated aqueous solution, as shown by the acrylate beads in Figure 7.6.a. PEG chains capped with lactide and terminated with an acrylate group formed micellar structures 1-3 nm in size as shown in Figure 7.6.b,[35, 51] with lactide and ethylene oxide beads forming the core and corona of the micelles, respectively. The acrylate-terminated peptide without (Figure 7.6.c) or with conjugation to PEG (Figure 7.6.d) formed irregularly-shaped aggregates (Figures 7.6.c,d) due to its amphiphilic nature. In the peptide case, hydrophobic side chains of the amino acids formed the core of the aggregates while ethylene oxide beads covered surface of the aggregates with hydrophilic amino acids (polar and charged) positioned at the core-corona interface (Figure 7.6.d). The size of the aggregates increased when the peptide-PEG macromer was capped with 2, 4 and 6 lactide units as shown in Figures 7.6.e, 7.6.f and 7.6.g, respectively, and the

number density of the aggregates decreased with increasing lactide segment length. The cross sections of one of the aggregates in the simulations of Figure 7.6 are shown in Figure 7.7 with green beads representing ethylene oxide (EO) units. The cross sections in Figure 7.7 show that the aggregates in aqueous solution are covered with ethylene oxide units of PEG to reduce the interfacial free energy between the aqueous phase and hydrophobic structures, thus stabilizing the aggregates. Notably, thickness of the EO layer increased with aggregate size.

The average aggregation number (n_{agg}) and fraction of the free peptide (P) and peptide conjugated to lactide-capped PEG (cPL0, cPL2, cPL4 and cPL6) are shown in Figure 7.7.h. Due to PEG hydrophilicity, n_{agg} decreased from 3.4 to 3.0 and aggregate distribution narrowed with conjugation of the peptide to PEG (cP). The n_{agg} increased from 3 to 3.9, 5.8 and 7.7 as the PEG macromer in peptide-PEG conjugate was capped with 2 (cPL2), 4 (cPL4) and 6 (cPL6) lactides, respectively. The n_{agg} increased from 3.4 to 4.3, 6.6 and 11.1 when the peptide was directly conjugated to lactide without PEG with segment length of 2, 4, and 6, respectively. On the other hand, the fraction of free peptide in solution increased from 0.06 to 0.1 with conjugation of the peptide to PEG (cP). Further, the fraction of free peptide decreased from 0.1 to 0.04, 0.03 and 0.02 for cPL2, cPL4 and cPL6, respectively.

To quantify the proximity of different beads, the average number of "b" beads in a sphere of radius R around bead "a" or the running integration number of beads "b" around bead "a", $IN_{ab}(R)$, was calculated by[35, 51]

$$IN_{ab}(R) = 4\pi\rho_{b0}\int_0^R g_{ab}(r)\, r^2 dr \qquad \text{(equation 7.6)}$$

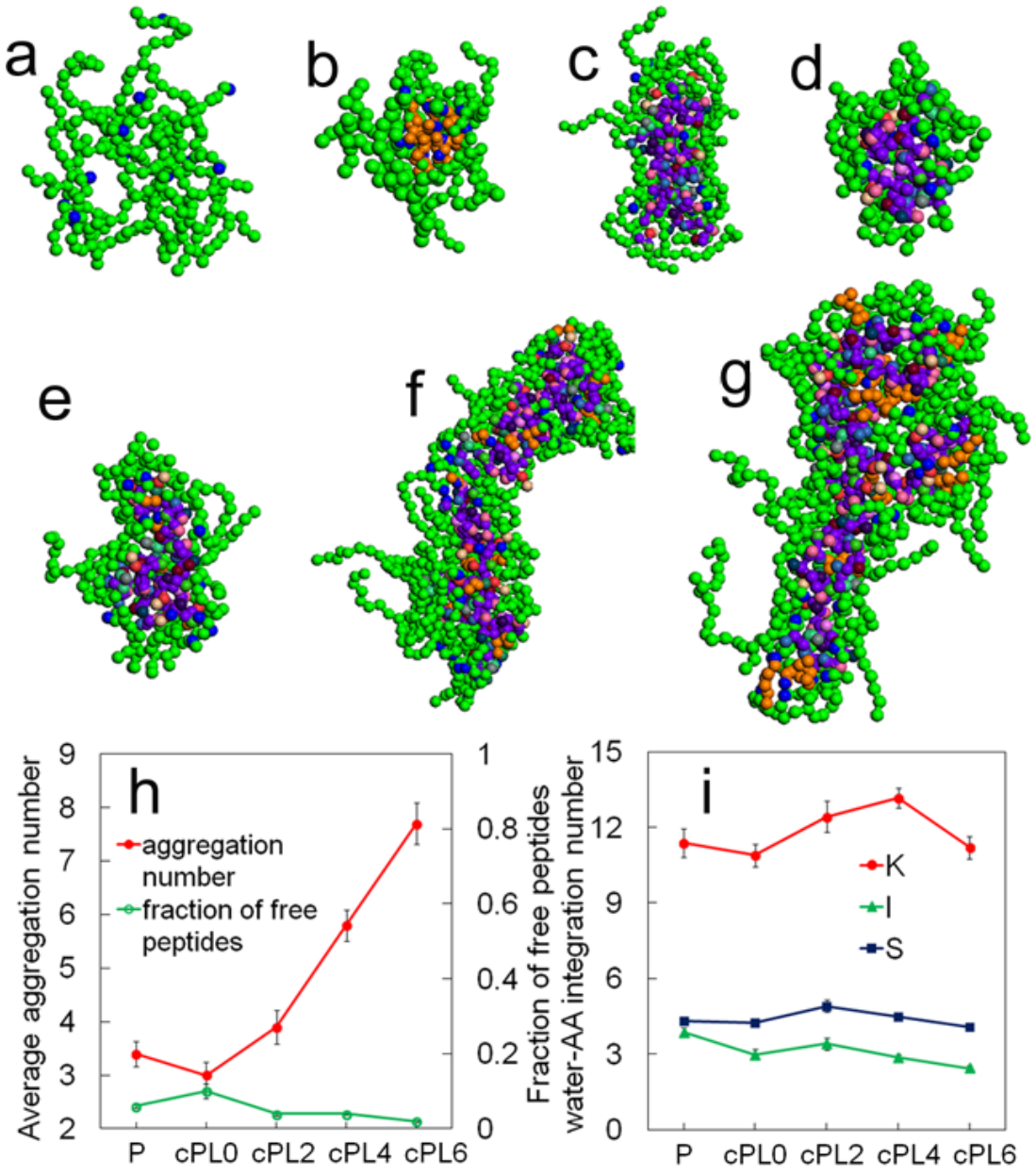

Figure 7.7. Cross-section of one of the BMP-2 peptide aggregates in Figure 5 with green beads representing ethylene oxide units. Images (a-g) correspond to aggregates without the peptide or lactide-capped PEG macromer (a), with lactide-capped PEG macromer (b), the peptide (c), peptide-PEG conjugate (d), peptide/lactide-capped PEG conjugate with 2 (e), 4 (f), and 6 (g) lactides. Water beads are not shown for clarity. (h) Simulated average aggregation number and the fraction of free peptide (h) and the water-amino acid integration number for lysine (charged), serine (uncharged but polar), and isoleucine (nonpolar) (i) for the peptide only (P), peptide-PEG conjugate attached to the hydrogel network (cPL0), peptide/lactide-capped PEG conjugate attached to the gel network with 2 (cPL2), 4 (cPL4), and 6 (cPL6) lactide units. Error bars correspond to means ± SD for 5 simulation runs.

where ρ_{b0} is the overall number density of "b" beads and $g_{ab}(r)$ is the radial distribution function of bead "b" around bead "a", located at the origin. The integration numbers between water and amino acids lysine (K), serine (S) and isoleucine (I) representing charged, polar and hydrophobic amino acids, respectively, are shown in Figure 7.7.i. Isoleucine with lowest $IN_{AA\text{-}w}$ (green curve in Figure 7.7.i) was confined to the center of the aggregates while lysine with highest $IN_{AA\text{-}W}$ was situated on the aggregate surface in proximity to the PEG layer (see Figures 7.7.b-g). The simulation results in Figure 7.7 indicated that, due to peptide aggregation, the encapsulated hMSCs may interact with the PEG layer on the surface of peptide-PEG aggregates or amino acids different from the BMP-2 peptide sequence, leading to a lower osteoinductive potential of the lactide-capped PEG conjugated peptide.

The effect of peptide aggregation on interaction of the peptide with the cell membrane was simulated by molecular dynamics and the results are shown in Figure 7.8. When a single peptide (not an aggregate) or a single peptide-PEG conjugate was in contact with the cell membrane, the distance between the center of masses of the peptide and cell membrane did not change significantly. However, when an aggregate of the BMP-2 peptides (P, upper left and right images) or an aggregate of the peptide-PEG conjugates (PL0, lower left and right images) were in contact with the cell membrane, higher energetic interaction, penetration of the peptide and pore formation in the membrane was observed. However, conjugation of the peptide to PEG (PL0) reduced the attractive interaction between the conjugate and cell membrane and the extent of pore formation. Notably, covalent attachment of the peptide-PEG conjugate to the hydrogel network eliminated pore formation in the cell membrane.

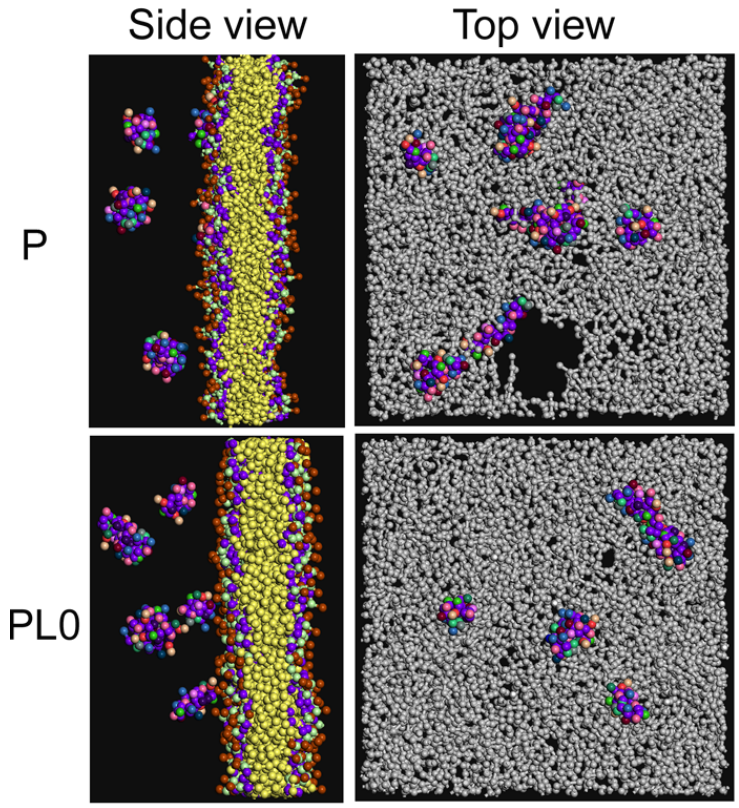

Figure 7.8. Effect of an aggregate of the BMP-2 peptide (top images) and an aggregate of the peptide-PEG conjugate (bottom images) on energetic interaction, penetration of the peptide and pore formation in the cell membrane. The water beads are not shown for clarity. The images on the left and right show the side and top views of the membrane, respectively. In the top view, all membrane beads are shown in gray for clarity.

7.4. DISCUSSION

Aside from cost efficiency, osteogenic peptides are less likely to lose their activity by denaturation than their corresponding protein. Therefore, a wider range of methods can be used for incorporation of osteogenic peptides in engineered scaffolds. Li and collaborators measured osteoinductivity of the BMP-2 peptide loaded in nano-hydroxy apatite/collagen/poly(L-lactic acid) scaffolds by implantation in a rat calvarial defect.[336] They reported that 3 mg of the BMP-2 peptide loaded in the scaffold had osteoinductive potential similar to 1 µg of BMP-2 protein, indicating that 3000-fold higher BMP-2 peptide concentrations are required to achieve the same activity as the

protein. Our results demonstrate that although the addition of the BMP-2 peptide significantly increased osteoinductive potential, but the level of activity was much less than that of BMP-2 protein even at 12000-fold higher molar concentrations (1000-fold higher mass concentrations). Further, the expression of RunX-2, a marker for the onset of osteogenic differentiation, was delayed with the BMP-2 peptide compared to BMP-2 protein (Figure 7.2.e). One factor that can lower osteoinductive potential of the peptide is aggregation in aqueous solution. The peptide is derived from BMP-2 protein based on its ability to differentiate MSCs to the osteogenic lineage without consideration for its stability in aqueous solution. Hydrophobicity index analysis of each amino acid indicated that the peptide is amphiphilic with an overall positive index of hydrophobicity. Therefore, the peptide tends to form aggregates above its CMC in aqueous solution to reduce the interfacial free energy. The BMP-2 peptide concentration range of 0.00025-0.005 mM was below the peptide's CMC concentration of 0.019 mM (or 0.040 mM based on the simulation results). Therefore, based on the experimental and simulated values for CMC, the peptides in cell encapsulation experiments with 0.00025-0.005 mM concentrations were most likely not aggregated. Above CMC concentration, the fraction of free peptide decreased with increasing peptide concentration but the free peptide density in the hydrogel slightly increased which could explain the slight increase in osteoinductive potential with increasing peptide concentration in Figure 7.2. Therefore, the experimental and computational results indicate that osteoinductive potential of the BMP-2 peptide is related to the density of free non-aggregated peptide in aqueous solution, not the overall concentration. Further, simulation results show that the amino acids in the peptide aggregates facing the aqueous phase may be different from those of

the free peptide (Figure 7.7.i) which may lead to non-specific interaction of the aggregates with cell surface receptors. In addition, simulation results in Figure 7.8 show that the peptide aggregates (P) had a higher energy of interaction with the cell membrane than the free peptide, leading to undesired pore formation on the membrane and reduced peptide activity. When the peptide was conjugated to PEG (PL0), the peptide aggregates were shielded from the cell membrane by surface-bound PEG chains, which slightly increased peptide activity. This is consistent with previous results that palmitoylation of pro-apoptotic peptides can affect micelle stability and cell uptake.[337]

The results show that there was higher osteogenic differentiation of encapsulated hMSCs when the BMP-2 peptide was dissolved in the hydrogel matrix as compared to conjugated peptide (Figure 7.5) which was similar to the previously reported lower activity of BMP-2 protein attached to immobilized heparin.[338] Conjugation of the peptide to the hydrophilic PEGDA matrix decreased the degree of freedom of the peptide beads, which decreased aggregation and increased the free peptide density. Further capping the PEG chain with hydrophobic lactide units increased aggregation number of the conjugated peptide which can be explained by a decrease in CMC. The free energy of micelle formation is related to CMC by [334, 339]

$$\Delta G_{mic}^{0} = RT\ln(CMC) \qquad \text{(equation 7.7)}$$

where R and T are the gas constant and absolute temperature respectively and ΔG_{mic}^{0} is the difference in free energy of the peptide between the dissolved and aggregated states. CMC and ΔG_{mic}^{0} increased with conjugation of the peptide to hydrophilic PEG, leading to an increase in free peptide concentration and higher osteoinductive potential of the PEG-conjugated peptide (cPL0) compared to cP. However, the addition of hydrophobic lactide

units to the PEG-peptide conjugate offset the positive effect of PEG conjugation to the peptide, leading to an insignificant change in osteoinductive potential of cPL2, cPL4 and cPL6 groups compared to cPL0.

7.5. CONCLUSION

In this work, the effect of concentration and hydrophobicity of the BMP-2 peptide, from residues 73-92 of the knuckle epitope of BMP-2 protein, on differentiation of hMSCs encapsulated in PEGDA hydrogel was investigated experimentally and by molecular dynamic simulation. The encapsulated cells were cultured in osteogenic medium without DEX supplemented with the BMP-2 peptide. The index of hydrophobicity of the peptide was varied by conjugation to a lactide-capped PEG chain with 0-6 lactide units. The BMP-2 peptide dissolved in the hydrogel had significantly higher osteoinductive potential than the attached peptide consistent with the fact that BMP-2 protein is associated with the soluble not the insoluble fraction of the bone matrix. The osteoinductive potential of the BMP-2 peptide was significantly less than the protein even at 12000-fold higher molar concentrations which was explained by peptide aggregation in aqueous solution. Based on simulation results, the fraction of free peptide in solution decreased while the concentration of free peptide increased slightly with 1000-fold increase in peptide concentration in aqueous solution, which reduced osteoinductive potential of the peptide. A decrease in the index of hydrophobicity of the peptide by conjugation to PEG increased CMC which increased osteoinductive potential of the peptide. Conversely, an increase in the index of hydrophobicity of the peptide by conjugation to lactide-capped PEG reduced CMC which reduced the peptide osteoinductive potential. Experimental and simulation results indicated that

osteoinductive potential of the BMP-2 peptide should be correlated with its hydrophobicity index, CMC concentration in aqueous medium, and the concentration of free peptide in solution, not the total peptide concentration.

CHAPTER 8

CONCLUDING REMARKS

This work showed that hydrogels based on star PEG macromonomers chain extended with short hydroxyl acid segments (SPEXA) with a wide range of degradation rate, gelation kinetics and mechanical properties are potential candidates for delivery of stem cells to the site of regeneration in tissue engineering. Although SPEXA hydrogels were applied in this work for osteogenic differentiation and mineralization of MSCs, these gels can be utilized for a wide range of applications including vasculogenic differentiation of endothelial progenitor cells or chondrocyte implantation in cartilage regeneration. Further, results of this work demonstrated that the nano-scale characteristics of the hydrogels' precursor solutions, predicted via meso-scale molecular simulation methods, can be utilized for anticipating the hydrogels' macroscopic properties including degradation rate, gelation kinetics and stiffness. In addition, experimental and simulation results revealed that activity of a model osteo-inductive peptide in PEG based hydrogels is correlated with the free peptide concentration in aqueous medium and not the total concentration. To continue this work it is necessary to study the effect of concentration and hydrophobicity of other osteo-inductive peptides on the activity of peptides and interaction of peptides with cell-surface receptors.

REFERENCES

1. Di Silvestre, M., F. Lolli, and G. Bakaloudis, *Degenerative lumbar scoliosis in elderly patients: dynamic stabilization without fusion versus posterior instrumented fusion.* Spine Journal, 2014. **14**(1): p. 1-10.

2. Agrawal, A., et al., *Primary Ewing's sarcoma of the frontal bone with intracranial extension.* Journal of Cancer Research and Therapeutics, 2009. **5**(3): p. 208-209.

3. Flierl, M.A., et al., *Outcomes and complication rates of different bone grafting modalities in long bone fracture nonunions: a retrospective cohort study in 182 patients.* Journal of Orthopaedic Surgery and Research, 2013. **8**.

4. Brydone, A.S., D. Meek, and S. Maclaine, *Bone grafting, orthopaedic biomaterials, and the clinical need for bone engineering.* Proceedings of the Institution of Mechanical Engineers Part H-Journal of Engineering in Medicine, 2010. **224**(H12): p. 1329-1343.

5. Giannoudis, P.V., H. Dinopoulos, and E. Tsiridis, *Bone substitutes: An update.* Injury-International Journal of the Care of the Injured, 2005. **36**: p. 20-27.

6. *2012 Spinal Industry Update.* Orthopedic Network News, 2012. **23**(4).

7. Goulet, J.A., et al., *Autogenous iliac crest bone graft - Complications and functional assessment.* Clinical Orthopaedics and Related Research, 1997(339): p. 76-81.

8. Fishman, J.A., M.A. Greenwald, and P.A. Grossi, *Transmission of Infection With Human Allografts: Essential Considerations in Donor Screening.* Clinical Infectious Diseases, 2012. **55**(5): p. 720-727.

9. Wheeler, D.L. and W.F. Enneking, *Allograft bone decreases in strength in vivo over time.* Clinical Orthopaedics and Related Research, 2005(435): p. 36-42.

10. Dawson, J.I., et al., *Concise Review: Bridging the Gap: Bone Regeneration Using Skeletal Stem Cell-Based Strategies-Where Are We Now?* Stem Cells, 2014. **32**(1): p. 35-44.

11. Jones, E. and X.B. Yang, *Mesenchymal stem cells and bone regeneration: Current status.* Injury-International Journal of the Care of the Injured, 2011. **42**(6): p. 562-568.

12. Guan, M., et al., *Directing mesenchymal stem cells to bone to augment bone formation and increase bone mass.* Nature Medicine, 2012. **18**(3): p. 456-U159.

13. Hoffman, M.D., et al., *The effect of mesenchymal stem cells delivered via hydrogel-based tissue engineered periosteum on bone allograft healing.* Biomaterials, 2013. **34**(35): p. 8887-8898.

14. Clarke, B., *Normal Bone Anatomy and Physiology*. Clinical Journal of the American Society of Nephrology, 2008. **3**: p. S131-S139.

15. Colnot, C., *Skeletal Cell Fate Decisions Within Periosteum and Bone Marrow During Bone Regeneration (vol 24, pg 274, 2009).* Journal of Bone and Mineral Research, 2009. **24**(4): p. 758-758.

16. Devescovi, V., et al., *Growth factors in bone repair*. La Chirurgia degli Organi di Movimento, 2008. **92**(3): p. 161-168.

17. Burdick, J.A. and K.S. Anseth, *Photoencapsulation of osteoblasts in injectable RGD-modified PEG hydrogels for bone tissue engineering.* Biomaterials, 2002. **23**(22): p. 4315-4323.

18. Saito, A., et al., *Activation of osteo-progenitor cells by a novel synthetic peptide derived from the bone morphogenetic protein-2 knuckle epitope.* Biochimica Et Biophysica Acta-Proteins and Proteomics, 2003. **1651**(1-2): p. 60-67.

19. Heino, T.J. and T.A. Hentunen, *Differentiation of Osteoblasts and Osteocytes from Mesenchymal Stem Cells.* Current Stem Cell Research & Therapy, 2008. **3**(2): p. 131-145.

20. Drury, J.L. and D.J. Mooney, *Hydrogels for tissue engineering: scaffold design variables and applications.* Biomaterials, 2003. **24**(24): p. 4337-4351.

21. Peppas, N.A. and S.R. Lustig,
solute diffusion in hydrophilic network structures, in hydrogels in medicine and pharmacy. I. Fundamentals. 2004: CRC Press.

22. Liang, S.M., et al., *Protein diffusion in agarose hydrogel in situ measured by improved refractive index method.* Journal of Controlled Release, 2006. **115**(2): p. 189-196.

23. Beruto, D.T. and R. Botter, *Role of the water matric potential (Psi(M)) and of equilibrium water content (EWC) on the water self-diffusion coefficient and on the oxygen permeability in hydrogel contact lenses.* Biomaterials, 2004. **25**(14): p. 2877-2883.

24. Sarvestani, A.S., X.Z. He, and E. Jabbari, *Viscoelastic characterization and modeling of gelation kinetics of injectable in situ cross-linkable poly(lactide-co-ethylene oxide-co-fumarate) hydrogels.* Biomacromolecules, 2007. **8**(2): p. 406-415.

25. Lapienis, G., *Star-shaped polymers having PEO arms.* Progress in Polymer Science, 2009. **34**(9): p. 852-892.

26. Seck, T.M., et al., *Designed biodegradable hydrogel structures prepared by stereolithography using poly(ethylene glycol)/poly(D,L-lactide)-based resins.* Journal of Controlled Release, 2010. **148**(1): p. 34-41.

27. Wang, H.B., et al., *Injectable cardiac tissue engineering for the treatment of myocardial infarction.* Journal of Cellular and Molecular Medicine, 2010. **14**(5): p. 1044-1055.

28. Zhao, L.A., M.D. Weir, and H.H.K. Xu, *An injectable calcium phosphate-alginate hydrogel-umbilical cord mesenchymal stem cell paste for bone tissue engineering.* Biomaterials, 2010. **31**(25): p. 6502-6510.

29. Klein, J., *CHEMISTRY Repair or Replacement-A Joint Perspective.* Science, 2009. **323**(5910): p. 47-48.

30. Cushing, M.C. and K.S. Anseth, *Hydrogel cell cultures.* Science, 2007. **316**(5828): p. 1133-1134.

31. Salinas, C.N. and K.S. Anseth, *Mesenchymal Stem Cells for Craniofacial Tissue Regeneration: Designing Hydrogel Delivery Vehicles.* Journal of Dental Research, 2009. **88**(8): p. 681-692.

32. Bosnakovski, D., et al., *Chondrogenic differentiation of bovine bone marrow mesenchymal stem cells (MSCs) in different hydrogels: Influence of collagen type II extracellular matrix on MSC chondrogenesis.* Biotechnology and Bioengineering, 2006. **93**(6): p. 1152-1163.

33. Kundu, A.K. and A.J. Putnam, *Vitronectin and collagen I differentially regulate osteogenesis in mesenchymal stem cells.* Biochemical and Biophysical Research Communications, 2006. **347**(1): p. 347-357.

34. Aamer, K.A., et al., *Rheological studies of PLLA-PEO-PLLA triblock copolymer hydrogels.* Biomaterials, 2004. **25**(6): p. 1087-1093.

35. Moeinzadeh, S., et al., *Gelation Characteristics and Osteogenic Differentiation of Stromal Cells in Inert Hydrolytically Degradable Micellar Polyethylene Glycol Hydrogels.* Biomacromolecules, 2012. **13**(7): p. 2073-2086.

36. Pollock, J.F. and K.E. Healy, *Mechanical and swelling characterization of poly(N-isopropyl acrylamide-co-methoxy poly(ethylene glycol) methacrylate) sol-gels.* Acta Biomaterialia, 2010. **6**(4): p. 1307-1318.

37. Wang, D., et al., *Hydrolytic degradation of POSS-PEG-lactide hybrid hydrogels.* Polymer Degradation and Stability, 2011. **96**(1): p. 123-130.

38. Sakai, T., et al., *Design and fabrication of a high-strength hydrogel with ideally homogeneous network structure from tetrahedron-like macromonomers.* Macromolecules, 2008. **41**(14): p. 5379-5384.

39. Wang, F., et al., *Synthesis and evaluation of a star amphiphilic block copolymer from poly(epsilon-caprolactone) and poly(ethylene glycol) as a potential drug delivery carrier.* Bioconjugate Chemistry, 2005. **16**(2): p. 397-405.

40. Nagahama, K., Y. Ohya, and T. Ouchi, *Suppression of cell and platelet adhesion to star-shaped 8-armed poly(ethylene glycol)-poly(L-lactide) block copolymer films.* Macromolecular Bioscience, 2006. **6**(6): p. 412-419.

41. He, X.Z. and E. Jabbari, *Material properties and cytocompatibility of injectable MMP degradable poly(lactide ethylene oxide fumarate) hydrogel as a carrier for marrow stromal cells.* Biomacromolecules, 2007. **8**(3): p. 780-792.

42. Lee, P.J., R. Langer, and V.P. Shastri, *Role of n-methyl pyrrolidone in the enhancement of aqueous phase transdermal transport.* Journal of Pharmaceutical Sciences, 2005. **94**(4): p. 912-917.

43. Ovsianikov, A., et al., *Three-dimensional laser micro- and nano-structuring of acrylated poly(ethylene glycol) materials and evaluation of their cytoxicity for tissue engineering applications.* Acta Biomaterialia, 2011. **7**(3): p. 967-974.

44. Fu, Y., et al., *3D cell entrapment in crosslinked thiolated gelatin-poly(ethylene glycol) diacrylate hydrogels.* Biomaterials, 2012. **33**(1): p. 48-58.

45. Sarvestani, A.S. and E. Jabbari, *Modeling and experimental investigation of rheological properties of injectable poly(lactide ethylene oxide fumarate)/hydroxyapatite nanocomposites.* Biomacromolecules, 2006. **7**(5): p. 1573-1580.

46. Gilbert, P.M., et al., *Substrate Elasticity Regulates Skeletal Muscle Stem Cell Self-Renewal in Culture.* Science, 2010. **329**(5995): p. 1078-1081.

47. van Dijk, M., et al., *Synthesis and Characterization of Enzymatically Biodegradable PEG and Peptide-Based Hydrogels Prepared by Click Chemistry.* Biomacromolecules, 2010. **11**(6): p. 1608-1614.

48. Adeloew, C., et al., *The effect of enzymatically degradable poly(ethylene glycol) hydrogels on smooth muscle cell phenotype.* Biomaterials, 2008. **29**(3): p. 314-326.

49. Nair, L.S. and C.T. Laurencin, *Biodegradable polymers as biomaterials.* Progress in Polymer Science, 2007. **32**(8-9): p. 762-798.

50. Barati, D., et al., *Time dependence of material properties of polyethylene glycol hydrogels chain extended with short hydroxy acid segments.* Polymer, 2014. **55**(16): p. 3894-3904.

51. Moeinzadeh, S., et al., *Nanostructure Formation and Transition from Surface to Bulk Degradation in Polyethylene Glycol Gels Chain-Extended with Short Hydroxy Acid Segments.* Biomacromolecules, 2013. **14**(8): p. 2917-2928.

52. Moeinzadeh, S., et al., *Synthesis and gelation characteristics of photo-crosslinkable star Poly (ethylene oxide-co-lactide-glycolide acrylate) macromonomers.* Polymer, 2011. **52**(18): p. 3887-3896.

53. Choi, Y.R., Y.H. Bae, and S.W. Kim, *Star-shaped poly(ether-ester) block copolymers: Synthesis, characterization, and their physical properties.* Macromolecules, 1998. **31**(25): p. 8766-8774.

54. Keys, K.B., F.M. Andreopoulos, and N.A. Peppas, *Poly(ethylene glycol) star polymer hydrogels.* Macromolecules, 1998. **31**(23): p. 8149-8156.

55. Sukumar, V.S. and S.T. Lopina, *Network model for the swelling properties of end-linked linear and star poly(ethylene oxide) hydrogels.* Macromolecules, 2002. **35**(27): p. 10189-10192.

56. Moeinzadeh, S., et al., *Synthesis and gelation characteristics of photo-crosslinkable star Poly (ethylene oxide-co-lactide-glycolide acrylate) macromonomers.* Polymer, 2011.

57. Hiemstra, C., et al., *Rapidly in situ forming biodegradable robust hydrogels by combining stereocomplexation and photopolymerization.* Journal of the American Chemical Society, 2007. **129**(32): p. 9918-9926.

58. Groot, R.D. and P.B. Warren, *Dissipative particle dynamics: Bridging the gap between atomistic and mesoscopic simulation.* Journal of Chemical Physics, 1997. **107**(11): p. 4423-4435.

59. Moeinzadeh, S. and E. Jabbari, *Mesoscale Simulation of the effect of Lactide Segment on Nanostructure of Poly(ethylene glycol-co-lactide)-Acrylate Macromonomers in Aqueous Solution.* Journal of physical chemistry B, 2012.

60. Moeinzadeh, S. and E. Jabbari, *Mesoscale Simulation of the Effect of a Lactide Segment on the Nanostructure of Star Poly(ethylene glycol-co-lactide)-Acrylate Macromonomers in Aqueous Solution.* Journal of Physical Chemistry B, 2012. **116**(5): p. 1536-1543.

61. Linkhart, T.A., S. Mohan, and D.J. Baylink, *Growth factors for bone growth and repair: IGF, TGF beta and BMP.* Bone, 1996. **19**(1): p. S1-S12.

62. Mckay, W.F., S.M. Peckham, and J.M. Badura, *A comprehensive clinical review of recombinant human bone morphogenetic protein-2 (INFUSE (R) Bone Graft).* International Orthopaedics, 2007. **31**(6): p. 729-734.

63. Burkus, J.K., J.D. Dorchak, and D.L. Sanders, *Radiographic assessment of interbody fusion using recombinant human bone morphogenetic protein type 2.* Spine, 2003. **28**(4): p. 372-377.

64. McKay, B. and H.S. Sandhu, *Use of recombinant human bone morphogenetic protein-2 in spinal fusion applications.* Spine, 2002. **27**(16): p. S66-S85.

65. Carragee, E.J., E.L. Hurwitz, and B.K. Weiner, *A critical review of recombinant human bone morphogenetic protein-2 trials in spinal surgery: emerging safety concerns and lessons learned.* Spine Journal, 2011. **11**(6): p. 471-491.

66. Jabbari, E., *Osteogenic Peptides in Bone Regeneration.* Current Pharmaceutical Design, 2013. **19**(19): p. 3391-3402.

67. Moeinzadeh, S., et al., *Experimental and Computational Investigation of the Effect of Hydrophobicity on Aggregation and Osteoinductive Potential of BMP-2 Derived Peptide in a Hydrogel Matrix.* Tissue Engineering Part A, 2014.

68. Grassel, S. and N. Ahmed, *Influence of cellular microenvironment and paracrine signals on chondrogenic differentiation.* Frontiers in Bioscience, 2007. **12**: p. 4946-4956.

69. Nombela-Arrieta, C., J. Ritz, and L.E. Silberstein, *The elusive nature and function of mesenchymal stem cells.* Nature Reviews Molecular Cell Biology, 2011. **12**(2): p. 126-131.

70. McBride, S.H., S.F. Evans, and M.L.K. Tate, *Anisotropic mechanical properties of ovine femoral periosteum and the effects of cryopreservation.* Journal of Biomechanics, 2011. **44**(10): p. 1954-1959.

71. Rho, J.Y., L. Kuhn-Spearing, and P. Zioupos, *Mechanical properties and the hierarchical structure of bone.* Medical Engineering & Physics, 1998. **20**(2): p. 92-102.

72. Ferretti, M., et al., *Does static precede dynamic osteogenesis in endochondral ossification as occurs in intramembranous ossification?* Anatomical Record Part a-Discoveries in Molecular Cellular and Evolutionary Biology, 2006. **288A**(11): p. 1158-1162.

73. Engler, A.J., et al., *Matrix elasticity directs stem cell lineage specification.* Cell, 2006. **126**(4): p. 677-689.

74. Nava, M.M., M.T. Raimondi, and R. Pietrabissa, *Controlling Self-Renewal and Differentiation of StemCells via Mechanical Cues.* Journal of Biomedicine and Biotechnology, 2012.

75. Huebsch, N., et al., *Harnessing traction-mediated manipulation of the cell/matrix interface to control stem-cell fate.* Nature Materials, 2010. **9**(6): p. 518-526.

76. Parekh, S.H., et al., *Modulus-driven differentiation of marrow stromal cells in 3D scaffolds that is independent of myosin-based cytoskeletal tension.* Biomaterials, 2011. **32**(9): p. 2256-2264.

77. Palumbo, C., M. Ferretti, and A. De Pol, *Apoptosis during intramernbranous ossification.* Journal of Anatomy, 2003. **203**(6): p. 589-598.

78. Pallotta, I., et al., *Bone Marrow Osteoblastic Niche: A New Model to Study Physiological Regulation of Megakaryopoiesis.* Plos One, 2009. **4**(12).

79. Govender, S., et al., *Recombinant human bone morphogenetic protein-2 for treatment of open tibial fractures - A prospective, controlled, randomized study of four hundred and fifty patients.* Journal of Bone and Joint Surgery-American Volume, 2002. **84A**(12): p. 2123-2134.

80. Flory, P.J., *Principles of Polymer Chemistry*. 1953, New York: Cornell University Press.

81. Uchida, R., et al., *Azulene incorporation and release by hydrogel containing methacrylamide propyltrimenthylammonium chloride, and its application to soft contact lens.* Journal of Controlled Release, 2003. **92**(3): p. 259-264.

82. Schultz, C.L., T.R. Poling, and J.O. Mint, *A medical device/drug delivery system for treatment of glaucoma.* Clinical and Experimental Optometry, 2009. **92**(4): p. 343-348.

83. Xu, J.K., X.S. Li, and F.Q. Sun, *Preparation and Evaluation of a Contact Lens Vehicle for Puerarin Delivery.* Journal of Biomaterials Science-Polymer Edition, 2010. **21**(3): p. 271-288.

84. Vukelja, S.J., et al., *Phase 1 study of escalating-dose OncoGel((R)) (ReGel((R))/paclitaxel) depot injection, a controlled-release formulation of paclitaxel, for local management of superficial solid tumor lesions.* Anti-Cancer Drugs, 2007. **18**(3): p. 283-289.

85. Meenach, S.A., J.Z. Hilt, and K.W. Anderson, *Poly(ethylene glycol)-based magnetic hydrogel nanocomposites for hyperthermia cancer therapy.* Acta Biomaterialia, 2010. **6**(3): p. 1039-1046.

86. Shim, W.S., et al., *pH- and temperature-sensitive, injectable, biodegradable block copolymer hydrogels as carriers for paclitaxel.* International Journal of Pharmaceutics, 2007. **331**(1): p. 11-18.

87. Cheng, Y.H., et al., *Thermosensitive Chitosan-Gelatin-Glycerol Phosphate Hydrogels as a Cell Carrier for Nucleus Pulposus Regeneration: An In Vitro Study.* Tissue Engineering Part A, 2010. **16**(2): p. 695-703.

88. Sarvestani, A.S., et al., *Gelation and degradation characteristics of< i> in situ</i> photo-crosslinked poly (l-lactide-< i> co</i>-ethylene oxide-< i> co</i>-fumarate) hydrogels.* Polymer, 2007. **48**(24): p. 7113-7120.

89. Wang, C.M., R.R. Varshney, and D.A. Wang, *Therapeutic cell delivery and fate control in hydrogels and hydrogel hybrids.* Advanced Drug Delivery Reviews, 2010. **62**(7-8): p. 699-710.

90. McLaughlin, C.R., et al., *Bioengineered corneas for transplantation and in vitro toxicology.* Frontiers in Bioscience-Landmark, 2009. **14**: p. 3326-3337.

91. Perez, R.A., et al., *Utilizing Core-Shell Fibrous Collagen-Alginate Hydrogel Cell Delivery System for Bone Tissue Engineering.* Tissue Engineering Part A, 2014. **20**(1-2): p. 103-114.

92. Hesse, E., et al., *Collagen type I hydrogel allows migration, proliferation, and osteogenic differentiation of rat bone marrow stromal cells.* Journal of Biomedical Materials Research Part A, 2010. **94A**(2): p. 442-449.

93. Wang, L.M., R.R. Rao, and J.P. Stegemann, *Delivery of Mesenchymal Stem Cells in Chitosan/Collagen Microbeads for Orthopedic Tissue Repair.* Cells Tissues Organs, 2013. **197**(5): p. 333-343.

94. Banerjee, A., et al., *The influence of hydrogel modulus on the proliferation and differentiation of encapsulated neural stem cells.* Biomaterials, 2009. **30**(27): p. 4695-4699.

95. DeKosky, B.J., et al., *Hierarchically Designed Agarose and Poly(Ethylene Glycol) Interpenetrating Network Hydrogels for Cartilage Tissue Engineering.* Tissue Engineering Part C-Methods, 2010. **16**(6): p. 1533-1542.

96. Yuan, T., et al., *Collagen hydrogel as an immunomodulatory scaffold in cartilage tissue engineering.* Journal of Biomedical Materials Research Part B-Applied Biomaterials, 2014. **102**(2): p. 337-344.

97. Roberts, J.J. and S.J. Bryant, *Comparison of photopolymerizable thiol-ene PEG and acrylate-based PEG hydrogels for cartilage development.* Biomaterials, 2013. **34**(38): p. 9969-9979.

98. Mirahmadi, F., et al., *Enhanced mechanical properties of thermosensitive chitosan hydrogel by silk fibers for cartilage tissue engineering.* Materials Science & Engineering C-Materials for Biological Applications, 2013. **33**(8): p. 4786-4794.

99. Park, H., et al., *Injectable chitosan hyaluronic acid hydrogels for cartilage tissue engineering.* Acta Biomaterialia, 2013. **9**(1): p. 4779-4786.

100. Chen, Y.C., et al., *Functional Human Vascular Network Generated in Photocrosslinkable Gelatin Methacrylate Hydrogels.* Advanced Functional Materials, 2012. **22**(10): p. 2027-2039.

101. Benoit, D.S.W., A.R. Durney, and K.S. Anseth, *Manipulations in hydrogel degradation behavior enhance osteoblast function and mineralized tissue formation.* Tissue Engineering, 2006. **12**(6): p. 1663-1673.

102. Bryant, S.J. and K.S. Anseth, *Hydrogel properties influence ECM production by chondrocytes photoencapsulated in poly(ethylene glycol) hydrogels.* Journal of Biomedical Materials Research, 2002. **59**(1): p. 63-72.

103. Lee, K.Y. and D.J. Mooney, *Hydrogels for tissue engineering.* Chemical Reviews, 2001. **101**(7): p. 1869-1879.

104. Brodsky, B. and J.A.M. Ramshaw, *The collagen triple-helix structure.* Matrix Biology, 1997. **15**(8-9): p. 545-554.

105. Yamamoto, M., Y. Tabata, and Y. Ikada, *Growth factor release from gelatin hydrogel for tissue engineering.* Journal of Bioactive and Compatible Polymers, 1999. **14**(6): p. 474-489.

106. Chevallay, B. and D. Herbage, *Collagen-based biomaterials as 3D scaffold for cell cultures: applications for tissue engineering and gene therapy.* Medical & Biological Engineering & Computing, 2000. **38**(2): p. 211-218.

107. Rault, I., et al., *Evaluation of different chemical methods for cross-linking collagen gel, films and sponges.* Journal of Materials Science-Materials in Medicine, 1996. **7**(4): p. 215-221.

108. Van Vlierberghe, S., P. Dubruel, and E. Schacht, *Biopolymer-Based Hydrogels As Scaffolds for Tissue Engineering Applications: A Review.* Biomacromolecules, 2011. **12**(5): p. 1387-1408.

109. Zhao, W., et al., *Degradable natural polymer hydrogels for articular cartilage tissue engineering.* Journal of Chemical Technology and Biotechnology, 2013. **88**(3): p. 327-339.

110. Ko, D.Y., et al., *Recent progress of in situ formed gels for biomedical applications.* Progress in Polymer Science, 2013. **38**(3-4): p. 672-701.

111. Atzet, S., et al., *Degradable Poly(2-hydroxyethyl methacrylate)-co-polycaprolactone Hydrogels for Tissue Engineering Scaffolds.* Biomacromolecules, 2008. **9**(12): p. 3370-3377.

112. Cha, C., et al., *Designing Biomaterials To Direct Stem Cell Fate.* Acs Nano, 2012. **6**(11): p. 9353-9358.

113. He, X.Z., J.Y. Ma, and E. Jabbari, *Effect of Grafting RGD and BMP-2 Protein-Derived Peptides to a Hydrogel Substrate on Osteogenic Differentiation of Marrow Stromal Cells.* Langmuir, 2008. **24**(21): p. 12508-12516.

114. Yang, F., et al., *The effect of incorporating RGD adhesive peptide in polyethylene glycol diacrylate hydrogel on osteogenesis of bone marrow stromal cells.* Biomaterials, 2005. **26**(30): p. 5991-5998.

115. Bryant, S.J., et al., *Encapsulating Chondrocytes in degrading PEG hydrogels with high modulus: Engineering gel structural changes to facilitate cartilaginous tissue production.* Biotechnology and Bioengineering, 2004. **86**(7): p. 747-755.

116. Liu, S.Q., et al., *Synthetic hydrogels for controlled stem cell differentiation.* Soft Matter, 2010. **6**(1): p. 67-81.

117. Hassan, C.M. and N.A. Peppas, *Structure and applications of poly(vinyl alcohol) hydrogels produced by conventional crosslinking or by freezing/thawing methods.* Biopolymers/Pva Hydrogels/Anionic Polymerisation Nanocomposites, 2000. **153**: p. 37-65.

118. Stauffer, S.R. and N.A. Peppas, *Poly(Vinyl Alcohol) Hydrogels Prepared by Freezing-Thawing Cyclic Processing.* Polymer, 1992. **33**(18): p. 3932-3936.

119. Cha, W.I., S.H. Hyon, and Y. Ikada, *Microstructure of Poly(Vinyl Alcohol) Hydrogels Investigated with Differential Scanning Calorimetry.* Makromolekulare Chemie-Macromolecular Chemistry and Physics, 1993. **194**(9): p. 2433-2441.

120. Bidault, L., et al., *Self-Supported Fibrin-Polyvinyl Alcohol Interpenetrating Polymer Networks: An Easily Handled and Rehydratable Biomaterial.* Biomacromolecules, 2013. **14**(11): p. 3870-3879.

121. Schmedlen, K.H., K.S. Masters, and J.L. West, *Photocrosslinkable polyvinyl alcohol hydrogels that can be modified with cell adhesion peptides for use in tissue engineering.* Biomaterials, 2002. **23**(22): p. 4325-4332.

122. Hartgerink, J.D., E. Beniash, and S.I. Stupp, *Self-assembly and mineralization of peptide-amphiphile nanofibers.* Science, 2001. **294**(5547): p. 1684-1688.

123. Holmes, T.C., et al., *Extensive neurite outgrowth and active synapse formation on self-assembling peptide scaffolds.* Proceedings of the National Academy of Sciences of the United States of America, 2000. **97**(12): p. 6728-6733.

124. Caplan, M.R., et al., *Control of self-assembling oligopeptide matrix formation through systematic variation of amino acid sequence.* Biomaterials, 2002. **23**(1): p. 219-227.

125. Niece, K.L., et al., *Modification of gelation kinetics in bioactive peptide amphiphiles.* Biomaterials, 2008. **29**(34): p. 4501-4509.

126. Tan, H.P. and K.G. Marra, *Injectable, Biodegradable Hydrogels for Tissue Engineering Applications.* Materials, 2010. **3**(3): p. 1746-1767.

127. Shimizu, T., et al., *Fabrication of pulsatile cardiac tissue grafts using a novel 3-dimensional cell sheet manipulation technique and temperature-responsive cell culture surfaces.* Circulation Research, 2002. **90**(3): p. E40-E48.

128. Ahn, S.K., et al., *Stimuli-responsive polymer gels.* Soft Matter, 2008. **4**(6): p. 1151-1157.

129. Jeong, B., S.W. Kim, and Y.H. Bae, *Thermosensitive sol-gel reversible hydrogels.* Advanced Drug Delivery Reviews, 2012. **64**: p. 154-162.

130. van der Linden, H.J., et al., *Stimulus-sensitive hydrogels and their applications in chemical (micro)analysis.* Analyst, 2003. **128**(4): p. 325-331.

131. Zhang, S.G., et al., *Spontaneous Assembly of a Self-Complementary Oligopeptide to Form a Stable Macroscopic Membrane.* Proceedings of the National Academy of Sciences of the United States of America, 1993. **90**(8): p. 3334-3338.

132. Zhang, S.G., et al., *Self-Complementary Oligopeptide Matrices Support Mammalian-Cell Attachment.* Biomaterials, 1995. **16**(18): p. 1385-1393.

133. Amsden, B.G., et al., *Synthesis and characterization of a photo-cross-linked biodegradable elastomer.* Biomacromolecules, 2004. **5**(6): p. 2479-2486.

134. Salaam, L.E., D. Dean, and T.L. Bray, *In vitro degradation behavior of biodegradable 4-star micelles.* Polymer, 2006. **47**(1): p. 310-318.

135. Bae, Y.H., et al., *Biodegradable amphiphilic multiblock copolymers and their implications for biomedical applications.* Journal of Controlled Release, 2000. **64**(1-3): p. 3-13.

136. Jeong, K.J. and A. Panitch, *Interplay between Covalent and Physical Interactions within Environment Sensitive Hydrogels.* Biomacromolecules, 2009. **10**(5): p. 1090-1099.

137. Dai, X.S., et al., *Free radical polymerization of poly(ethylene glycol) diacrylate macromers: Impact of macromer hydrophobicity and initiator chemistry on polymerization efficiency.* Acta Biomaterialia, 2011. **7**(5): p. 1965-1972.

138. Johnson, L.M., et al., *Enzyme-Mediated Redox Initiation for Hydrogel Generation and Cellular Encapsulation.* Biomacromolecules, 2009. **10**(11): p. 3114-3121.

139. Hong, Y., et al., *Covalently crosslinked chitosan hydrogel: Properties of in vitro degradation and chondrocyte encapsulation.* Acta Biomaterialia, 2007. **3**(1): p. 23-31.

140. Park, H., et al., *Effect of Swelling Ratio of Injectable Hydrogel Composites on Chondrogenic Differentiation of Encapsulated Rabbit Marrow Mesenchymal Stem Cells In Vitro.* Biomacromolecules, 2009. **10**(3): p. 541-546.

141. Sarvestani, A.S., X. He, and E. Jabbari, *Viscoelastic characterization and modeling of gelation kinetics of injectable in situ cross-linkable poly(lactide-co-ethylene oxide-co-fumarate) hydrogels.* Biomacromolecules, 2007. **8**(2): p. 406-15.

142. Zhu, W. and J.D. Ding, *Synthesis and characterization of a redox-initiated, injectable, biodegradable hydrogel.* Journal of Applied Polymer Science, 2006. **99**(5): p. 2375-2383.

143. Ye, Q., et al., *Relationship of solvent to the photopolymerization process, properties, and structure in model dentin adhesives.* Journal of Biomedical Materials Research Part A, 2007. **80A**(2): p. 342-350.

144. Billiet, T., et al., *The 3D printing of gelatin methacrylamide cell-laden tissue-engineered constructs with high cell viability.* Biomaterials, 2014. **35**(1): p. 49-62.

145. Williams, C.G., et al., *Variable cytocompatibility of six cell lines with photoinitiators used for polymerizing hydrogels and cell encapsulation.* Biomaterials, 2005. **26**(11): p. 1211-1218.

146. Nettles, D.L., et al., *Photocrosslinkable hyaluronan as a scaffold for articular cartilage repair.* Annals of Biomedical Engineering, 2004. **32**(3): p. 391-397.

147. Hao, Y.T., et al., *Visible light cured thiol-vinyl hydrogels with tunable degradation for 3D cell culture.* Acta Biomaterialia, 2014. **10**(1): p. 104-114.

148. Killion, J.A., et al., *Mechanical properties and thermal behaviour of PEGDMA hydrogels for potential bone regeneration application.* Journal of the Mechanical Behavior of Biomedical Materials, 2011. **4**(7): p. 1219-1227.

149. Tan, G.X., et al., *Synthesis and characterization of injectable photocrosslinking poly (ethylene glycol) diacrylate based hydrogels.* Polymer Bulletin, 2008. **61**(1): p. 91-98.

150. Sarvestani, A.S., et al., *Gelation and degradation characteristics of in situ photo-crosslinked poly(L-lactid-co-ethylene oxide-co-fumarate) hydrogels.* Polymer, 2007. **48**(24): p. 7113-7120.

151. Nichol, J.W., et al., *Cell-laden microengineered gelatin methacrylate hydrogels.* Biomaterials, 2010. **31**(21): p. 5536-5544.

152. Moller, L., et al., *Preparation and evaluation of hydrogel-composites from methacrylated hyaluronic acid, alginate, and gelatin for tissue engineering.* International Journal of Artificial Organs, 2011. **34**(2): p. 93-102.

153. Xu, K.D., et al., *Thiol-ene Michael-type formation of gelatin/poly(ethylene glycol) biomatrices for three-dimensional mesenchymal stromal/stem cell administration to cutaneous wounds.* Acta Biomaterialia, 2013. **9**(11): p. 8802-8814.

154. Zhang, Z.F., et al., *Synthesis of Poly(ethylene glycol)-based Hydrogels via Amine-Michael Type Addition with Tunable Stiffness and Postgelation Chemical Functionality.* Chemistry of Materials, 2014. **26**(12): p. 3624-3630.

155. Malkoch, M., et al., *Synthesis of well-defined hydrogel networks using Click chemistry.* Chemical Communications, 2006(26): p. 2774-2776.

156. Huynh, C.T., M.K. Nguyen, and D.S. Lee, *Injectable Block Copolymer Hydrogels: Achievements and Future Challenges for Biomedical Applications.* Macromolecules, 2011. **44**(17): p. 6629-6636.

157. Riess, G., *Micellization of block copolymers.* Progress in Polymer Science, 2003. **28**(7): p. 1107-1170.

158. Cohn, D., et al., *PEO-PPO-PEO-based poly(ether ester urethane)s as degradable reverse thermo-responsive multiblock copolymers.* Biomaterials, 2006. **27**(9): p. 1718-1727.

159. Kim, H.K., et al., *Injectable In Situ-Forming pH/Thermo-Sensitive Hydrogel for Bone Tissue Engineering.* Tissue Engineering Part A, 2009. **15**(4): p. 923-933.

160. O'Lenick, T.G., et al., *Rheological Properties of Aqueous Micellar Gels of a Thermo- and pH-Sensitive ABA Triblock Copolymer.* Journal of Physical Chemistry B, 2011. **115**(12): p. 2870-2881.

161. Moeinzadeh, S. and E. Jabbari, *Nanostructure Formation in Hydrogels*, in *Handbook of Nanomaterials Properties*, B. Bhushan, et al., Editors. 2014, Springer Berlin Heidelberg. p. 285-297.

162. Sanson, N. and J. Rieger, *Synthesis of nanogels/microgels by conventional and controlled radical crosslinking copolymerization.* Polymer Chemistry, 2010. **1**(7): p. 965-977.

163. Peppas, N.A., et al., *Hydrogels in pharmaceutical formulations.* European Journal of Pharmaceutics and Biopharmaceutics, 2000. **50**(1): p. 27-46.

164. Ganji, F., S. Vasheghani-Farahani, and E. Vasheghani-Farahani, *Theoretical Description of Hydrogel Swelling: A Review.* Iranian Polymer Journal, 2010. **19**(5): p. 375-398.

165. Amsden, B., *Solute diffusion within hydrogels. Mechanisms and models.* Macromolecules, 1998. **31**(23): p. 8382-8395.

166. Peppas, N.A. and S.R. Lustig, *Solute diffusion in hydrophilic network structures*, in *Hydrogels in medicine and pharmacy. I. Fundumentals*, P.N. A., Editor. 1986, CRC Press: Boca Raton. p. 57-84.

167. Zhang, N.L. and D.H. Kohn, *Using Polymeric Materials to Control Stem Cell Behavior for Tissue Regeneration.* Birth Defects Research Part C-Embryo Today-Reviews, 2012. **96**(1): p. 63-81.

168. Anseth, K.S., C.N. Bowman, and L. BrannonPeppas, *Mechanical properties of hydrogels and their experimental determination.* Biomaterials, 1996. **17**(17): p. 1647-1657.

169. Bryant, S.J. and K.S. Anseth, *Controlling the spatial distribution of ECM components in degradable PEG hydrogels for tissue engineering cartilage.* Journal of Biomedical Materials Research Part A, 2003. **64A**(1): p. 70-79.

170. Boontheekul, T., et al., *Regulating myoblast phenotype through controlled gel stiffness and degradation.* Tissue Engineering, 2007. **13**(7): p. 1431-1442.

171. Khetan, S., et al., *Degradation-mediated cellular traction directs stem cell fate in covalently crosslinked three-dimensional hydrogels.* Nature Materials, 2013. **12**(5): p. 458-465.

172. Ye, Q., et al., *Fibrin gel as a three dimensional matrix in cardiovascular tissue engineering.* European Journal of Cardio-Thoracic Surgery, 2000. **17**(5): p. 587-591.

173. Jin, R., et al., *Synthesis and characterization of hyaluronic acid-poly(ethylene glycol) hydrogels via Michael addition: An injectable biomaterial for cartilage repair*. Acta Biomaterialia, 2010. **6**(6): p. 1968-1977.

174. Ashton, R.S., et al., *Scaffolds based on degradable alginate hydrogels and poly(lactide-co-glycolide) microspheres for stem cell culture.* Biomaterials, 2007. **28**(36): p. 5518-5525.

175. Kharkar, P.M., K.L. Kiick, and A.M. Kloxin, *Designing degradable hydrogels for orthogonal control of cell microenvironments.* Chemical Society Reviews, 2013. **42**(17): p. 7335-7372.

176. Lutolf, M.R., et al., *Repair of bone defects using synthetic mimetics of collagenous extracellular matrices.* Nature Biotechnology, 2003. **21**(5): p. 513-518.

177. Kraehenbuehl, T.P., et al., *Cell-responsive hydrogel for encapsulation of vascular cells.* Biomaterials, 2009. **30**(26): p. 4318-4324.

178. Nakayama, Y., et al., *Preparation of well-defined poly(ether-ester) macromers: Photogelation and biodegradability.* Acta Biomaterialia, 2011. **7**(4): p. 1496-1503.

179. Ko, C.Y., et al., *Cartilage formation through alterations of amphiphilicity of poly(ethylene glycol)-poly(caprolactone) copolymer hydrogels.* Rsc Advances, 2013. **3**(48): p. 25769-25779.

180. Jiang, Z.Q., et al., *Biodegradable Thermogelling Hydrogel of P(CL-GL)-PEG-P(CL-GL) Triblock Copolymer: Degradation and Drug Release Behavior.* Journal of Pharmaceutical Sciences, 2009. **98**(8): p. 2603-2610.

181. Yu, L., Z. Zhang, and J.D. Ding, *Influence of LA and GA Sequence in the PLGA Block on the Properties of Thermogelling PLGA-PEG-PLGA Block Copolymers.* Biomacromolecules, 2011. **12**(4): p. 1290-1297.

182. Rodriguez-Galan, A., L. Franco, and J. Puiggali, *Degradable Poly(ester amide)s for Biomedical Applications.* Polymers, 2011. **3**(1): p. 65-99.

183. He, J.L., M.Z. Zhang, and P.H. Ni, *Rapidly in situ forming polyphosphoester-based hydrogels for injectable drug delivery carriers.* Soft Matter, 2012. **8**(22): p. 6033-6038.

184. Wang, Y.C., W.J. Lee, and S.P. Ju, *Modeling of the polyethylene and poly(L-lactide) triblock copolymer: A dissipative particle dynamics study.* Journal of Chemical Physics, 2009. **131**(12): p. -.

185. Zheng, Y.T., et al., *Biodegradable pH- and temperature-sensitive multiblock copolymer hydrogels based on poly(amino-ester urethane)s.* Macromolecular Research, 2010. **18**(10): p. 974-980.

186. Kloxin, A.M., et al., *Photodegradable Hydrogels for Dynamic Tuning of Physical and Chemical Properties.* Science, 2009. **324**(5923): p. 59-63.

187. Chatterjee, K., et al., *The effect of 3D hydrogel scaffold modulus on osteoblast differentiation and mineralization revealed by combinatorial screening.* Biomaterials, 2010. **31**(19): p. 5051-5062.

188. Henderson, J.A., X.Z. He, and E. Jabbari, *Concurrent differentiation of marrow stromal cells to osteogenic and vasculogenic lineages.* Macromolecular Bioscience, 2008. **8**(6): p. 499-507.

189. Cukierman, E., R. Pankov, and K.M. Yamada, *Cell interactions with three-dimensional matrices.* Current Opinion in Cell Biology, 2002. **14**(5): p. 633-639.

190. Dalby, M.J., N. Gadegaard, and R.O.C. Oreffo, *Harnessing nanotopography and integrin-matrix interactions to influence stem cell fate.* Nature Materials, 2014. **13**(6): p. 558-569.

191. Gloe, T. and U. Pohl, *Laminin binding conveys mechanosensing in endothelial cells.* News in Physiological Sciences, 2002. **17**: p. 166-169.

192. Aplin, A.E., et al., *Signal transduction and signal modulation by cell adhesion receptors: The role of integrins, cadherins, immunoglobulin-cell adhesion molecules, and selectins.* Pharmacological Reviews, 1998. **50**(2): p. 197-263.

193. Silva, A.K.A., et al., *Growth Factor Delivery Approaches in Hydrogels.* Biomacromolecules, 2009. **10**(1): p. 9-18.

194. Chen, R. and J.A. Hunt, *Biomimetic materials processing for tissue-engineering processes.* Journal of Materials Chemistry, 2007. **17**(38): p. 3974-3979.

195. Zhu, J.M., *Bioactive modification of poly(ethylene glycol) hydrogels for tissue engineering.* Biomaterials, 2010. **31**(17): p. 4639-4656.

196. Liu, S.Q., et al., *Injectable Biodegradable Poly(ethylene glycol)/RGD Peptide Hybrid Hydrogels for in vitro Chondrogenesis of Human Mesenchymal Stem Cells.* Macromolecular Rapid Communications, 2010. **31**(13): p. 1148-1154.

197. Weber, L.M., et al., *The effects of cell-matrix interactions on encapsulated beta-cell function within hydrogels functionalized with matrix-derived adhesive peptides.* Biomaterials, 2007. **28**(19): p. 3004-3011.

198. Park, K.M., et al., *In Situ SVVYGLR Peptide Conjugation into Injectable Gelatin-Poly(ethylene glycol)-Tyramine Hydrogel via Enzyme-Mediated Reaction for Enhancement of Endothelial Cell Activity and Neo-Vascularization.* Bioconjugate Chemistry, 2012. **23**(10): p. 2042-2050.

199. He, X.Z., X.M. Yang, and E. Jabbari, *Combined Effect of Osteopontin and BMP-2 Derived Peptides Grafted to an Adhesive Hydrogel on Osteogenic and Vasculogenic Differentiation of Marrow Stromal Cells.* Langmuir, 2012. **28**(12): p. 5387-5397.

200. Salinas, C.N. and K.S. Anseth, *Decorin moieties tethered into PEG networks induce chondrogenesis of human mesenchymal stem cells.* Journal of Biomedical Materials Research Part A, 2009. **90A**(2): p. 456-464.

201. Saito, A., et al., *Prolonged ectopic calcification induced by BMP-2-derived synthetic peptide.* Journal of Biomedical Materials Research Part A, 2004. **70A**(1): p. 115-121.

202. Saito, A., et al., *Accelerated bone repair with the use of a synthetic BMP-2-derived peptide and bone-marrow stromal cells.* Journal of Biomedical Materials Research Part A, 2005. **72A**(1): p. 77-82.

203. Jabbari, E., et al., *Injectable polymers and hydrogels for orthopedic and dental applications. In: Tissue engineering in musculoskeletal clinical practice,* in *Tissue engineering in musculoskeletal clinical practice*, L. Sandell and A. Grodzinsky, Editors. 2004, American Academy of Orthopaedic Surgeons: Rosemont.

204. Ballios, B.G., et al., *A hydrogel-based stem cell delivery system to treat retinal degenerative diseases.* Biomaterials, 2010. **31**(9): p. 2555-2564.

205. He, X. and E. Jabbari, *Material properties and cytocompatibility of injectable MMP degradable poly(lactide ethylene oxide fumarate) hydrogel as a carrier for marrow stromal cells.* Biomacromolecules, 2007. **8**(3): p. 780-92.

206. Dembczynski, R. and T. Jankowski, *Characterisation of small molecules diffusion in hydrogel-membrane liquid-core capsules.* Biochem Eng J, 2000. **6**(1): p. 41-44.

207. Beruto, D.T. and R. Botter, *Role of the water matric potential (psi(M)) and of equilibrium water content (EWC) on the water self-diffusion coefficient and on the oxygen permeability in hydrogel contact lenses.* Biomaterials, 2004. **25**(14): p. 2877-83.

208. Liang, S., et al., *Protein diffusion in agarose hydrogel in situ measured by improved refractive index method.* J Control Release, 2006. **115**(2): p. 189-96.

209. Saadi, T., et al., *Hepatocyte Cell Line Function in a Biosynthetic Hydrogel Scaffold for Liver Tissue Engineering.* Liver Transplantation, 2010. **16**(6): p. S122-S122.

210. Sarvestani, A.S., X. He, and E. Jabbari, *Effect of osteonectin-derived peptide on the viscoelasticity of hydrogel/apatite nanocomposite scaffolds.* Biopolymers, 2007. **85**(4): p. 370-8.

211. Sarvestani, A.S. and E. Jabbari, *Modeling and experimental investigation of rheological properties of injectable poly(lactide ethylene oxide fumarate)/hydroxyapatite nanocomposites.* Biomacromolecules, 2006. **7**(5): p. 1573-80.

212. Pang, X.A. and C.C. Chu, *Synthesis, characterization and biodegradation of poly(ester amide)s based hydrogels.* Polymer, 2010. **51**(18): p. 4200-4210.

213. Chan, G. and D.J. Mooney, *New materials for tissue engineering: towards greater control over the biological response.* Trends in Biotechnology, 2008. **26**(7): p. 382-392.

214. Puppi, D., et al., *Polymeric materials for bone and cartilage repair.* Progress in Polymer Science, 2010. **35**(4): p. 403-440.

215. Ifkovits, J.L. and J.A. Burdick, *Review: Photopolymerizable and degradable biomaterials for tissue engineering applications.* Tissue Engineering, 2007. **13**(10): p. 2369-2385.

216. Miller, O.N. and G. Bazzano, *Propanediol metabolism and its relation to lactic acid metabolism.* Ann N Y Acad Sci, 1965. **119**(3): p. 957-73.

217. Sodergard, A. and M. Stolt, *Properties of lactic acid based polymers and their correlation with composition.* Progress in Polymer Science, 2002. **27**(6): p. 1123-1163.

218. Buwalda, S.J., et al., *Influence of Amide versus Ester Linkages on the Properties of Eight-Armed PEG-PLA Star Block Copolymer Hydrogels.* Biomacromolecules, 2010. **11**(1): p. 224-232.

219. Park, S.Y., et al., *Micellization and gelation of aqueous solutions of star-shaped PLLA-PEO block copolymers.* Macromolecules, 2003. **36**(11): p. 4115-4124.

220. Lin, H.H. and Y.L. Cheng, *In-situ thermoreversible gelation of block and star copolymers of poly(ethylene glycol) and poly(N-isopropylacrylamide) of varying architectures.* Macromolecules, 2001. **34**(11): p. 3710-3715.

221. Oberti, T.G., M.S. Cortizo, and J.L. Alessandrini, *Novel Copolymer of Diisopropyl Fumarate and Benzyl Acrylate Synthesized Under Microwave Energy and Quasielastic Light Scattering Measurements.* Journal of Macromolecular Science Part a-Pure and Applied Chemistry, 2010. **47**(7): p. 725-731.

222. Wei, H.Y., et al., *Characterization and photopolymerization of divinyl fumarate.* Macromolecules, 2007. **40**(17): p. 6172-6180.

223. Xu, Q.M., et al., *Effects of organic solvents on membrane of Taxus cuspidata cells in two-liquid-phase cultures.* Plant Cell Tissue and Organ Culture, 2004. **79**(1): p. 63-69.

224. Rey, A., et al., *Radius of Gyration and Viscosity of Linear and Star Polymers in Different Regimes.* Macromolecules, 1992. **25**(4): p. 1311-1315.

225. Jabbari, E. and X. He, *Synthesis and characterization of bioresorbable in situ crosslinkable ultra low molecular weight poly(lactide) macromer.* J Mater Sci Mater Med, 2008. **19**(1): p. 311-8.

226. Jabbari, E., et al., *Material properties and bone marrow stromal cells response to In situ crosslinkable RGD-functionlized lactide-co-glycolide scaffolds.* J Biomed Mater Res A, 2009. **89**(1): p. 124-137.

227. Silverstein, R.M., G.C. Bassler, and T.C. Morrill, *Spectrometric identification of organic compounds*. 1991, New YorK: John Wiley. 91.

228. Kim, J.W., J.Y. Ko, and K.D. Suh, *A useful poly(ethylene oxide)-poly(propylene oxide)-poly(ethylene oxide) triblock crosslinker in a diffusion-controlled polymerization method.* Macromolecular Rapid Communications, 2001. **22**(4): p. 257-261.

229. Odian, G., *Principles of polymerization*. 1981, New York: John Wiley.

230. Wang, J. and V.M. Ugaz, *Using in situ rheology to characterize the microstructure in photopolymerized polyacrylarnide gels for DNA electrophoresis.* Electrophoresis, 2006. **27**(17): p. 3349-3358.

231. Potoczek, M. and E. Zawadzak, *Initiator effect on the gelcasting properties of alumina in a system involving low-toxic monomers.* Ceramics International, 2004. **30**(5): p. 793-799.

232. Nowers, J.R., J.A. Costanzo, and B. Narasimhan, *Structure-property relationships in acrylate/epoxy interpenetrating polymer networks: Effects of the reaction sequence and composition.* Journal of Applied Polymer Science, 2007. **104**(2): p. 891-901.

233. Flory, P.J. and J. Rehner, *Statistical mechanics of cross-linked polymer networks I Rubberlike elasticity.* Journal of Chemical Physics, 1943. **11**(11): p. 512-520.

234. He, Z.Q. and L.Z. Xiong, *A Comparative Study on In vitro Degradation Behaviors of Poly(L-lactide-co-glycolide) Scaffolds and Films.* Journal of Macromolecular Science Part B-Physics, 2010. **49**(1): p. 66-74.

235. Fu, S.Z., et al., *Injectable Biodegradable Thermosensitive Hydrogel Composite for Orthopedic Tissue Engineering. 1. Preparation and Characterization of Nanohydroxyapatite/Poly(ethylene glycol)-Poly(epsilon-caprolactone)-Poly(ethylene glycol) Hydrogel Nanocomposites.* Journal of Physical Chemistry B, 2009. **113**(52): p. 16518-16525.

236. Metters, A.T., K.S. Anseth, and C.N. Bowman, *Fundamental studies of a novel, biodegradable PEG-b-PLA hydrogel.* Polymer, 2000. **41**(11): p. 3993-4004.

237. Jie, P., et al., *Micelle-like nanoparticles of star-branched PEO-PLA copolymers as chemotherapeutic carrier.* Journal of Controlled Release, 2005. **110**(1): p. 20-33.

238. He, X.Z., J.Y. Ma, and E. Jabbari, *Migration of marrow stromal cells in response to sustained release of stromal-derived factor-1 alpha from poly(lactide ethylene oxide fumarate) hydrogels.* International Journal of Pharmaceutics, 2010. **390**(2): p. 107-116.

239. Mercado, A.E., et al., *Release characteristics and osteogenic activity of recombinant human bone morphogenetic protein-2 grafted to novel self-assembled poly(lactide-co-glycolide fumarate) nanoparticles.* Journal of Controlled Release, 2009. **140**(2): p. 148-156.

240. Ciarmela, P., et al., *Presence, Actions, and Regulation of Myostatin in Rat Uterus and Myometrial Cells.* Endocrinology, 2009. **150**(2): p. 906-914.

241. Pfaffl, M.W., *A new mathematical model for relative quantification in real-time RT-PCR.* Nucleic Acids Research, 2001. **29**(9).

242. Espanol, P. and P. Warren, *Statistical-Mechanics of Dissipative Particle Dynamics.* Europhysics Letters, 1995. **30**(4): p. 191-196.

243. Hoogerbrugge, P.J. and J.M.V.A. Koelman, *Simulating Microscopic Hydrodynamic Phenomena with Dissipative Particle Dynamics.* Europhysics Letters, 1992. **19**(3): p. 155-160.

244. Groot, R.D. and T.J. Madden, *Dynamic simulation of diblock copolymer microphase separation.* Journal of Chemical Physics, 1998. **108**(20): p. 8713-8724.

245. Sun, H., *COMPASS: An ab initio force-field optimized for condensed-phase applications - Overview with details on alkane and benzene compounds.* Journal of Physical Chemistry B, 1998. **102**(38): p. 7338-7364.

246. Silverstein, R.M., G.C. Bassler, and T.C. Morril, *Spectrometric identification of organic compounds*. 1991, New York: John Wiley.

247. Cima, L.G. and S.T. Lopina, *Network Structures of Radiation-Cross-Linked Star Polymer Gels.* Macromolecules, 1995. **28**(20): p. 6787-6794.

248. Fioroni, M., et al., *Model of 1,1,1,3,3,3-hexafluoro-propan-2-ol for molecular dynamics simulations.* Journal of Physical Chemistry B, 2001. **105**(44): p. 10967-10975.

249. Nicolai, T., O. Colombani, and C. Chassenieux, *Dynamic polymeric micelles versus frozen nanoparticles formed by block copolymers.* Soft Matter, 2010. **6**(14): p. 3111-3118.

250. Choquet, M. and F. Rietsch, *Characterization of Radical Polystyrene Gels.* Polymer, 1978. **19**(5): p. 513-518.

251. Sawhney, A.S., C.P. Pathak, and J.A. Hubbell, *Bioerodible Hydrogels Based on Photopolymerized Poly(Ethylene Glycol)-Co-Poly(Alpha-Hydroxy Acid) Diacrylate Macromers.* Macromolecules, 1993. **26**(4): p. 581-587.

252. Wang, L.M., et al., *Osteogenic Differentiation of Human Umbilical Cord Mesenchymal Stromal Cells in Polyglycolic Acid Scaffolds.* Tissue Engineering Part A, 2010. **16**(6): p. 1937-1948.

253. Oliveira, J.M., et al., *The osteogenic differentiation of rat bone marrow stromal cells cultured with dexamethasone-loaded carboxymethylchitosan/poly(amidoamine) dendrimer nanoparticles.* Biomaterials, 2009. **30**(5): p. 804-813.

254. Sieber, C., et al., *Recent advances in BMP receptor signaling.* Cytokine & Growth Factor Reviews, 2009. **20**(5-6): p. 343-355.

255. Kim, J., et al., *Bone regeneration using hyaluronic acid-based hydrogel with bone morphogenic protein-2 and human mesenchymal stem cells.* Biomaterials, 2007. **28**(10): p. 1830-1837.

256. Na, K., et al., *Osteogenic differentiation of rabbit mesenchymal stem cells in thermo-reversible hydrogel constructs containing hydroxyapatite and bone morphogenic protein-2 (BMP-2).* Biomaterials, 2007. **28**(16): p. 2631-2637.

257. Seliktar, D., *Designing Cell-Compatible Hydrogels for Biomedical Applications.* Science, 2012. **336**(6085): p. 1124-1128.

258. Sharma, B., et al., *Human Cartilage Repair with a Photoreactive Adhesive-Hydrogel Composite.* Science Translational Medicine, 2013. **5**(167): p. 167ra6.

259. Joshi, A., et al., *Functional compressive mechanics of a PVA/PVP nucleus pulposus replacement.* Biomaterials, 2006. **27**(2): p. 176-184.

260. Graf, N., et al., *alpha(V)beta(3) Integrin-Targeted PLGA-PEG Nanoparticles for Enhanced Anti-tumor Efficacy of a Pt(IV) Prodrug.* Acs Nano, 2012. **6**(5): p. 4530-4539.

261. Jabbari, E., et al., *Drug release kinetics, cell uptake, and tumor toxicity of hybrid VVVVVVKK peptide-assembled polylactide nanoparticles.* European Journal of Pharmaceutics and Biopharmaceutics, 2013.

262. Kersey, F.R., et al., *Stereocomplexed Poly(lactic acid)-Poly(ethylene glycol) Nanoparticles with Dual-Emissive Boron Dyes for Tumor Accumulation.* Acs Nano, 2010. **4**(9): p. 4989-4996.

263. Saito, N., et al., *A biodegradable polymer as a cytokine delivery system for inducing bone formation.* Nature Biotechnology, 2001. **19**(4): p. 332-335.

264. Xiao, L., et al., *Role of cellular uptake in the reversal of multidrug resistance by PEG-b-PLA polymeric micelles.* Biomaterials, 2011. **32**(22): p. 5148-5157.

265. Zhang, Z., et al., *Cellular uptake and intracellular trafficking of PEG-b-PLA polymeric micelles.* Biomaterials, 2012. **33**(29): p. 7233-7240.

266. Zhao, Z.X., et al., *Self-assembly nanomicelles based on cationic mPEG-PLA-b-Polyarginine(R-15) triblock copolymer for siRNA delivery.* Biomaterials, 2012. **33**(28): p. 6793-6807.

267. *Materials Studio V 5.5*. 2011, Accelrys Inc. : San Diego, California.

268. Maniatopoulos, C., J. Sodek, and A.H. Melcher, *Bone formation in vitro by stromal cells obtained from bone marrow of young adult rats.* Cell and Tissue Research, 1988. **254**(2): p. 317-330.

269. Chen, K.L., et al., *A Hybrid Silk/RADA-Based Fibrous Scaffold with Triple Hierarchy for Ligament Regeneration.* Tissue Engineering Part A, 2012. **18**(13-14): p. 1399-1409.

270. Nagarajan, R. and K. Ganesh, *Block Copolymer Self-Assembly in Selective Solvents - Spherical Micelles with Segregated Cores.* Journal of Chemical Physics, 1989. **90**(10): p. 5843-5856.

271. Meng, X.X. and W.B. Russel, *Structure and size of spherical micelles of telechelic polymers.* Macromolecules, 2005. **38**(2): p. 593-600.

272. Li, Z.L. and E.E. Dormidontova, *Equilibrium chain exchange kinetics in block copolymer micelle solutions by dissipative particle dynamics simulations.* Soft Matter, 2011. **7**(9): p. 4179-4188.

273. Nicodemus, G.D. and S.J. Bryant, *Cell encapsulation in biodegradable hydrogels for tissue engineering applications.* Tissue Engineering Part B-Reviews, 2008. **14**(2): p. 149-165.

274. Yan, C.Q. and D.J. Pochan, *Rheological properties of peptide-based hydrogels for biomedical and other applications.* Chemical Society Reviews, 2010. **39**(9): p. 3528-3540.

275. Hawkins, A.M., et al., *Synthesis and analysis of degradation, mechanical and toxicity properties of poly(beta-amino ester) degradable hydrogels.* Acta Biomaterialia, 2011. **7**(5): p. 1956-1964.

276. Jabbari, E. and X.Z. He, *Synthesis and characterization of bioresorbable in situ crosslinkable ultra low molecular weight poly(lactide) macromer.* Journal of Materials Science-Materials in Medicine, 2008. **19**(1): p. 311-318.

277. Clapper, J.D., et al., *Development and characterization of photopolymerizable biodegradable materials from PEG-PLA-PEG block macromonomers.* Polymer, 2007. **48**(22): p. 6554-6564.

278. Leach, A.R., *Molecular modeling principles and applications*. 2nd ed. 2001, London: Longman Press.

279. Dotera, T. and A. Hatano, *The diagonal bond method: A new lattice polymer model for simulation study of block copolymers.* Journal of Chemical Physics, 1996. **105**(18): p. 8413-8427.

280. van Vlimmeren, B.A.C., et al., *Simulation of 3D mesoscale structure formation in concentrated aqueous solution of the triblock polymer surfactants (ethylene oxide)(13)(propylene oxide)(30)(ethylene oxide)(13) and (propylene oxide)(19)(ethylene oxide)(33)(propylene oxide)(19). Application of dynamic mean-field density functional theory.* Macromolecules, 1999. **32**(3): p. 646-656.

281. Groot, R.D., T.J. Madden, and D.J. Tildesley, *On the role of hydrodynamic interactions in block copolymer microphase separation.* Journal of Chemical Physics, 1999. **110**(19): p. 9739-9749.

282. Guo, X.D., et al., *Effect of composition on the formation of poly(DL-lactide) microspheres for drug delivery systems: Mesoscale simulations.* Chemical Engineering Journal, 2007. **131**(1-3): p. 195-201.

283. Guo, X.D., et al., *Dissipative Particle Dynamics Studies on Microstructure of pH-Sensitive Micelles for Sustained Drug Delivery.* Macromolecules, 2010. **43**(18): p. 7839-7844.

284. Scocchi, G., et al., *Polymer-clay nanocomposites: A multiscale molecular modeling approach.* Journal of Physical Chemistry B, 2007. **111**(9): p. 2143-2151.

285. Thakkar, F.M. and K.G. Ayappa, *Effect of Polymer Grafting on the Bilayer Gel to Liquid-Crystalline Transition.* Journal of Physical Chemistry B, 2010. **114**(8): p. 2738-2748.

286. Cao, X.R., et al., *Aggregation of poly(ethylene oxide)-poly(propylene oxide) block copolymers in aqueous solution: DPD simulation study.* Journal of Physical Chemistry A, 2005. **109**(45): p. 10418-10423.

287. Posocco, P., M. Fermeglia, and S. Pricl, *Morphology prediction of block copolymers for drug delivery by mesoscale simulations.* Journal of Materials Chemistry, 2010. **20**(36): p. 7742-7753.

288. Xia, J. and C.L. Zhong, *Dissipative particle dynamics study of the formation of multicompartment micelles from ABC star triblock copolymers in water.* Macromolecular Rapid Communications, 2006. **27**(14): p. 1110-1114.

289. Xu, Y., et al., *Microphase separation of star-diblock copolymer melts studied by dissipative particle dynamics simulation.* Molecular Simulation, 2006. **32**(5): p. 375-383.

290. Zhao, Y., et al., *Dissipative particle dynamics study on the multicompartment micelles self-assembled from the mixture of diblock copolymer poly(ethyl ethylene)-block-poly(ethylene oxide) and homopolymer poly(propylene oxide) in aqueous solution.* Polymer, 2009. **50**(22): p. 5333-5340.

291. Groot, R.D. and K.L. Rabone, *Mesoscopic simulation of cell membrane damage, morphology change and rupture by nonionic surfactants.* Biophysical Journal, 2001. **81**(2): p. 725-736.

292. Loverde, S.M., et al., *Curvature-driven molecular demixing in the budding and breakup of mixed component worm-like micelles.* Soft Matter, 2010. **6**(7): p. 1419-1425.

293. Ortiz, V., et al., *Dissipative particle dynamics simulations of polymersomes.* Journal of Physical Chemistry B, 2005. **109**(37): p. 17708-17714.

294. Flory, P.J., *Statistical mechanics of chain molecules*. 1969, New York: Interscience.

295. Devanand, K. and J.C. Selser, *Asymptotic-Behavior and Long-Range Interactions in Aqueous-Solutions of Poly(Ethylene Oxide).* Macromolecules, 1991. **24**(22): p. 5943-5947.

296. Nagarajan, R., *Molecular packing parameter and surfactant self-assembly: The neglected role of the surfactant tail.* Langmuir, 2002. **18**(1): p. 31-38.

297. Tanford, C., *The hydrophobic effect: formation of micelles and biological membranes*. 2nd ed. 1980, New York: JOHN WILEY & SONS.

298. Sliozberg, Y.R., et al., *Modeling Viscoelastic Properties of Triblock Copolymers: A DPD Simulation Study*. Journal of Polymer Science Part B-Polymer Physics, 2010. **48**(1): p. 15-25.

299. Hansen, J.P. and I.R. McDonald, *Theory of simple liquids*. 2nd ed. 1990, London: Academic Press.

300. Yang, H.S., et al., *Heparin-Conjugated Fibrin as an Injectable System for Sustained Delivery of Bone Morphogenetic Protein-2.* Tissue Engineering Part A, 2010. **16**(4): p. 1225-1233.

301. Mercado, A.E. and E. Jabbari, *Effect of Encapsulation or Grafting on Release Kinetics of Recombinant Human Bone Morphogenetic Protein-2 From Self-Assembled Poly(lactide-co-glycolide ethylene oxide fumarate) Nanoparticles.* Microscopy Research and Technique, 2010. **73**(9): p. 824-833.

302. Shields, L.B.E., et al., *Adverse effects associated with high-dose recombinant human bone morphogenetic protein-2 use in anterior cervical spine fusion.* Spine, 2006. **31**(5): p. 542-547.

303. Raida, M., et al., *Bone morphogenetic protein 2 (BMP-2) and induction of tumor angiogenesis.* Journal of Cancer Research and Clinical Oncology, 2005. **131**(11): p. 741-750.

304. Kirsch, T., W. Sebald, and M.K. Dreyer, *Crystal structure of the BMP-2-BRIA ectodomain complex.* Nature Structural Biology, 2000. **7**(6): p. 492-496.

305. Liu, F., et al., *Human Type-Ii Receptor for Bone Morphogenic Proteins (Bmps) - Extension of the 2-Kinase Receptor Model to the Bmps.* Molecular and Cellular Biology, 1995. **15**(7): p. 3479-3486.

306. Zhang, S.M., et al., *A self-assembly pathway to aligned monodomain gels.* Nature Materials, 2010. **9**(7): p. 594-601.

307. Anderson, J.M., et al., *Modulating the Gelation Properties of Self-Assembling Peptide Amphiphiles.* Acs Nano, 2009. **3**(11): p. 3447-3454.

308. Luo, J.N. and Y.W. Tong, *Self-Assembly of Collagen-Mimetic Peptide Amphiphiles into Biofunctional Nanofiber.* Acs Nano, 2011. **5**(10): p. 7739-7747.

309. Ellis-Behnke, R.G., et al., *Nano neuro knitting: Peptide nanofiber scaffold for brain repair and axon regeneration with functional return of vision (vol 103, pg 5054, 2006).* Proceedings of the National Academy of Sciences of the United States of America, 2006. **103**(19): p. 7530-7530.

310. Santoso, S., et al., *Self-assembly of surfactant-like peptides with variable glycine tails to form nanotubes and nanovesicles.* Nano Letters, 2002. **2**(7): p. 687-691.

311. Marrink, S.J., A.H. de Vries, and A.E. Mark, *Coarse grained model for semiquantitative lipid simulations.* Journal of Physical Chemistry B, 2004. **108**(2): p. 750-760.

312. Monticelli, L., et al., *The MARTINI coarse-grained force field: Extension to proteins.* Journal of Chemical Theory and Computation, 2008. **4**(5): p. 819-834.

313. White, P., et al., *Expediting the Fmoc solid phase synthesis of long peptides through the application of dimethyloxazolidine dipeptides.* Journal of Peptide Science, 2004. **10**(1): p. 18-26.

314. Kaiser, E., et al., *Color test for detection of free terminal amino groups in the solid-phase synthesis of peptides.* Anal Biochem, 1970. **34**(2): p. 595-8.

315. Jabbari, E., et al., *Drug release kinetics, cell uptake, and tumor toxicity of hybrid VVVVVVKK peptide-assembled polylactide nanoparticles.* European Journal of Pharmaceutics and Biopharmaceutics, 2013. **84**(1): p. 49-62.

316. Yang, S.J. and S.G. Zhang, *Self-assembling behavior of designer lipid-like peptides.* Supramolecular Chemistry, 2006. **18**(5): p. 389-396.

317. Khoe, U., Y.L. Yang, and S.G. Zhang, *Self-Assembly of Nanodonut Structure from a Cone-Shaped Designer Lipid-like Peptide Surfactant.* Langmuir, 2009. **25**(7): p. 4111-4114.

318. Meinel, A.J., et al., *Optimization strategies for electrospun silk fibroin tissue engineering scaffolds.* Biomaterials, 2009. **30**(17): p. 3058-3067.

319. Chung, E.J., et al., *Osteogenic potential of BMP-2-releasing self-assembled membranes.* Tissue Engineering Part A, 2013. **19**(23-24): p. 2664-2673.

320. Livak, K.J. and T.D. Schmittgen, *Analysis of relative gene expression data using real-time quantitative PCR and the 2(T)(-Delta Delta C) method.* Methods, 2001. **25**(4): p. 402-408.

321. Brocos, P., et al., *Multiscale molecular dynamics simulations of micelles: coarse-grain for self-assembly and atomic resolution for finer details.* Soft Matter, 2012. **8**(34): p. 9005-9014.

322. Gkeka, P. and L. Sarkisov, *Interactions of Phospholipid Bilayers with Several Classes of Amphiphilic alpha-Helical Peptides: Insights from Coarse-Grained Molecular Dynamics Simulations.* Journal of Physical Chemistry B, 2010. **114**(2): p. 826-839.

323. Zhang, H., et al., *A molecular dynamics simulation of N-(fluorenyl-9-methoxycarbonyl)-dipeptides supramolecular hydrogel.* Colloids and Surfaces a-Physicochemical and Engineering Aspects, 2013. **417**: p. 217-223.

324. Santo, K.P. and M.L. Berkowitz, *Difference between Magainin-2 and Melittin Assemblies in Phosphatidylcholine Bilayers: Results from Coarse-Grained Simulations.* Journal of Physical Chemistry B, 2012. **116**(9): p. 3021-3030.

325. Yang, S.C. and R. Faller, *Pressure and Surface Tension Control Self-Assembled Structures in Mixtures of Pegylated and Non-Pegylated Lipids.* Langmuir, 2012. **28**(4): p. 2275-2280.

326. Lee, H. and R.W. Pastor, *Coarse-Grained Model for PEGylated Lipids: Effect of PEGylation on the Size and Shape of Self-Assembled Structures.* Journal of Physical Chemistry B, 2011. **115**(24): p. 7830-7837.

327. Martyna, G.J., M.L. Klein, and M. Tuckerman, *Nose-Hoover chains: The Canonical ensemble via Continuous dynamics.* Journal of Chemical Physics, 1992. **97**(4): p. 2635-2643.

328. Marrink, S.J., et al., *The MARTINI force field: Coarse grained model for biomolecular simulations.* Journal of Physical Chemistry B, 2007. **111**(27): p. 7812-7824.

329. Gobin, A.S. and J.L. West, *Effects of epidermal growth factor on fibroblast migration through biomimetic hydrogels.* Biotechnology Progress, 2003. **19**(6): p. 1781-1785.

330. DeLong, S.A., J.J. Moon, and J.L. West, *Covalently immobilized gradients of bFGF on hydrogel scaffolds for directed cell migration.* Biomaterials, 2005. **26**(16): p. 3227-3234.

331. Swiontkowski, M.F., et al., *Recombinant human bone morphogenetic protein-2 in open tibial fractures - A subgroup analysis of data combined from two prospective randomized studies.* Journal of Bone and Joint Surgery-American Volume, 2006. **88A**(6): p. 1258-1265.

332. Mygind, T., et al., *Mesenchymal stem cell ingrowth and differentiation on coralline hydroxyapatite scaffolds.* Biomaterials, 2007. **28**(6): p. 1036-1047.

333. Kyte, J. and R.F. Doolittle, *A Simple Method for Displaying the Hydropathic Character of a Protein.* Journal of Molecular Biology, 1982. **157**(1): p. 105-132.

334. Owen, S.C., D.P.Y. Chan, and M.S. Shoichet, *Polymeric micelle stability.* Nano Today, 2012. **7**(1): p. 53-65.

335. Scheufler, C., W. Sebald, and M. Hülsmeyer, *Crystal structure of human bone morphogenetic protein-2 at 2.7 Å resolution.* Journal of Molecular Biology, 1999. **287**(1): p. 103-115.

336. Li, J.F., et al., *Repair of Rat Cranial Bone Defects with nHAC/PLLA and BMP-2-Related Peptide or rhBMP-2.* Journal of Orthopaedic Research, 2011. **29**(11): p. 1745-1752.

337. Missirlis, D., H. Khant, and M. Tirrell, *Mechanisms of Peptide Amphiphile Internalization by SJSA-1 Cells in Vitro.* Biochemistry, 2009. **48**(15): p. 3304-3314.

338. Ruppert, R., E. Hoffmann, and W. Sebald, *Human bone morphogenetic protein 2 contains a heparin-binding site which modifies its biological activity.* European Journal of Biochemistry, 1996. **237**(1): p. 295-302.

339. Zana, R., *Critical micellization concentration of surfactants in aqueous solution and free energy of micellization.* Langmuir, 1996. **12**(5): p. 1208-1211.

APPENDIX A

PERMISSION TO REPRINT

ELSEVIER LICENSE
TERMS AND CONDITIONS

Nov 13, 2014

This is a License Agreement between Seyedsina Moeinzadeh ("You") and Elsevier ("Elsevier") provided by Copyright Clearance Center ("CCC"). The license consists of your order details, the terms and conditions provided by Elsevier, and the payment terms and conditions.

All payments must be made in full to CCC. For payment instructions, please see information listed at the bottom of this form.

Supplier	Elsevier Limited The Boulevard,Langford Lane Kidlington,Oxford,OX5 1GB,UK
Registered Company Number	1982084
Customer name	Seyedsina Moeinzadeh
Customer address	301 Main street, Rm 2B46 COLUMBIA, SC 29208
License number	3507200674222
License date	Nov 13, 2014
Licensed content publisher	Elsevier
Licensed content publication	Polymer
Licensed content title	Synthesis and gelation characteristics of photo-crosslinkable star Poly(ethylene oxide-co-lactide-glycolide acrylate) macromonomers
Licensed content author	Seyedsina Moeinzadeh,Saied Nouri Khorasani,Junyu Ma,Xuezhong He,Esmaiel Jabbari
Licensed content date	18 August 2011
Licensed content volume number	52
Licensed content issue number	18
Number of pages	10
Start Page	3887
End Page	3896
Type of Use	reuse in a thesis/dissertation

Portion	full article
Format	both print and electronic
Are you the author of this Elsevier article?	Yes
Will you be translating?	No
Title of your thesis/dissertation	BIO-ACTIVE DEGRADABLE MICELLAR HYDROGELS FOR OSTEOGENIC DIFFERENTIATION OF MESENCHYMAL STEM CELLS
Expected completion date	Dec 2014
Estimated size (number of pages)	200
Elsevier VAT number	GB 494 6272 12
Permissions price	0.00 USD
VAT/Local Sales Tax	0.00 USD / 0.00 GBP
Total	0.00 USD
Terms and Conditions	

INTRODUCTION

1. The publisher for this copyrighted material is Elsevier. By clicking "accept" in connection with completing this licensing transaction, you agree that the following terms and conditions apply to this transaction (along with the Billing and Payment terms and conditions established by Copyright Clearance Center, Inc. ("CCC"), at the time that you opened your Rightslink account and that are available at any time at http://myaccount.copyright.com).

GENERAL TERMS

2. Elsevier hereby grants you permission to reproduce the aforementioned material subject to the terms and conditions indicated.

3. Acknowledgement: If any part of the material to be used (for example, figures) has appeared in our publication with credit or acknowledgement to another source, permission must also be sought from that source. If such permission is not obtained then that material may not be included in your publication/copies. Suitable acknowledgement to the source must be made, either as a footnote or in a reference list at the end of your publication, as follows:

"Reprinted from Publication title, Vol /edition number, Author(s), Title of article / title of

chapter, Pages No., Copyright (Year), with permission from Elsevier [OR APPLICABLE SOCIETY COPYRIGHT OWNER].” Also Lancet special credit - “Reprinted from The Lancet, Vol. number, Author(s), Title of article, Pages No., Copyright (Year), with permission from Elsevier.”

4. Reproduction of this material is confined to the purpose and/or media for which permission is hereby given.

5. Altering/Modifying Material: Not Permitted. However figures and illustrations may be altered/adapted minimally to serve your work. Any other abbreviations, additions, deletions and/or any other alterations shall be made only with prior written authorization of Elsevier Ltd. (Please contact Elsevier at permissions@elsevier.com)

6. If the permission fee for the requested use of our material is waived in this instance, please be advised that your future requests for Elsevier materials may attract a fee.

7. Reservation of Rights: Publisher reserves all rights not specifically granted in the combination of (i) the license details provided by you and accepted in the course of this licensing transaction, (ii) these terms and conditions and (iii) CCC's Billing and Payment terms and conditions.

8. License Contingent Upon Payment: While you may exercise the rights licensed immediately upon issuance of the license at the end of the licensing process for the transaction, provided that you have disclosed complete and accurate details of your proposed use, no license is finally effective unless and until full payment is received from you (either by publisher or by CCC) as provided in CCC's Billing and Payment terms and conditions. If full payment is not received on a timely basis, then any license preliminarily granted shall be deemed automatically revoked and shall be void as if never granted. Further, in the event that you breach any of these terms and conditions or any of CCC's Billing and Payment terms and conditions, the license is automatically revoked and shall be void as if never granted. Use of materials as described in a revoked license, as well as any use of the materials beyond the scope of an unrevoked license, may constitute copyright infringement and publisher reserves the right to take any and all action to protect its copyright in the materials.

9. Warranties: Publisher makes no representations or warranties with respect to the licensed material.

10. Indemnity: You hereby indemnify and agree to hold harmless publisher and CCC, and their respective officers, directors, employees and agents, from and against any and all claims arising out of your use of the licensed material other than as specifically authorized pursuant to this license.

11. No Transfer of License: This license is personal to you and may not be sublicensed, assigned, or transferred by you to any other person without publisher's written

permission.

12. No Amendment Except in Writing: This license may not be amended except in a writing signed by both parties (or, in the case of publisher, by CCC on publisher's behalf).

13. Objection to Contrary Terms: Publisher hereby objects to any terms contained in any purchase order, acknowledgment, check endorsement or other writing prepared by you, which terms are inconsistent with these terms and conditions or CCC's Billing and Payment terms and conditions. These terms and conditions, together with CCC's Billing and Payment terms and conditions (which are incorporated herein), comprise the entire agreement between you and publisher (and CCC) concerning this licensing transaction. In the event of any conflict between your obligations established by these terms and conditions and those established by CCC's Billing and Payment terms and conditions, these terms and conditions shall control.

14. Revocation: Elsevier or Copyright Clearance Center may deny the permissions described in this License at their sole discretion, for any reason or no reason, with a full refund payable to you. Notice of such denial will be made using the contact information provided by you. Failure to receive such notice will not alter or invalidate the denial. In no event will Elsevier or Copyright Clearance Center be responsible or liable for any costs, expenses or damage incurred by you as a result of a denial of your permission request, other than a refund of the amount(s) paid by you to Elsevier and/or Copyright Clearance Center for denied permissions.

LIMITED LICENSE

The following terms and conditions apply only to specific license types:

15. **Translation**: This permission is granted for non-exclusive world **English** rights only unless your license was granted for translation rights. If you licensed translation rights you may only translate this content into the languages you requested. A professional translator must perform all translations and reproduce the content word for word preserving the integrity of the article. If this license is to re-use 1 or 2 figures then permission is granted for non-exclusive world rights in all languages.

16. **Posting licensed content on any Website**: The following terms and conditions apply as follows: Licensing material from an Elsevier journal: All content posted to the web site must maintain the copyright information line on the bottom of each image; A hyper-text must be included to the Homepage of the journal from which you are licensing at http://www.sciencedirect.com/science/journal/xxxxx or the Elsevier homepage for books at http://www.elsevier.com; Central Storage: This license does not include permission for a scanned version of the material to be stored in a central repository such as that provided by Heron/XanEdu.

Licensing material from an Elsevier book: A hyper-text link must be included to the

Elsevier homepage at http://www.elsevier.com . All content posted to the web site must maintain the copyright information line on the bottom of each image.

Posting licensed content on Electronic reserve: In addition to the above the following clauses are applicable: The web site must be password-protected and made available only to bona fide students registered on a relevant course. This permission is granted for 1 year only. You may obtain a new license for future website posting.

For journal authors: the following clauses are applicable in addition to the above: Permission granted is limited to the author accepted manuscript version* of your paper.

***Accepted Author Manuscript (AAM) Definition:** An accepted author manuscript (AAM) is the author's version of the manuscript of an article that has been accepted for publication and which may include any author-incorporated changes suggested through the processes of submission processing, peer review, and editor-author communications. AAMs do not include other publisher value-added contributions such as copy-editing, formatting, technical enhancements and (if relevant) pagination.

You are not allowed to download and post the published journal article (whether PDF or HTML, proof or final version), nor may you scan the printed edition to create an electronic version. A hyper-text must be included to the Homepage of the journal from which you are licensing at http://www.sciencedirect.com/science/journal/xxxxx. As part of our normal production process, you will receive an e-mail notice when your article appears on Elsevier's online service ScienceDirect (www.sciencedirect.com). That e-mail will include the article's Digital Object Identifier (DOI). This number provides the electronic link to the published article and should be included in the posting of your personal version. We ask that you wait until you receive this e-mail and have the DOI to do any posting.

Posting to a repository: Authors may post their AAM immediately to their employer's institutional repository for internal use only and may make their manuscript publically available after the journal-specific embargo period has ended.

Please also refer to Elsevier's Article Posting Policy for further information.

18. **For book authors** the following clauses are applicable in addition to the above: Authors are permitted to place a brief summary of their work online only.. You are not allowed to download and post the published electronic version of your chapter, nor may you scan the printed edition to create an electronic version. **Posting to a repository:** Authors are permitted to post a summary of their chapter only in their institution's repository.

20. **Thesis/Dissertation**: If your license is for use in a thesis/dissertation your thesis may be submitted to your institution in either print or electronic form. Should your thesis be published commercially, please reapply for permission. These requirements include

permission for the Library and Archives of Canada to supply single copies, on demand, of the complete thesis and include permission for Proquest/UMI to supply single copies, on demand, of the complete thesis. Should your thesis be published commercially, please reapply for permission.

Elsevier Open Access Terms and Conditions

Elsevier publishes Open Access articles in both its Open Access journals and via its Open Access articles option in subscription journals.

Authors publishing in an Open Access journal or who choose to make their article Open Access in an Elsevier subscription journal select one of the following Creative Commons user licenses, which define how a reader may reuse their work: Creative Commons Attribution License (CC BY), Creative Commons Attribution – Non Commercial - ShareAlike (CC BY NC SA) and Creative Commons Attribution – Non Commercial – No Derivatives (CC BY NC ND)

Terms & Conditions applicable to all Elsevier Open Access articles:

Any reuse of the article must not represent the author as endorsing the adaptation of the article nor should the article be modified in such a way as to damage the author's honour or reputation.

The author(s) must be appropriately credited.

If any part of the material to be used (for example, figures) has appeared in our publication with credit or acknowledgement to another source it is the responsibility of the user to ensure their reuse complies with the terms and conditions determined by the rights holder.

Additional Terms & Conditions applicable to each Creative Commons user license:

CC BY: You may distribute and copy the article, create extracts, abstracts, and other revised versions, adaptations or derivative works of or from an article (such as a translation), to include in a collective work (such as an anthology), to text or data mine the article, including for commercial purposes without permission from Elsevier

CC BY NC SA: For non-commercial purposes you may distribute and copy the article, create extracts, abstracts and other revised versions, adaptations or derivative works of or from an article (such as a translation), to include in a collective work (such as an anthology), to text and data mine the article and license new adaptations or creations under identical terms without permission from Elsevier

CC BY NC ND: For non-commercial purposes you may distribute and copy the article and include it in a collective work (such as an anthology), provided you do not alter or

modify the article, without permission from Elsevier

Any commercial reuse of Open Access articles published with a CC BY NC SA or CC BY NC ND license requires permission from Elsevier and will be subject to a fee.

Commercial reuse includes:

- <!--[if !supportLists]-->· <!--[endif]-->Promotional purposes (advertising or marketing)

- <!--[if !supportLists]-->· <!--[endif]-->Commercial exploitation (e.g. a product for sale or loan)

- <!--[if !supportLists]-->· <!--[endif]-->Systematic distribution (for a fee or free of charge)

Please refer to Elsevier's Open Access Policy for further information.

21. **Other Conditions**:

v1.7

LiebertPub Website Customer Question

Ballen, Karen <KBallen@liebertpub.com>
Wed 7/23/2014 2:52 PM
Inbox

To: MOEINZADEH, SEYEDSINA;

Dear Seyedsina:

Copyright permission is granted for use of your article from TISSUE ENGINEERING, Parts A, B & C in your thesis/dissertation.

Kind regards,

Karen Ballen

Manager, Copyright Permissions